THE UNIVERSITY *of* EDINBURGH

Dynamic Platinum(II)-Based Metallosupramolecular Architectures

Sarah J. Pike

Degree of Doctor of Philosophy

School of Chemistry

The University of Edinburgh

May 2011

Contents

Abstract and Layout of Thesis

Over the past two decades, transitions metals have been extensively employed towards the construction (using coordination driven assembly) and operation (using reversible metal-ligand switching motifs) of supramolecular architectures. This Thesis details the investigation of an array of dynamic platinum(II)-based metallosupramolecular architectures and includes a series of model studies on switchable platinum(II) coordination modes.

Chapter Two describes the synthesis and study of a series of prototype non-interlocked molecular machines. The inherent dynamics of intramolecular metal-ligand substitution reactions (metallotrophic shifts) are exploited to drive a d^8 platinum(II-)-phenanthroline component along different ligating architectures to achieve translational (and in one case rotary) motion of the sub-molecular components. Variable temperature NMR studies of these complexes have established the kinetic parameters for the observed shuttling processes.

In Chapter Three, the switchable behaviour of a metal-ligand coordination motif is reported in which a proton input is employed to modify the overall thermodynamic bias and light is orthogonally utilized to selectively lower the energetic barrier for the binding event to re-equilibration. A discussion of the light-promoted ligand exchange reaction is presented, supported by a combination of TD-DFT calculations and kinetic studies.

Chapter Four describes the exploitation of this discovered pH-switchable metal-ligand motif for the stimuli-responsive reversible assembly of two dimensional and three dimensional metallosupramolecular architectures. Whilst Chapter Five details how this reversible motif can be exploited to induce controlled exchange between "3+1" and "2+2" square planar platinum donor sets in response to the application of acid-base stimuli.

Declaration

The scientific work described in this Thesis was carried out in the School of Chemistry at the University of Edinburgh between September 2007 and September 2010. Unless otherwise stated, it is the work of the author and has not been submitted in whole or in support of an application for another degree or qualification at this or any other University or institute of learning.

Signed .....

Date.....

Lectures and Meetings Attended and Presentations Given

1. **Organic Research Seminars**, School of Chemistry, University of Edinburgh, UK, 2007–2010.
   Oral presentations:
   i) "*Towards Linear Non-Interlocked Molecular Machines"*, December 2007.
   ii) *"From Metal-based Molecular Machines to Switchable Metallosupramolecular Assemblies"*, March 2008.

2. **School of Chemistry Visiting Speaker Colloquia**, School of Chemistry, University of Edinburgh, UK, 2007–2010.

3. **Supra-Nano 2008**, University of Birmingham, 16th-18th December, 2008.
   Poster presentation: *"Towards Synthetic Molecular Machines Driven Through Metal Ligand Exchange Reactions"*

4. **USIC 2009**, Heriot-Watt University, UK, 3rd-4th September 2009.
   Poster presentation: **"***Reversibly, Allosterically Driven Assembly of 2- and 3-D Metallosupramolecular Architectures."*

5. **Supra-Nano 2009**, University of Cambridge, 15th-16th December, 2009.
   Poster presentation: *"Stimuli-Responsive Reversible Assembly of 2D and 3D Metallosupramolecular Architectures."* RSC *Chem. Soc. Rev.* Poster Prize.

6. **RSC Photochemistry Group – Young and Early Researchers' Meeting**, University of Durham, UK, 13th January 2010.
   Poster presentation: *"pH and Light Responsive Heteroleptic Platinum Coordination Compounds."*

7. **ISMSC 2010- 5th International Symposium on Macrocyclic and Supramolecular Chemistry**., Nara Prefecture, Japan, 6 - 10th June 2010.
   Poster presentation: *"Stimuli-Responsive Reversible Assembly of 2D and 3D Metallosupramolecular Architectures."* RSC *Org. Bio. Chem*. Poster Prize.

8. **USIC - 44th Universities of Scotland Inorganic Conference**, University of Durham, UK, 9th July 2010. Oral presentation:*"From Metal-based Molecular Machines to Switchable Metallosupramolecular Assemblies."*

Acknowledgements

I would like to thank my supervisor Dr. Paul Lusby, to whom I am grateful for the opportunity to work on these exciting projects and for all his support during my Ph.D studies and during the writing of this Thesis.

I would like to thank Professor Alex Slawin at St. Andrews for solving all my crystal structures presented in this Thesis and Dr. Patricia Richardson for all her support and guidance particularly with the computational studies described in this Thesis. Thanks go to Dr. Martin De Cecco and Dr. Perdita Barran who undertook the electrospray mass spectrometry on the molecular square and trigonal prism species. I would also like to thank Oleg Chepelin and Paul Symmers for their camaraderie in the lab. Dr. Roy McBurney for his proof-reading of Chapter Two and for his guidance in the lab during my first year and Gordon Nimmo-Smith for proof-reading Chapter Three.

Finally, special thanks go to my family for their continuous support during my studies.

List of Abbreviations

3,5-Lut	3,5-lutidine
4,4`-bipy	4,4`-bipyridine
[9]aneS_3	1,4,7-trithiocyclononane
Ac	acetate
aq.	aqueous
ATP	adenosine triphosphate
BET	back electron transfer
bipy	2,2`-bipyridine
bp	base pair
Boc	di-*tert*-butyl dicarbonate
Bn	benzyl
CD	cyclodextrin
CSA	camphor-10-sulfonic acid
CuAAC	Cu(I) catalyzed azide-alkyne 1,3-cycloaddition
DCC	dynamic covalent chemistry
DCM	dichloromethane
dec.	decomposed
DFT-TD	density functional theory time dependent
dmbipy	5,5`-dimethyl-2,2'-bipyridyl
DMF	*N*,*N*`-dimethylformamide
DMSO	dimethylsulfoxide
DNA	deoxyribonucleic acid
EI	electron ionisation
en	ethylenediamine
eq	equivalent(s)
ESI	electrospray ionisation
Et	ethyl
FAB	fast atom bombardment
GlyGly	glycylglycine
h	hour(s)

HOMO	highest occupied molecular orbital
HR	high resolution
Hz	hertz
IPr	isopropyl
ISC	intersystem crossing
k	rate constant
K	kelvin
LUMO	lowest unoccupied molecular orbital
LR	low resolution
M	molarity
max	maximum
MC	metal centred
Me	methyl
MeCN	acetonitrile
min	minute(s)
MLCT	metal-to-ligand charge- transfer
MO	molecular orbital
MS	mass spectrometry
MT	microtubule
m/z	mass to charge ratio
N_3	azide
NEt_3	triethylamine
n-BuLi	*n*-butyllithium
NMR	nuclear magnetic resonance
NOE	nuclear overhausser effect
m.p.	melting point
m/z	mass to charge ratio
nm	nanometre
NMP	*N*-methylmorpholine
NMR	nuclear magnetic resonance
p-TsCl	*para*-tosylchloride
PCM	polarisable continuum model

PEPPSI	[trans-Dichloro(1,3-bis-(2,6-di-isopropylphenyl)imidazolylidinium)(3-chloro-pyridine)palladium]
PET	photoinduced electron transfer
Ph	phenyl
phen	phenanthroline
P_1-^{t}Bu	phosphazene base
Pr	propyl
PS	photostationary
py	pyridyl
pyCN	4-cyanopyridine
pyOMe	4-methoxypyridine
$pyNMe_2$	4-dimethylaminopyridine
PTZ	phenothiazine
pyrdm	pyridinium
RCM	ring closing metathesis
RT	room temperature
sat.	saturated
TEOA	triethanolamine
Terpy	terpyridine
TFA	trifluoroacetic acid
THF	tetrahydrofuran
TLC	thin layered chromatography
TsOH	*para*-toluenesulfonic acid
UV-Vis	ultraviolet-visible
VT	variable temperature
W	Watt

CHAPTER ONE

Recent Advances in the Synthesis and Operation of Artificial Molecular Machines

Acknowledgements

Dr. Paul Lusby is gratefully thanked for his proof-reading of this introduction.

1.1 Overview of Thesis

There has been extensive development and remarkable advances in the employment of transition metals in the field of supramolecular chemistry over the past two decades. The versatility and efficacy of metal-ligand coordination chemistry has been widely demonstrated not only in the context of construction of supramolecular architectures but additionally as a means to operate/manipulate these large assemblies. This Thesis presents work on the synthesis and investigation of an array of dynamic group 10-based metallosupramolecular architectures. The work detailed in this Thesis addresses the synthesis of prototype non-interlocked molecular machines which are able to exhibit processive translational motion. The presented work additionally outlines the development of novel molecular switching motifs which will ultimately provide innovative methods by which to induce molecular motion in artificial interlocked systems. Model studies into sophisticated switching mechanisms in which control over both the kinetics and thermodynamics of the binding event are explored and additional molecular switching motifs which exploit different metal coordination modes have been developed to induce controlled molecular exchange between different ligand sets. This work is also concerned with the development of novel methods by which to induce stimuli-responsive reversible assembly of multidimensional metallosupramolecular architectures.

1.2 Artificial Molecular Machines: Background

Biological molecular motors, such as kinesin[1] and dynein[2] which are responsible for cellular transport, eloquently demonstrate Natures' ability to accomplish controlled motion at the molecular level in order to perform tasks. Inspired by natural molecular machines, great interest has been shown in the synthesis and operation of fully artificial systems, such as stimuli-responsive rotaxanes and catenanes, which are capable of demonstrating controlled, large amplitude sub-molecular motion.[3] The structural integrity of the nanomachinery during its operation is maintained by the physical interlocking (mechanical bonding) of sub-molecular components. [2]Rotaxanes are chemical structures in which a macrocycle is mechanically bonded

onto a linear thread (axle) by the presence of bulky, terminal "stopper" groups. [2]Catenanes are comprised of two interlocked rings (Figure 1.1). The number prefix terminology describes, in part, the topology[4] of these architectures by denoting the number of constituents in each structure (Figure 1.1). The molecular motion which can be displayed by these systems can be either rotary or translational in nature. In the former case, pirouetting motions of the macrocycle about the thread (rotaxane) or other ring (catenane) are observed. In the latter form, translocation of the ring along the thread (rotaxane) or about the other ring (catenane) is seen. Usually two (or more) recognition sites, termed stations, which are capable of interacting with the macrocycle, are incorporated into the axle (rotaxane) or one ring (catenane). These stations classically bind the macrocycle using a series of non-covalent interactions such as hydrogen-bonding and π-π stacking interactions. The application of an external stimulus, electrochemical, photochemical or chemical, can manipulate these intrinsically weak interactions such that control over the binding affinity of the macrocycle for a particular station can be accomplished. As a result, large amplitude motion of the ring between the two (or more) recognition sites can be achieved.

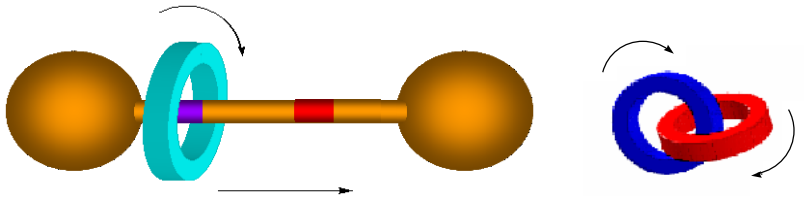

Figure 1.1 Representation of a [2]rotaxane and a [2]catenane and the possible motions of the sub-components.

1.3 First Reported Synthesis of a Rotaxane

In 1967, the first reported rotaxane synthesis was communicated by Harrison.[5] An undirected "statistical" approach was employed wherein favourable interactions between the thread and macrocycle were absent (Figure 1.2). The formation of **1** relied exclusively on the statistical distribution of the two components, the resin bound macrocycle and the ether thread, residing in the correct orientation to give the desired threaded compound. This approach whilst establishing the proof of concept for the formation of rotaxane architectures, was synthetically exhaustive. Seventy

treatments of a column containing the resin-bound macrocycle with a solution of the ether thread precursors, decane-10-diol and triphenylmethyl chloride in the presence of pyridine, were required to afford **1** in an extremely modest 6%.

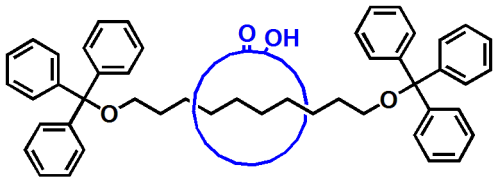

1

Figure 1.2 First reported of a rotaxane by Harrison and Harrison. **1** was synthesised using an undirected "statistical" approach were favourable interactions between the sub-molecular components were absent.[5]

1.4 Templating Strategies

The introduction of templating strategies permitted the construction of mechanically bonded structures in greatly improved yields. This synthetic approach relied upon the establishment of favorable non-covalent interactions (i.e. hydrogen-bonding, hydrophobic effect and/or π-π stacking interactions) or metal-ligand interactions between the sub-molecular components. As such, the constituents are held in mutual proximity to each other and in the correct orientation that upon covalent capture the desired interlocked architecture is formed.

Two principal methodologies exist for the construction of rotaxanes based on templating techniques. These are the 'clipping' and 'threading-followed-by-stoppering' strategies (Figure 1.3). In the former method, the precursor macrocycle ligand is bound to the acyclic thread with subsequent intramolecular cyclisation affording the interlocked structure. The latter technique, involves the threading of an axle through a macrocycle followed by subsequent attachment of bulky, terminal "stopper" groups. In a similar manner, catenanes can be constructed using a 'double-clipping' or 'threading-followed-by-clipping' strategy. The first methodology involves two intramolecular cyclisation reactions of pre-organised acyclic ligands. The second approach is achieved through threading one acyclic ligand through a cyclic ligand followed by intramolecular cyclisation.

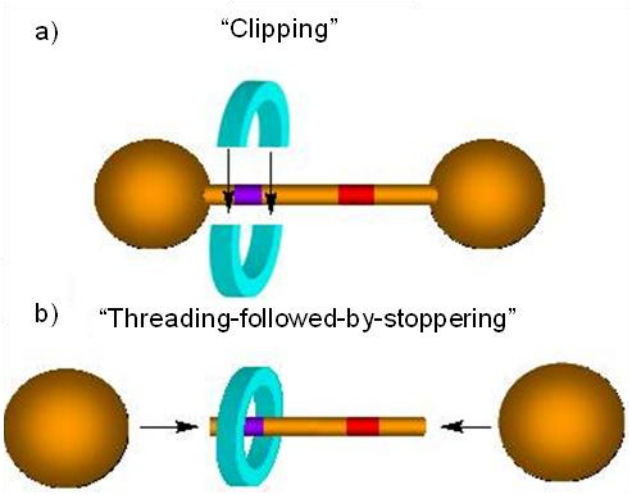

Figure 1.3 Two principle methods for employed for the construction of rotaxanes a) 'clipping' and b) 'threading-followed-by-stoppering' techniques.

1.4.1 Organic Templating Strategies

1.4.1.1 π-π Stacking Interactions

In 1991, Stoddart and co-workers published the first example of a molecular shuttle.[6] The synthesis of $\mathbf{2}^{4+}$ was achieved using an organic templating strategy and a 'clipping' technique. Favourable π-π stacking and charge-transfer interactions between the electron deficient bipyridinium units of the macrocycle and electron rich hydroquinol stations on the thread arranged the sub-components in the correct orientation such that 'clipping' of the macrocycle about the thread afforded $\mathbf{2}^{4+}$ in 32%. Unbiased temperature-dependent shuttling of the macrocycle between the two degenerate hydroquinol stations was observed by a series of variable temperature (VT) NMR experiments.

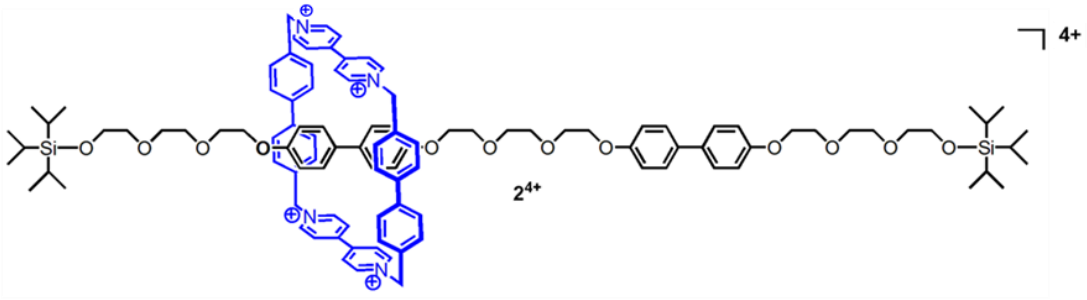

Figure 1.4 The first reported molecular shuttle, **2**. The assembly of **2** relied upon the templating effect and the 'clipping' technique. Unbiased shuttling motion of the macrocycle between the degenerate stations was established *via* a series of VT NMR experiments.[6]

In 1994, Stoddart reported on the first stimuli-responsive molecular shuttle.[7] $\mathbf{3}^{4+}$ demonstrated translocation of the macrocycle between two distinct recognition sites upon the addition of acid or base (Scheme 1.1). At room temperature rapid shuttling of the macrocycle along the thread was observed but upon cooling to 229 K the ring was found to principally reside over the benzidine station, $\mathbf{3}^{4+}$, as evidenced by ^{1}H NMR spectroscopy. Treatment with trifluoroacetic acid (TFA) caused protonation of nitrogen donors of the benzidine unit and electrostatic repulsion of the tetracationic macrocycle to the secondary hydroquinol station to generate $[2H.\mathbf{3}]^{6+}$. The original co-conformer, $\mathbf{3}^{4+}$, was reformed upon the addition of pyridine.

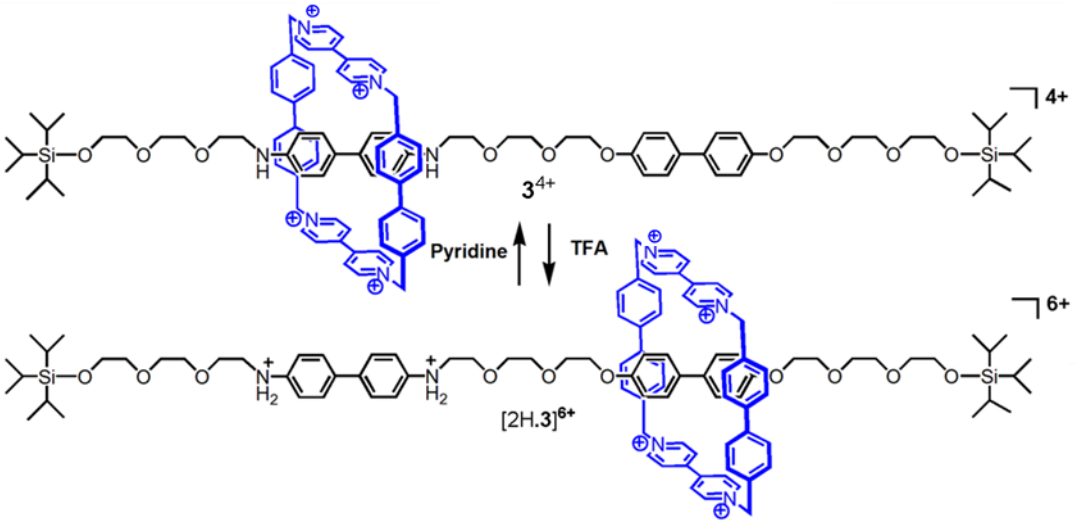

Scheme 1.1 The first non-generate shuttle, $\mathbf{3}^{4+}$, in which translocation of the macrocycle between two distinct recognition sites, benzidine and hydroquinol stations, was achieved in response to treatment with acid or base.[7]

1.4.1.2 Hydrophobic Effect

In 1997, the first light-driven molecular shuttle was reported.[8] Nakashima and co-workers described the high-yielding formation of a photoresponsive cyclodextrin (CD)-based [2]rotaxane through an organic templating strategy.[8,9] In water, the linear azobenzene-based axle was "threaded" through the cavity of the CD macrocycle and the subsequent instalment of bulky, 2,6-dinitrobenzene "stopper" groups afforded the interlocked architecture, $\mathbf{4}^{4+}$, in 30%. Shuttling of the CD ring was achieved through photoisomerisation of an integrated, central azobenzene group (Scheme 1.2). In *trans*-$\mathbf{4}^{4+}$, the azo-linkage resides within the cavity of the cyclodextrin unit. Irradiation at 360 nm for 11 min caused *trans*-*cis* isomerisation of the double bond to generate *cis*-$\mathbf{4}^{4+}$. Two-dimensional (2D) NMR experiments suggested that upon formation of this *cis* co-conformer the CD ring expels the *cis*-azo group and as a result the macrocycle translates to a secondary, ethylene spacer moiety. The original *trans*-$\mathbf{4}^{4+}$ co-conformer was regenerated upon irradiation of *cis*-**4** at 430 nm for 15 min to complete the switching cycle.

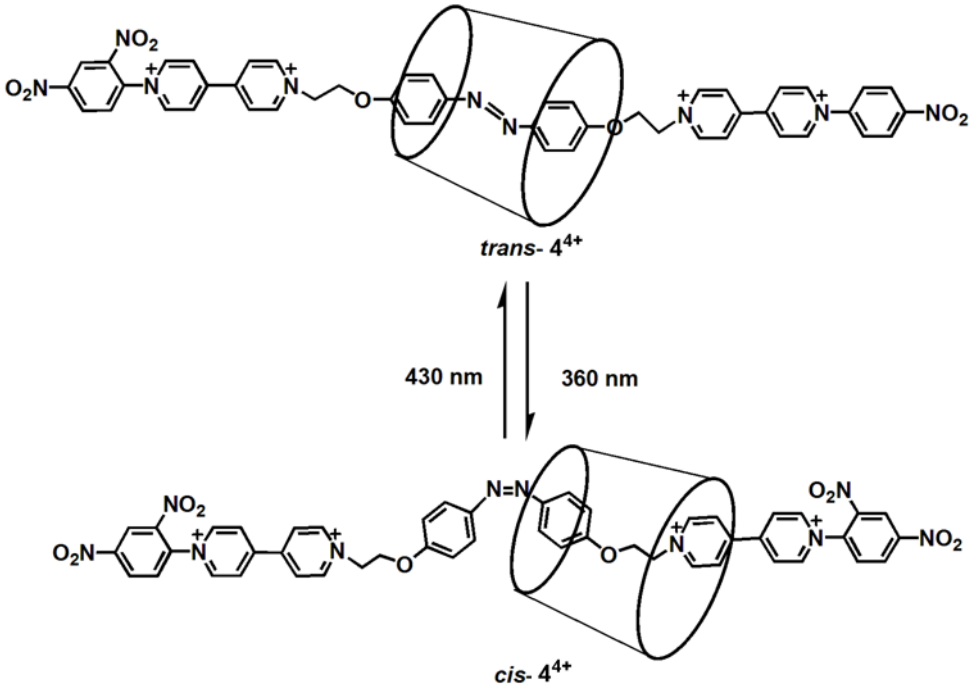

Scheme 1.2 The first example of light driven molecular shuttle, $\mathbf{4}^{4+}$, in which translation of a cyclodextrin ring was achieved upon photoisomerisation of the central *azo*benzene unit.[8]

1.4.1.3 Hydrogen-bonding Templates

In 2001, Leigh and co-workers reported on a hydrogen-bonded molecular shuttle in which fast, reversible translational motion of a macrocycle between two non-degenerate stations was achieved upon the application of photochemical stimulus.[10] Two years later, the group of Leigh showed that **5** could be prepared in a similar manner, using a hydrogen-bonding template.[11] In the bistable [2]rotaxane, **5**, exceptional positional discrimination of the macrocycle between a photoswitchable fumaramide-maleamide unit and a secondary succinamide station was realised in response to photochemical stimulus and elevated temperatures. In *trans*-**5**, macrocycle binds to the fumaramide station. This co-conformer is stabilised by the presence of four intramolecular H-bonding interactions between the fumaramide recognition site and the ring. Furthermore, unlike the other stations (maleamide and succinamide) which can intramolecularly hydrogen bond to itself, the fumaramide site is not able to fold to participate in "self-binding" (Scheme 1.3). Irradiation of *trans*-**5** at 350 nm for 5 min in the presence of benzophenone sensitizer principally afforded the *cis*-co-conformer. In *cis*-**5**, the maleamide station displays a weaker binding affinity for the macrocycle as the H-bonding interactions between the ring and the axle were reduced from four (in *trans*-**5**) to two (in *cis*-**5**). As a result, shuttling of the macrocycle to the succinamide station, which possesses an intermediate binding affinity for the ring was observed. Heating *cis*-**5** at 120 ºC for seven days returned the system to its original state, *trans*-**5**. The shuttling motion of the macrocycle was monitored by ^{1}H NMR spectroscopy.

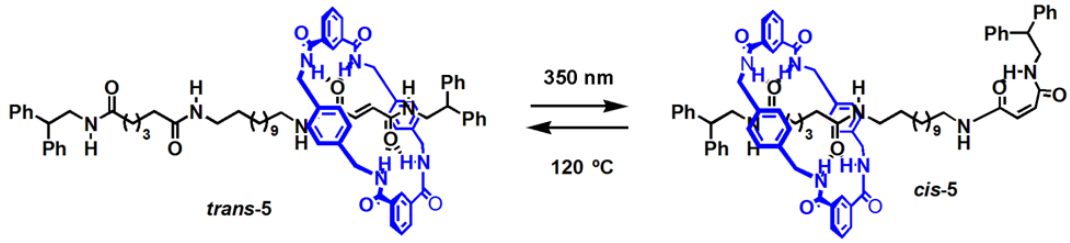

Scheme 1.3 Bistable [2]rotaxane, **5**, was constructed using a hydrogen-bonding template and motion was induced through photoisomerisation of a fumaramide-maleamide unit wherein shuttling of the macrocycle to a secondary succinamide station was observed.[11]

1.5 Metal-Template Strategies

1.5.1 Tetrahedral Geometries

The first metal templated synthesis of an interlocked structure was reported in 1983.[12] The construction of [2]catenane, Cu(I)-**6**, exploited the preference of copper(I) to adopt a tetrahedral geometry to position two appropriately substituted rigid phenanthroline (phen) ligands, **7**, in a mutually orthogonal arrangement about the metal centre. Upon pre-organisation of the acyclic phen ligands, **7**, the reactive alcohol end groups underwent intramolecular cyclisation reactions to afford the desired interlocked species, Cu(I)-**6**. Both 'threading-followed-by-clipping' and 'double clipping' strategies were employed to synthesise Cu(I)-**6** (Scheme 1.4).[12,13] In the former approach, both the phen-based macrocycle, **8**, and the acyclic ligand, **7,** coordinated to the copper(I) centre to generate pre-catenane Cu(I)-**9** (Scheme 1.4a). Single cyclisation of Cu(I)-**9** *via* a Williamson alkylation reaction between the hydroxyl end groups and the di-iodopolyether, **10**, in the presence of Cs_2CO_3, afforded Cu(I)-**6** in 42%. In the latter methodology, two acyclic phen ligand were orthogonally coordinated around a copper(I) centre to give pre-interlocked species, Cu(I)-**11**. Subsequent double macrocyclization undertaken again *via* a Williamson alkylation reaction of the phenol end groups with **10** gave Cu(I)-**6** in 27% (Scheme 1.4b).

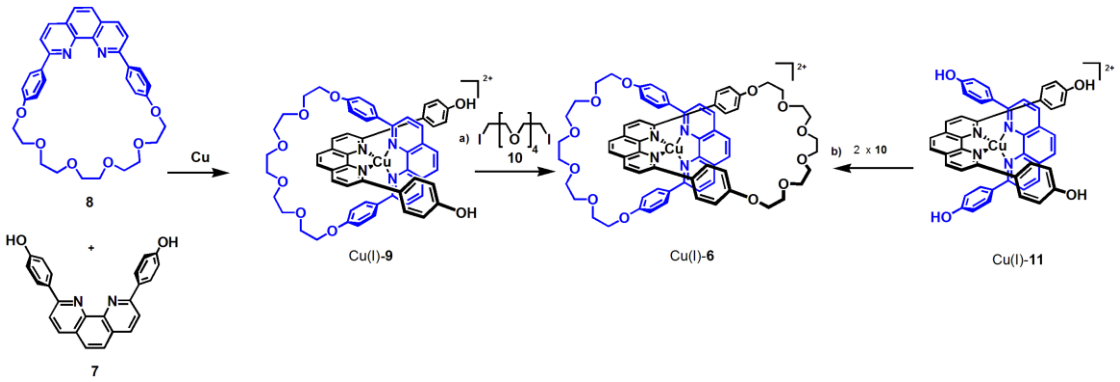

Scheme 1.4 Synthesis of [2]catenane, Cu(I)-**6**, using the "passive" metal template technique. Cu(I)-**6** was constructed *via* two methodologies a) "threading-followed-by-stoppering" technique from macrocycle, **8** and acyclic ligand, **7**;[12] b) double "clipping" technique from pre-catenane, Cu(I)-**11**.[13]

Nearly a decade after the original "passive" metal template was reported,[12] Gibson and co-workers demonstrated that the same Cu(I)-phen motif could be employed to construct [2]rotaxanes.[14] Using the pre-catenane, Cu(I)-**9**, as previously described by Sauvage and co-workers,[12] Williamson alkylation reactions were subsequently employed on both of the reactive phenol end groups of the acyclic phen ligand, **7**, to covalently attach bulky "stopper" units. Following demetallation, upon treatment with potassium cyanide, the [2]rotaxane, **12**, was generated in 42%.

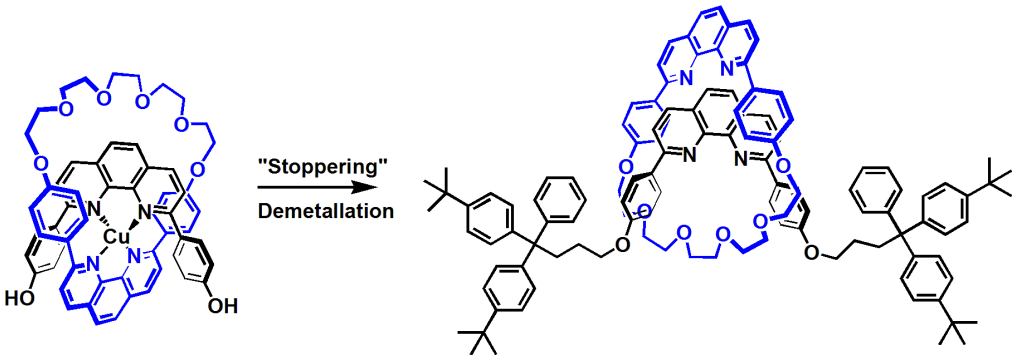

Scheme 1.5 Synthesis of **12** *via* the 'threading-followed-by-stoppering' strategy from pre-rotaxane Cu(I)-**9** with the attachment of bulky stopper groups.[14]

Following on from this report, the group of Sauvage prepared the metal-containing [2]rotaxane, Cu(I)-**15**, from the singly porphyrin "stoppered" pre-catenane, Cu(I)-**14**, in 25%.[15a] Interestingly, the incorporation of bulky porphyrin units as "stopper" end groups permitted the introduction of multiple metal centers into the system such that electron transfer processes could be investigated in [2]rotaxane architectures for the first time.[15b,15c]

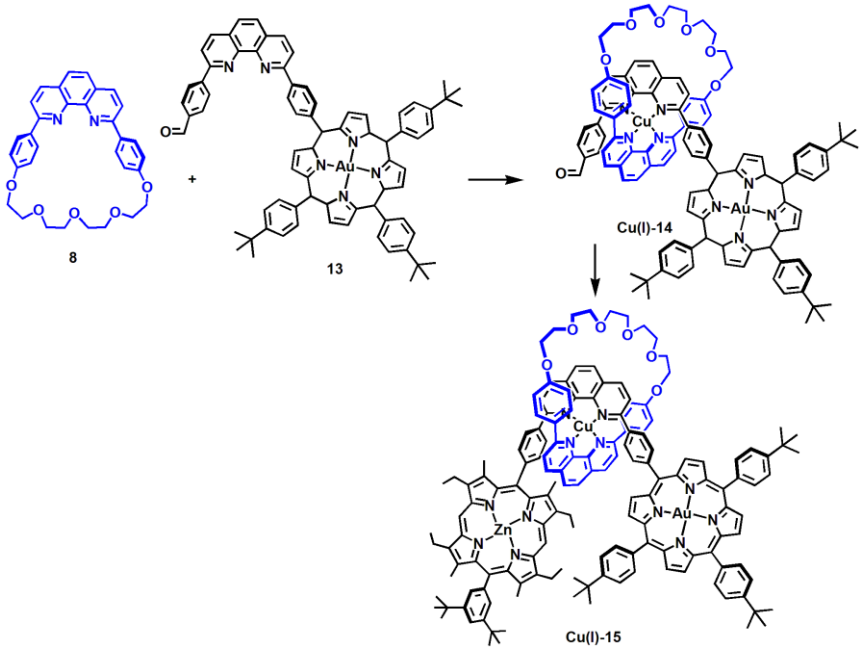

Scheme 1.6 Synthesis of the porphyrin 'stoppered' [2]rotaxane, Cu(I)-**15**, which was assembled using the 'threading-followed-by-stoppering' technique about a tetrahedral Cu(I) template.[15a]

Sauvage demonstrated that metal-ligand bonding interactions were not exclusively restricted to a templating capacity but rather that the incorporated metal centre could be further exploited, upon the application of external stimuli, to achieve controlled motion in these Cu(I)-phen-based systems.[16-19] In 1997, the bistable [2]catenane, Cu(I)-**16**, was prepared.[17] It was comprised of two distinct macrocycles; one which possessed a single phen unit and a second asymmetric macrocycle containing a bidentate phen unit and a tridentate terpyridine (terpy) unit. Rotary motion of the dual stationed ring about the second phen-based macrocycle was observed through exploitation of the Cu(I)/Cu(II) redox couple (Scheme 1.7). The preferred tetrahedral

geometry of copper(I) was satisfied by two phen ligands in the monovalent state Cu(I)-**16**. Electrochemical oxidation of the copper centre triggered rotation of the asymmetric ring to ligate the terpy chelate to the metal ion. As such, the preferred trigonal bipyramidal coordination mode of the copper(II) centre in Cu(II)-**16** was satisfied. Molecular switching between the two co-conformers was determined by monitoring the absorption spectrum of the reaction mixture as a function of time.

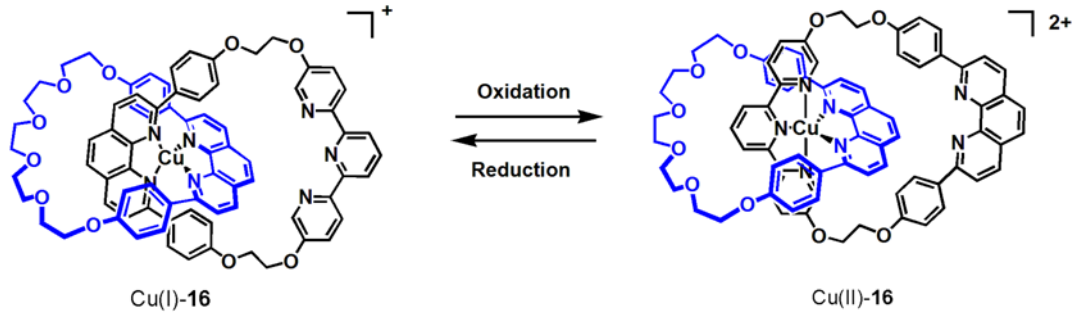

Scheme 1.7 Controlled rotary motion of one interlocked phen-based ring in [2]catenane, Cu(I)-**16**, through manipulation of the Cu(I)/Cu(II) redox couple.[17]

The redox-responsive Cu(I)-phen motif was exploited in the same manner to achieve controlled translational motion in [2]rotaxane, Cu(I)-**17** (Figure 1.5).[18] Translocation of a phen containing macrocycle along a dual terpy- and phen-stationed axle was observed in an analogous fashion.

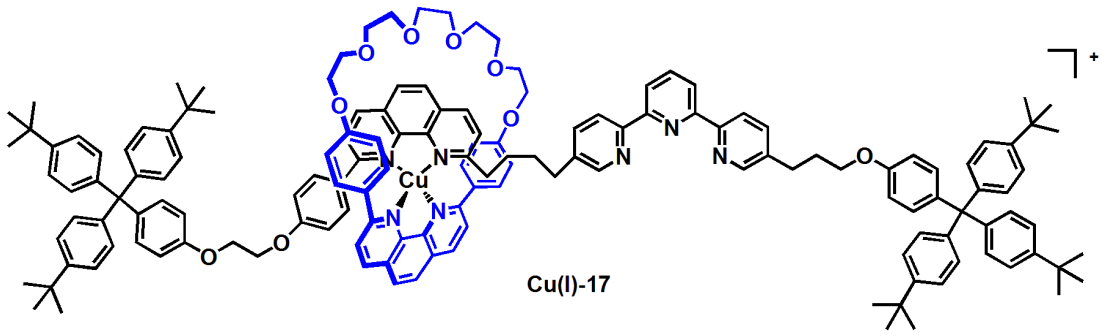

Figure 1.5 [2]rotaxane, Cu(I)-**17**, prepared about the Cu(I)-phen motif. Controlled translation of the phen-containing macrocycle along the thread can be achieved in response to electrochemical stimuli.[18]

Modification of the system such that the phen and terpy units were incorporated into the macrocycle component and the single phen group in the axle, in Cu(I)-**18**, meant that pirouetting motions of a macrocycle around the thread could also be accomplished (Scheme 1.8).[19a] It should be noted t-hat the shuttling rates in this class of Cu(I)-phen-based systems are relatively slow such that metastable states were often observed.[16-19]

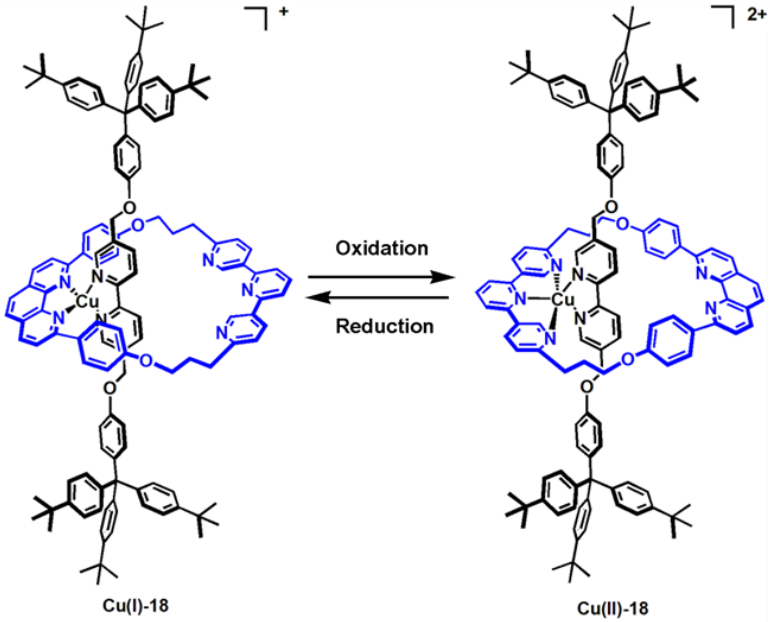

Scheme 1.8 [2]Rotaxane, Cu(I)-**18**, was prepared about a Cu(I)-phen motif. Directed rotation of the dual station macrocycle was realised upon the application of electrochemical stimulus.[19a]

Recently, Sauvage and co-workers reported that when the phen group of the macrocycle of Cu(I)-**17** is replaced by a bi-isoquinoline-based unit and rigid aromatic groups are incorporated into the thread between the phen and terpy stations then a pronounced increase, of several orders of magnitudes, in the molecular shuttling rates are observed.[20]

The group of Sauvage also reported that demetallation/metallation processes could invoke controlled motion in interlocked ring systems.[13] In metallated Cu(I)-**6**, the two phen units on the macrocycles were orientated towards the centre of the interlocked structure as a result of coordination to the tetrahedral copper(I) centre.

Treatment of Cu(I)-**6** with potassium cyanide quantitatively afforded the catenand, **6**. The demetallation procedure was readily monitored by ^{1}H NMR spectroscopy.[13] When in its metal free state, **6**, the phen rings are positioned from the centre of the structure and as a result point away from each other (Scheme 1.9). The observed orientation of the rings in this co-conformer, is presumably due to lone pair repulsion, although removal of the metal centre from Cu(I)-**6** permits the two non-coordinated rings to freely rotate unless bulky groups are incorporated into the structure.[21] Cu(I)-**6** was afforded upon re-introduction of the copper(I) templating ion to realise reversible molecular switching between the two co-conformers. The structural arrangement of the interlocked phen rings in both species was evidenced by X-ray crystallography.[22] Demetallation of the catenated species, Cu(I)-**6**, could not be achieved electrochemically as with acyclic analogues. Furthermore, kinetic studies undertaken on the demetallation process of Cu(I)-**6** in acetonitrile:water 1:9, through treatment with the potassium cyanide, ascertained that formation of the catenand, **6**, was significantly slower when compared to acyclic analogues.[23] These studies highlighted the high stability of the catenated species, Cu(I)-**6**.

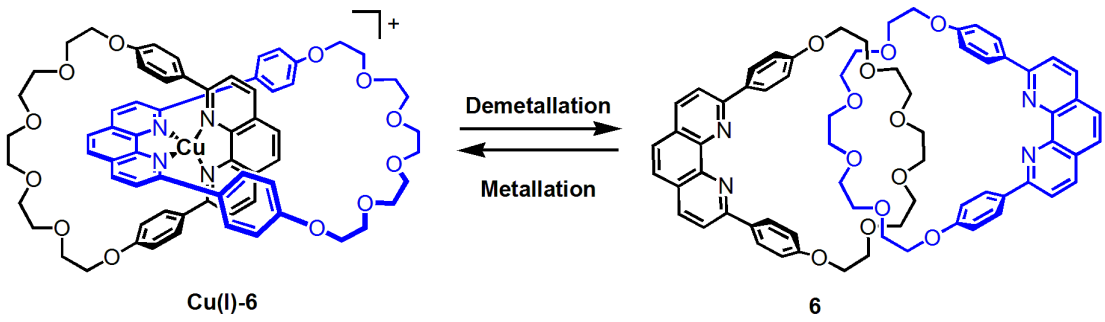

Scheme 1.9 The metallation/demetallation process of a [2]catenane was exploited by Sauvage and co-workers to achieve controlled rotational motion of the two interlocked phen-based rings.[12]

1.5.2 Octahedral Geometries

In 1991, Sauvage and co-workers reported the synthesis of the first interlocked architecture constructed about an octahedral metal template.[24] Two appropriately di-substituted, acyclic terpy ligands were complexed to a ruthenium(II) centre to afford Ru(II)-**18** (Scheme 1.10). Double macrocyclization using Williamson-ether alkylation reactions between the hydroxyl end groups and two equivalents of the di-iodopolyether species, **19**, in DMF (*N*,*N'*-dimethylformamide), in the presence of Cs_2CO_3 under high dilution conditions, led to formation of Ru(II)-**20** in 11% (Scheme 1.10). The templated synthesis was termed a "3+3" approach to reflect the assembly of two tridentate terpy-based ligands about the metal template centre in the pre-interlocked species, Ru(II)-**18**.

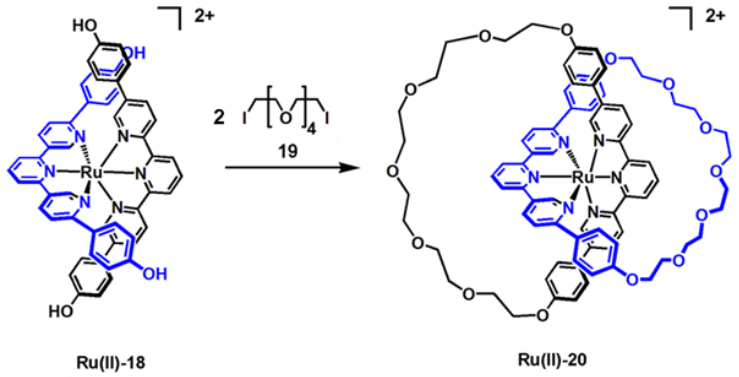

Scheme 1.10 Octahedral Ru(II)-template employed to assemble [2]catenane, Ru(II)-**20**.

In 2003, Sauvage and co-workers published work on a photochemical and thermal responsive [2]catenane.[25] An octahedral $[Ru(II)(diimine)_3]^{2+}$ motif was employed for its preparation. Two phen chelates were incorporated into one macrocycle and a third bidentate chelate, 2,2'-bipyridine (bipy), was contained in an acyclic ligand. Coordination of the *bis*-phen macrocycle to the ruthenium(II) centre with subsequent threading of the bipy-based ligand through the cavity of the cycle afforded the pre-catenane, Ru(II)-**21**. Macrocyclization of the acyclic ligand using ring closing metathesis (RCM) generated Ru(II)-**22** in 68% (Scheme 1.11). One year later, a second Ru(II)(diimine)-based [2]catenane was prepared by the same synthetic approach.[26] Whilst this later system retained the *bis*-phen macrocycle of Ru(II)-**22**,

the 42-membered bipy-based cycle was replaced by a larger, 63-membered, *bis*-phenol A and bipy-containing ring. Stimuli-responsive rotation of the bipy cycle was achieved in both of these Ru(II)-based [2]catenanes using irradiative conditions and elevated temperatures (see Section 1.5.3).

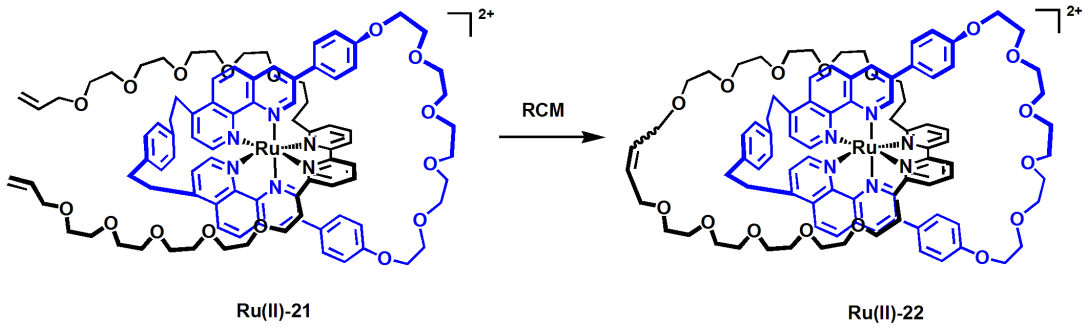

Scheme 1.11 Synthesis of [2]catenane, Ru(II)-**22**, using the "threading-followed-by-clipping" technique about an octahedral Ru(II) template. RCM was employed to covalently capture the interlocked architecture.[25]

A pseudo-[2]rotaxane and a [2]rotaxane were also prepared about the same octahedral $[Ru(II)(diimine)_3]^{2+}$ core.[27,28] In both structures, "threading" of a *bis*-phen containing axle through the cavity of a bipy-based macrocycle in ethylene glycol at 140 ºC was undertaken. To afford the [2]rotaxane bulky triarylmethyl derivatized "stoppers"[28b] were subsequently installed. As with the Ru(II)(diimine)-based interlocked ring systems, these two complexes were exposed to photonic stimulus and elevated temperatures to realise unbiased rotary motion of the bipy containing macrocycle about the axle. Section 1.5.3 elaborates on the molecular switching process and more particularly on the mechanism operating under irradiative conditions.

The template synthesis of interlocked architectures using octahedral templates is not exclusively restricted to the use of ruthenium(II) metal centres.[29-31] The Leigh group reported on the synthesis of a series of [2]catenanes using a diverse range of divalent octahedral transition metals. Two tridentate, 2,6-diiminopyridine-based acyclic ligands were complexed to an appropriate divalent metal ion (Mn(II), Fe(II), Co(II), Ni(II), Cu(II), Zn(II), Cd(II) and Hg(II)). Subsequent RCM of the terminal alkene groups in each of the ligands afforded the desired [2]catenane in good yields.

1.5.3 Square Planar Geometries

In 2003, Sauvage and co-workers reported the exploitation of a square planar palladium(II) metal centre for the preparation of a pseudo-[2]rotaxane using a "3+1" approach.[32] A tridentate terpy-based ligand was incorporated into a macrocycle and coordinated to a Pd(II)-centre. Subsequent threading of an acyclic, pyridine derivatized ligand through the cavity of the ring quantitatively afforded a pseudo-[2]rotaxane.

The construction of a three-dimensional interlocked architecture from a two-dimensional template was first reported by the group of Leigh in 2004.[33] A tridentate 2,6-dipyridinecarboxamide-containing macrocycle was complexed to a square planar palladium(II) metal centre and subsequent coordination of a pyridine "stoppered" thread, in chloroform at 50 ºC, afforded the pre-rotaxane, Pd(II)-**23** in 63%. 'Clipping' of the acyclic alkene-based ligand using RCM, followed by hydrogenation, gave Pd(II)-**24** in 77% yield (Scheme 1.12). The coordination bonds were not necessary to ensure the stability of the interlocked architecture as demetallation of Pd(II)-**24**, upon treatment with potassium cyanide, generated the corresponding metal-free mechanically bonded structure in 97%. A year later, the same square planar palladium(II)-dipyridinecarboxamide motif was employed to construct a [2]catenane in 78%.[34]

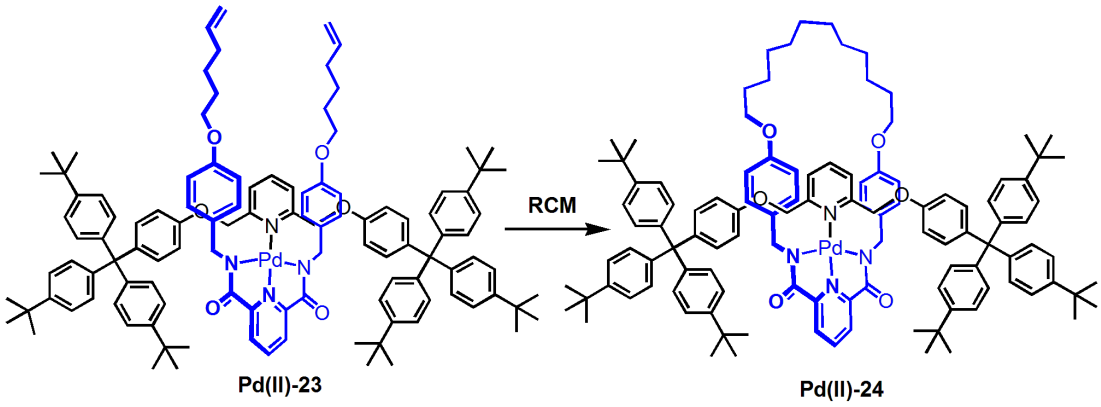

Scheme 1.12 Pd(II)-**24** was prepared using a square planar palladium(II)-dipyridinecarboxamide template followed by 'clipping' of the acyclic alkene-based pre-macrocycle using RCM to afford the desired interlocked structure.[34]

The palladium(II)-dipyridinecarboxamide motif was additionally employed to prepare [*n*]-rotaxanes *via* a sequential, single template site iterative approach.[35] A pyridine-based station was incorporated into the thread and a square planar Pd(II)-based 'clipping' methodology exploited to mechanically bond a series of tridentate 2,6-dipyridinecarboxamide-based pre-macrocycles (*vide supra*), to the axle, to afford an interlocked structure. Complexation of the palladium(II)-based pre-macrocycle to the pyridine unit of the thread was followed by RCM to covalently capture the architecture whilst subsequent demetallation left the pyridine recoginition site free to bind another Pd(II)-containing ligand. This iterative cycle was then twice repeated to generate the [4]rotaxane in 68%.

Leigh and co-workers have recently described the assembly and operation of a pH-responsive Pd(II)-complexed [2]rotaxane.[36] Tridentate 2,6-dipyridinecarboxamide and an appropriately derivatized pyridine ligand was complexed to a square planar palladium(II)-template. The [2]rotaxane, Pd(II)-**25**, was then formed upon the covalent attachment of bulky, triarylmethyl derivatized, "stopper" groups.[28b] Translocation of the palladium(II)-based macrocycle between two monodentate *N*-heterocycles, *N*,*N'*-dimethylaminopyridine ($PyNMe_2$) and pyridine (PyH) was achieved as a function of basicity. In the ground state, *PyNMe*$_2$-Pd(II)-**25**,[37] the macrocycle was bound to the more basic $PyNMe_2$ station. Upon treatment with *para*-toluenesulfonic acid (TsOH) the metastable co-conformer, *PyNMe*$_2$-[HPd(II)-**25**]OTs, was formed. The Pd-N ($PyNMe_2$) bond was found to be remarkably stable with no change in the co-conformer ratio being observed at ambient temperature over 24 h. However, upon heating a sample of *PyNMe*$_2$-[HPd(II)-**25**]OTs at 383 K, positional switching of the palladium-based macrocycle was observed, attaining an equilibration of 89:11; *PyH:PyNMe*$_2$-[HPd(II)-**25**]OTs after 16 h ($[D_7]$-DMF) and 36 h ($C_2D_2Cl_4$). Subsequent treatment of this isomeric mixture in dichloromethane with Na_2CO_3 for 30 min generated a mixture of the neutral co-conformers *PyH:PyNMe*$_2$-Pd(II)-**25** 89:11 (Scheme 1.13). Heating either a pure sample of *PyH*-Pd(II)-**25** or the isomeric mixture, *PyH:PyNMe*$_2$-Pd(II)-**25** 89:11, at 383 K for 90 min in $[D_7]$-DMF reversed the coordinative bias of the *N*-heterocycles at the metal centre. As such, an

equilibrium ratio of 86:14; *PyH:PyNMe*$_2$-Pd(II)-**25** was obtained. An associative solvent (or anion) mediated mechanism was proposed for translocation of the palladium-based macrocycle between the two recognition sites.[36]

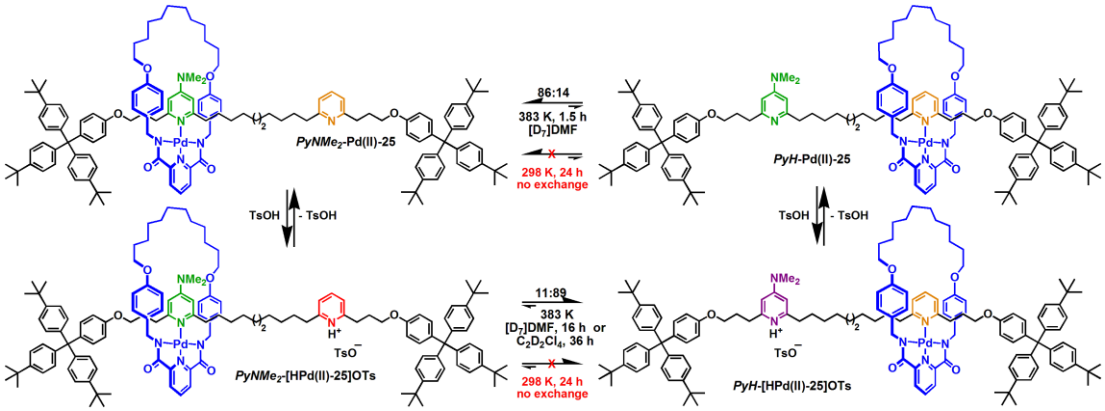

Scheme 1.13 Operation of the pH shuttle, Pd(II)-**25**, in which metastable states *PyNMe*$_2$-[HPd(II)-**25**]OTs and *PyH*-Pd(II)-**25** were formed with the addition of a proton input. Reversible molecular switching of the palladium(II)-based macrocycle was achieved in four discrete steps upon the sequential application of pH and thermal stimuli.[36]

Three years later, a second generation pH-switchable molecular shuttle, Pd(II)-**26**, was reported.[38] A related square planar "3+1" palladium(II)-templating motif was employed in conjunction with the 'threading-followed-by-stoppering' procedure to afford Pd(II)-**26** in 15% yield. The benzylic amide ring (of Pd(II)-**25**) was replaced by a larger *bis*-anilide macrocyle (Figure 1.6). A significant increase in the shuttling rates and more pronounced positional discrimination in both chemical states (neutral and protonated) was observed. Presumably, the observed increase in the shuttling rates is because the less sterically hindered environment around the palladium(II) centre better accommodates the solvent (or anion) mediated associative mechanism thought to be operating. Whilst, in the protonated state, the better positional bias of Pd(II)-macrocycle in Pd(II)-**26**, compared to Pd(II)-**25**, suggests that the Pd(II)-benzylic amide ring binds more strongly to the track than the Pd(II)-*bis*-anilide ring. As such, the weaker Pd-N (thread) interaction in Pd(II)-**26** would be expected to generate poorer co-conformational bias of the Pd(II)-based macrocycle between the two stations in the neutral states. However, even in the absence of acid, improved positional discrimination of the Pd(II)-complexed macrocycle was observed. This is

most probably a consequence of a subtle balance of solvation, metal-ligand coordination and π-stacking effects.

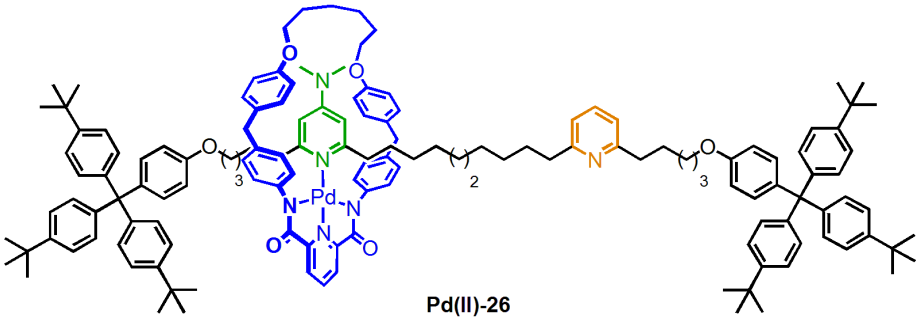

Figure 1.6 Second generation Pd(II)-based pH-responsive molecular shuttle, Pd(II)-**26**. Improved dynamics and positional bias of the palladium(II)-based macrocycle between the two heterocyclic stations was observed.[38]

The bistable [2]rotaxane, Pd(II)-**27**, exhibits controlled translocation of a palladium(II)-based macrocycle between pyridinium (pyrdm) and triazole recognition sites with exceptional positional integrity (>98%) using anion-switching (Scheme 1.14).[39] A pyridinium containing ligand was threaded through the cavity of a tridentate 2,6-dipyridinecarboxamide palladium(II)-based macrocycle. A subsequent Cu(I) catalyzed azide-alkyne 1,3-cycloaddition (CuAAC) "Click" reaction[40] between a terminal alkyne incorporated on the acyclic ligand and an appropriately stoppered azide moiety afforded the interlocked structure, Pd(II)-**27**, in 64%. The resultant triazole unit served as a secondary station for the palladium(II)-based macrocycle. In *pyrdm*-[Pd(II)-**27**]Cl, tight ion pairing between the pyridinium nitrogen atom and the formally negatively charged metal complex, combined with aromatic stacking interactions and aryl and alkyl hydrogen bonding between the oxygen atoms (in the polyether moiety) of the macrocycle and the protons adjacent to the nitrogen of the pyridinium atom in the thread caused the ring to reside in close proximity to the protonated recognition site. The addition of $AgPF_6$ to *pyrdm*-[Pd(II)-**27**]Cl induced positional switching of the macrocycle to afford *triazole*-Pd(II)-**27** wherein the palladium-based macrocycle was bound to the nitrogen of the triazole unit. The system was returned to its original state, *pyrdm*-[Pd(II)-**27**]Cl, upon treatment with tetrabutylammonium chloride.

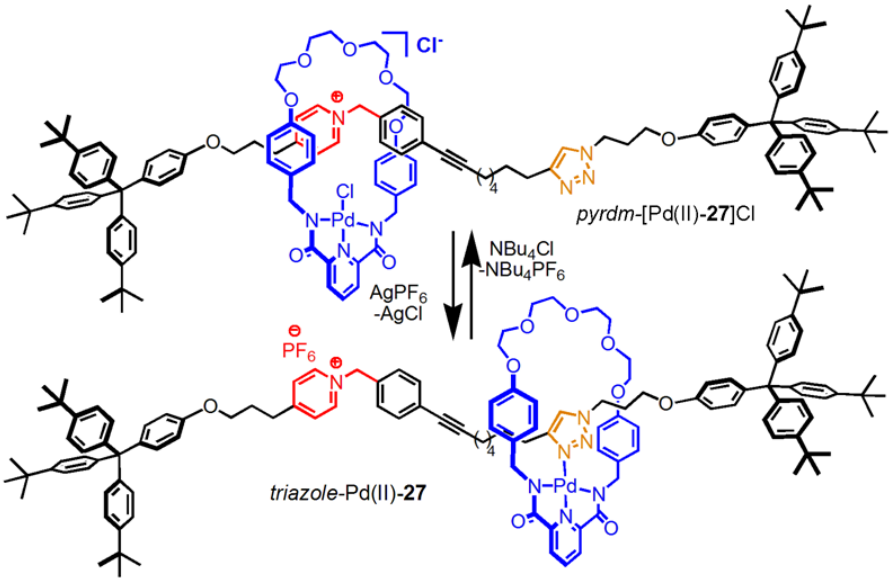

Scheme 1.14 [2]Rotaxane, Pd(II)-**27**, was assembled using a square planar palladium(II) template. Shuttling of the Pd(II)-macrocycle between the triazole and pyrdm recognition sites was achieved through anion switching.

1.5.4 "Active" Metal Template

Pioneering work by the Leigh group demonstrated that metal ions could play an "active" role in preparation of the interlocked structures (Scheme 1.15).[41] Firstly, the metal centre binds three sub-molecular components, the macrocycle and two "half-threads," so that they are in close proximity and the correct orientation for construction of a mechanically bonded architecture. Secondly, the metal catalyses covalent bond formation between the two "half-threads" through the cavity of the macrocycle to covalently capture the interlocked structure.

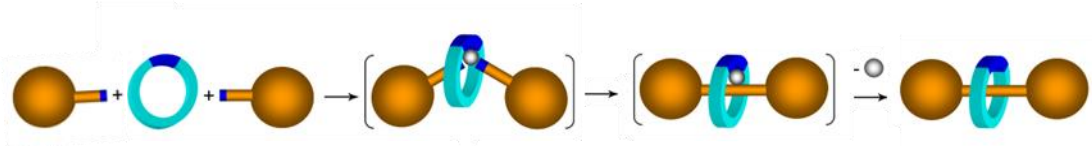

Scheme 1.15 Outline of the "active" metal templating strategy for the construction of mechanically bonded architectures such as [2]rotaxanes. Organisation of a macrocycle and two "half-threads" about a metal centre permits the constituents to be arranged such that covalent capture of the interlocked architecture is realised upon catalysis of a bond forming reaction by the metal centre. As such, the metal centre plays a dual role in both pre-organising the components of the system and catalyzing a covalent bond forming reaction within the cavity of the macrocycle.

In 2006, the first "active" metal template strategy was reported wherein a CuAAC reaction was employed to facilitate the construction of a [2]rotaxane (Scheme 1.16).[41a] Treatment of an equimolar solution of macrocycle, **29**, and terminal alkyne and azide "half-threads," **28** and **30** respectively, with a stiochiometric amount of a Cu(I) salt in dichloromethane at ambient temperature overnight afforded the interlocked species, **31**, in 57%. The macrocycle **29** coordinates to the copper centre of the added Cu(I) salt and the resultant copper(I)-complex subsequently catalyses a CuAAC reaction between **28** and **30** to form a triazole group in the cavity of **29**. Improved yields of 94% were observed when an excess of **28** and **30** were employed and with prolonged reaction times (72 h). Additionally, a series of analogous triazole-containing [2]rotaxanes were formed with a range of differently functionalized macrocycles demonstrating the tolerance of the "Click" reaction in this synthetic approach.[42]

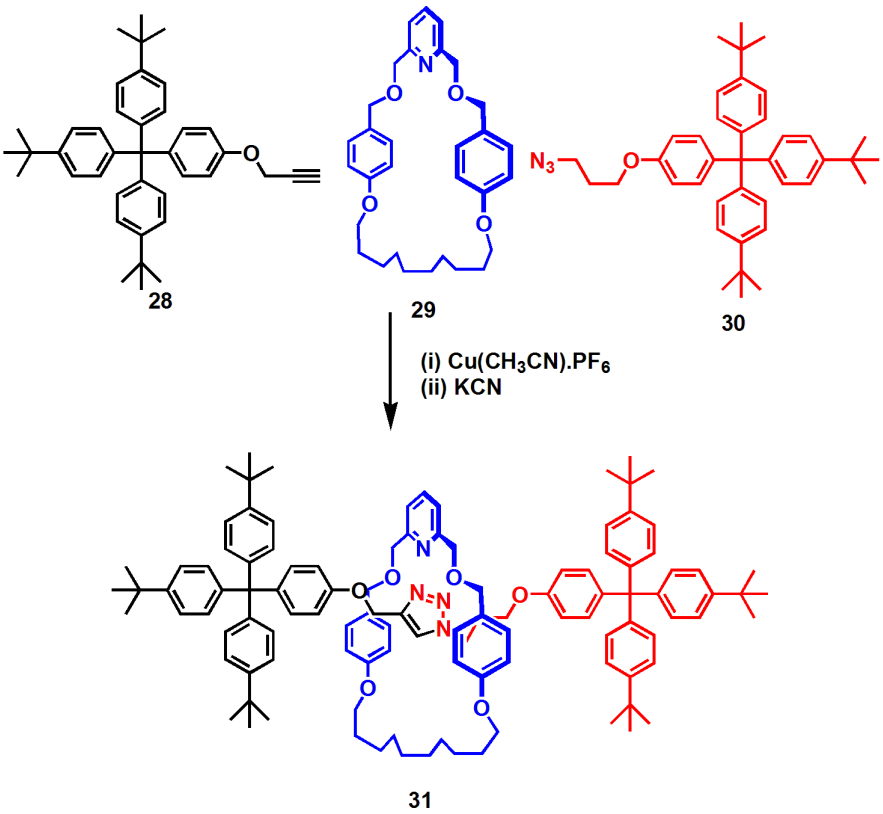

Scheme 1.16 "Active" metal templating strategy between macrocycle, **29**, and "half-threads," **28** and **29**, in the presence of Cu(I) which catalyzed the CuAAC reaction to covalent capture the [2]rotaxane, **31**.[41a]

The versatility of the active metal template strategy has been demonstrated with the construction of interlocked architectures using different copper-based reactions[43] and more recently mediated by a different transition metal templating ion.[44] Glaser couplings[43a] and Cadiot-Chodkiewicz procedures[43b] have been employed in this manner towards the formation of interlocked structures. Whilst, palladium(II)-catalysed reactions; homocoupling of alkynes,[44a] oxidative Heck cross-coupling reactions[44b] and Michael additions,[44c] have been additionally been exploited in this context.

1.6 Prototype Light-Driven Molecular Machines

In Nature, light-driven molecular processes are extensively employed to perform a diverse range of tasks. Photoresponsive systems, generally exhibit fast response times, are controlled with relative ease and often operate without forming by-products. As such, great interest has been shown in the development of synthetic photochemically-driven molecular machines.[45] Photoisomerism, photoinduced electron transfer and photoinduced ligand exchange are, to date, the three principal techniques by which motion is induced in artificial, photoresponsive molecular machines.

1.6.1 Photoisomerisation

1.6.1.1 Azobenzene and Stilbene Units

Reversible *cis*-*trans* photoisomerisation of stilbene and azobenzene motifs have been widely exploited for realising large amplitude motion in rotaxane-based systems.[3b] In the pseudo-[2]rotaxane, [*trans*-**32**⊂**33**], the azobiphenoxy acyclic ligand, **32**, resides within the centre of the macrocycle, **33** (Scheme 1.17).[46] This self-assembled "threaded" structure, [*trans*-**32**⊂**33**], was stabilised by π-electron donor-acceptor interactions between the two diazapyrenium, electron accepting units in cyclophane, **33**, and electron donating azobiphenoxy moiety. Photoirradiation (436 nm) of [*trans*-**32**⊂**33**] (which exists as the major species (~ 80%) in an equilibrium between the "threaded," [*trans*-**32**⊂**33**]**,** and two "dethreaded" species, **33** and *trans*-**32**) in

acetonitrile caused *trans*-*cis* isomerisation of the azo double bond moiety. Resultant, "dethreading" of *cis*-**32** from the cavity of the macrocycle, **33**, was observed (Scheme 1.17). Upon the application of photonic stimuli (365 nm) to the "dethreaded" components, *cis*-**32** and **33**, reversal of the *cis*-*trans* isomerisation process occurred to return the system to [*trans*-**32**⊂**33**]. The strong fluorescence signal of free cyclophane unit, **33**, was quenched upon "threading," as a result of electron transfer between the diazapyrenium and azobiphenoxy units which were in close proximity in the *trans* co-conformer. As such, light could be employed as a means to both induce and monitor motion in the system.

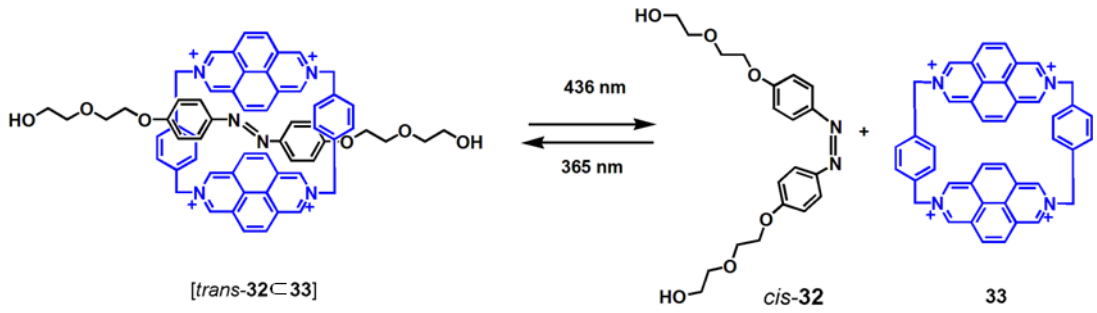

Scheme 1.17 "Threading/dethreading" process in pseudo-[2]rotaxane which was a direct consequence of photoisomerisation of the azo double bond in the acyclic ligand, **32**.[43]

Anderson and co-workers published work on a stilbene-based bistable [2]rotaxane which demonstrated unprecedented directional shuttling of an asymmetric cyclodextrin macrocycle, smaller 6-rim *vs* larger 3-rim, along a symmetric organic axle (Scheme 1.18).[47] In *trans*-**34**, a rapid gliding motion of the CD ring along the thread was observed by 2D NMR spectroscopy. Irradiation at 340 nm led to *cis*-*trans* isomerisation to afford *cis*-**34**. In the *cis*-conformer, the stilbene unit of the thread is located in close proximity to the 6-rim of the CD ring whilst the wider 3-rim is able to better accommodate the bulky "stopper" group. The molecular switching cycle between the two co-conformers was completed upon irradiation of *cis*-**34** at 265 nm.

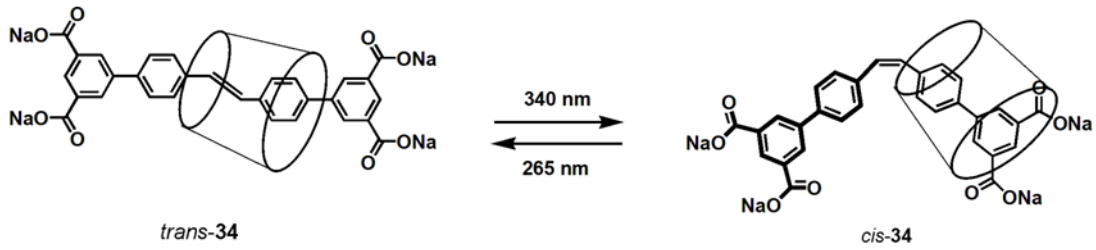

trans-**34** *cis*-**34**

Scheme 1.18 In [2]rotaxane **34**, an organic templating strategy was employed for its self-assembly whilst the installation of bulky "stopper" groups ensured covalent capture of the interlocked species. Photoisomerisation of the central stilbene unit caused translocation of the CD ring along the symmetric thread.[47]

In 2004, a lockable photoresponsive molecular shuttle, **35**, with a fluorescent output signal was published.[48] Shuttling of a CD ring between biphenyl and stilbene recognition sites on an organic thread was accomplished through light-induced *cis*-*trans* isomerisation of the photoactive station (Scheme 1.19). The presence of intramolecular hydrogen-bonding interactions between the hydroxyl groups of the cyclodextrin ring and to the carbonyl groups of the isophthalic acid "stopper" unit prevented photoisomerisation of the stilbene unit. As such, manipulation of these non-covalent interactions, through treatment with base, formed the foundation of a "molecular lock" for the system. In *trans*-**35**, the CD ring resides over the stilbene station and prevents its photoisomerisation, as such the structure is "locked." Treatment of *trans*-**35**, with Na_2CO_3 afforded *trans*-**35**$^{2-}$ where the intramolecular H-bonding interactions are disrupted. Subsequent irradiation at 335 nm for 65 min led to *trans*-*cis* isomerisation of the stilbene unit. In this state, the system is "unlocked." The CD ring shuttles towards the biphenyl station upon formation of the alternative co-conformer, *cis*-**35**$^{2-}$. Irradiation of this isomer at 280 nm shifted the equilibrium back to *trans*-**35**$^{2-}$. The distinct fluorescent output signals of *trans*-**35**$^{2-}$ and *cis*-**35**$^{2-}$ meant that shuttling motion of the CD ring could be readily monitored.

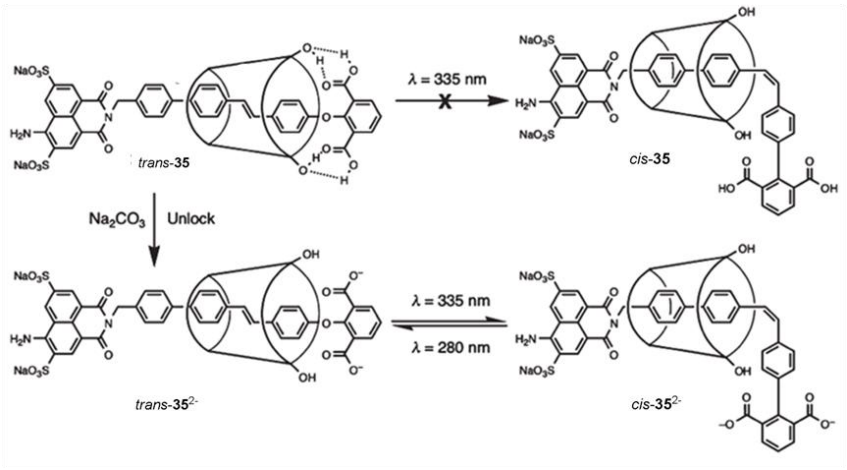

Scheme 1.19 A "lockable" light driven molecular shuttle. Intramolecular H-bonding interactions between the isophthalic acid "stopper" group and the CD ring cause "molecular locking" of the system making it non-responsive to photoisomerisation of the central stilbene unit. Upon the treatment with base, disruption of the intramolecular H-bonding interactions permits photoisomerisation such that resultant shuttling of the CD ring is observed. Reproduced from reference 48.

1.6.1.2 Fumaramide-Maleamide Units

The Leigh group have previously reported on bi-stable H-bonded [2]rotaxanes in which a macrocycle was translocated between two recognition sites in response to photostimulus (see Section 1.3.2).[10,49] In 2004, the molecular shuttle, **36**, was prepared.[49a] **36** displayed a readable fluorescence output, which exhibited a remarkable intensity ratio between the "on-off" states, in response to large, controlled positional change of the macrocycle. As such **36** can be thought to be functioning as a light-activated switch for fluorescence (Scheme 1.20). **36** was comprised of two stations; a photoresponsive fumaramide-maleamide station and a nonreactive glycylglycine (GlyGly) unit which was of intermediate binding affinity between the fumaramide and maleamide units. The two binding sites were separated by an alkyl chain spacer group. A bulky fluorophore "stopper" unit, 9-carboxyanthracene, was incorporated into the thread in close proximity to the peptide station. The two pyridinium groups in the macrocycle are capable of quenching the fluorescence signal of anthracene through electron transfer when the two sub-

components are in close proximity to each other. In cis-**36** ("off"-state), the macrocycle resides over the GlyGly station wherein the fluorescence of the system is almost completely quenched by the pyridinium groups of the ring. In *trans*-**36**, the ring principally binds the fumaramide station with significant spatial separation between the fluorophore and the quenching pyridinium units. Photoisomerisation of pure samples of either isomeric state at 312 nm in CH_2Cl_2 for 20 min afforded the photostationary (PS) state, *trans*-**36**:*cis*-**36** 40:60. This "on"-state was relatively stable ($T_{1/2}$ ~ 24 h). The observed difference in the intensity ratio of the fluorescence signal of the *cis*-**36** "off"-state and the PS "on"-state was pronounced, with the PS state emitting around eighty-five times more light than the pure *cis* co-conformer.

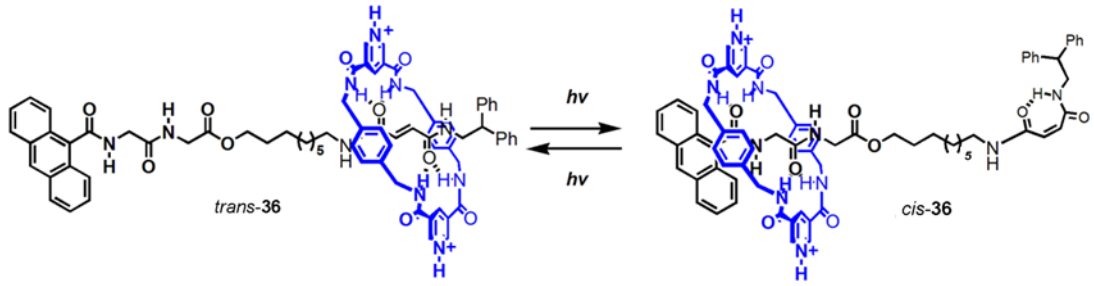

Scheme 1.20 In [2]rotaxane **36**, shuttling of the macrocycle between the fumaramide-maleamide motif and the GlyGly station occurs in response to photochemical stimuli. Fluorescence spectroscopy was employed to monitor the motion.[49]

1.6.1.3 Unidirectional Molecular Rotors

In 1999, the groups of Feringa and Harada reported on the first synthetic unidirectional molecular rotor.[50] The molecular rotor was comprised of two identical biphenanthrylidene halves connected by a carbon-carbon double bond. The upper part (rotor) underwent a unidirectional 360º rotation relative to the lower half (stator) around the central olefin bond (rotary axle) by a sequence of four discrete photochemically or thermally driven isomerisation steps. The principle behind the system involved the exploitation of two chiral photochemical and thermal responsive constituents, the stereogenic centres and the molecular helicity, to demonstrate unidirectional motion.

In the resting state, *(P,P)-trans*-**37**, the two methyl groups are diaxial. Photoirradiation ($\lambda \geq 280$ nm) at -55 ºC in *n*-hexane led to *trans-cis* isomerisation causing 180º rotation about the central olefin bond and simultaneous helical switching to give the disfavoured (*M,M*)-*cis*-**37** species. This isomerisation process was readily reversible with irradiation at $\lambda \geq 380$ nm causing the photoequilibrium to shift towards the original *(P,P)-trans*-**37** co-conformer. This reversible light-driven isomerisation step was extremely fast.[51] In *(M,M)-cis*-**37**, the chiral methyl substituents occupied equatorial positions. The disfavoured (*M,M*)-*cis*-**37** conformer was rapidly and irreversibly converted to the stable (*P,P*)-*cis*-**37** isomer by thermal helix inversion at 20 ºC. The two methyl groups in (*P,P*)-*cis*-**37** occupied axial positions. Irradiation of (*P,P*)-*cis*-**37** at $\lambda \geq 280$ nm induced a second 180º rotation about the central axle as a result of the *cis-trans* isomerisation of the photoactive olefin bond and simultaneous helical reversal was observed to give the disfavoured (*M,M*)-*trans*-**37**. The methyl substituents of (*M,M*)-*trans*-**37** now occupied equatorial positions. Irreversible conversion of the (*M,M*)-*trans*-**37** isomer to the stable *(P,P)-trans*-**38** was achieved thermally at 60 ºC to complete the unidirectional cycle (Scheme 1.21).

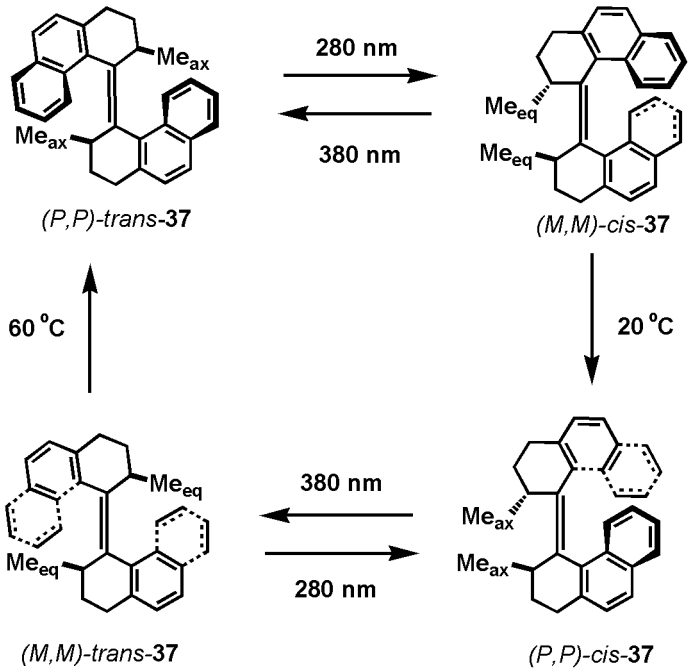

Scheme 1.21 Unidirectional rotary motor, **37**, controlled by light and thermal stimuli.[50]

After this initial communication, a second generation of light-powered sterically overcrowded molecular rotors, **38**-**45**, were produced.[52-60] All described systems, **38**-**45**, achieved unidirectional motion by an analogous fashion to **37** using four distinct photochemically- or thermally-driven isomerisation steps. **38**-**45** aimed to accelerate the rotary motion observed in the system by lowering the barrier for the rate determining thermal helix inversion steps. The two factors controlling the rate of the thermal helical switching steps are the steric hinderance in the "fjord" region (Figure 1.7) and the electronic nature of the substituents on the rotor and stator components. Accordingly, a diverse range of structural modifications to the upper and lower parts of the molecule were investigated.[52-60]

In **38**, napthiopyran propeller and thioxanthene stator units were incorporated into the structure (Figure 1.7).[53] The introduction of a bridging sulfur atom served to reduce the steric hinderance in the "fjord" region of the molecule. As a result, a dramatic increase in the kinetics of the rotary motion was observed. Reducing the size of the bridging atom in the rotor and stator facilitated the slippage of the upper and lower halves of the molecule over each other thus lowering the rate determining helix inversion steps. Interestingly, these studies demonstrated that the inclusion of a single stereogenic centre in the upper ring was sufficient to induce unidirectional rotary motion. The development of this class of sulfur-based systems also provided the opportunity to attach this series of sterically, overcrowded, alkene motors to gold surfaces.[54] Modification of **38** through the replacement of the thioxanthene unit for a xanthene group gave **39** which displayed increased kinetics for the rotation process.[53] Presumably, the smaller oxygen atom further reduced the steric hinderance in the "fjord" region to better assist the slippage of the propeller and stator units over each other.

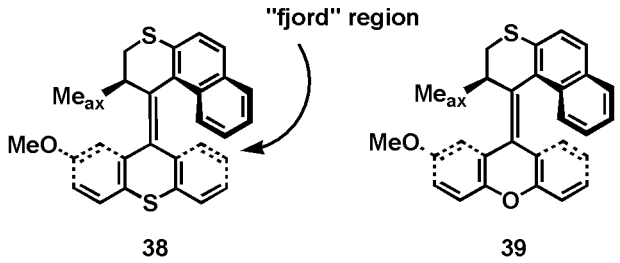

Figure 1.7 Second generation of the sterically, overcrowded alkenes, **38** and **39**, which operate as molecular rotors.[53]

The introduction of five-membered ring systems (fluorene groups) in both the upper and lower parts of the molecule were found to significantly lower the barriers for the thermal helix inversion steps compared to their six-membered analogues, **37** (Figure 1.8).[55]As such, a drastic increase (1.2 million-fold) in the rotary speed of the motion was observed compared to **37**. The rotary speed achieved in **40** was 80 revolutions per second which was astonishingly close to that observed for the natural nanomachine ATPase (135 revolutions s^{-1}).[56] Reduction in the steric bulk of the rotor component, in **40**, was also investigated with the replacemernt of the naphthalene unit by the less sterically hindered benzothiophene in **41**. This caused a significant $3.5x10^3$ fold increase in the speed of the rotation process relative to **40**.[57] Furthermore, combining the two structural modifications, five-membered ring systems (fluorene groups) and bridging heteroatoms, as in **42** (sulfur) and **43** (oxygen), gave even a pronounced increase in the rotational speed (Figure 1.8)[58] such that **42** and **43** were operational at ambient temperatures.

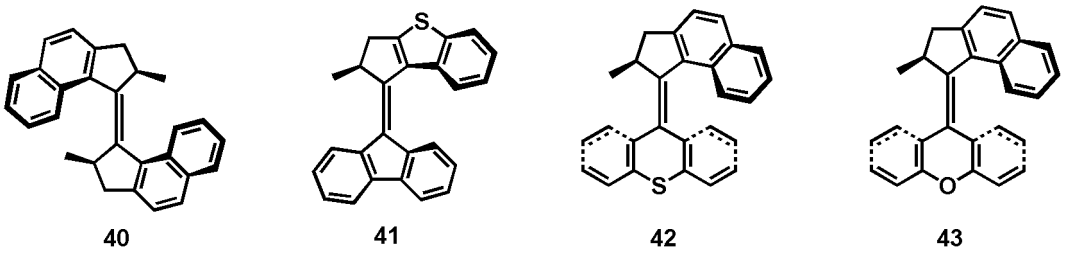

Figure 1.8 Second generation of the sterically, overcrowded alkenes, **40**-**43**, which operate as molecular rotors.[55-58]

Electronic effects were also investigated to determine their influence on the speed of rotation in these molecular rotor systems. In **44**, an amine moiety was introduced into the rotor component and a ketone group in the lower stator part.[59] The lone electron pair on the amine could be delocalised by direct conjugation with the ketone (Figure 1.9). This generated a push-pull electronic system which had a large polarising effect on the central alkene bond. As a result, the rotational axis had greater single bond character. The rate of thermal helical switching steps was accordingly increased through significant lowering of the activation barrier. As such, full unidirectional 360º rotation of the upper part of **44** was observed at 20 ºC in a matter of minutes and not hours as in earlier systems. In **45**, the incorporation of electron-withdrawing and electron-donating groups (Figure 1.9) led to a bathochromic shift in the optimal wavelength of irradiation for the system such that the rotor component underwent full 360º unidirectional motion through four distinct sequential steps with visible light and thermal stimuli.[60]

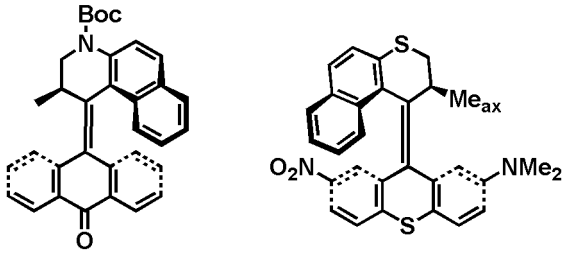

44 **45**

Figure 1.9 Second generation of the sterically, overcrowded alkenes, **44** and **45**, which operate as molecular rotors.[59,60]

1.6.2 Photoinduced Electron Transfer: Molecular Abacuses

In 2006, the group of Stoddart published work on a light-driven molecular abacus.[61] The multicomponent [2]rotaxane, **46**, relied upon photoinduced electron transfer to generate large amplitude motion of the polyether macrocycle between two aromatic recognition sites (Figure 1.10). In its resting state, the macrocycle resides over the stronger π-electron acceptor station, 4,4'-bipyridinium station, A_1^{2+}. Photosensitisation of the bulky ruthenium(II)-based "stopper" group, P^{2+}, at 532 nm causes formation of an excited state, $*P^{2+}$, from which photoinduced electron

transfer (PET) to A_1^{2+} occurs. The newly reduced species, $A_1^{+\cdot}$, drives the electron rich macrocycle towards the secondary 3,3'-dimethyl-4,4'-bipyridinium station, A_2^{2+}. Back electron transfer processes from $A_1^{+\cdot}$ to ruthenium(II) unit, $*P^{2+}$, occurred. As a result, A_1^{2+} was reformed and the macrocycle restored to the starting 4,4'-bipyridinium station. Sacrifical[61a] and autonomous[61b] mechanisms were employed to induce shuttling of the ring. In the former case, a stiochiometric quantity of triethanolamine (TEOA) was required to prolong the lifetime of the reduced station A_1^{+}, sufficiently so that repulsion (and hence motion) of the macrocycle could occur. In the autonomous mechanism, treatment of the system with phenothiazine (PTZ) induced reversible shuttling of the cycle between the two recognition sites. PTZ acted as a dual redox reagent, both prolonging the lifetime of the radical cation, A_1^{+}, and oxidising A_1^{+}. The reduction potential of $PTZ^{+/0}$ was equal to that of the oxidation potential of the $A_1^{+\cdot/2+}$ site allowing the desired electronic-phase recombination to occur. No additional reagents were required when PTZ was employed as it was regenerated upon completion of the cycle. In contrast, TEOA was degraded into by-products during operation requiring a further stiochiometric amount to reinitiate the cycle. A second generation abacus was published shortly after the initial report.[62] The positions of the two stations were reversed so that the stronger π-acceptor station A_1^{2+} was closer to the photosensitising unit, P^{2+}, so that the induced motion of the macrocycle was now directed away from the ruthenium(II)-based "stopper group", P^{2+}.

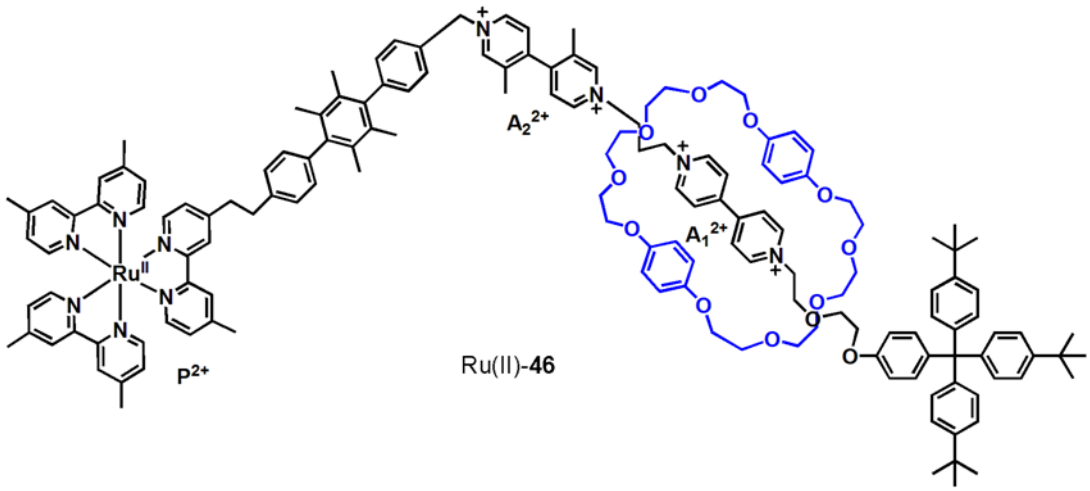

Figure 1.10 Representation of [2]rotaxane, **46**, wherein translocation of the polyether macrocycle between two aromatic recognition sites, 4,4'-bipyridinium and 3,3'-dimethyl-4,4'-bipyridinium station was observed.[61]

1.6.3 Photoinduced Ligand Exchange

In the [2]catenane, Ru(II)-**22**, Sauvage and co-workers[25,26] reported the first example of the use of photoinduced ligand exchange reactions to realise motion in one of the sub-molecular components in an interlocked architecture. Upon irradiation of Ru(II)-**22** at $\lambda > 300$ nm for 90 min in CD_3CN, in the presence of an excess of the salt $NEt_4^+Cl^-$, decoordination (expulsion) of the smaller bipy containing cycle was observed to quantitatively afford Ru(II)(L_2)-**22** (where L = Cl) (Scheme 1.22). In Ru(II)(Cl_2)-**22**, uncontrolled rotary motion of the uncoordinated macrocycle about the second *bis*-phen ring occurs. The reverse thermal recoordination reaction to regenerate Ru(II)-**22** was achieved in >95% as evidenced by ^{1}H NMR spectroscopy.

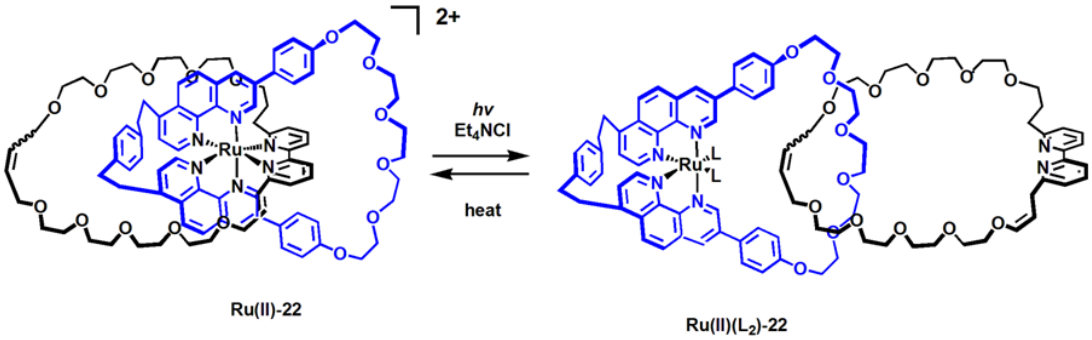

Scheme 1.22 Thermal- and photoresponsive [2]catenane, Ru(II)-**22**. Selective expulsion of the bipy chelate-containing macrocycle was observed upon the application of photochemical stimuli such that uncontrolled rotation of the liberated ring was seen. Recoordination was achieved with heating. L = Cl.[25,26]

The Ru(diimine)-based [2]catenane, Ru(II)-**47**, displayed improved reaction kinetics for the photochemically induced rotation of the bipy macrocycle.[26] The light-driven decoordination of the bipy-containing macrocycle was found to be significantly quicker in Ru(II)-**47** taking only 9 min to reach completion in CD_3CN with irradiation at $\lambda > 300$ nm in the presence of an excess of $NEt_4^+Cl^-$ (*cf* Ru(II)-**22**). In Ru(II)-**47** photochemically-driven decomplexation of the bipy chelate could also be achieved in the absence of chloride ions where the vacant coordination sites of the metal centre were then occupied by two molecules of acetonitrile (Scheme 1.23). Heating Ru(II)-**47** in ethylene glycol at 140 ºC for 15 min or 80 ºC for 2 h quantitatively reproduced the starting complex Ru(II)-**47**.

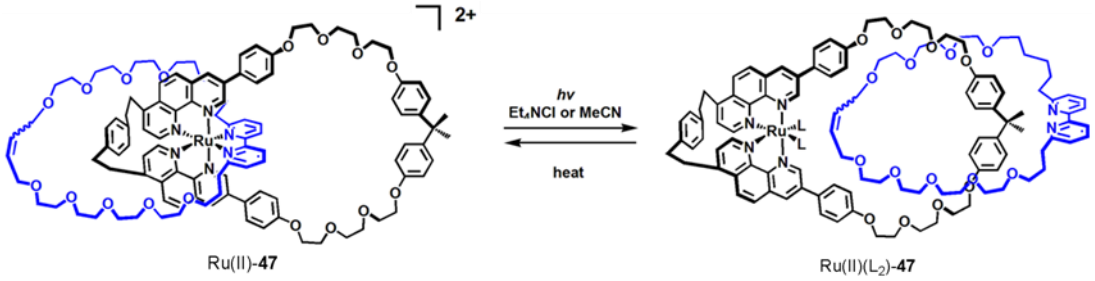

Scheme 1.23 Thermal- and photoresponsive [2]catenane, Ru(II)-**47**. Selective expulsion of the bipy chelate-containing macrocycle was observed upon the application of photochemical stimuli such that uncontrolled rotation of the liberated ring was seen. Recoordination was achieved with heating. L = CD_3CN or Cl.[26]

The selective photochemically-driven chelate expulsion in pseudo-[2]rotaxane, Ru(II)-**48**, was explored.[27] An isomeric mixture of, endo-Ru(II)-**48** and exo-Ru(II)-**48** complexes (Figure 1.11) was formed upon complexation of a *bis*-phenol A bipy-containing (dpbipy) macrocycle to a *bis*-phen-based axle. Irradiation of this isomeric mixture at 470 nm, in 1,2-dichloroethane, in the presence of a chloride salt, selectively decoordinated the dpbipy ring in a quantitative manner.[27] Thermal recoordination of the bipy ring to the axle only occurred in 15%. The low yield was most likely a result of the relatively small cavity of the bipy ring compared to the sterically hindered Ru(II)-axle.

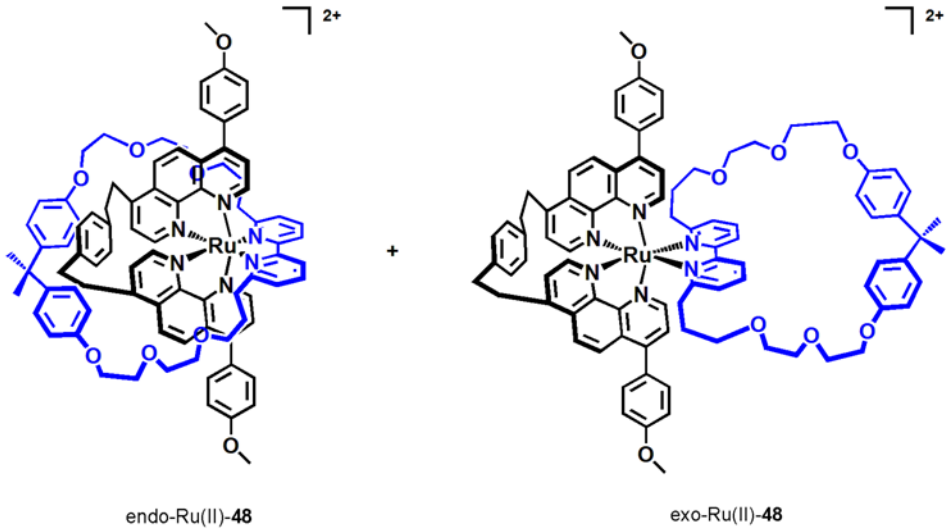

Figure 1.11 Pseudo-[2]rotaxane, endo-Ru(II)-**48**, and its isomer exo-Ru(II)-**48** formed through the complexation of of a *bis*-phenol A bipy-containing macrocycle to a *bis*-phen-based axle.[27]

Following on from this work, the photoresponsive behaviour of [2]rotaxane, Ru(II)-**49**, was investigated (Figure 1.12).[28] Irradiation of Ru(II)-**49** at 470 nm, in 1,2-dichloroethane, in the presence of an excess of $NEt_4^+Cl^-$, selectively decoordinated the bipy ring in a quantitative manner**.** Thermal recoordination of the bipy chelate was neither selective nor clean.

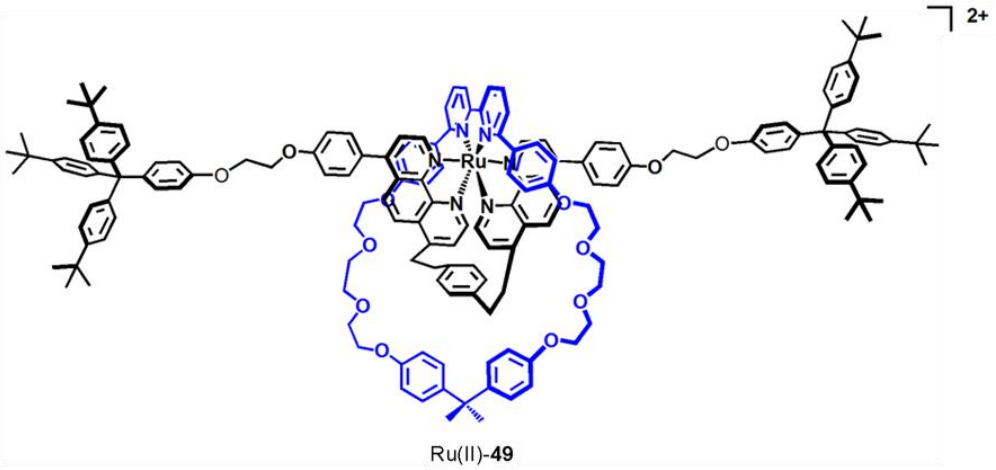

Figure 1.12 [2]rotaxane, Ru(II)-**49**, was assembled using an octahedral ruthenium(II) motif. Expulsion of the bipy-based macrocycle was achieved under irradiative conditions.[28]

The mechanism of the photoinduced ligand exchange reaction was postulated to rely upon the population of dissociative triplet ligand-field excited states (^{3}d-d*). The mechanism most likely proceeds *via* singlet and triplet metal-to-ligand charge transfer excited states (Figure 1.13).[26] Upon initial irradiation of a $[Ru(diimine)_3]^{2+}$ complex, photoexcitation into ^{1}MLCT (metal-to-ligand charge-transfer) occurs but this newly populated state rapidly undergoes intersystem crossing (ISC) into the ^{3}MLCT state. The fate of the ^{3}MLCT state is determined by the magnitude of the ligand-field splitting in the $[Ru(diimine)_3]^{2+}$ complexes. If there is no distortion of the ligand-field splitting then fluorescence (and non-radiative decay i.e. heat) would be anticipated. However, if distortion of the coordination octahedron is significant then the desired strongly dissociative metal-centred (MC) ligand field state (^{3}d-d*) would be effectively populated. $[Ru(diimine)_3]^{2+}$ complexes are well adapted to this approach. They display intense absorption in the visible region and furthermore the magnitude of the ligand field splitting can be readily tuned such that it can be significantly decreased through the incorporation of sterically bulky ligands into the structure.

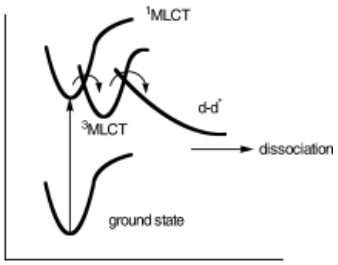

Figure 1.13 Representation of the different excited states accessed by the Ru(II)-based complexes illustrating the population of d-d* dissociative states. Reproduced from reference 26**.**

1.7 Molecular Locks: Thermal and Photoinduced Self-Assembly of Pt(II)-Linked Ring and Cage Structures

Fujita and co-workers have demonstrated that platinum(II)-py (pyridyl) "molecular locks" could be exploited towards the self-assembly of interlocked architectures with elevated temperatures in highly polar media.[63] The one way catenation of the platinum(II)-py containing ring, Pt(II)-**50**, was achieved with prolonged heating at 100 ºC in D_2O for 24 h in the presence of an excess of $NaNO_3$ to quantitatively afford Pt(II)-**51** (Scheme 1.24a). In the absence of salt and without heating the Pt(II)-py bond in Pt(II)-**50** was inert such that the structure is "locked." However, upon releasing the lock, using the specified reaction conditions (*vide supra*), equilibration between the Pt(II)-**50** and the catenated dimer Pt(II)-**51** was observed by ^{1}H NMR spectroscopy. Once, the self-assembly process was complete the system was cooled to ambient temperature and the excess sodium salt removed, effectively "locking" the [2]catenane structure (Scheme 1.24a). The interlocked nature of Pt(II)-**53** was unambiguously confirmed by X-ray crystallography. Twelve years after this initial report, the group of Fujita demonstrated that platinum(II)-py "molecular locks" were also photoresponsive.[64] The catenation of Pt(II)-**52** was achieved upon irradiation (330 ± 70 nm) for 15 min, in polar media, DMSO-d_6:D_2O 1:2, to quantitatively afford Pt(II)-**53** (Scheme 1.24b). For comparison, thermally induced catenation of Pt(II)-**52** required heating at 90 ºC in DMSO-d_6:D_2O 1:2 for several days to reach equilibration. In the absence of irradiation, once formed [2]catenane, Pt(II)-**53**, was

"locked" such that dissociation into the constituent rings did not occur. Kinetic studies of the catenation process of Pt(II)-**53** established that under non-irradiative conditions (simply with heating) the self-assembly process proceeds by an associative mechanism, however, upon the application of photochemical stimuli the mechanism switches from being associative (non-irradiative conditions) to dissociative (irradiative conditions).[64] This proposition was supported by time dependent-density function theory (TD-DFT) calculations undertaken by the authors on an analogue of Pt(II)-**52**. These established that the LUMO (lowest occupied molecular orbital) was a ^{1}MC state with significant σ-antibonding $d_{x^2-y^2}$ orbital character and furthermore identified an absorption band around 305 nm which could be ascribed to a HOMO-LUMO transition (where HOMO = highest occupied molecular orbital). Direct excitation into this dissociative (d-d*) state under irradiative conditions was proposed to result in dissociation (and hence labilization) of the coordinate platinum-py bond.

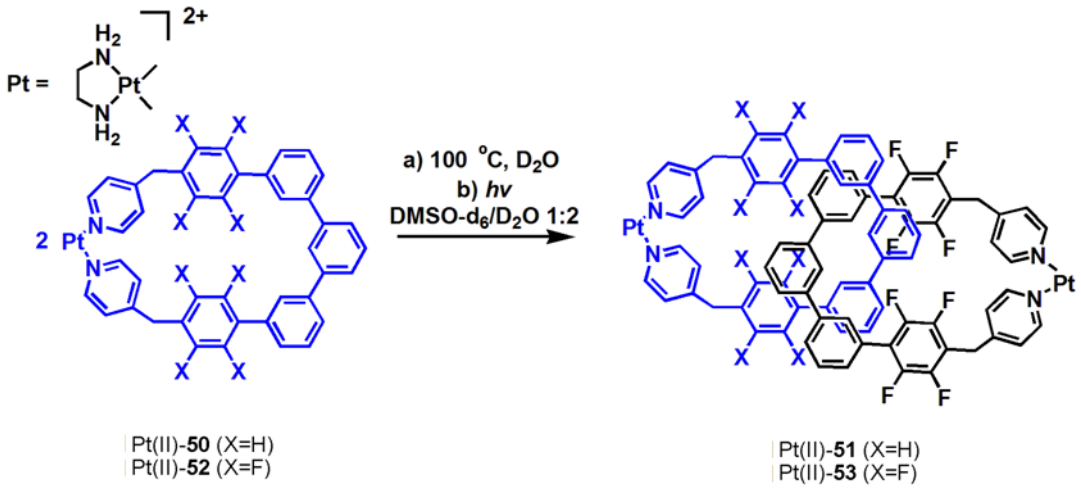

Scheme 1.24 One way catenation of the platinum(II) metallocycle, Pt(II)-**50** and Pt(II)-**52**, under irradiative and non-irradiative conditions gave [2]catenane Pt(II)-**51** and Pt(II)-**53** respectively.[63,64]

The "molecular lock" principle has also been employed under thermal[63] and photochemical[65] stimuli to self-assemble two and three-dimensional metallosupramolecular architectures. Prolonged heating of [Pt(en)]$(NO_3)_2$, (en = ethylenediamine), Pt(II)-**54**, and 4,4'-bipyridine, **55**, at 100 ºC in D_2O the presence of an excess of $NaNO_3$, afforded the tetranuclear Pt(II)-**56** in 50% yield. Initially

heating the two constituents, Pt(II)-**54** and **55**, generated an oligomeric mixture of products under kinetic control. However, over time ^{1}H NMR spectroscopy evidenced the self-assembly of the thermodynamically favourable molecular square, Pt(II)-**56**. In the absence of $NaNO_3$, the formation of Pt(II)-**56**, from the oligomeric mixture of kinetic products, was extremely slow requiring over a month of heating at 100 ºC.

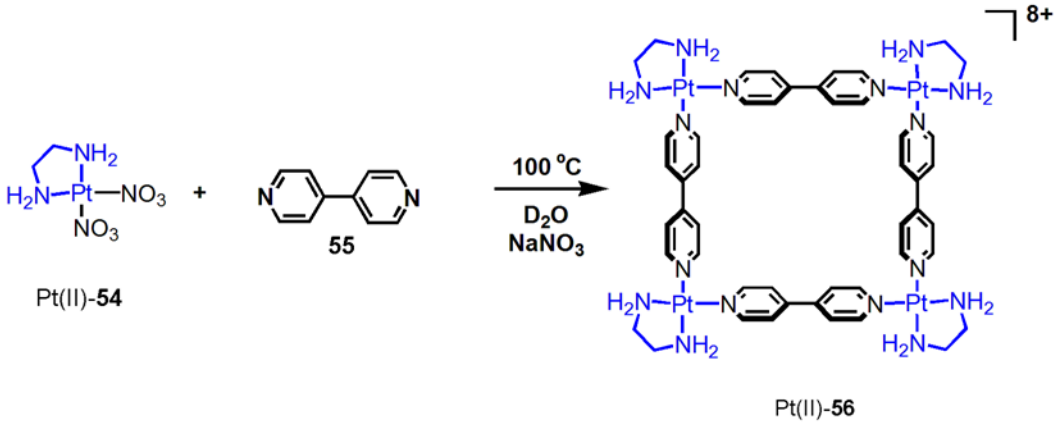

Scheme 1.25 Self-assembly of Pt(II)-**56** from Pt(II)-**54** and **55** with prolonged heating at 100 ºC in the presence of $NaNO_3$.[63]

In 2009, Fujita reported on the light-driven self-assembly of metallosupramolecular architectures *via* labilisation of a photoswitchable platinum(II)-py coordination bond (or "molecular lock").[65] Photoirradiation (330 ± 70 nm) of **57** and $[Pt(en)](NO_3)_2$, Pt(II)-**54**, in highly polar media, D_2O:1,4-dioxane-d_8 1:1, for 4 h at ambient temperature quantitatively afforded the bimetallic macrocycle Pt(II)-**58** (Scheme 1.26a)**.** The formation of Pt(II)-**58** was monitored over time by ^{1}H NMR spectroscopy. Under non-irradiative conditions and at ambient temperatures the metallocycle, Pt(II)-**58**, was not formed cleanly but upon heating at 80 ºC for several days the desired Pt(II)-py based ring structure was formed. The triangle species, Pt(II)-**59**, was assembled from $[Pt(en)](NO_3)_2$, Pt(II)-**54**, and **60** in 4 h at ambient temperature under irradiative conditions (330 ± 70 nm) in highly polar media, D_2O:1,4-dioxane-d_8 (1:1) (Scheme 1.26b). The molecular connectivity of Pt(II)-**59** was unambiguously proved by X-ray crystallography. DFT calculations undertaken on Pt(II)-**59** identified the LUMO as a ^{1}MC state with σ-antibonding $d_{x^2-y^2}$ orbital character (Figure 1.14). As previously described, the dissociative mechanism thought

to be operating under irradiative conditions was proposed to be facilitated by the promotion of electron density into this excited dissociative (d-d*) state.

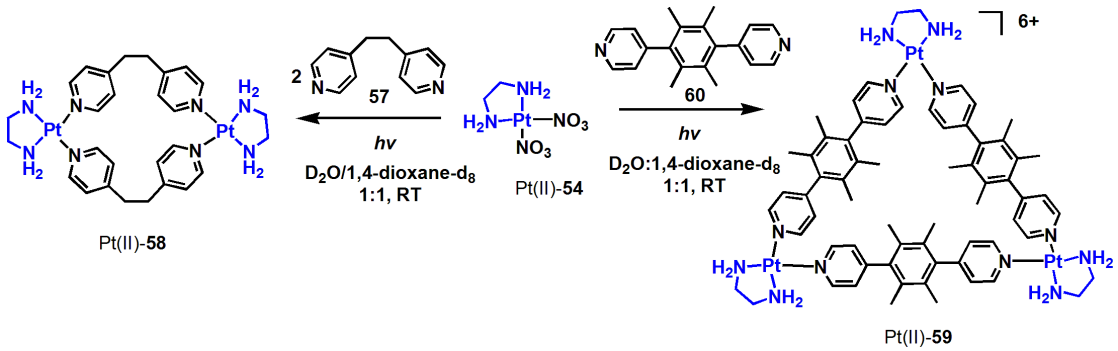

Scheme 1.26 Assembly of Pt(II)-**58** (from Pt(II)-**54** and **57**) and Pt(II)-**60** (from Pt(II)-**54** and **60**) using the photoswitchable molecular lock priniciple.[65]

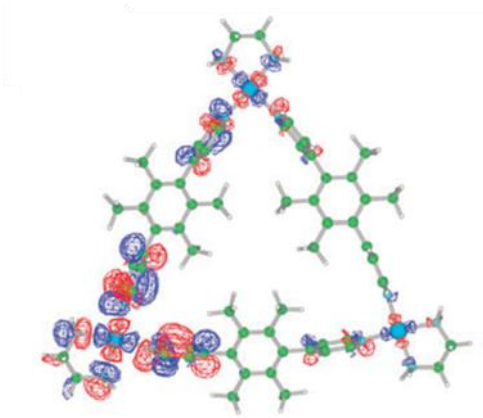

Figure 1.14 DFT calculations undertaken on Pt(II)-**61** identified the LUMO as a ^{1}MC state with σ-antibonding $d_{x^2-y^2}$ orbital character. Reproduced from reference 65.

The molecular cage, Pt(II)-**61**, with M_6L_4 stiochiometry,[66] was self-assembled under irradiative conditions using the photoswitchable "molecular lock" principle (Scheme 1.27).[65] Photoirradiation of a mixture of six equivalents of [Pt(en)]$(NO_3)_2$, Pt(II)-**54**, and the four equivalents of tridentate ligand, **62**, in D_2O:1,4-dioxane-d_8 1:1 for 2 h at ambient temperature afforded the molecular cage complex. The formation of Pt(II)-**61** was evidenced by both ^{1}H NMR spectroscopy and mass spectrometry.

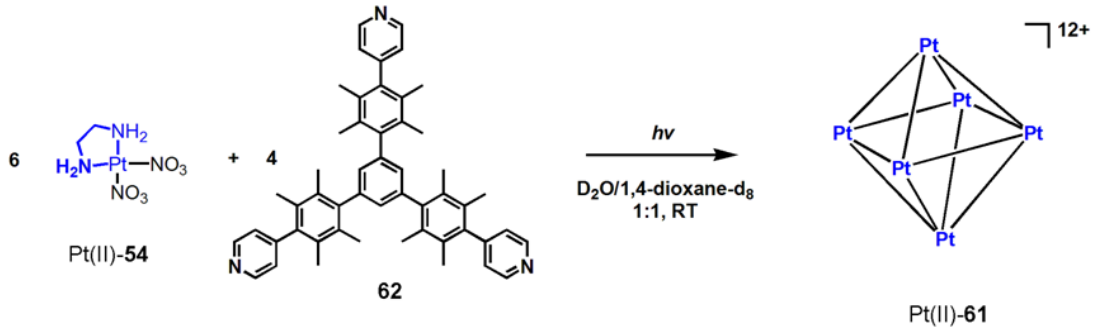

Scheme 1.27 Self-assembly of Pt(II)-**61** from Pt(II)-**54** and **62** under irradiative conditions.[64]

1.8 Kinesin: Natural Molecular Machine

Since its discovery in 1985,[67] kinesin has been one of the most extensively studied of the molecular motor proteins. Kinesin, is essential for the intracellular transport of organelles and membrane-bound vesicles.[68,69] The unidirectional processive manner by which kinesin moves large cargoes by walking along microtubule profilaments has long been admired.[70] Interlocked architectures form the basis for virtually all artificial molecular machines capable of exhibiting translational motion to date. Kinesin, however, serves to illustrate how Nature has efficiently overcome the need for interlocked architectures to effectively demonstrate linear motion at the molecular level.

1.8.1 Kinesin and Microtubule Structure

Prototypical kinesin (kinesin-1) is comprised of two chains each consisting of 960 identical amino acids which dimerise to form the coiled stalk (sometimes referred to as the rod) (Figure 1.15a).[71-74] The three structural constituents are the motor, neck and tail domains. The motor domain consists of two identical globular heads which each contain nucleotide (microtubule) binding sites and catalytically active ATPase for the hydrolysis of ATP.[75] The neck domain, also known as the linker domain, is vital for the connection of the motor domains. The flexibility of the linker domain additionally allows motor stepping to occur by regulating the internal strain of the system such that it can negotiate walking along microtubules even in high load states. The tail domain is responsible for attaching (and detaching) the appropriate

cargo. The microtubule and cargo binding sites, the motor and tail domains respectively, are associated at opposite ends of the coiled stalk (Figure 1.15b).

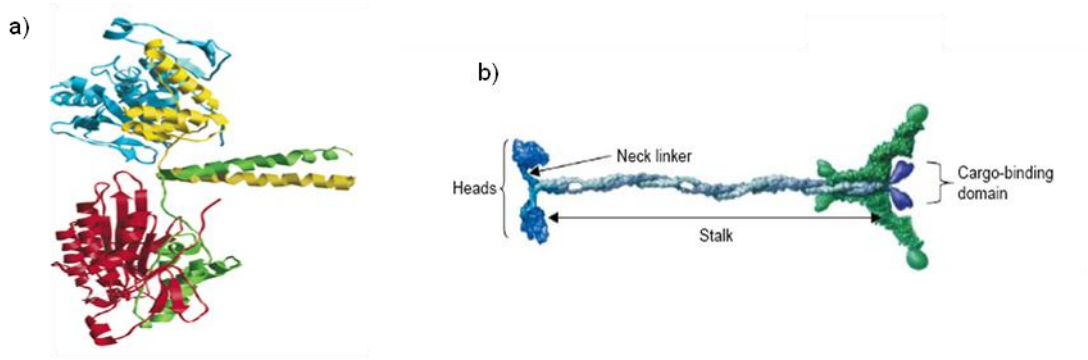

Figure 1.15 Crystal structure of conventional kinesin(I) and schematic representation of dimeric rat kinesin. a) reproduced from reference 73, b) reproduced from reference 74.

Microtubules are comprised of arrays of linearly self assembled, head-to-tail protein sub-unit dimers, α and β tubulin, which form a protofilament. The association of several protofilaments gives rise to the formation of a sheet which when closed generates the cylindrical microtubule upon which kinesin can bind. Microtubules are hollow assemblies which have a diameter of 24 nm and an 8 nm repetitive structural unit brought about from its composition from tubulin heterodimers (Figure 1.16).

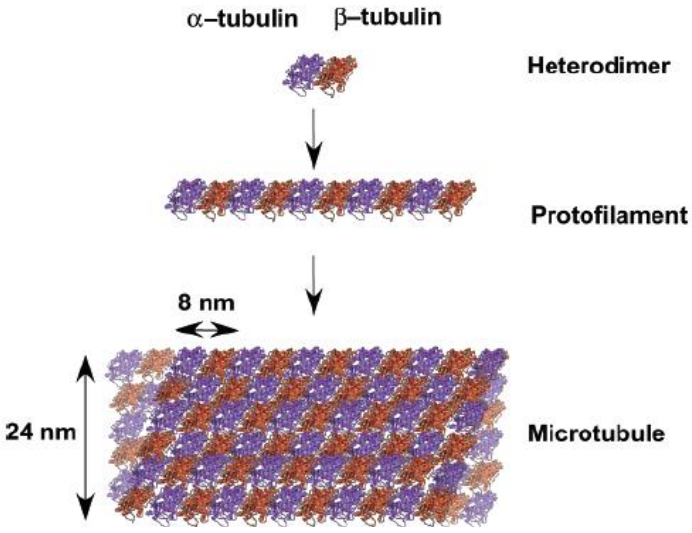

Figure 1.16 Representation of microtubule constituents; α and β tubulin, which form a protofilament. This then gives rise to the formation of a sheet which when closed generates the cylindrical microtubule structure. Reproduced from reference 73.

Microtubules possess inherent polarity as a result of the way in which their constituent proteins, α and β tubulin, associate. More specifically, each end of the microtubule polymer has a different heterodimer exposed. This has led to the development of the terminology for the system of 'plus' and 'minus' ends where the former refers to a β-tubulin terminus and the latter a α-tubulin. This inbuilt polarity plays a vital role in establishing control over the directionality of the intracellular cargo transport as it forms the basis for the organisation (and classification) of the kinesin enzymes in the "kinesin superfamily proteins."[70] Specifically, different kinesin species are known to walk to different ends of the microtubule track. Conventional kinesin (kinesin-1) is known to drive motion to the "plus" terminus of microtubule towards the cell periphery.[76]

1.8.2 The Motion of Kinesin

Kinesin is known to move in a stepwise manner along the microtubule profilament axis[72] with high fidelity in 8 nm increments[77-79] hydrolysing one molecule of ATP per step.[81] The distance of each stepwise advancement is equivalent to the distance between adjacent tubulins so for each step kinesin traverses one tubulin heterodimer. The motion is highly processive, with kinesin being able to take hundreds of steps before dissociation from the microtubule track,[71,80,81] even against loads of several piconewtons.[82,83] This has implications towards the mode of action of kinesin, suggesting that the twin globular heads of kinesin don't act independently of one another but rather act in a coordinated manner to ensure that at least one of the heads of motor domain is bound to the microtubule profilament at all times.[84,85]

The mechanism of kinesin's motility has been extensively studied.[86] The two stepping models which hold the greatest potential to describing its motion are the "inchworm" and "hand-over-hand" mechanisms. The major difference between these two mechanisms is that of head equivalence of the motor domains. In the "inchworm" model, head inequivalency was assumed with the postulation of one catalytically active head and one passive head; the forwards head, which is responsible for ATP binding and hydrolysis, always advances by an 8 nm steps subsequently followed by an 8 nm step by the trailing head. In contrast, in the "hand-

over-hand" mechanism head equivalency is assumed (Section 1.7.3). The homodimeric structure of kinesin,[87] lends great weight to the supposition of head equivalency. Currently, an asymmetric version of the "hand-over-hand" mechanism stands as the most widely accepted model to explain the processive nature by which conventional kinesin transports cargos intracelluarly.[88,89]

1.8.3 Asymmetric "Hand-Over-Hand" Mechanism

In this model the protein returns to its original three-dimensional conformation only after two complete steps. Each alternate step taken by the globular head is distinct. The two identical motor domains take alternative steps forwards with the trailing head moving successively from the left to right hand side of the coiled stalk (Figure 1.16).[74,90] The neck linker is key to reducing the strain in the system; wrapping itself around the chain during the first step and unwinding during the second step. The linker domain is also integral for the processivity and unidirectionality of the motility of kinesin. The catalytic cycle for the hydrolysis of ATP by the motor domain of kinesin is "gated" so that one head is always tightly bound to the microtubule. "Gating" is thought to be achieved by communication of the respective enzymatic state of each individual motor domain system between partner heads by relaying information about the internal strain of the system through the neck linker.[91,92]

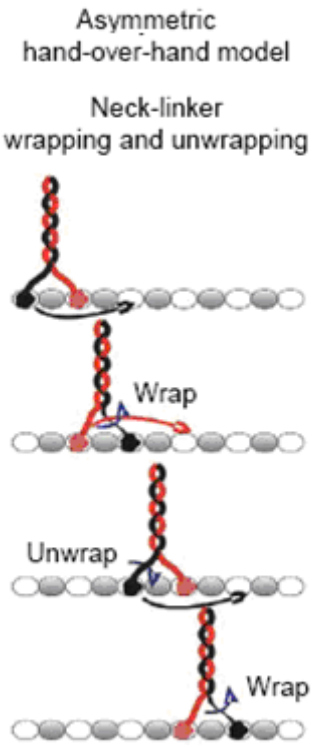

Figure 1.16 Schematic representation of two steps undertaken by kinesin using the asymmetric "hand-over-hand" mechanism. Reproduced from reference 73.

1.9 DNA-Based Molecular Walkers

In 2004, three independent research groups reported a major breakthrough in the field of DNA nanomachines. Each group described the synthesis and operation of unique DNA-based bipedal molecular walkers capable of demonstrating unidirectional, processive translational motion.[93-97]

The first report was published by Seeman and co-workers.[93] The mode of action of the DNA-based walker was reminiscent of the "inchworm" mechanism. One walker leg always advanced forwards whilst the second leg constantly trailed behind (Scheme 1.28). The bipedal walker unit was comprised of two double stranded helices termed legs (labelled black regions) from each of which protruded a single strand sequence (foot) (purple and orange regions). The legs of the walker unit were linked by three flexible linkers which were comprised of nine nucleotide linker strands of DNA. Three anchorages (footholds) (red, green and blue regions) were incorporated into the track. These footholds consisted of single-stranded

oligonucleotide sequences and protruded from the rigid backbone at regular spaced intervals and situated at the end of each foothold was an eight-base single strand overhang termed a toehold (pink region). Motion of the walker unit along the track was achieved through sequential addition of specific attachment/detachment fuel strands which could selectively initiate competitive hybridization between the toehold of a specific foothold and foot of the walker fragment. Initially, both feet of the biped are attached to the track, at the footholds A and B (Scheme 1.28a). Release of the front foot (orange region) from foothold B (green region) is achieved upon treatment with an unset detachment fuel strand whose sequence is complimentary to the leg of the front foot and the second foothold (Scheme 1.28b). Competitive hybridization is initiated at the toehold position of the second foothold. Upon its release, the front foot is still indirectly connected to the rigid backbone by means of the three flexible linkers but was also able to advance towards the third anchorage site. The leading foot is anchored to the third foothold (Scheme 1.28c) through addition of an attachment set strand which sequence is complimentary to the advancing leg (orange region) and the third foothold (blue region). The trailing leg (purple region) is then subjected to same sequential addition of appropriately sequenced detachment (Scheme 1.28d) and attachment (Scheme 1.28e) set fuel strands. As such, motion of the trailing leg from the first foothold (red region) to the newly vacated, second, foothold position is achieved (Scheme 1.28d→e). Over this four step procedure the total distance travelled by the walker unit in the biped relative to the track was 2 nm (*cf* the 8 nm steps undertaken by kinesin).

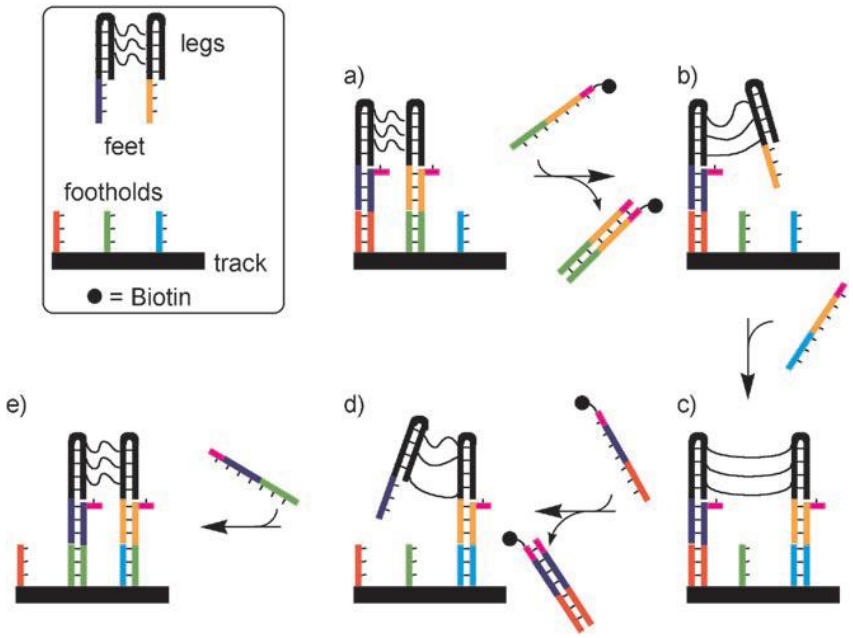

Scheme 1.28 Schematic representation of the processive motion of the walker unit in the bipedal DNA-based walker by Seeman and co-workers which is reminiscent of the "inchworm" mechanism. Reproduced from reference 4b.

In collaborative work between the groups of Pierce and Shin a non-autonomous DNA molecular walker, which mimicked the asymmetric "hand-over-hand" (or "passing-leg") mechanism was synthesised.[94] Unidirectional translational motion of the walker unit (labelled black region) was induced in the system again through the sequential addition of appropriate attachment and detachment fuel strands (Scheme 1.29). The walker unit consisted of two partially complimentary oligonucleotides which formed a twenty base pair (bp) helix. From this structure, protruded two single-stranded feet each consisting of twenty-three bases. The track was comprised of six oligonucleotides from which four regularly spaced single-stranded twenty base branches "footholds" (coloured red, green blue and yellow regions) extended out. The walker unit is bound to the track at the two first two footholds with both feet anchored (Scheme 1.29a). The addition of a detachment fuel strand, which is complimentary to the trailing leg (purple region), causes its liberation from the first foothold (Scheme 1.29b). In this state, the walker is directly bound to the track exclusively by the leading foot. The trailing leg is able to advance towards the third anchorage (yellow region). Treatment with a specific attachment fuel strand initiates

competitive hybridisation between the trailing foot (purple region) and the third foothold (yellow region). In this state, the walker unit is once again bound to the track by two feet (Scheme 1.29c). In a similar manner, the walker fragment progresses along the track to the fourth foothold through the sequential addition of appropriate attachment and detachment strands (Scheme 1.29d→e).

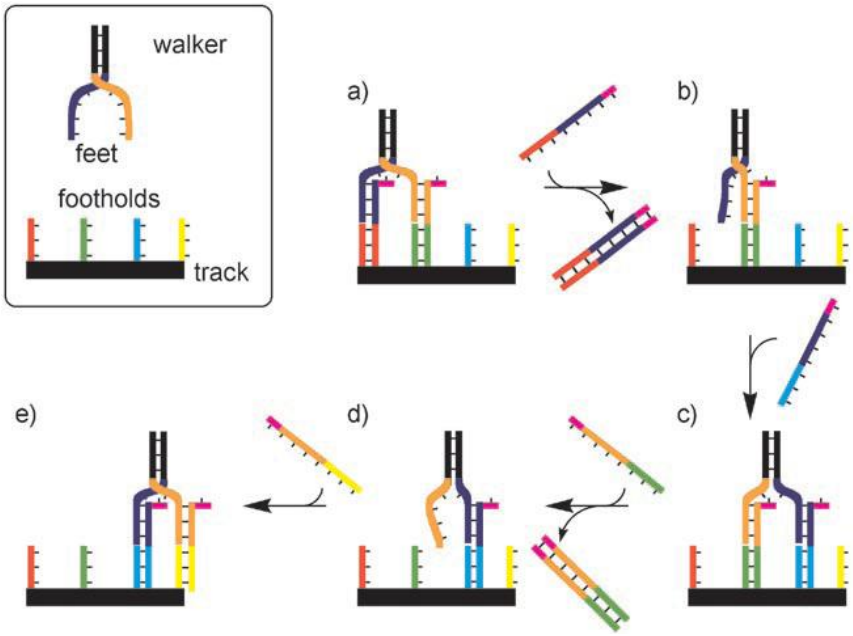

Scheme 1.29 Schematic representation of the processive motion of the walker unit in the bipedal DNA-based walker by the groups of Pierce and Shin which is reminiscent of the "hand-over-hand" mechanism. Reproduced from reference 4b.

The groups of Turberfield, Reif and Yan published an autonomous, unidirectional, DNA-walker.[95] The walker unit (red region) consisted of a six-nucleotide DNA sequence which processed along the track through binding to three distinct anchorages (footholds A, B and C) on the track (Scheme 1.30). Initially, the walker is covalently bound to the first anchorage (A*) (Scheme 1.30a). Competitive hybridisation between the complimentary three base nucleotide single strand overhang on the walker and the second foot causes its motion towards the adjacent site (A* + B) (Scheme 2.30b). The flexible four-nucleotide hinge unit incorporated into the "foothold" is fundamental in permitting the degrees of freedom required to form A* + B. The formation of the A* + B species provides a substrate for enzyme T4 ligase and resultant covalently linking of the two anchorages *via* the walker

fragment to generate A*B is achieved (Scheme 1.30b). This ligating step is irreversible. The newly formed helix is cleaved by the restriction enzyme (PfM 1) (Scheme 1.30c) in such a manner that the walker is selectively transferred onto the second anchorage (Scheme 1.30d). In a similar fashion, motion of the walker fragment between the second and third anchorages (B* → C) is accomplished. The action of enzyme T4 ligase on the newly created helix (B* + C) (Scheme 1.30e) forms the covalently attached state B*C (Scheme 1.30f) which provides a substrate for a second distinct restriction endonuclease (BstAP 1). Cleavage of B*C resulted in advancement of the walker unit onto the third anchorage (Scheme 1.30g). The processive motion of this DNA-based walker is reportedly autonomous but for thoroughness the authors additionally demonstrated that it could operate in a stepwise manner through the sequential addition of the enzyme T4 ligase and the appropriate restriction endonucleases.

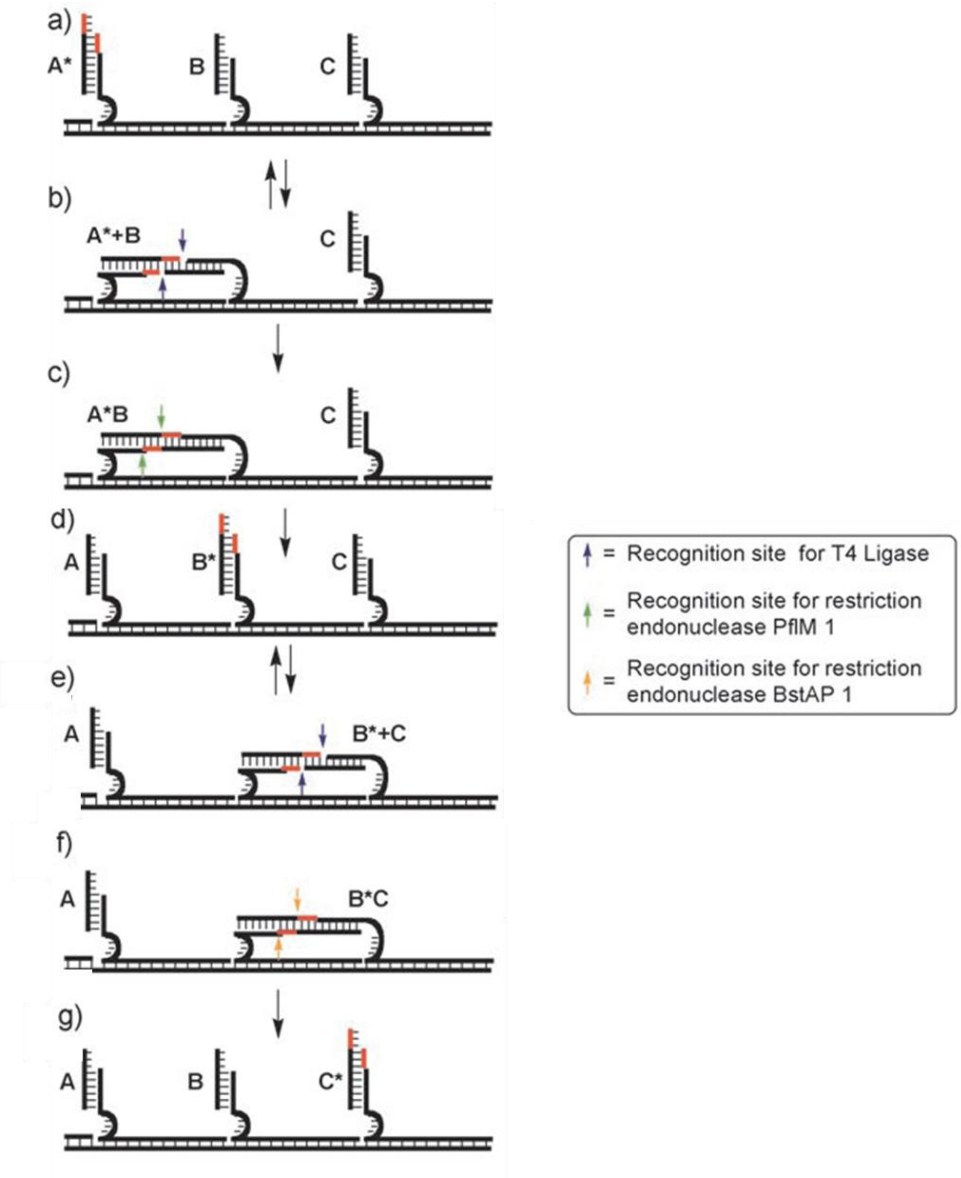

Scheme 1.30 Schematic representation of the processive motion of the walker unit in the bipedal DNA-based walker by the groups of Turberfield, Reif and Yan. Reproduced from reference 4b.

1.10 Molecular Walkers: Dynamic Covalent Chemistry Approach

In 2010, the Leigh group reported on the operation of a small molecule that walks down a linear track in a "passing-leg" gait using a dynamic covalent chemistry (DCC) approach.[98-100] A two-legged molecular walker (red region) was translated along a four-foothold (green and blue regions) track in response to sequential

treatment with acid and base (Scheme 1.31). Exploitation of orthogonally controlled, reversible, covalent bond formation of disulfide and hydrazone bonds between the foot and track units ensured the processivity of the system. As such, the track-binding interactions of the two feet of the walker unit were labile under different conditions. Initially, the two feet of the walker are bound to the first two footholds of the track. Under acidic conditions, the disulfide bond between the front leg of the walker unit and the track kinetically "locks" this leg in position. Meanwhile, the hydrazone group linking the trailing leg and track is labile permitting its advancement towards the third foothold through dynamic exchange. Reversal of the kinetic stabilities of the foot-track interactions (the disulfide and hydrazone moieties) was achieved upon treatment of the system with base. As a result, the now trailing leg is able to advance forwards towards the fourth foothold whilst the foot at the third position is kinetically locked into place. The motion was studied using ^{1}H NMR spectroscopy and high purity liquid chromatography (HPLC).

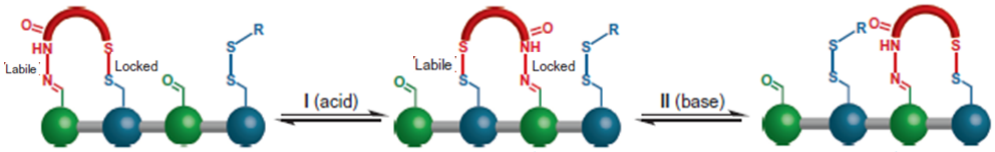

Scheme 1.31 Schematic representation of a DCC-based approach for the processive translational motion of a small molecular along a four foothold track upon sequential treatment with of acid and base. Scheme reproduced from reference 98.

Following on from this pioneering work, the Leigh group reported on the light-driven transport of a molecular walker which could also reversibly translate along a track.[102] The incorporation of a stilbene unit between the second and third footholds permitted the photochemical induction of *cis-trans* isomerisation of the photoactive group to bring about a significant conformational change in the structure. As such, control over the relative position of the second and third footholds (in close promixity in *cis* conformation or with larger spatial separation in *trans* isomer) could be realised through photoisomerisation of this central double bond unit. When exploited, in conjunction with the acid-based induce reverse foot-migration

processes, remarkable directional bias of the small walker molecule along the track was accomplished.

1.11 Work Presented in This Thesis

At present artificial molecular machines that are capable of exhibiting progressive linear motion are principally, but not exclusively, based on rotaxane-based systems wherein physical interlocking of the molecular sub-components is required. As a consequence of the presence of the mechanical bond the motion is restricted to one dimension. The work presented in Chapter Two of this Thesis addresses the synthesis of non-interlocked molecular machines which display processive translational motion of the sub-components. A square planar d^8 platinum(II)-phenanthroline component is driven along different ligating architectures through exploitation of a series of intramolecular metal-ligand substitution reactions (metallotrophic shifts). Determination of the kinetic parameters of the shuttling processes has been achieved using a series of VT NMR experiments.

Chapter Three presents model studies on a platinum(II)-based motif in which dual control over the kinetics and thermodynamics of a reversible binding event at the metal centre is achieved using pH and light stimuli. This novel, interconvertable, heteroleptic platinum coordination mode should ultimately provide a means to accessing interlocked molecular machines which are of a more sophisticated nature than most existing systems, wherein both the kinetics and thermodynamics of a stimuli-responsive switchable event can be orthogonally controlled.

Few examples of stimuli-responsive reversible switching between metallosupramolecular assemblies in solution are described in the literature. Chapter Four describes the exploitation of the discovered interconvertable platinum(II) coordination mode, as a novel method towards the proton-driven self-assembly and disassembly of two and three dimensional metallosupramolecular architectures in the presence of suitable exotopic ligands.

Whilst reversible metal-ligand motifs have been extensively employed to induce molecular switching in interlocked architectures, namely catenanes and rotaxanes,

there are few reports of systems which exploit a change in the coordination mode of the metal centre to achieve molecular motion. Chapter Five details an investigation of the exploitation of the reversible metal-ligand motif to induce controlled exchange between “3+1” and “2+2” square planar platinum donor sets in response to the application of acid-base stimuli.

1.12 References and Notes

[1] For discussion of the motor protein kinesin which is responsible for the intracellular transport of organelles see: (a) M. C. Alonso, D. R. Drummond, S. Kain, J. Hoeng, L. Amos, R. A. Cross; *Science,* 2007, **316**, 120; (b) C. L. Asbury; *Curr. Opin. Cell. Bio.*, 2005, **17**, 89; (c) K. Svoboda, C. F. Schmidt, B. J. Schnapp, S. M. Block; *Nature,* 1993, **365**, 721; (d) R. D. Vale, T. S. Reese, M. P. Sheetz; *Cell*, 1985, **42**, 39.

[2] For a recent report on the motor protein dynein which is responsible for intracellular transport see: S. Toba, T. M. Watanabe, L. Yamaguchi-Okimoto, Y. Y. Toyoshima, H. Higuchi, *Proc. Natl. Acad. Sci. USA* **2006**, *103*, 5741.

[3] For a review on molecular machines see: V. Balzani, M. Gómez-Lopez, J. F. Stoddart, *Acc. Chem. Res.,* 1998, **31**, 405; (b) E. R. Kay, D. A. Leigh, F. Zerbetto, *Angew. Chem. Int. Ed.*, 2007, **46**, 72.

[4] H. L. Frisch, E. Wasserman, *J. Am. Chem. Soc.*, 1961, **83**, 3789.

[5] I. T. Harrison, S. Harrison, *J. Am. Chem. Soc.,* 1967, **89**, 5723.

[6] P. L. Anelli, N. Spencer, J. F. Stoddart, *J. Am. Chem. Soc.*, 1991, **113**, 5131.

[7] The electrochemically-driven translocation of the tetracationic macrocycle between the two recoginition sites in bistable [2]rotaxane, **3**, is also described in this report: R. A. Bissell, E. Cordova, A. E. Kaifer, J. F. Stoddart, *Nature*, 1994, **369**, 133.

[8] H. Kurakami, A. Kawabuchi, K. Kotoo, M. Kunitake, N. Nakashima, *J. Am. Chem. Soc.*, 1997, **119**, 7605.

[9] For a more recent example of the use of a hydrophobic effect and CD rings and organic threads to construct [2]rotaxanes see: H. Murakami, A. Kawabuchi, R. Matsumoto, T. Ido, N. Nakashima, *J. Am. Chem. Soc.,* 2005, **127**, 15891.

[10] For an example of H-bonded molecular shuttle in which fast, reversible translational motion is realised through photoinduction see: (a) A. M. Brouwer, C. Frochot, F. G. Gatti, D. A. Leigh, L. Mottier, F. Paolucci, S. Roffia, G. W. Wurpel, *Science*, 2001, **291**, 2124.

[11] A. Altieri, G. Bottari, F. Dehez, D. A. Leigh, J. K. Y. Wong, F. Zerbetto, *Angew. Chem. Int. Ed.*, 2003, **42**, 2296.

[12] C. O. Dietrich-Buchecker, J. –P Sauvage, J. P. Kintzinger, *Tetrahedron Lett.*, 1983, **124**, 5095.

[13] C. O. Dietrich-Buchecker, J. –P Sauvage, J. –M. Kern, *J. Am. Chem. Soc.*, 1984, **106**, 3043.

[14] C. Wu, P. R. Lecavalier, Y. X. Shen, H. W. Gibson, *Chem. Mater.*, 1991, **3**, 569.

[15] (a) J. –C. Chambron, V. Heitz, J. –P. Sauvage, *J. Chem. Soc., Chem. Comm.*, 1992, 1131; (b) M. –J. Blanco, J. –C. Chambron, V. Heitz, J. –P. Sauvage, *Org. Lett.*, 2000, **2**, 3051; (c) M. Linke, J. –C. Chambron, V. Heitz, J. –P Sauvage, *J. Am. Chem. Soc.*, **119**, 11329.

[16] (a) J. –P. Sauvage, *Chem. Comm.*, 2005, 1507. (b) J. –P. Collin, A. C. Laemmel, J. –P. Sauvage, *New J. Chem.*, 2001, **25**, 22; (c) A. –C. Laemmel, J. –P. Collin, J. –P. Sauvage, G. Accorsi, N. Armaroli, *Eur. J. Inorg. Chem.*, 2003, 467; (d) S. Bonnet, J. –P. Collin, J. –P. Sauvage, *Inorg. Chem.*, 2007, **46**, 10520.

[17] A. Livoreil, J. –P. Sauvage, N. Armaroli, V. Balzani, L. Flamigni, B. Ventura, *J. Am. Chem. Soc.*, 1997, **119**, 12114.

[18] (a) N. Armaroli, V. Balzani, J. –P Sauvage, *J. Am. Chem. Soc.*, 1999, **121**, 4397. For the initial report on the synthesis of Cu-**17** see: (b) P. Gaviña, J. –P Sauvage, *Tetrahedron Lett.*, 1997, **38**, 3521. For other examples of stimuli-responsive Cu(I)/Cu(II) interlocked systems which exhibit metastable states see: (c) A. Livoreil, C. O. Dietrich-Buchecker, J. –P. Sauvage, *J. Am. Chem.*

Soc., 1994, **116**, 9399 ; (d) D. Cardenas, A. Livoreil and J. –P. Sauvage, *J. Am. Chem. Soc.*, 1996, **118**, 11980; (e) N. Weber, C. Hamann, J. –M. Kern and J. –P. Sauvage, *Inorg. Chem.*, 2003, **42**, 6780; (f) N. Armaroli, V. Balzani, J. –P. Collin, P. Gavina and J. –P. Sauvage, *Angew. Chem. Int. Ed.*, 2007, **121**, 4397. For reviews of transitions metal-ligand complexed molecular machines; (g) J. –P. Collin, V. Heitz and J. –P. Sauvage, *Top. Curr. Chem.*, 2005, **262**, 29. (h) S. Bonnet, J. –P. Collin, M. Koizumi, P. Mobian and J. –P. Sauvage, *Adv. Mat.*, 2006, **18**, 1239.

[19] (a) U. Letinois-Hanss, J. M. Beierle, J. –P. Collin, J. –P. Sauvage, *Org. Lett.*, 2005, **7**, 5753. For a preliminary account of electrochemically induced pirouetting motion of a phen- and terpy-containing ring about a phen-based axle see: (b) L. Raehm, J. M. Kern, J. –P. Sauvage, *Chem. Eur. J.*, 1999, **5**, 3310; For a recent example of the implementation of redox-responsive Cu(I)/Cu(II) motif in [2]rotaxanes towards the construction of set-reset molecular logic gate see: (c) G. Peryasamy, J. –P Collin, J. –P Sauvage, R. D. Levine, F. Remacle, *Chem. Eur. J.*, 2009, **15**, 1310.

[20] (a) F. Durola, J. Lux, J. –P. Sauvage, *Chem. Eur.- J.*, 2009, **15**, 4124; (b) J. –P. Collin, F. Durola, J. Lux, J. –P. Sauvage, *New J. Chem.*, 2010, **34**, 34. For a preliminary account of the electrochemical and dynamic properties of the biisoquinoline-copper-based [2]rotaxane see: (c) F. Durola, J. –P. Sauvage, *Angew. Chem.*, 2007, **119**, 3607; *Angew. Chem. Int. Ed.*, 2007, **46**, 3537.

[21] For an example of the incorporation of bulky groups to prevent rotation of the rings in the metal free state see: C. O. Dietrich-Buchecker, J. –P. Sauvage, J. Weiss, *Tetrahedron Lett.*, 1986, **27**, 2257.

[22] M. Cesario, C. O. Dietrich-Buchecker, J. Guilhem, C. Pascard, J. –P. Sauvage, *J. Chem. Soc., Chem. Comm.*, 1985, 244.

[23] A. –M. Albrecht-Gary, Z. Saad, C. O. Dietrich-Buchecker, J. –P Sauvage, *J. Am. Chem. Soc.*, 1985, **107**, 3205.

[24] J. –P. Sauvage, M. Ward, *Inorg. Chem.*, 1991, **30**, 3869.

[25] P. Mobian, J. –M. Kern, J. –P. Sauvage, *J. Am. Chem. Soc.*, 2003, **125**, 2016.

[26] P. Mobian, J. –M. Kern, J. –P. Sauvage, *Angew. Chem. Int. Ed.*, 2004, **43**, 2392.

[27] (a) D. Pomeranc, D. Jouvenot, J. –C. Chambron, J. –P. Collin, V. Heitz, J. –P. Sauvage, *Chem. Eur. J.*, 2003, **9**, 4247. For a preliminary account of the coordination of substituted bipy based ligands and *bis*-phen containing macrocycles to an octahedral ruthenium(II) template see: (b) D. Pomeranc, V. Heitz, J. –C. Chambron, J. –P. Sauvage, *J. Am. Chem. Soc.*, 2001, **123**, 12215.

[28] (a) J. –P. Collin, D. Jouvenor, M. Koizumi, J. –P. Sauvage, *Eur. J. Inorg. Chem.*, 2005, 1850. (b) For an account of the synthesis of triarylmethyl derivatized stopper groups for use in rotaxane architectures see: (a) H. W. Gibson, S. –H. Lee, P. T. Engen, P. Lecavalier J. Sze, Y. X. Shen, M. Bheda, *J. Org. Chem.*, 1993, **58**, 3748.

[29] For a recent example of the preparation of catenanes about Fe(II) and Ru(II) transition metal templates see: J. C. Loren, P. Gantzel, A. Linden, J. S. Siegel, *Org. Biomol. Chem.*, 2005, **3**, 3105.

[30] For a recent example of the assembly of a series of [2]catenanes using a wide variety of divalent transition metal templates as described but additionally through a thermodynamic approach, with reversible imine bond formation between amine and diformylpyridine constitutents, in the presence of the metal salt see: D. A. Leigh, P. J. Lusby, S. J. Teat, A. J. Wilson, J. K. Y. Wong, *Angew. Chem. Int. Ed.*, 2001, **40**, 1538.

[31] For an example of the construction of [2]rotaxanes using reversible bond formation between constitutents in the presence of a metal salt as in ref 30 see: L Hogg, D. A. Leigh, P. J. Lusby, A. Morelli, S. Parsons, J. K. Y. Wong, *Angew. Chem. Int. Ed.*, 2004, **43**, 1218.

[32] C. Hamann, J. –M. Kern, J. –P. Sauvage, *Dalton Trans.*, 2003, 3770.

[33] A. –M. Fuller, D. A. Leigh, P. J. Lusby, D. H. Oswald, S. Parsons, D. B. Walker, *Angew. Chem. Int. Ed.*, 2004, **43**, 3914

[34] A. –M. Fuller, D. A. Leigh, P. J. Lusby, A. M. Z. Slawin, D. B. Walker, *J. Am. Chem. Soc.*, 2005, **127**, 12612.

[35] A. –M. Fuller, D. A. Leigh, P. J. Lusby, *Angew. Chem. Int. Ed.*, 2007, **46**, 5015.

[36] J. D. Crowley, D. A. Leigh, P. J. Lusby, R. T. McBurney, L-E. Perret-Aebi, C. Petzold, A. M. Z. Slawin, M. D. Symes, *J. Am. Chem. Soc.* **2007**, *129*, 15085.

[37] The prefix PyH and $PyNMe_2$ refers to the station at which the macrocycle is bound.

[38] D. A. Leigh, P. J. Lusby, R. T. McBurney, M. D. Symes, *Chem. Comm.* **2010**, *46*, 2382.

[39] M. J. Barrell, D. A. Leigh, P. J. Lusby, A. M. Z. Slawin, *Angew. Chem. Int. Ed.*, 2008, **47**, 8036.

[40] For some recent examples of the CuAAC reaction see; (a) M. A. White, J. A. Johnson, J. T. Koberstein, N. J. Turro, *J. Am. Chem. Soc.*, 2006, **128**, 11356; (b) B. Helms, J.L. Mynar, C. J. Hawker, J. M. Frechet, *J. Am. Chem. Soc.*, 2004, **126**, 15020; (c) P. Wu, M. Malkoch, J. N. Hunt, R. Vestberg, E. Kaltgrad, M. G. Finn, V. V. Fokin, K. B. Sharpless, C. J. Hawker, *Chem. Comm.* 2005, 5775.

[41] For the first example of the use of the "active" metal templating strategy towards the construction of [2]rotaxanes see: (a)V. Aucagne, K. D. Hänni, D. A. Leigh, P. J. Lusby, D. B. Walker, *J. Am. Chem. Soc.*, 2006, **128**, 2186. For a recent review on active metal template synthesis of rotaxanes, catenanes and molecular shuttles see: (b) J. D. Crowley, S. M. Goldup, A. –L Lee, D. A. Leigh, R. T. McBurney, *Chem. Rev. Soc.*, 2009, **38**, 1530; For a recent

review on the application of the CuAAC reaction for the construction of rotaxane and catenane structures see: (c) K. D. Hänni, D. A. Leigh, *Chem. Soc. Rev.,* 2010, **39**, 1240. For a recent example of the use of the CuAAC reaction to construct [2]catenanes see: (d) S. M. Goldup, D. A. Leigh, T. Long, P. McGonigal, M. D. Symes, J. Wu, *J. Am. Chem. Soc.,* 2009, **131**, 15924.

[42] V. Aucagne, J. Berná, J. D. Crowley, S. M. Goldup, K. D. Hänni, D. A. Leigh, P. J. Lusby, V. E. Ronaldson, A. M. Z. Slawin, A. Viterisi, D. B. Walker, *J. Am. Chem. Soc.,* 2007, **129**, 11950.

[43] (a) S. Saito, E. Takahashi, K. Nakazono, *Org. Lett.,* 2006, **8**, 5133; (b) J. Berná, S. M. Goldup, A.-L. Lee, D. A. Leigh, M. D. Symes, G. Teobaldi, F. Zerbetto, *Angew. Chem.* 2008, **120,** 4464; *Angew. Chem. Int. Ed.* 2008, **47**, 4392. For a recent example of the use of the CuAAC reaction to form [3]rotaxanes wherein two axles are threaded using a single template site see: (c) S. M. Goldup, D. A. Leigh, P. R. Mc Gonigal, V. E. Ronaldson, A. M. Z. Slawin, *J. Am. Chem. Soc.,* 2010, **132**, 315. For a report on nickel-copper mediated alkyne homocoupling reactions for the synthesis of [2]rotaxanes see: (d) J. D. Crowley, S. M. Goldup, N. D. Gowans, D. A. Leigh, V. E. Ronaldson, A. M. Z. Slawin, *J. Am. Chem. Soc.,* 2010, **132**, 6243.

[44] (a) J. Berná, J. D. Crowley, S. M. Goldup, K. D. Hänni, A.-L. Lee, D. A. Leigh, *Angew. Chem.* 2007, **119**, 5811; *Angew. Chem. Int. Ed.* 2007, **46**, 5709; (b) J. D. Crowley, K. D. Hänni, A.-L. Lee, D. A. Leigh, *J. Am. Chem. Soc.* 2007, **129**, 12092; (c) S. M. Goldup, D. A. Leigh, P. J. Lusby, R. T. McBurney, A. M. Z. Slawin, *Angew. Chem.* 2008, **120**, 3429; *Angew. Chem. Int. Ed.* 2008, **47**, 3381.

[45] For a recent review on light powered molecular machines see: (a) M. Clemente-León, F. Marchioni, S. Silvi, A. Credi, *Synthetic Metals,* 2003, **139**, 773. For a recent review on Ru(II)-based light powered molecular machines see: (b) S. Bonnet, J. –P. Collin, *Chem. Soc. Rev.*, 2008, **37**, 1207

[46] V. Balzani, A. Credi, F. Marchioni, J. F. Stoddart, *Chem. Comm.*, 2001, 1860.

[47] C. A. Stanier, S. J. Alderman, T. D. W. Claridge, H. L. Anderson, *Angew. Chem. Int. Ed.*, 2002, **41**, 1769.

[48] Q. –C. Wang, D. –H. Qu, J. Ren, K. Chen, H. Tian, *Angew. Chem. Int. Ed.*, 2004, **43**, 2661.

[49] E. M. Pérez, D. T. F. Dryden, D. A. Leigh G. Teobaldi, F. Zerbetto, *J. Am. Chem. Soc.*, 2004, **126**, 12210. For other examples of bi-stable H-bonded [2]rotaxanes which contain photoswitchable furmaramide-maleamide motifs see (b) G. Bottari, D. A. Leigh, P. J. Nash, E. M. Pérez, J. K. Y. Wong, F. Zerbetto, *Angew. Chem. Int. Ed.*, 2003, **42**, 5886; (c) G. Bottari, D. A. Leigh, E. M. Pérez, *J. Am. Chem. Soc.*, 2003, **125**, 13360; (d) G. W. H. Wurpel, A. M. Brouwer, I. H. van Stokkum, A. Farran, D. A. Leigh, *J. Am. Chem. Soc.*, 2001, **123**, 11327.

[50] N. Koumura, R. W. J. Zijlstra, R. A. van Delden, N. Harada, B. L. Feringa, *Nature*, 1999, **401**, 152.

[51] Photochemical *cis-trans* isomerisation has been shown to occur in the picoseconds timescale for reported examples see: (a) W. Schuddeboom, S. A. Jonker, J. M. Warman, M. P. de Haas, M. J. W. Vermeulen, W. F. Jager, B. de Lange, B. L. Feringa, R. W. Fessenden, *J. Am. Chem. Soc.*, 1993, **115**, 3286; (b) R. W. J. Zijlstra, P. T. Van Duijnen, B. L. Feringa, T. Steffen, K. Duppen, D. A. Wiersma, *J. Phys. Chem.*, 1997, **101**, 9828.

[52] For recent review articles on light-powered unidirectional molecular motors see: (a) W. R. Browne, B. L. Feringa, *Nature Rev.*, 2006, **1**, 25; (b) B. L. Feringa, R. A. van Delden, N. Koumura, E. M. Geertsema, *Chem. Rev.*, 2000, **100**, 1789; (c) B. L. Feringa, *Acc. Chem. Res.*, 2001, **34**, 504.

[53] (a) N. Koumura, E. M. Geertsema, M. B. van Gelder, A. Meetsma, B. L. Feringa, *J. Am. Chem. Soc.*, 2002, **124**, 5037; (b) R. A. van Delden, M. K. J.

ter Wiel, H. de Jong, A. Meetsma, B. L. Feringa, *Org. Biomol. Chem.*, 2004, **2**, 1531.

[54] R. A. van Delden, M. K. J. ter Wiel, M. M. Pollard, J. Vicario, N. Koumura, B. L. Feringa, *Nature*, 2005, **437**, 1337.

[55] J. Vicario, A. Meetsma, B. L. Feringa, *Chem. Comm.*, 2005, 5910.

[56] B. L. Feringa, *J. Org. Chem.*, 2007, **72**, 6635.

[57] T. Fernández Landaluce, G. London, M. M. Pollard, P. Rudolf, B. L. Feringa, *J. Org. Chem.*, 2010, **75**, 5323.

[58] M. Klok, N. Boyle, M. T. Pryce, A. Meetsma, W. R. Browne, B. L. Feringa, *J. Am. Chem. Soc.*, 2008, **130**, 10484.

[59] D. Pijper, R. A. Delden, A. Meetsma, B. L. Feringa, *J. Am. Chem. Soc.*, 2005, **127**, 17612.

[60] R. A. van Delden, N. Koumora, A. Schoevaars, A. Meetsma, B. L. Feringa, *Org. Biomol. Chem.*, 2003, **1**, 33.

[61] (a) P. R. Ashton, R. Ballardini, V. Balzani, A. Credi, K. R. Dress, E. Ishow, C. J. Kleverlaan, O. Kocian, J. A. Preece, N. F. Spencer, J. F. Stoddart, M. Venturi, S. Wenger, *Chem. –Eur. J.*, 2000, **6**, 3558; (b) V. Balzani, M. Clemente-León, A. Credi, B. Ferrer, M. Venturi, A. H. Flood, J. F. Stoddart, *Proc. Natl. Acad. Sci. U. S. A.*, 2006, **103**, 1178.

[62] V. Balzani, M. Clemente-León, A. Credi, M. Semeraro, M. Venturi, H. –R Tseng, S. Wenger, S. Saha, J. F. Stoddart, *Aust. J. Chem.*, 2006, **59**, 193.

[63] M. Fujita, F. Ibukuro, K. Yamaguchi, K. Ogura, *J. Am. Chem. Soc.*, 1995, **117**, 4175.

[64] K. –I. Yamashita, M. Kawano, M. Fujita, *J. Am. Chem. Soc.*, 2007, **129**, 1850.

[65] K. –I. Yamashita, K. I- Sato, M. Kawano, M. Fujita, *New Journal of Chem.,* 2009, **33**, 264.

[66] For other examples of palladium(II) containing M_6L_4 cages see: (a) M. Yoshizawa, M. Nagao, K. Kumazawa, M. Fujita, *J. Organometallic Chem.,* 2005, **690**, 5383; (b) T. Kusukawa, M Fujita, *J. Am. Chem. Soc.,* 2002, **124**, 13576; (c) F. Ibukuro, T. Kusukawa, M. Fujita, *J. Am. Chem. Soc.,* 1998, **120**, 8561; (d) M. Fujita, D. Ogura, M. Miyazawa, H. Oka, K. Yamaguchi, K. Ogura, *Nature,* 1995, **378**, 469; (e) M. Yoshizawa, M. Nagao, K. Kumazawa, M. Fujita, *J. Organometallic Chem.,* 2005, **690**, 5383; For a recent review article on the self-assembly of discrete nanostructures mediated by transition metals including examples of palladium(II) containing M_6L_4 cages see: (f) S. Leininger, B. Olenyuk, P. J. Stang, *Chem. Rev.,* 2000, **100**, 853; (g) M. Fujita, M. Tominaga, A. Hori, B. Therrien, *Acc. Chem. Res.,* 2005, **38**, 369.

[67] R. D. Vale, T. S. Reese, M. P. Sheetz, *Cell,* 1985, **42**, 39.

[68] S. M. Block, *J. Cell Bio.,* 1998, **140**, 1281.

[69] For a recent review article on kinesin superfamily motor proteins and intracellular transport see: N. Hirokawa, Y. Noda, Y. Tanaka, S. Niwa, *Nature Rev.,* 2009, **10**, 682.

[70] S. Ray, E. Meyhöfer, R. A. Milligan, J. Howard, *J. Cell. Bio.,* 1993, **121**, 1083.

[71] S. M. Block, L. S. Goldstein, B. J. Schnapp, *Nature,* 1990, **348**, 348.

[72] E. J. Kull, E. P. Sablin, R. Lau, R. J. Fletterick, R. D. Vale, *Nature,*1996, **380**, 550.

[73] K. Kinbara, T. Aida, *Chem. Rev. Soc.,* 2005, **105**, 1377.

[74] A. Yildiz, P. R. Selvin, *Trends In Cell Biology,* 2005, **15**, 112.

[75] E. Mandelkow, K. A. Johnson, *J. Cell Bio.,* 1998, **140**, 1281.

[76] B. J. Schnapp, T. S. Reese, R. Bechtold, *J. Cell. Bio.,*1992, **119**, 389.

[77] K. Svoboda, C. F. Schmidt, B. J. Schnapp, S. M. Block, *Nature,* 1993, **365**, 721.

[78] W. Hua, E. C. Young, M. L. Fleming, J. Gelles, *Nature,* 1997, **388**, 390.

[79] S. J. Schnitzer, S. M. Block, *Nature,* 1997, **388**, 386.

[80] J. Howard, A. J. Huspeth, R. D. Vale, *Nature*, 1989, **342**, 154.

[81] D. D. Hackney, *Nature,* 1995, **377**, 448.

[82] K. Svoboda, S. M. Block, *Cell,* 1994, **77**, 773.

[83] E. Meyhöfer, J. Howard, *Proc. Natl. Acad. Sci. USA.*, **92**, 574.

[84] E. Berliner, E. C. Young, K. Anderson, H. K. Mahtani, J. Gelles, *Nature*., 1995, **373**, 718.

[85] W. O. Hancock, J. Howard, *J. Cell. Bio.*,1998, **140**, 1395.

[86] N. Hirokawa, R. Nitta, Y. Okada, *Nature Rev.*, 2009, **10**, 877.

[87] W. Hancock, J. Howard, *Proc. Nat. Aca. Sci.*, 1999, **96**, 13147.

[88] A, Yildiz, M. Tomishige, R. D. Vale P. R. Selvin, *Science,* 2004, **303**, 676.

[89] C. L. Asbury, A. N. Fehr, S. M. Block, *Science,* 2003, **302**, 2130.

[90] W. Hua, J. Chung, J. Gelles, *Science*, 2003, **295**, 844.

[91] C. V. Sindelar, K. H. Downing, *Proc. Natl. Acad. Sci.*, 2010, **107**, 4111.

[92] D. S. Martin, R. Fathi, T. J. Mitchison, J. Gelles, *Proc. Natl. Aca. Sci.,* 2010, **107**, 5453.

[93] (a) W. B. Sherman, N. C. Seeman, *Nano. Lett.,* 2004, **7**, 1203. For a review article of the three linear DNA based molecular walkers see: (b) R. Kelly, *Angew. Chem. Int. Ed.,* 2005, **44**, 4124.

[94] J. –S. Shin, N. A. Pierce, *J. Am. Chem. Soc.*, 2004, **126**, 10834.

[95] P. Yin, H. Yan, X. G. Daniell, A. J. Tuberfield, J. H. Reif, *Angew. Chem. Int. Ed.*, 2004, **43**, 4906.

[96] For a recent example of DNA-based molecular machine which employs set and unset fuel strands to achieve rotary motion see: (a) Y. Tian, C. Mao, *J. Am. Chem. Soc.*, 2004, **126**, 11410.

[97] For a recent review of processive motion in bipedal DNA walkers see: F. C. Simmel, *ChemPhysChem.*, 2009, **10**, 2593.

[98] M. Von Delius, E. M. Geertsema, D. A. Leigh, *Nature Chem.*, 2010, **2**, 96.

[99] For an example of the use of DCC chemistry with disulfide and hydrazone units to selectively open and close a macrocycle under acidic and basic conditions see: M. Von Delius, E. M. Geertsema, D. A. Leigh, A. M. Z. Slawin, *Org. Biomol. Chem.*, 2010, **8**, 4617.

[100] M. von Delius, E. M. Geertsema, D. A. Leigh, D. –T. D. Tang, *J. Am. Chem. Soc.*, 2010, **132**, 16134.

[101] For a recent example of a small molecule that walks down a track see: M. von Delius, E. M. Geertsema, D. A. Leigh, D. –T. D. Tang, *J. Am. Chem. Soc.*, 2010, **132**, 16134.

[102] M. J. Barrell, A. G. Campaña, M. von Delius, E. M. Geertsema, D. A. Leigh, D. –T. D. Tang, *Angew. Chem. Int. Ed.*, 2011, **50**, 285.

CHAPTER TWO

Towards Non-Interlocked Molecular Machines

Acknowledgements

Professor Alexandra Slawin is gratefully acknowledged for solving the crystal structure of [Pt(phen)(**L5**)]$(PF_6)_2$ and Nicholas Baxter for the preliminary studies with the palladium "U-shape" complex. Dr. Paul Lusby and Dr. Roy McBurney are gratefully thanked for their proof-reading of this chapter.

Synopsis

The motor protein kinesin is vital to cellular transport being responsible for the movement of organelles within cells, by "walking" along microtubule "tracks." The translational molecular motion demonstrated by this biological nanomachine is highly processive such that kinesin is able to take many hundreds of steps before dissociation from the track occurs. Inspired by molecular machines abound in Nature many groups have reported on the synthesis and operation of fully artificial systems, such as stimuli-responsive molecular shuttles, capable of controlled, large amplitude, sub-molecular translational motion. However, these synthetic systems rely on mechanical bonding, the physical interlocking of the sub-molecular components, in order to ensure kinetic association of nanomachinery during operation. This consequently limits the motion of these interlocked architectures (rotaxanes) to one dimension. Whilst reports of non-interlocked systems capable of displaying processive linear molecular motion are known, these are almost exclusively restricted to DNA-based walkers or molecular walkers based on a DCC approach. To the best of our knowledge, there are no reports in the literature of the exploitation of metal-ligand bonding interactions to achieve processive translational motion in non-interlocked molecular architectures. The inherent dynamics of the intramolecular, metal-ligand substitution reactions (metallotrophic shifts) have been exploited to drive a square planar d^8 platinum(II) component along different ligating architectures.

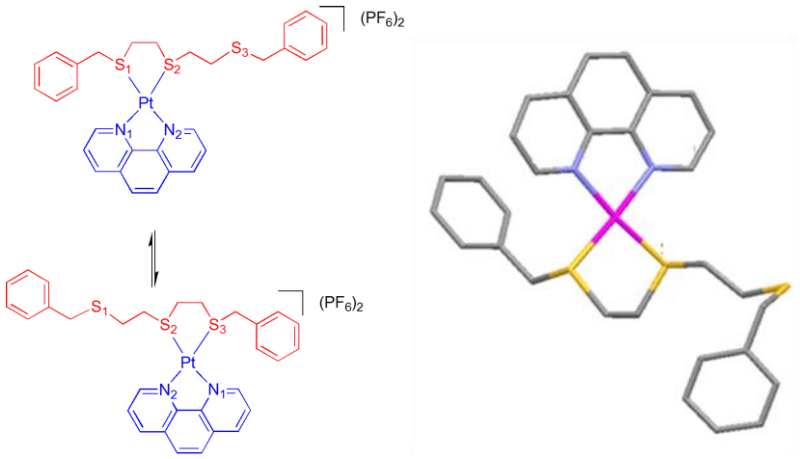

A platinum(II)-phenanthroline, thioether crown complex was investigated to establish if the observed fluxional ligand exchange process was dominantly intra- or intermolecular in nature. If the former was correct then this complex could be thought of as being a prototype, non-biased molecular rotor. The dominant intramolecular nature of the observed ligand substitution reaction was determined by following an intermolecular ligand exchange experiment with a deuterated analogue of the thioether crown. An unbiased, non-interlocked molecular shuttle was then synthesised following the coordination of the platinum(II)-phenanthroline motif to an acyclic tridentate thioether track. At room temperature, this complex also displayed rapid fluxional ligand exchange, which was found to be predominantly intramolecular as determined by studying the relative rates of the intra- and intermolecular ligand exchange processes. A variable temperature NMR study of this complex established the kinetic parameters for the observed shuttling process. A second non-interlocked molecular shuttle was synthesised through coordination of the platinum(II)-phen motif to an acyclic, tridentate, mixed donor track consisting of two sulfur donors and one nitrogen pyridyl donor. Interestingly, whilst this complex displayed fluxional ligand exchange, which was also rapid on the NMR timescale at room temperature, an apparent difference in the fluxional ligand exchange mechanism of the two non-interlocked molecular shuttles was observed. A variable temperature NMR study of this complex determined the kinetic parameters for the observed shuttling process in coordinating and non-coordinating solvent to determine the effect of solvent on the operating mechanism. This series of non-interlocked, square planar, platinum(II)-phenanthroline based complexes have been unambiguously characterized using ^{1}H and ^{13}C NMR spectroscopy, low and high resolution mass spectrometry and (in some cases) X-ray crystallography.

2.1 Introduction

Nature has developed a vast array of molecular motors to perform a wide range of biological processes. The motor protein, kinesin,[1] for instance is vital for cellular transport, being responsible for the movement of organelles within a cell by "walking" along microtubule "tracks".[2] Kinesin, remains kinetically associated throughout its operation,[3] i.e. it does not detach and exchange with the bulk and then re-attach at either a different point or with another track. In contrast to biological nanomachines,[4] which employ a complex array of weak non-covalent interactions (e.g. hydrogen bonding) to maintain structural integrity, fully synthetic linear molecular machines have almost exclusively been based on rotaxane or rotaxane-type architectures.[5-12] Such interlocked systems rely upon mechanical bonding to ensure the kinetic association of the nanomachinery during operation. Despite the great success achieved in these pioneering systems,[5-12] particularly in terms of controlling the directionality of the motion, the physical interlocking of the sub-molecular components means that the molecular motion is topologically constrained to a single dimension. A synthetic non-interlocked nanomachine however would not be limited by such topological constraints. Given the highly processive nature of the molecular motion demonstrated by the non-interlocked nanomachine, kinesin, Nature effectively demonstrates that mechanical bonding is not a prerequisite for efficient translational motion at the molecular scale. Currently there are few reports of non-interlocked systems capable of demonstrating processive translational molecular motion and these are almost exclusively restricted to DNA-based walkers[13a-d] and molecular walkers based on a DCC approach.[13e-h] The use of metal-ligand bonding interactions[14-16] to achieve processive translational motion in non-interlocked molecular architectures remains to be reported.

2.2 Preliminary Studies

2.2.1 Initial Design of a Non-Interlocked Molecular Shuttle: Palladium(II) "U-Shape" Complex

In order to ensure that the motion of the non-interlocked system was processive a kinetically stable molecular shuttle needed to be realised. This non-interlocked architecture required a linear thread with two degenerate binding sites and a non-interlocked component which could translate between them in an exclusively intramolecular manner. Weak, covalent metal-ligand bonding seems the most promising form of binding interaction between the sub-molecular components, as weaker forms of bonding such as H-bonding, the hydrophobic effect and π-π stacking interactions, (Section 1.2-1.4) would probably lack the kinetic stability required for exclusively intramolecular motion. The Pd-complexed, pH shuttle [2]rotaxane reported by Leigh and co-workers[17] presented an attractive model for the basic synthetic design of a non-interlocked architecture due to its exceptional kinetic stability. However, adaption of the existing pH shuttle was necessary as the probable solvent-mediated mechanism, which brings about translocation of the palladium(II)-macrocycle component between the PyH and $PyNMe_2$ stations, would be unsuitable for a shuttling mechanism in a non-interlocked architecture. Attack by coordinating solvent would result in dissociation of the palladium(II)-macrocycle and subsequent intermolecular scrambling (Scheme 2.1) which would render it useless as a molecular machine.

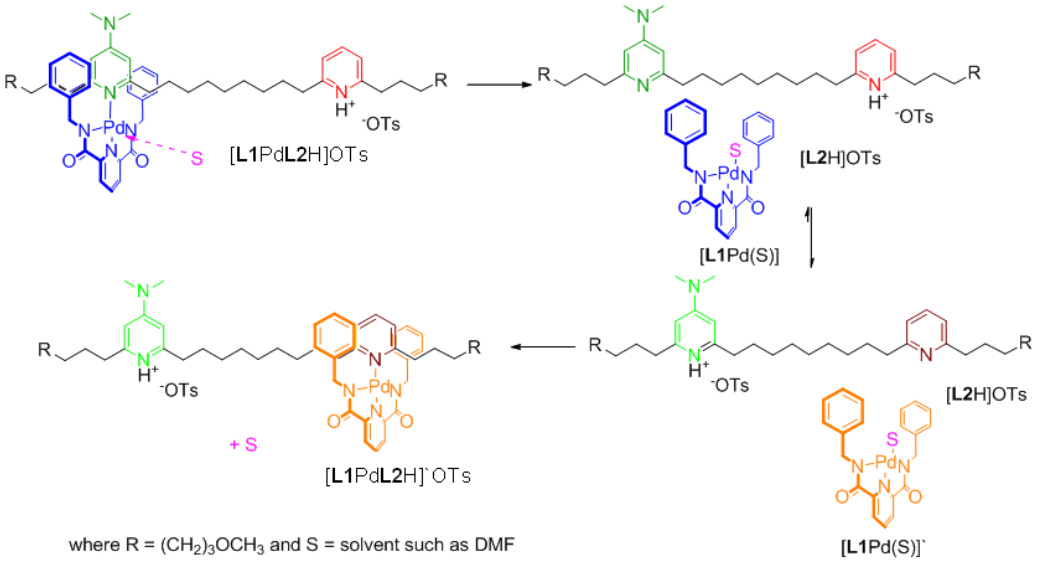

Scheme 2.1 The anticipated solvent-mediated mechanism in a non-interlocked system wherein dissociation of the molecular subcomponents leading to intermolecular scrambling would be expected as a result of the operation of the associative solvent-mediated mechanism.

An alternative strategy, based on well known coordination chemistry, which negates the need for interlocking components was proposed with the incorporation of coordinating functionalities capable of ligating the metal-based component between the two recognition sites. These groups would be capable of binding to the metal centre between the two stations, promoting intramolecular interactions over intermolecular ones, to facilitate processive translational motion. This approach was inspired by previous work involving intramolecular fluxional ligand exchange processes in square planar d^8 Pd(II) and Pt(II) complexes wherein an associative mechanism reportedly operates *via* a series of metallotrophic shifts.[15,16]

The principal aim was to create a degenerate non-switchable system in which shuttling between two identical stations could be achieved. Pyridine binding sites were chosen as suitable stations for synthetic reasons, as 2,6-dibromopyridine was a readily available starting material. The presence of stopper groups and a macrocycle were not appropriate in the non-interlocked architecture as a mechanical bond was not required for the kinetic stability of architecture. Instead, a simpler design was employed wherein the stoppers were replaced by acetate groups and the reported

macrocycle by the palladium(II) "U-shape" complex, [**L1**Pd]. The non-interlocked shuttle, [**L1**Pd**L3**], should benefit from additional π-stacking interactions with the pyridine sites to favor coordination at these stations as in the pH shuttle. Thioether groups were selected as suitable donors for inclusion into the track as they would compliment the "soft" nature of the palladium(II) centre (Figure 2.1).

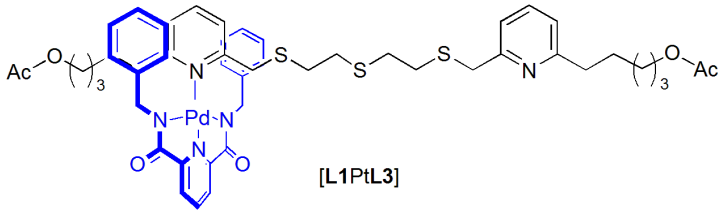

Figure 2.1 Initial design for a non-biased non-interlocked molecular shuttle, [**L1**Pd**L3**], based on the translocation of the palladium-U-shape complex between two pyridine stations employing exclusively intramolecular interactions to achieve processive motion.

The anticipated mechanism of motion in [**L1**Pd**L3**], is that the square planar d^8 Pd(II) centre would undergo a series of ligand substitutions reaction *via* an associative mechanism (*cf* solvent mediated mechanism operating in pH shuttle).[17] Initially the adjacent sulfur donor would coordinate to the metal centre to give a five-coordinate species (Scheme 2.2b). The penta-coordinate species formed would be of relatively high energy and thus rapidly generate the four-coordinate species (Scheme 2.2c) with coordination of the metal centre to the sulfur group of the track. A further five-coordinate species (Scheme 2.2d) would be formed, with coordination of the metal centre to two neighboring sulfur groups of the track, **L3**. This in turn would lead to the formation of another four coordinate species such that [**L1**Pd] (Scheme 2.2e) would be situated in the centre of the track. It was anticipated that there would be some element of thermodynamic advantage towards the binding of [**L1**Pd] at the pyridine recognition sites.

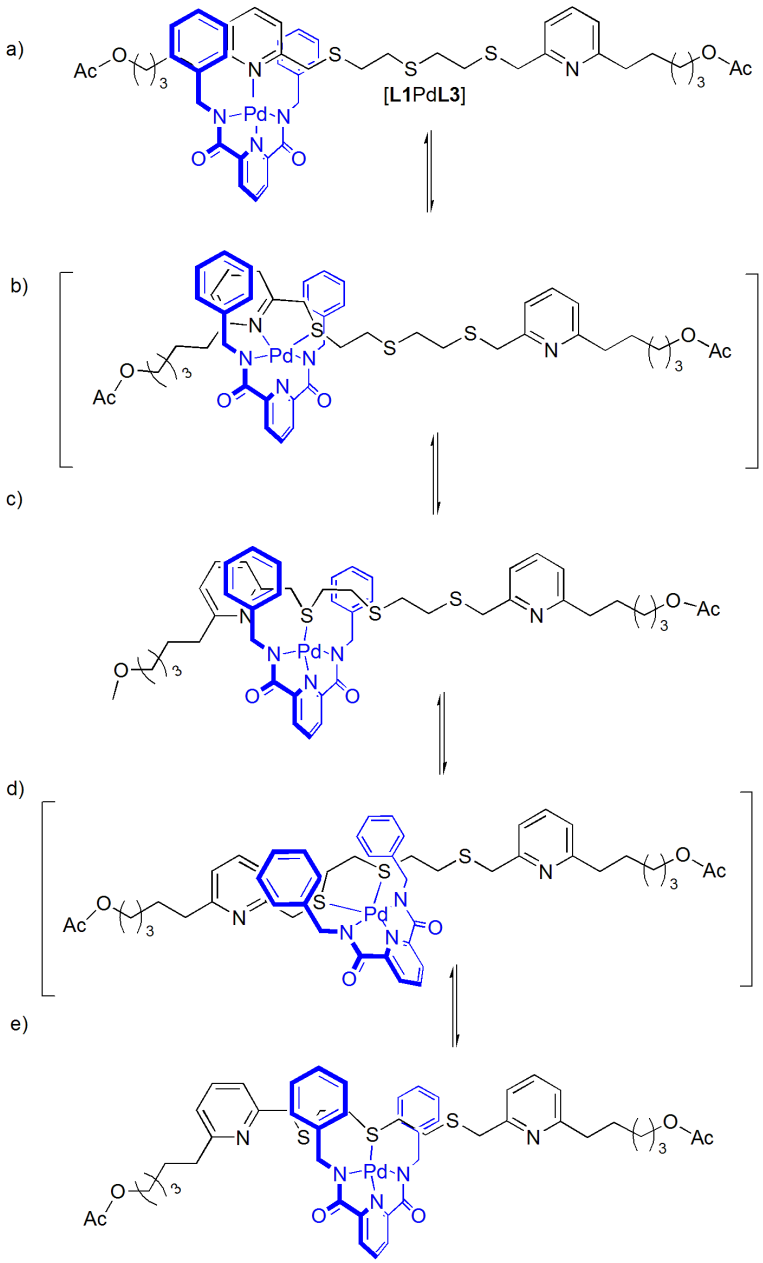

Scheme 2.2 Anticipated mechanism of non-interlocked unbiased molecular shuttle, [**L1**Pd**L3**].

2.2.2 Preliminary Results With Palladium(II)-"U-Shape" Complex

When [**L1**Pd(CH_3CN)] was complexed with **L3**, the expected statistical distribution of 1:2:1 **L3**:[**L1**Pd**L3**]:[(**L1**Pd)$_2$**L3**] was observed by ^{1}H NMR spectroscopy. However, upon purification by flash column chromatography (methanol:dichloromethane 3:97) only **L3** and [(**L1**Pd)$_2$**L3**] were isolated (Scheme 2.3). It was proposed that during the purification procedure a coordinating species, most likely either methanol or silica, caused dissociation of [**L1**Pd] from [**L1**Pd**L3**] to generate free **L3** and [**L1**Pd(X)] (where X = coordinating factor). **L3** would elute much faster than either [(**L1**Pd)$_2$**L3**] or [**L1**Pd(X)]. As a result, [**L1**Pd(X)] resided on the column such that it was able to re-coordinate to the vacant pyridine site on [**L1**Pd**L3**] to afford [(**L1**Pd)$_2$**L3**] (Scheme 2.3). In essence, dynamic resolution of the statistical mixture yielded only **L3** and [(**L1**Pd)$_2$**L3**] and not the desired complex, [**L1**Pd**L3**]. Crucially, this showed that the Pd-track interaction was too labile for use in a non-interlocked assembly.

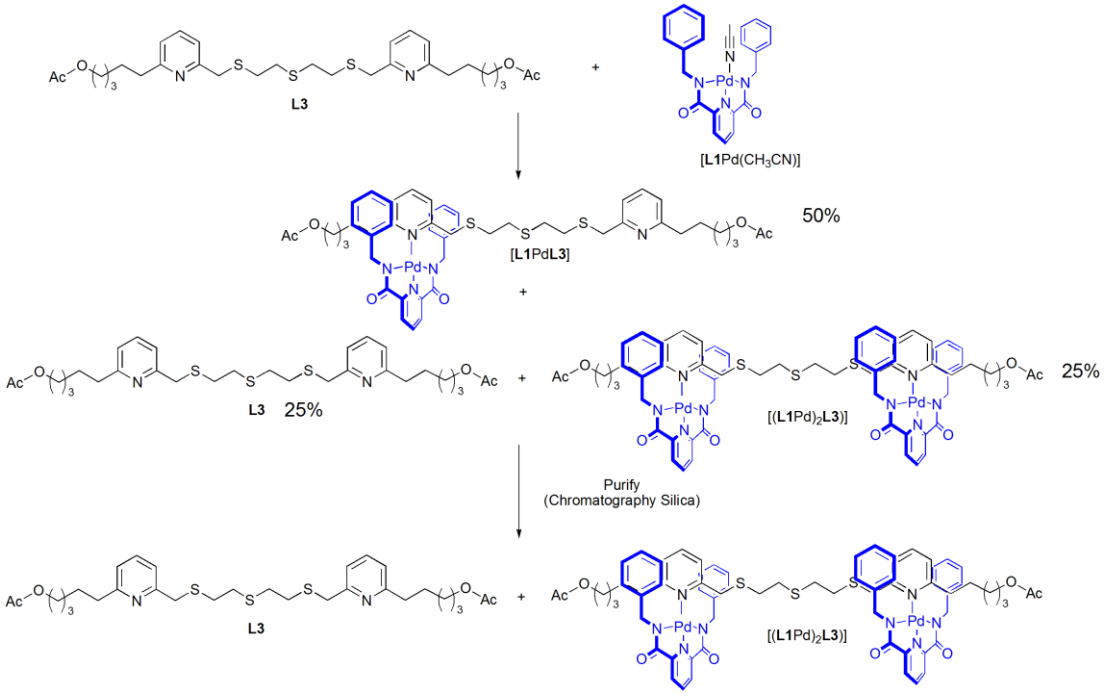

Scheme 2.3 Initial complexation of [**L1**Pd(CH_3CN)] to **L3** led to a statistical distribution of 1:2:1; **L3**:[**L1**Pd**L3**]:[(**L1**Pd)$_2$**L3**]. However, upon flash column chromatography only **L3** and [(**L1**Pd)$_2$**L3**] were isolated.

2.3 Results and Discussion

2.3.1 Initial Design of the Non-Interlocked Molecular Shuttle: Platinum(II)-C^N^C Complex

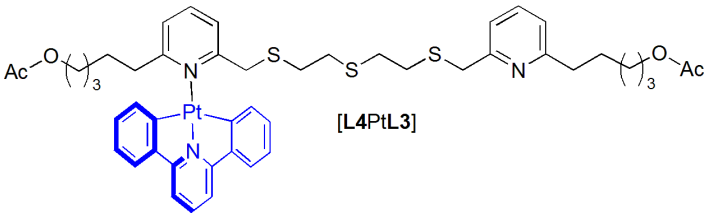

Figure 2.2 Initial target system for an unbiased, non-interlocked, synthetic molecular shuttle, [**L4**Pt**L3**], capable of exhibiting processive translational motion of the platinum-C^N^C component between the pyridine stations of the track.

The modified design for a non-interlocked molecular shuttle, [**L4**Pt**L3**] (Figure 2.2) retained the degenerate, linear track component, **L3**, but it was anticipated that the use of a platinum(II) centre would address the instability presented in the initial studies undertaken with the palladium(II)-based "U-shape" complex (Section 2.2). Consequently the system should be less susceptible to dissociation. Whilst a variety of tridentate-Pt motifs are known[18] the cyclometallated C^N^C motif [**L4**Pt(DMSO)],[19] (DMSO = dimethylsulphoxide) was decided upon as it was anticipated that its charge neutrality would facilitate purification of subsequent complexes. Like palladium(II), platinum(II) species are known to exhibit associative mechanisms under non-irradiative conditions. It was anticipated therefore that the operation of metal-ligand substitution reactions in [**L4**Pt**L3**] would be exclusively intramolecular proceeding *via* pentacoordinate transition states (*cf* Scheme 2.2). As such, non-biased shuttling of the platinum-C^N^C component between the degenerate pyridine stations of **L3** was envisaged.

The synthesis of **L3** was undertaken *via* a six step procedure from commercially available materials (Scheme 2.4). A modified literature procedure[20] was undertaken for the formylation reaction of 2,6-dibromopyridine to generate the desired aldehyde, **64**, in 83%. The protected alcohol containing alkyne, **66**, was prepared from 5-

hexyn-1-ol in 96%, and then a Sonogashira reaction[21] between **64** and **66**, gave the anticipated cross-coupled product **67** in 87%. Simultaneous reduction of the alkyne and aldehyde functionalities of **67** was achieved under a hydrogen atmosphere using 20% $Pd(OH)_2/C$ in tetrahydrofuran to generate **68** almost quantitatively. Chlorination of the hydroxyl group was accomplished in an excellent 96% simply by stirring **68** with an excess of thionyl chloride in dichloromethane for 3 h. A modified Williamson ether procedure,[22] was employed to generate the desired ligand, **L3**, in 23% by refluxing a solution of **7** and 2,2'-thiodiethanolthiol in butanone in the presence of K_2CO_3 for 48 h.

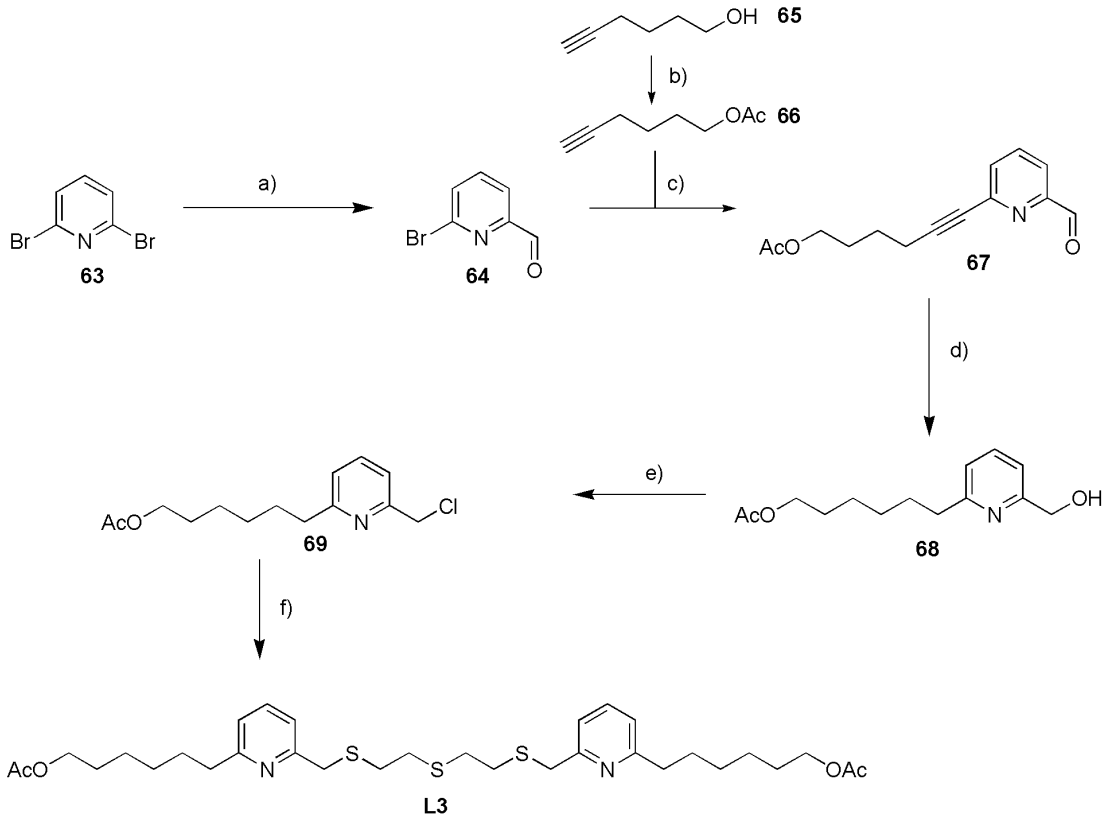

Scheme 2.4 Six step procedure towards the synthesis of **L3**. Reagents and conditions: (a) (i) *n*-BuLi, THF, 30 mins, 195 K (ii) DMF, 195 K → 298 K, 83%; (b) Ac_2O, pyridine, dichloromethane, 3 h, 298 K, 96%; (c) $Pd(PPh_3)_2Cl_2$, CuI, NEt_3,THF, 18 h, 298 K, 87%; (d) H_2, $Pd(OH)_2/C$, THF, 32 h, 298 K, 99%; (e) Thionyl chloride, dichloromethane, 18 h, 298 K, 96%; (f) 2,2'-thiodiethanolthiol, K_2CO_3, butanone, 48 h, reflux, 23%.

The platinum(II)-C^N^C precursor complex, [**L4**Pt(DMSO)], was prepared *via* a two step procedure from commercially available materials (Scheme 2.5). A Suzuki cross-coupling reaction[23] between 2,6-dibromopyridine and 4-phenylboronic acid was employed to generate 2,6-diphenylpyridine, H_2**L4**, in 81%. A modified Rourke procedure[19] was then carried out for the introduction of platinum into the C^N^C scaffold to generate the cyclometallated complex, [**L4**Pt(DMSO)], in a respectable 43%.

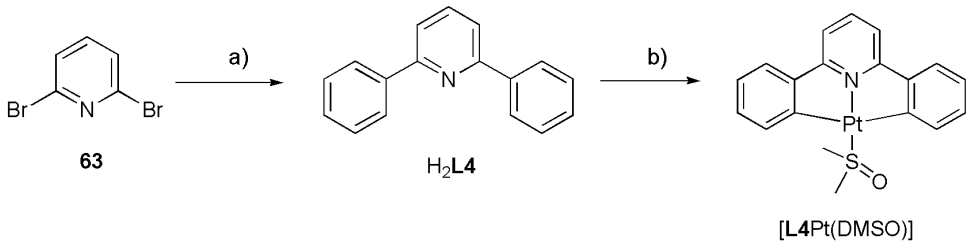

Scheme 2.5 Two step procedure for the synthesis of [**L4**Pt(DMSO)]. Reagents and conditions: (a) 4-phenylboronic acid, $Pd(PPh_3)_4$, Na_2CO_3, toluene, H_2O, 298 K, 81%; (b) (i) K_2PtCl_4, H_2O, acetic acid, 358 K, 18 h. (ii) DMSO, K_2CO_3, H_2O, reflux, 1 h, 43%.

To promote formation of the desired mono-complexed species, [**L4**Pt**L3**], over the di-complexed species, [(**L4**Pt)$_2$**L3**], dilute reaction conditions were employed for the complexation step. Dropwise addition of a dilute solution of the platinum(II)-C^N^C precursor, [**L4**Pt(DMSO)], to a dilute solution of multidentate track, **L3**, was undertaken. A ^{1}H NMR spectrum of the crude reaction mixture established that the initially coordinated sulfoxide ligand, DMSO, in [**L4**Pt(DMSO)], had been partially displaced in solution with unbound DMSO observed at δ 3.7. Electrospray mass spectrometry of the crude mixture confirmed the presence of the desired mono-complexed species, [**L4**Pt**L3**], at 1045.38 ([**L4**Pt**L3**]H$^+$), **L3** at 621.9 (**L3**H$^+$) and the di-complexed species, [(**L4**Pt)$_2$**L3**] at 1470.5 ([(**L4**Pt)$_2$**L3**]H$^+$). However, all attempts to isolate the desired complex, [**L4**Pt**L3**], using flash column chromatography proved unsuccessful and only free track was recovered in 18%. This was presumably due to the instability of [**L4**Pt**L3**] which most likely led to its decomposition or dissociation of its molecular subcomponents during the purification procedure.

2.3.2 A Prototype Non-Biased Molecular Rotor

It was envisaged that the problematic instability encountered upon the purification of [**L4**Pt**L3**] could be addressed by increasing the number of metal-ligand bonding interactions between the platinum centre and the multidentate track. To this end, known $[Pt(phen)([9]aneS_3)][PF_6]_2$ ([9]aneS$_3$ = 1,4,7-trithiocyclononane) was investigated as a prototype, non-biased, artificial molecular rotor. The modified design (Scheme 2.6) incorporated a minimum of two metal-ligand bonding interactions between the platinum centre and the thioether crown at all times. It was anticipated that this adaptation of the system would improve its kinetic stability in comparison to [**L1**Pt**L3**] (wherein the platinum centre is only bound to the track *via* a single point in the ground state (Scheme 2.2a)). Gray and co-workers established, through a series of VT ^{1}H NMR experiments, that $[Pt(phen)([9]aneS_3)][PF_6]_2$ exhibits fluxional behaviour in which the coordinated and non-coordinated thio donors exchange.[16d] They calculated the free energy of activation ($\Delta G^{\ddagger}$) for this ligand substitution reaction to be 9.1 kcal mol^{-1}. Gray postulated that this was a rapid intramolecular rearrangement which proceeded through an associative mechanism *via* pentacoordinate intermediates. The authors did not ascertain whether simultaneous, intermolecular ligand exchange takes place. To determine if this was the case, an intermolecular ligand exchange experiment between $[Pt(phen)([9]aneS_3)][PF_6]_2$ and a deuterated analogue of the thioether crown was undertaken and the progress of the reaction monitored by ^{1}H NMR spectroscopy. Demonstration of the dominant intramolecular nature of this ligand substitution process would establish $[Pt(phen)([9]aneS_3)][PF_6]_2$ as a prototype, non-biased molecular rotor wherein the thioether crown acts as a rotor processing around the platinum(II)-phenanthroline stator (Scheme 2.6).

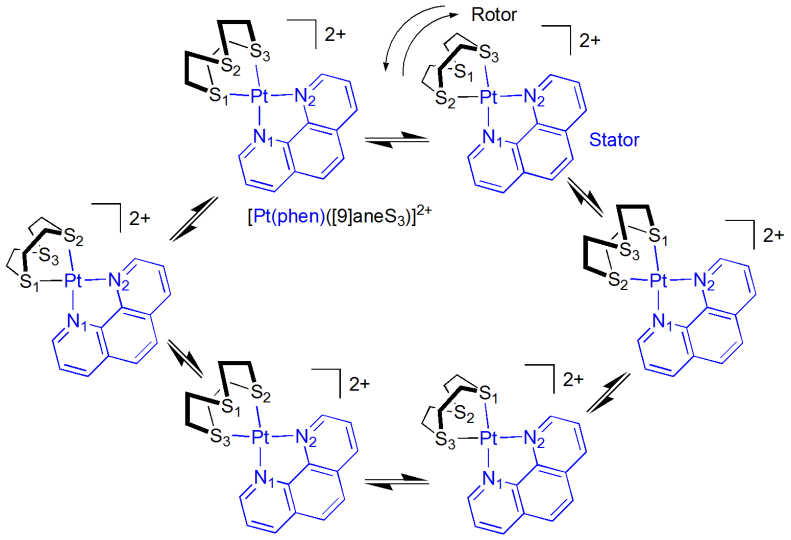

Scheme 2.6 [Pt(phen)([9]aneS$_3$)][PF$_6$]$_2$ as a prototype non-biased molecular rotor. Wherein [9]aneS$_3$ acts as the rotor processing around the platinum(II)-phenanthroline stator.

[Pt(phen)([9]aneS$_3$)][PF$_6$]$_2$ was prepared according to a literature procedure from [Pt(phen)Cl$_2$][24] and the commercially available thioether crown, [9]aneS$_3$ (Scheme 2.7). An exchange experiment between [Pt(phen)([9]aneS$_3$)][PF$_6$]$_2$ and a deuterated analogue of the thioether crown, [D$_4$]-[9]aneS$_3$, was undertaken to determine the rate of the intermolecular ligand exchange process. [D$_4$]-[9]aneS$_3$ was prepared from 2,2'-thiodiethanolthiol and [D$_4$]-1,2-dichloroethane, under high dilution conditions, in the presence of a slight excess of Cs$_2$CO$_3$, according to a literature procedure.[25]

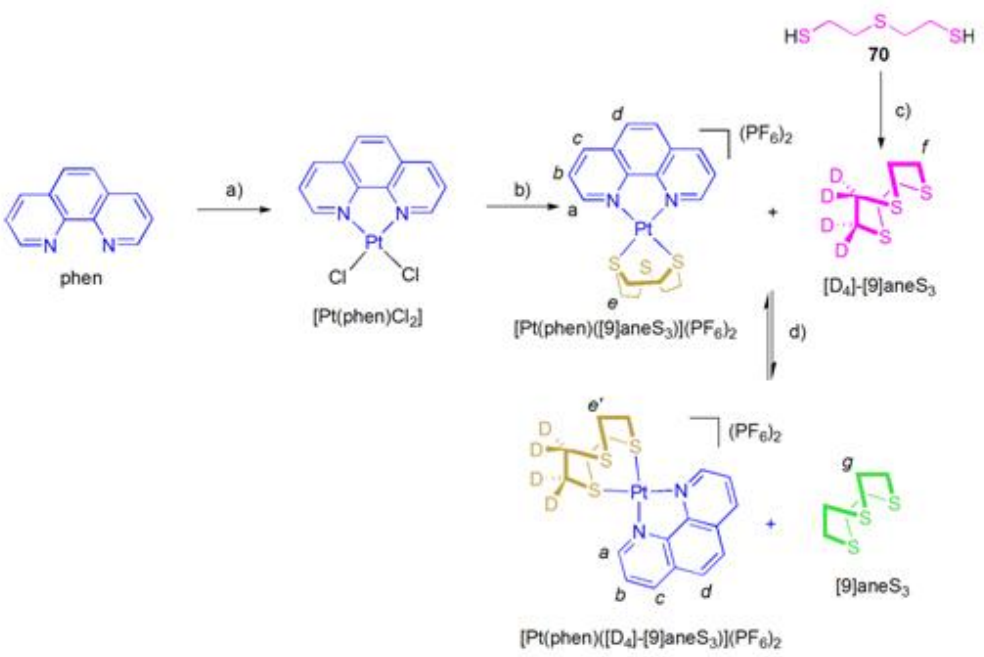

Scheme 2.7 Synthesis of $[D_4]$-[9]aneS_3 and ligand exchange experiment between $[Pt(phen)([9]aneS_3)][PF_6]_2$ and $[D_4]$-[9]aneS_3 in $[D_6]$-acetone at 298 K for 168 h. Reagents and conditions: (a) (i) K_2PtCl_4, H_2O, DMSO, 338 K, 92%; (b) (i) [9]aneS_3, MeOH, H_2O, MeCN, reflux, 3 h, (ii) NH_4PF_6, acetone, 60%; (c) K_2CO_3, DMF, $[D_4]$-1,2-dichloroethane, 373 K, 1%; (d) $[D_6]$-acetone, 0.01 M, 298 K.

One equivalent of $[D_4]$-[9]aneS_3 was added to a 0.01 M solution of $[Pt(phen)([9]aneS_3)][PF_6]_2$ in $[D_6]$-acetone and the formation of $[Pt(phen)([D_4]$-$[9]aneS_3)][PF_6]_2$ and liberation of [9]aneS_3 was monitored over time using ^{1}H NMR spectroscopy (Figure 2.3). Whilst there was no discernable difference in the spectra of $[Pt(phen)([9]aneS_3)](PF_6)_2$ and $[Pt(phen)([D_4]$-$[9]aneS_3)](PF_6)_2$, i.e. for $H_{a\text{-}e`}$, the substitution reaction could be easily monitored through comparison of the distinct resonances for free $[D_4]$-[9]aneS_3 and [9]aneS_3, H_f and H_g, respectively (see Figure 2.3 inset).[26] After 0.5 h, no detectable exchange between [9]aneS_3 and the deuterated analogue, $[D_4]$-[9]aneS_3, had been observed as only a single peak at δ 3.11 corresponding to free $[D_4]$-[9]aneS_3 was apparent. Whilst for comparison in this same time period, it was calculated (Section 2.6.2a) that the rotor, [9]aneS_3, had undertaken 2.43 x10^9 steps (Table 2.1) around the stator as a direct result of intramolecular 1,4-metallotrophic shifts between the platinum centre and [9]aneS_3.

As a full rotation of [9]aneS$_3$ about Pt(phen) requires six sequential steps (Scheme 2.6), the maximum number of full rotations which could be potentially achieved in this time frame (i.e. from 2.43 x10^9 steps) is 4.05x10^8. However, as the rotary motion of [9]aneS$_3$ about Pt(phen) is unbiased, upon formation of the pentacoordinate intermediate there is an equal chance of displacement of any of the three sulphur atoms (S_{1-3}) from the platinum centre. Therefore for every metallotrophic shift (step) undertaken by the system the statistical likelihood that the displacement of the sulphur atoms from the platinum centre occurs in a manner which generates the overall desired directionality of motion is one third of the total number of steps. As a result, whilst the maximum number of full rotations which could be realised is 4.05x10^8 in 0.5 h, the average number of full rotations undertaken statistically would be 1.35x10^8. After three and four days the intermolecular ligand exchange process had only proceeded to 7% and 13% respectively (Figure 2.3) whilst the number of steps taken by [9]aneS$_3$ had increased to 3.50 x10^{11} (which is an average of 1.94x10^{10} full rotations after statistical analysis and potentially a maximum of 5.83 x10^{10} full rotations) (three days) and 4.67 x10^{11} (an average of 2.59x10^{10} full rotations and potentially 7.78 x10^{10} full rotations) (four days) (Table 2.1). Complete intermolecular substitution of [9]aneS$_3$ in [Pt(phen)([9]aneS$_3$)][PF$_6$]$_2$ by [D$_4$]-[9]aneS$_3$ to generate a 1:1 mixture of Pt(phen)([D$_4$]-[9]aneS$_3$)][PF$_6$]$_2$:[Pt(phen)([9]aneS$_3$)][PF$_6$]$_2$ had not been achieved even after seven days at 298 K. The reaction had instead only proceeded to 33% i.e. 33:66; Pt(phen)([D$_4$]-[9]aneS$_3$)][PF$_6$]$_2$:[Pt(phen)([9]aneS$_3$)][PF$_6$]$_2$ (Figure 2.3). In contrast, the intramolecular ligand substitution reaction had progressed to allow 8.16 x10^{11} steps to be taken (an average of 5.83x10^{10} full rotations and potentially 1.75 x10^{11} full rotations) of the rotor around the stator in 168 h. Clearly, the dominant intramolecular nature of the ligand exchange process in [Pt(phen)([9]aneS$_3$)][PF$_6$]$_2$ had been established.

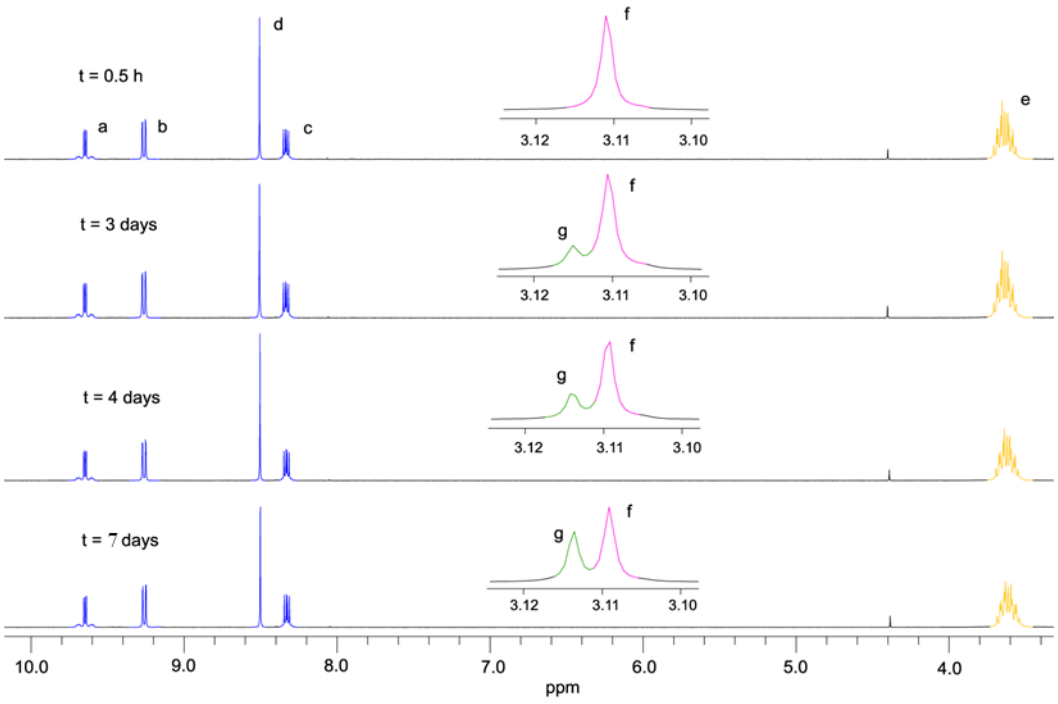

Figure 2.3 ^{1}H NMR spectra, (400 MHz, [D_6]-acetone, 298 K) for the ligand exchange reaction between [Pt(phen)([9]aneS_3)][PF_6]$_2$ and [D_4]-[9]aneS_3 monitored over seven days. Inset: The signals for free [D_4]-[9]aneS_3 and [9]aneS_3. The assignments and colouring of peaks correspond to those shown in Scheme 2.7.

Time (s)	Number of steps	Average number of full rotations	Number of maximum full rotations
1800	$2.43\text{x}10^{9}$	$1.35\text{x}10^{8}$	$4.05\text{x}10^{8}$
$2.59\text{x}10^{5}$	$3.50\text{x}10^{11}$	$1.94\text{x}10^{10}$	$5.83\text{x}10^{10}$
$3.46\text{x}10^{5}$	$4.67\text{x}10^{11}$	$2.59\text{x}10^{10}$	$7.78\text{x}10^{10}$
$7.77\text{x}10^{5}$	$1.05\text{x}10^{12}$	$5.83\text{x}10^{10}$	$1.75\text{x}10^{11}$

Table 2.1 Table showing the number of steps and full rotations taken by the rotor in [Pt(phen)([9]aneS_3)](PF_6)$_2$ at a given time over seven days.

2.3.3 Prototype Non-Biased Molecular Machines Exhibiting Translational Motion

Based on the model studies undertaken on the prototype molecular rotor (Section 2.3.2), a non-interlocked molecular shuttle, [Pt(phen)(**L5**)]$(PF_6)_2$, was investigated to determine its capacity to exhibit processive non-biased translational motion. The design of the non-interlocked shuttle, [Pt(phen)(**L5**)]$(PF_6)_2$ (Scheme 2.8) retained the platinum(II)-phenanthroline moiety of the molecular rotor but modification of the cyclic, tridentate sulfur donor, [9]aneS_3, for an acyclic analogue, **L5**, was required. This adaptation of the ligating architecture would allow the relative motion of the sub-molecular components to be translational and not rotary in nature. A series of low energy 1,4-metallotrophic shifts, between the square planar d^8 platinum(II) centre and the sulfur donors of **L5**, were envisaged to promote processive translational motion in [Pt(phen)(**L5**)]$(PF_6)_2$ (*vide supra*).

L5 was prepared in 69% through a Williamson ether procedure[23] between 2,2-thiodiethanolthiol and an excess of benzyl bromide, in DMF, in the presence of an excess of K_2CO_3 with stirring at ambient temperature for 3 h. The complexation of **L5** to the highly insoluble platinum(II)-phenanthroline precursor, [Pt(phen)Cl_2],[24] was undertaken using the same procedure employed to give [Pt(phen)([9]aneS_3)][PF_6]$_2$.[16d] [Pt(phen)(**L5**)]$(PF_6)_2$ was isolated in 54% yield (Scheme 2.8).

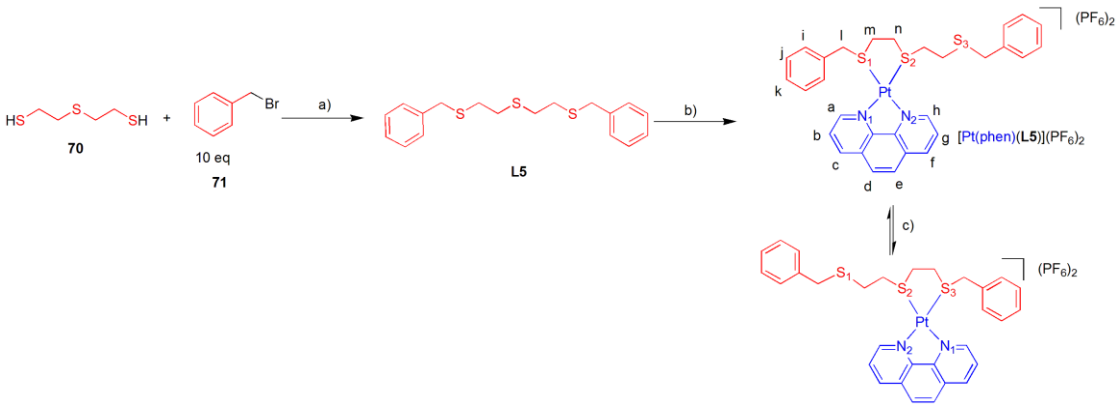

Scheme 2.8 Two step procedure for the synthesis of [Pt(phen)(**L5**)]$(PF_6)_2$ and schematic representation of its capability to achieve processive translational motion of its molecular subcomponents. Reagents and conditions: (a) K_2CO_3, DMF, 3 h, 298 K, 69% (b) (i) [Pt(phen)Cl_2], MeOH, H_2O, MeCN, reflux, 3 h; (ii) NH_4PF_6, 5 min, 298 K, acetone, 54%; (c) [D_6]-acetone, 298 K, 0.01 M.

The modest yield obtained for [Pt(phen)(**L5**)]$(PF_6)_2$ was caused by competing C-S bond cleavage reactions which gave **72** and **73** as side products (Scheme 2.9). It has been previously reported that it is possible to Lewis-acid activate thioether-CH_2 moieties through the coordination of transition metals[27] which can ultimately result in C-S bond cleavage.[28] The formation of **73** from the thio-vinyl containing complex, **74**, would be driven by coordination of the thiolate group (over the poorer thioether donor) and the chelate effect (Scheme 2.9i). Alternatively, polarisation of the C-S bond occurs upon coordination of the sulfur donor to the platinum centre such that the carbon atom becomes susceptible to attack by a nucleophile (e.g. H_2O) in solution to generate either **73** or **74** (Scheme 2.9ii). Due to the formation of multiple products it was necessary to subject the crude reaction mixture to flash column chromatography (acetonitrile:dichloromethane 10:90) to isolate [Pt(phen)(**L5**)]$(PF_6)_2$ as a bright orange solid.

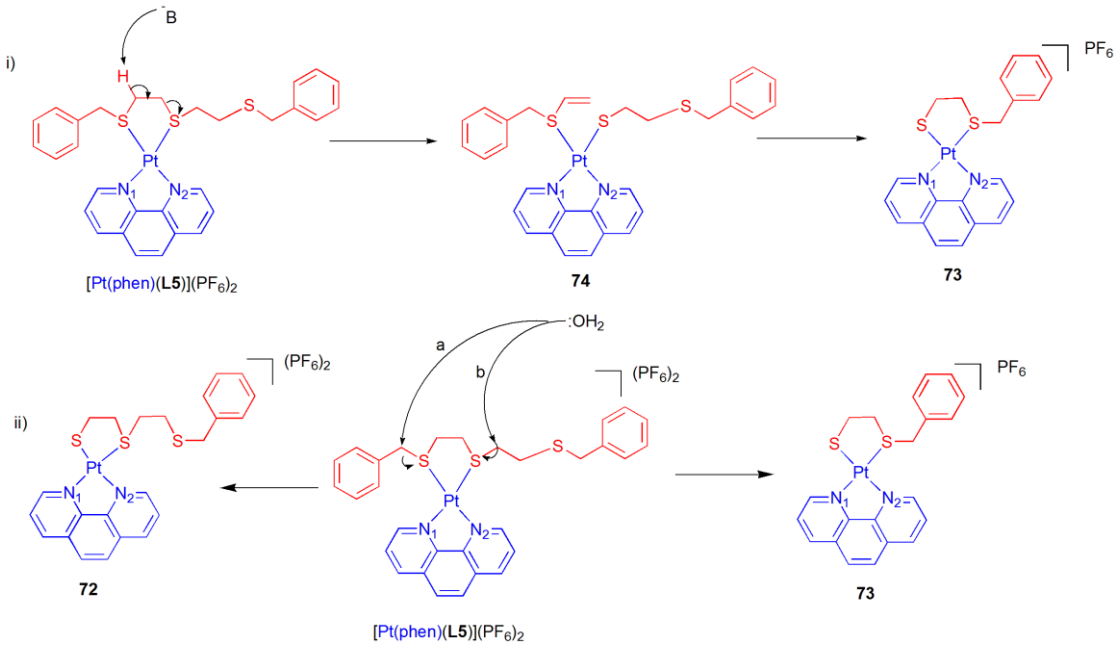

Scheme 2.9 Proposed mechanisms (i and ii) in which a basic species in solution such as water attacks the δ+ carbon atom adjacent to the coordinated sulfur atom to cause C-S bond cleavage at S12 and S15 to give the two novel thiolate containing platinum species, **72** and **73**.

Electrospray mass spectrometry confirmed the presence of [Pt(phen)(**L5**)](X) (where X = PF_6 and Cl) with the observation of molecular ion peaks at *m/z* = 854 (X = PF_6) and 745 (X = Cl) respectively. Furthermore, upon acquiring the spectrum of a pure sample of [Pt(phen)(**L5**)]$(PF_6)_2$, fragmentation of the parent ion in the gaseous phase was observed with peaks corresponding to the thiolate containing complexes **72** and **73** appearing at *m/z* = 618 and 558 respectively. The formation of these two novel species, **72** and **73**, was a direct result of cleavage of **L5** at the S12 and S15 positions respectively (Figure 2.4). The stability of [Pt(phen)(**L5**)]$(PF_6)_2$ in the gaseous phase was analyzed through a tandem MS-MS study on the parent peak *m/z* = 853 of [Pt(phen)(**L5**)](PF_6). It was observed that fragmentation of this species exclusively generated **73** as evidenced through the presence of a peak at *m/z* = 558 and absence of a peak at *m/z* = 618. The ^{1}H NMR spectrum of the crude mixture for the complexation reaction of **L5** to the precursor, [Pt(phen)Cl_2], showed the presence of multiple platinum containing species. This indicated that **72** and **73** were likely formed under the complexation conditions employed. However, once isolated

[Pt(phen)(**L5**)]$(PF_6)_2$ appeared to be stable as monitoring the complex in $[D_6]$-acetone, at 298 K, over 18 h using ^{1}H NMR spectroscopy showed no formation of the thiolate-containing side products, **72** and **73**.

Single crystals suitable for X-ray diffraction were grown *via* vapour diffusion of a saturated solution of the complex in di-isopropylethyl ether and acetone (Figure 2.4). The solid state structure of [Pt(phen)(**L5**)]$(PF_6)_2$ confirmed the pseudo-square planar geometry around the metal centre; N1-Pt1-N10, 80.70(16)°; N1-Pt1-S12, 95.73(12)°; S12-Pt1-S15, 89.24(5)°; N10-Pt1-S15, 94.40(12)°. The Pt-S bonds, between the metal centre and the ligand, **L5**, were observed to be longer and thus weaker than the Pt-N bonds, between the metal centre and bidentate phen ligand, Pt1-N1, 2.061(4) Å; Pt1-N10, 2.051(4) Å; Pt1-S12, 2.2766(15) Å; Pt1-S15, 2.2760(17) Å.

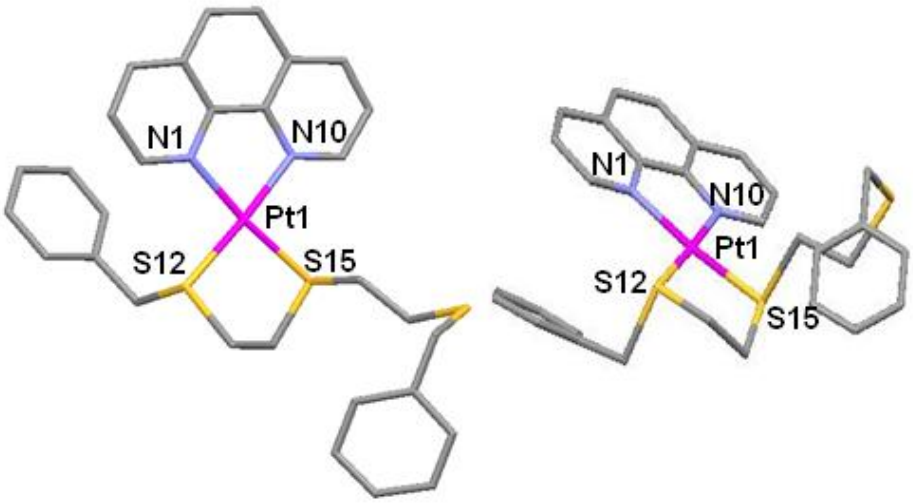

Figure 2.4 Two views of the X-ray crystal structure of [Pt(phen)(**L5**)]$(PF_6)_2$. The carbon atoms of phen and **L5** are shown in grey, nitrogen atoms of phen in light blue, platinum atom in magenta and sulfur atoms in yellow. The PF_6 counteranions and one di-isopropyl ether solvent molecule have been removed for clarity. Selected bond lengths and angles [Å and °]: Pt1-N1, 2.061(4); Pt1-N10, 2.051(4); Pt1-S12, 2.2766(15); Pt1-S15, 2.2760(17). N1-Pt1-N10, 80.70(16); N1-Pt1-S12, 95.73(12); S12-Pt1-S15, 89.24(5); N10-Pt1-S15, 94.40(12).

The ^{1}H NMR spectrum of [Pt(phen)(**L5**)]$(PF_6)_2$ at 298 K in $[D_6]$-acetone (Figure 2.5) suggested the operation of a fluxional ligand exchange process. The presence of only one set of phenyl signals (H_i at δ 7.5) was indicative of an exchange process that was fast on the NMR timescale. Furthermore, an insight into the mechanistic pathway

operating for this fluxional, ligand exchange process at 298 K was gained by closer inspection of the phenanthroline protons, H_{a-g}. The inequivalence displayed by these protons was indicative of the operation of a classic, platinum(II) associative mechanism wherein retention of the stereochemistry of the system would be anticipated. H_a would always be directed towards H_i, the outside of the track, whilst H_h would remain in close proximity to the aliphatic thioether moiety, H_{l-n}, causing the observed desymmetrisation of the signals. Rotation of **L5** about the platinum centre could also lead to the observed inequivalence of phenanthroline protons. To determine the kinetic parameters, *k* and $\Delta G^{\ddagger}$, for this exchange reaction, a VT NMR study of [Pt(phen)(**L5**)]$(PF_6)_2$ in [D_6]-acetone was undertaken (Figure 2.5). It was apparent through the desymmetrisation of H_i, which was observed to reach coalescence at 235 K and re-appeared as two well defined singlet peaks at lower temperatures (see Figure 2.5) that upon cooling the fluxional ligand exchange process was slowed relative to the NMR timescale. This was supported further by the observed coalescence of aliphatic protons, H_{l-n}, at depressed temperatures although resolution of these peaks was not achieved due to limitations of the instrumentation employed.[29] The resonance peak H_i, was useful for interpretation to determine *k* and $\Delta G^{\ddagger}$ values for the activation barrier of the ligand exchange process (Section 7). From the VT NMR data, it was established that the coalescence temperature, T_c, of H_i was 235 K and the maximum peak separation $\Delta\nu_o$ was 190 ± 9.5 Hz, as it is estimated that there will be a ± 5% error in calculation of $\Delta\nu_o$ from the relevant ^{1}H NMR spectra. From this data an estimation of k_{obs} was obtained as 422 ± 21 s^{-1} and subsequently $\Delta G^{\ddagger}$ for the ligand substitution reaction was estimated (using a modified Eyring equation, Section 2.6.2) to be 10.8 ± 0.03 kcal mol^{-1}. The free energy of activation for the fluxional ligand exchange process in [Pt(phen)(**L5**)]$(PF_6)_2$ was slightly higher than the value of 9.1 kcal mol^{-1} determined for [Pt(phen)([9]aneS_3)]$(PF_6)_2$ by Gray and co-workers.[16d] The differing values of $\Delta G^{\ddagger}$ obtained for these two systems is unsurprising given that the rigid cyclic thioether crown, [9]aneS_3, is better pre-organised for an intramolecular ligand substitution reaction with the platinum(II) centre of [Pt(phen)([9]aneS_3)]$(PF_6)_2$ in comparison to the acyclic thioether track, **L5** of [Pt(phen)(**L5**)]$(PF_6)_2$. In essence, a

higher entropic penalty is incurred on proceeding to the pentacoordinate species for [Pt(phen)([9]aneS$_3$)](PF$_6$)$_2$.

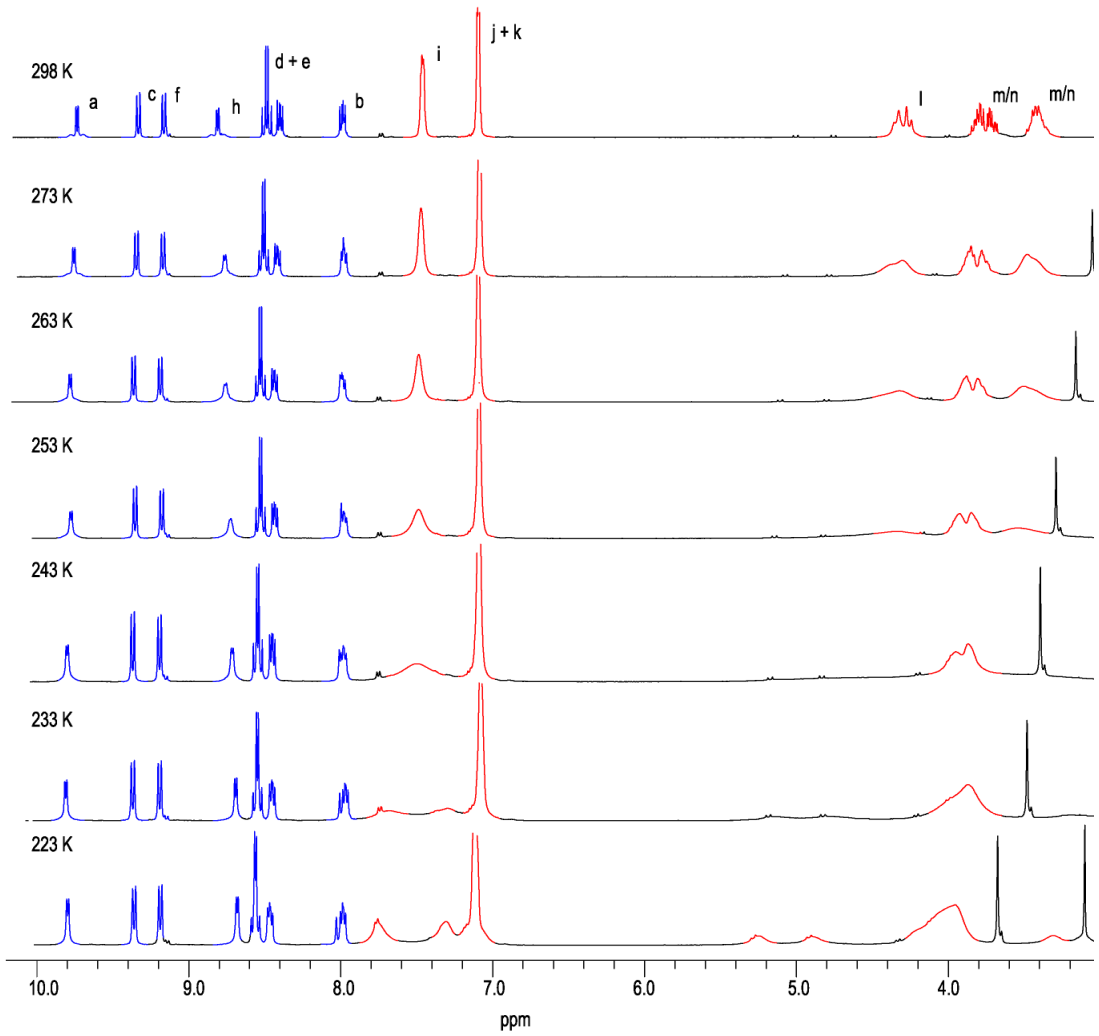

Figure 2.5 VT ^{1}H NMR spectra (400 MHz, [D$_6$]-acetone, 298 K). The assignments and colouring of peaks correspond to those shown in Scheme 2.8.

To determine the relative rates of the inter- and intramolecular exchange processes for [Pt(phen)(**L5**)](PF$_6$)$_2$, an exchange experiment between [Pt(phen)(**L5**)](PF$_6$)$_2$ and [D$_{14}$]-**L5** was undertaken at room temperature in [D$_6$]-acetone (Scheme 2.10). The deuterated analogue of the acyclic thioether ligand, [D$_{14}$]-**L5**, was prepared in 94% *via* a modified Williamson ether reaction[22] between [D$_7$]-benzyl choride and 2,2-thiodiethanolthiol in the presence of an excess of K$_2$CO$_3$, in DMF, with stirring for 18 h at ambient temperature.

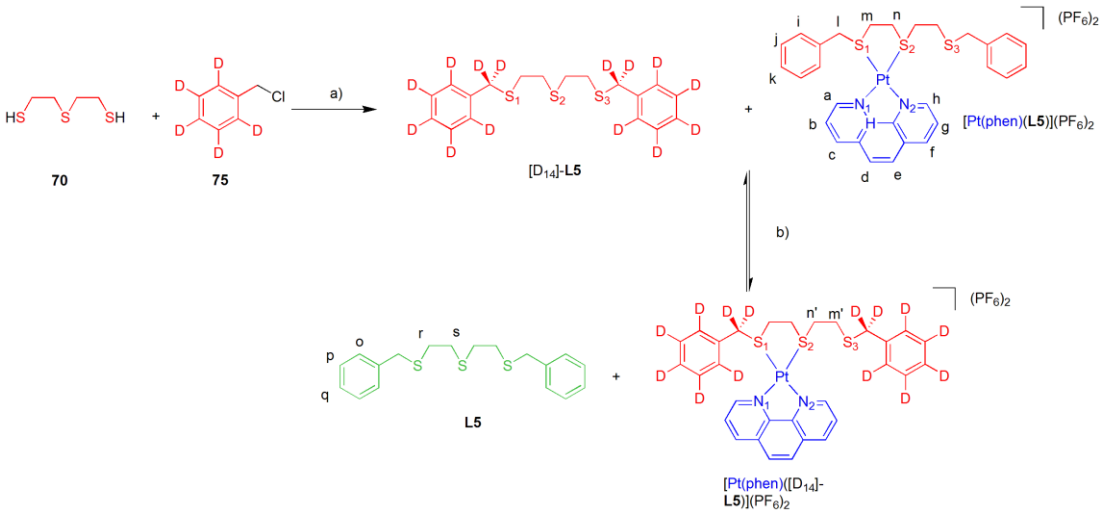

Scheme 2.10 Synthesis of $[D_{14}]$-**L5** and exchange experiment between [Pt(phen)(**L5**)]$(PF_6)_2$ and $[D_{14}]$-**L5** in $[D_6]$-acetone at 298 K for 150 min. Reagents and conditions: (a) K_2CO_3, DMF, 18 h, 298 K, 94%; (b) $[D_6]$-acetone, 0.01 M, 298 K.

One equivalent of $[D_{14}]$-**L5** was added to a 0.01 M solution of [Pt(phen)(**L5**)]$(PF_6)_2$ and the formation of [Pt(phen)($[D_{14}]$-**L5**)]$(PF_6)_2$ and liberation of **L5** monitored over time using ^{1}H NMR spectroscopy (Figure 2.6).[26] The spectra for [Pt(phen)(**L5**)]$(PF_6)_2$ and [Pt(phen)($[D_{14}]$-**L5**)]$(PF_6)_2$, specifically the resonances H_{a-n}, were not distinct and thus could not be employed to monitor the progression of the substitution reaction. However, a peak corresponding to the aromatic region of liberated **L5**, H_o, was useful for analysis as it was distinct and not complicated by overlap with other signals.[30] Upon the time taken to acquire the initial spectrum, after the addition of $[D_{14}]$-**L5** (5 min), it could be seen that **L5** had undergone partial displacement as a multiplet resonance at δ 7.4 (which corresponds to H_o for free **L5**) was observed (Figure 2.6). The intermolecular ligand substitution reaction had progressed to 97:3 [Pt(phen)(**L5**)]$(PF_6)_2$:[Pt(phen)($[D_{14}]$-**L5**)]$(PF_6)_2$ after 5 min, whilst the data obtained from the series of VT NMR experiments could be used to calculate that 2.15×10^7 steps had been taken by the Pt(phen) component (Table 2.2). Using the crystal structure data obtained for [Pt(phen)(**L5**)]$(PF_6)_2$ it was calculated that the distance between S12 and S18, the two terminal sulfur donors of **L5**, was 0.663 nm. One "step" taken by [Pt(phen)(**L5**)]$(PF_6)_2$, wherein coordination of the platinum centre changes from $S_{1\text{-}2}$ and $S_{2\text{-}3}$ (i.e. replacement of S_1 by S_3), would led

to the desired translation of the Pt(phen) component along the track resulting in a 0.663 nm motion of Pt(phen) relative to **L5**. However, as the motion of the molecular subcomponents is unbiased, upon formation of the pentacoordinate intermediate there is an equal chance that the displaced ligand will be any of the three sulphur atoms ($S_{1\text{-}3}$). As a result, whilst the potential number of steps which could be realised if the system always progressed between S_1 and S_3 i.e the platinum centre shifts in coordination between $S_{1\text{-}2}$, and $S_{2\text{-}3}$, the statistical likelihood is a third of this maximum value as every metallotrophic shift could result in coordination of the platinum centre to $S_{1\text{-}2}$, $S_{1\text{-}3}$ or the desired $S_{2\text{-}3}$. From this data, it was calculated that (after 5 min) the distance of 0.004 m was likely to have been travelled in an unbiased manner along the track whilst 0.086 m ($3.88\text{x}10^8$ steps) and 0.11 m ($5.18\text{x}10^8$ steps) should statistically have been traversed by the Pt(phen) component in 1.5 h and 2 h respectively (Table 2.2). The intermolecular exchange reaction had meanwhile progressed to 65:35 and 57:43 (for [Pt(phen)(**L5**)]$(PF_6)_2$:[Pt(phen)([D_{14}]-**L5**)]$(PF_6)_2$). A 1:1 ratio of [Pt(phen)(**L5**)]$(PF_6)_2$:[Pt(phen)([D_{14}]-**L5**)]$(PF_6)_2$ was observed after 2.5 h. In contrast, [Pt(phen)(**L5**)]$(PF_6)_2$ had statistically translated a distance of 0.14 m in a processive unbiased manner along **L5** (Table 2.2).

The rate of the intermolecular exchange reaction for [Pt(phen)([9]aneS_3)][PF_6]$_2$ is significantly slower than for [Pt(phen)(**L5**)]$(PF_6)_2$ as evidenced by the timescales of the ligand exchange reactions with the respective deuterated analogues. Additionally, the *k* value for the intramolecular exchange process differed by four orders of magnitude, yet in the opposite direction - 422 s^{-1} in [Pt(phen)(**L5**)]$(PF_6)_2$ and $1.3\ \text{x}10^6\ s^{-1}$ in [Pt(phen)([9]aneS_3)][PF_6]$_2$. The ratio of the intra to intermolecular exchange rates is therefore significantly diminished for [Pt(phen)(**L5**)]$(PF_6)_2$ in comparison to [Pt(phen)([9]aneS_3)][PF_6]$_2$. From this data, it appears that this metallotropic shift seems more suited to the preparation of molecular rotors.

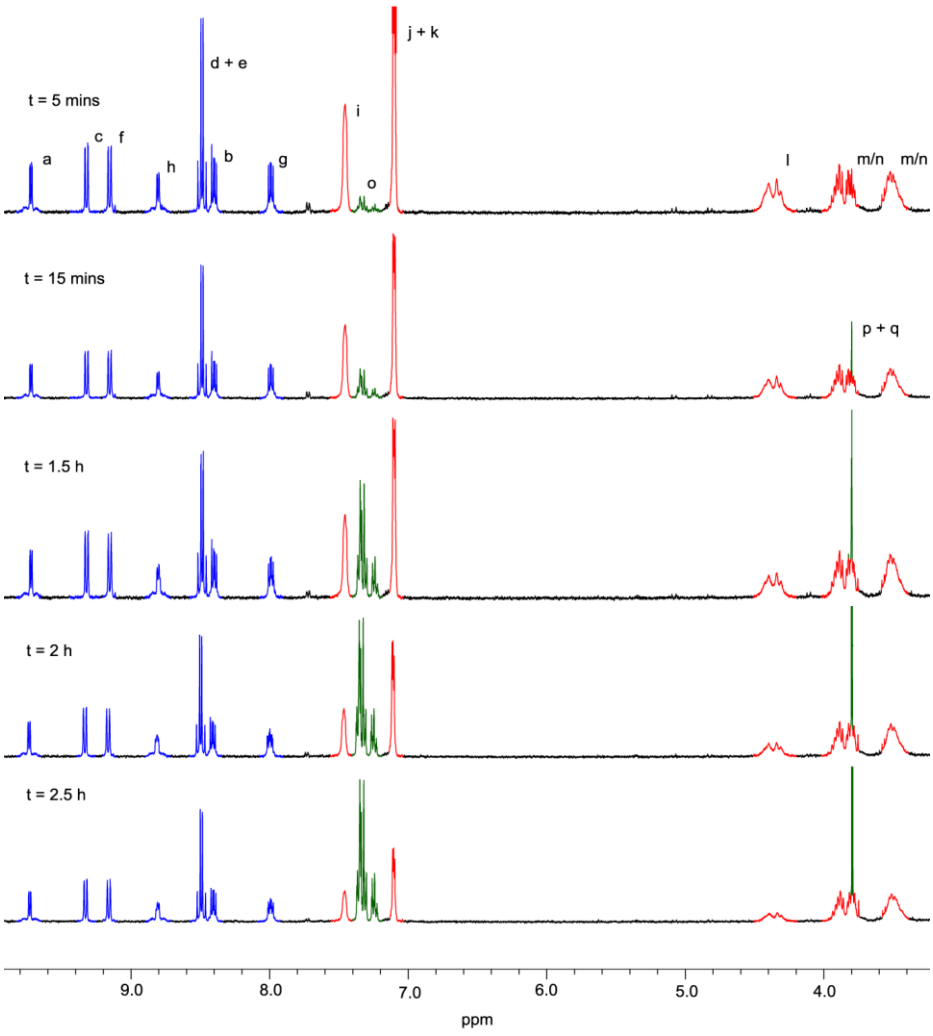

Figure 2.6 ^{1}H NMR spectra (400 MHz, [D_6]-acetone, 298 K) for the ligand exchange reaction between [D_{14}]-**L5** and [Pt(phen)(**L5**)](PF_6)$_2$ monitored over 2.5 h, showing the incorporation of [D_{14}]-**L5** and liberation of **L5**. The assignments and colouring of peaks correspond to those shown in Scheme 2.10.

Time (s)	Number of steps	Average distance travelled (m)
300	$2.15x10^7$	0.004
900	$6.47x10^7$	0.014
5400	$3.88x10^8$	0.086
7200	$5.18x10^8$	0.11
9000	$6.47x10^8$	0.14

Table 2.2 Table showing the number of steps and average distance travelled by Pt(phen) component in [Pt(phen)(**L5**)]$(PF_6)_2$ relative to **L5** at a given time over 2.5 h.

The associative mechanism known for ligand exchange in platinum(II) square planar complexes, under non-irradiative conditions, has been widely acknowledged to proceed *via* two main pathways; direct ligand substitution which produces a more sterically hindered reaction intermediate or *via* a solvent mediated pathway.[31] Usually, the solvent mediated mechanism dominates as (a) the solvent is present in high concentration and (b) solvent molecules are usually less sterically crowded. The preferred mechanisms in the inter- and intramolecular reaction pathways are likely to be different. In the former pathway, a solvent mediated mechanism is likely to operate as the resultant pentacoordinate intermediate would be significantly less crowded than the corresponding species formed in a direct exchange mechanism. In contrast, the intramolecular exchange mechanism most likely proceeds *via* direct ligand exchange as this would produce a less sterically hindered intermediate in comparison to the solvent mediated pathway. Therefore, non-coordinating solvents should hinder the intermolecular reaction pathway as the solvent mediated mechanism will be repressed. To investigate the relative rate of the intermolecular ligand exchange reaction in non-coordinating solvent a simple anion exchange of the PF_6 counter-ion in [Pt(phen)(**L5**)]$(PF_6)_2$ for BPh_4 generated [Pt(phen)(**L5**)]$(BPh_4)_2$, which was soluble in CD_2Cl_2. To a 0.01 M solution of [Pt(phen)(**L5**)]$(BPh_4)_2$ in CD_2Cl_2 was added one equivalent of $[D_{14}]$-**L5** and the liberation of **L5** monitored over time using ^{1}H NMR spectroscopy. In contrast to the study undertaken in

acetone, 40 h were required for complete substitution of **L5** by [D_{14}]-**L5** to generate a 1:1 ratio of [Pt(phen)([D_{14}]-**L5**)][BPh_4]$_2$ although approximately 10% decomposition of the charged square planar platinum species was observed over this period. However, clearly the nature of the solvent has a pronounced effect on the relative rates of the intermolecular and intramolecular ligand substitution reactions, where non-coordinating solvents significantly repressed the "scrambling" process as anticipated.

2.3.4 Fluxional Ligand Exchange Process in Other Platinum(II) Complexes

[Pt(phen)(**L6**)](PF_6)$_2$ was also investigated as prototype molecular shuttle capable of exhibiting translational motion (Scheme 2.11). This target molecule, [Pt(phen)(**L6**)](PF_6)$_2$, aimed to address the synthetic problems associated with the preparation of [Pt(phen)(**L5**)](PF_6)$_2$, with regards to the undesired side reaction which led to the observed C-S bond cleavage. Accordingly, modification of **L5** to tridentate **L6**, consisting of two sulfur ligating groups and one *N*-heterocyclic donor, was deemed appropriate. As before, it was anticipated that a series of low energy 1,4-metallotrophic shifts would result in translational motion of the Pt(phen) component with respect to **L6**. **L6** was prepared from benzyl mercaptan, **76**, and 2,6-bis(bromomethyl)pyridine, **77**, in the presence of K_2CO_3, in DMF, in 93% yield.[32] Complexation of **L6** to [Pt(phen)Cl_2][24] was undertaken *via* a modified literature procedure[16d] by refluxing for 20 min (Scheme 2.11). Anion exchange was subsequently undertaken on this crude mixture through the addition of a solution of acetone containing ten equivalents of NH_4PF_6. The desired charged complex, [Pt(phen)(**L6**)](PF_6)$_2$, was obtained as a bright orange solid in 41% yield.

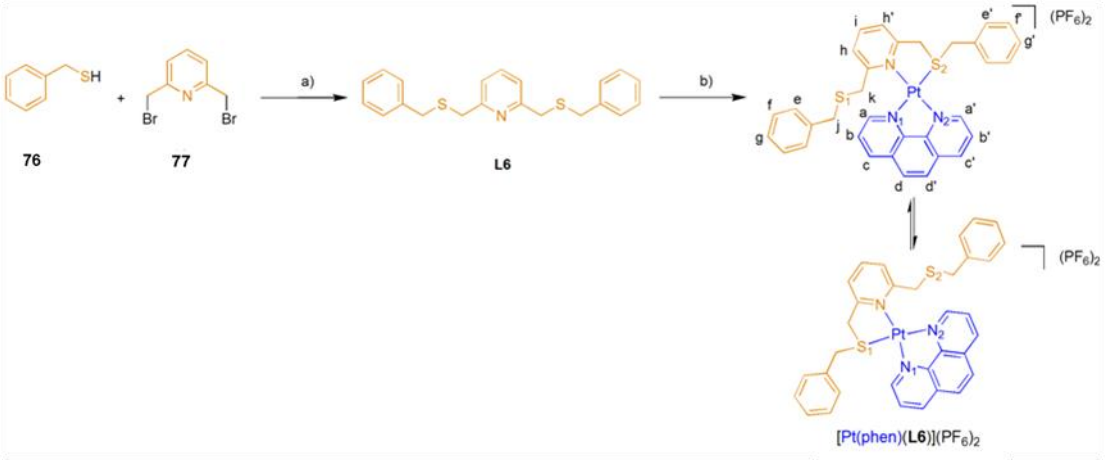

Scheme 2.11 Two step procedure for synthesis of [Pt(phen)(**L6**)]$(PF_6)_2$ and schematic representation of its capability to achieve processive translational motion of its molecular subcomponents. Reagents and conditions: (a) K_2CO_3, DMF, 3 h, 298 K, 93% (b) (i) [Pt(phen)Cl_2], MeOH:H_2O:MeCN, 1:1:1, reflux 3 h, (ii) NH_4PF_6, 41%; (c) [D_6]-acetone, 298 K.

Electrospray mass spectrometry confirmed the presence of the desired complex with the molecular ion peak at *m/z* = 761 which corresponded to [Pt(phen)(**L6**)](Cl).[33] Fragmentation of the parent ion was seen in the gaseous phase with the presence of a peak at *m/z* = 634, which corresponds to the thiolate-platinum complex wherein Bn-S (Bn = benzyl) bond cleavage occurred (*cf* analogous fragmentation pattern observed by electrospray mass spectrometry for [Pt(phen)(**L5**)]$(PF_6)_2$).

The ^{1}H NMR spectrum of [Pt(phen)(**L6**)]$(PF_6)_2$ at 298 K in [D_6]-acetone (Figure 2.7) showed several features which suggested the occurrence of a ligand exchange process which was rapid on the NMR timescale. These included the broad signal at δ 7.2, which corresponded to H_e, and the singlet signals at δ 5.1 and δ 4.5, which corresponded to H_j and H_k respectively. All of these signals appeared as time averaged resonances (Figure 2.7) as a direct result of the non-biased shuttling of the Pt(phen) component along the track, **L6**. A similar pattern of signals had been observed for the thread resonances of **L5** in [Pt(phen)(**L5**)]$(PF_6)_2$. However, in contrast, the pattern of the phenanthroline protons, H_{a-d}, suggested that a different mechanism occurs for the exchange process in [Pt(phen)(**L6**)]$(PF_6)_2$. The equivalence displayed by H_{a-d} indicated that unlike with [Pt(phen)(**L5**)]$(PF_6)_2$, where stereochemistry of the system was retained, a twist to the system was introduced,

possibly through rotation of an intermediate in the intramolecular ligand substitution reaction in [Pt(phen)(**L6**)](PF$_6$)$_2$. Whilst the Berry pseudo-rotation[34] (BPR) mechanism is most frequently proposed to explain the observation of stereomutation in associative, ligand exchange reactions,[35] it is unlikely that it is able to operate in [Pt(phen)(**L6**)](PF$_6$)$_2$. The substitution pattern on the pyridine moiety of **L6**, with the covalent linkages between the pyridine moiety and the thioether arms, would most probably prevent the bending motions required for this BPR reaction pathway to proceed.[15c] An atypical turnstile[36] (TS) mechanism, which is not often taken into account to explain stereomutation in literature,[37] is proposed to describe the fluxional behavior of [Pt(phen)(**L6**)](PF$_6$)$_2$ (Scheme 2.12). The operation of this mechanism would plausibly generate the observed pattern of the phenanthroline signals in [Pt(phen)(**L6**)](PF$_6$)$_2$. TS mechanisms are generally considered to be higher energy pathways than BPR but it has been shown in main group complexes that the introduction of a rigid ligand into a system can favour the TS pathway over the BPR.[38,39] Alternatively, the stereomutation could proceed *via* a planar intermediate as has been previously described by Orrell[40] in a simple platinum(II) complex containing a fluxional, bidentate 2,2`-6,2``-terpyridine ligand.

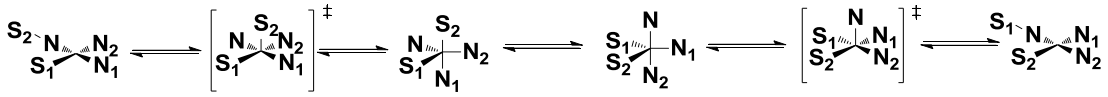

Scheme 2.12 The operation of the turnstile mechanism leading to stereomutation in [Pt(phen)(**L6**)](PF$_6$)$_2$. The labeling of the atoms corresponds to those shown in Scheme 2.11.

To determine the kinetic parameters, k and $\Delta G^{\ddagger}$, for the ligand exchange reaction, a VT ^{1}H NMR study of [Pt(phen)(**L6**)](PF$_6$)$_2$ in [D$_6$]-acetone was undertaken (Figure 2.7). Upon cooling, desymmetrisation of the phen signals, H$_{a\text{-}d}$, was observed as the exchange process became slow on the NMR timescale. Coalescence was reached at 250 K for H$_a$, 253 K for H$_c$, 249 K for H$_d$, 248 K for H$_e$ and 240 K for H$_f$ (Table 2.3). Furthermore, the observed coalescence and subsequent desymmetrisation of the aliphatic H$_{j+k}$ protons of **L6** supported the proposed reduction in the rate of the ligand exchange process at depressed temperatures. However, these aliphatic signals were

too complex at lower temperatures to be used for quantitative analysis of the ligand substitution reaction. The resonance peaks $H_{a\text{-}c}$, H_e and H_f were useful for interpretation and were employed to determine values for *k* and $\Delta G^{\ddagger}$ for the fluxional ligand exchange process (Section 2.8.3b). It was calculated that $\Delta G^{\ddagger} = 12.0 \pm 0.04$ kcal mol^{-1} (Table 2.3). This value for the activation barrier of the ligand exchange process was slightly higher than the value calculated for [Pt(phen)(**L5**)]$(PF_6)_2$ (10.8 kcal mol^{-1}). This difference in the energy barrier was most likely a consequence in the switch of mechanism between the two systems. The $\Delta G^{\ddagger}$ value for the fluxional ligand exchange process in [Pt(phen)(**L6**)]$(PF_6)_2$ was higher than that observed in [Pt(phen)([9]aneS_3)]$(PF_6)_2$ (9.1 kcal mol^{-1}) presumably for the same reasons outlined in Section 2.3.3.

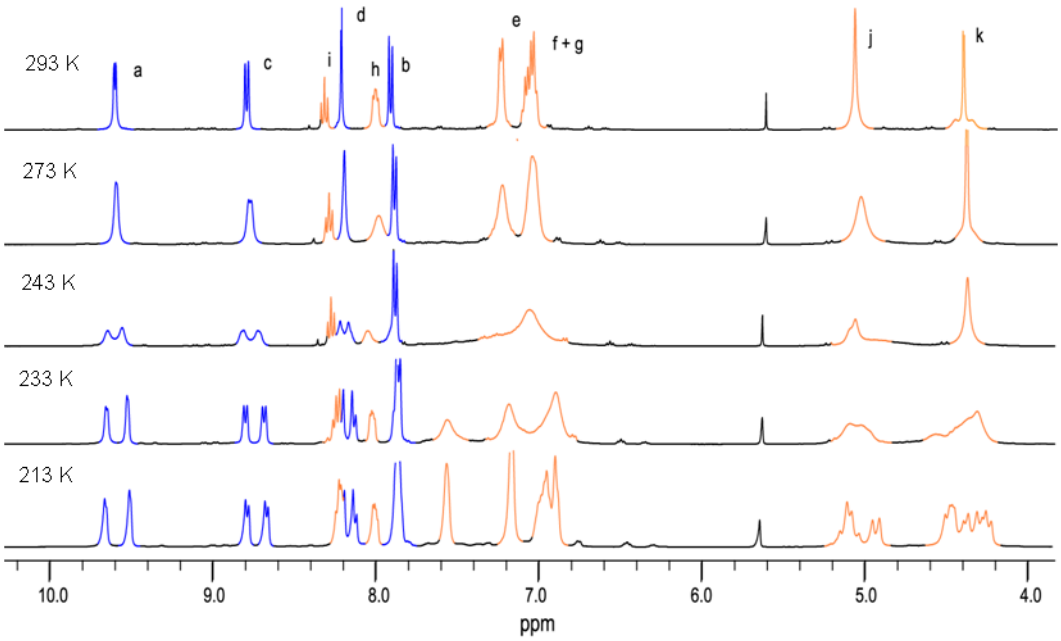

Figure 2.7 VT ^{1}H NMR spectra of [Pt(phen)(**L6**)]$(PF_6)_2$ in (400 MHz, [D_6]-acetone, 298 K). The assignments and colouring of peaks correspond to those shown in Scheme 2.11.

Resonance	T_c (K)	$\Delta\nu_o$ (Hz)	k_{obs} (s^{-1})	$\Delta G^{\ddagger}$ (kcal mol^{-1})
H_a	250	53 ± 3	118 ± 7	12.2 ± 0.05
H_c	253	46 ± 2	102 ± 5	12.4 ± 0.02
H_d	249	24 ± 2	53 ± 5	12.5 ± 0.07
H_e	248	244 ± 12	542 ± 27	11.4 ± 0.09
H_f	240	55 ± 3	123 ± 7	11.7 ± 0.04
				12.0 ± 0.04[a]

Table 2.3 Estimation of kinetic parameters for the fluxional ligand exchange process in [Pt(phen)(**L6**)]$(PF_6)_2$ in [D_6]-acetone from VT ^{1}H NMR studies. [a]Average value for $\Delta G^{\ddagger}$.

To investigate the role of solvent in the fluxional ligand exchange process, a ^{1}H NMR spectrum of [Pt(phen)(**L6**)]$(PF_6)_2$ was taken in 4:1 CD_2Cl_2:[D_2]-tetrachloroethane (Figure 2.8). Broad peaks at δ 4.7 and δ 4.1, which corresponded to H_{j+k} protons respectively, and a broad singlet at δ 7.9, corresponding to H_h, suggested that the ligand exchange process, which was fast on the NMR timescale, did operate even in non-coordinating solvents. The observed equivalence of the phenanthroline protons, H_{a-d}, indicated that despite changing the coordinating nature of the solvent, stereomutation was persisting. The observed ligand substitution reaction operating in [Pt(phen)(**L6**)]$(PF_6)_2$ therefore does not appear to proceed *via* a solvent mediated mechanism. A VT ^{1}H NMR study of the ligand substitution reaction was undertaken to determine k and $\Delta G^{\ddagger}$ for [Pt(phen)(**L6**)]$(PF_6)_2$ in 4:1 CD_2Cl_2:[D_2]-tetrachloroethane (Figure 2.8). Upon cooling, it was observed that the ligand exchange process became slow on the NMR timescale. The splitting of the resonance peaks, H_a and H_h, was observed upon cooling of the system with coalescence being reached at 240 K (H_a) and 254 K (H_h). These two latter resonance peaks, H_a and H_h, were used to determine values for k and $\Delta G^{\ddagger}$ for the ligand exchange process (Section 2.6.3c). From this data, the $\Delta G^{\ddagger}$ value for the fluxional ligand exchange process was estimated (using a modified Eyring equation, Section 2.6.3) to be 12.1 ± 0.06 kcal mol^{-1} (Table 2.4). This value for $\Delta G^{\ddagger}$ closely matched that obtained for the fluxional ligand exchange process for [Pt(phen)(**L6**)]$(PF_6)_2$ in [D_6]-acetone (12.0 kcal mol^{-1}) which established that the mechanism was solvent independent.

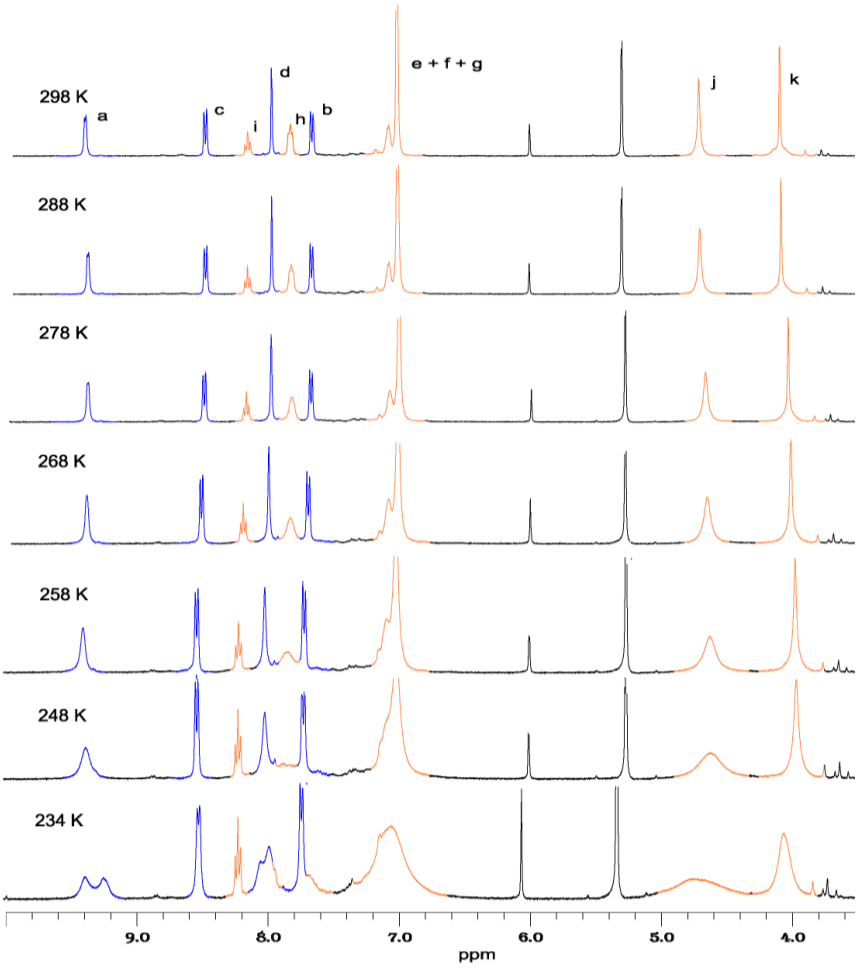

Figure 2.8 VT ^{1}H NMR spectra (400 MHz, 4:1 CD_2Cl_2:[D_2]-tetrachloroethane, 298 K). The assignments and colouring of peaks correspond to those shown in Scheme 2.11.

Resonance	T_c (K)	$\Delta\nu_o$ (Hz)	k_{obs} (s^{-1})	$\Delta G^{\ddagger}$ (kcal mol^{-1})
H_a	240	41 ± 2	92 ± 6	11.8 ± 0.04
H_h	254	38 ± 2	85 ± 5	12.5 ± 0.06
				12.1 ± 0.06[a]

Table 2.4 Estimation of kinetic parameters for the fluxional ligand exchange process in [Pt(phen)(**L3**)]$(PF_6)_2$ in 4:1 CD_2Cl_2:[D_2]-tetrachloroethane from VT ^{1}H NMR studies. [a]Average value for $\Delta G^{\ddagger}$.

2.4 Conclusions

A ligand exchange reaction between [Pt(phen)([9]aneS$_3$)][PF$_6$]$_2$ and a deuterated analogue of the thioether crown, [D$_4$]-[9]aneS$_3$, has determined that there is a marked difference in relative rates for the inter- and intramolecular ligand exchange processes displayed by this complex. The dominance of the intramolecular mechanism led to high processivity of the observed molecular motion. As such, [Pt(phen)([9]aneS$_3$)][PF$_6$]$_2$ can be thought of as a prototype non-biased molecular rotor. Reported kinetic parameters of the ligand exchange process in [Pt(phen)([9]aneS$_3$)][PF$_6$]$_2$ have been employed to calculate the number of steps (and full rotations) undertaken by the [9]aneS$_3$ rotor around the phenanthroline stator at various time intervals. The novel complex, [Pt(phen)(**L5**)](PF$_6$)$_2$, has been synthesized and unambiguously characterized by mass spectrometry, NMR spectroscopy and X-ray crystallography. A ligand exchange reaction between [Pt(phen)(**L5**)](PF$_6$)$_2$ and a deuterated analogue of the thioether ligand, [D$_{14}$]-**L5**, established that there was a significant difference in relative rates of the inter- and intramolecular ligand exchange although not as marked as with [Pt(phen)([9]aneS$_3$)][PF$_6$]$_2$. As in the molecular rotor system, the intramolecular ligand exchange process dominates. The kinetic parameters, k and $\Delta G^{\ddagger}$, have been calculated for the identified ligand exchange process using a series of VT ^{1}H NMR experiments. From this data, the distance travelled by the Pt(phen) moiety of [Pt(phen)(**L5**)](PF$_6$)$_2$ along **L5**, in a processive manner, has been determined to establish that over a period of hours impressively large distances on the molecular scale are traversed. A second non-interlocked, unbiased molecular shuttle, [Pt(phen)(**L6**)](PF$_6$)$_2$, has been synthesised and the operation of a fluxional ligand substitution reaction, which was rapid on the NMR timescale at ambient temperature, has been established. Determination of the kinetic parameters, k and $\Delta G^{\ddagger}$, for the ligand exchange reaction has been undertaken *via* a series of VT NMR experiments. Interestingly, stereomutation of the ligand exchange process was observed for [Pt(phen)(**L6**)](PF$_6$)$_2$, in both coordinating and non-coordinating solvents, indicating that different mechanisms operate for the substitution reactions in the two novel complexes, [Pt(phen)(**L5**)](PF$_6$)$_2$ and [Pt(phen)(**L6**)](PF$_6$)$_2$.

2.5 References and Notes

[1] (a) M. C. Alonso, D. R. Drummond, S. Kain, J. Hoeng, L. Amos, R. A. Cross; *Science,* 2007, **316**, 120; (b) C. L. Asbury; *Curr. Opin. Cell. Bio.,* 2005, **17**, 89; (c) K. Svoboda, C. F. Schmidt, B. J. Schnapp, S. M. Block; *Nature,* 1993, **365**, 721; (d) R. D. Vale, T. S. Reese, M. P. Sheetz; *Cell,* 1985, **42**, 39.

[2] (a) K. Kinbara, T. Aida; *Chem. Rev.,* 2005, **205**, 1377; (b) R. B. Case, D. W. Pierce, N. Hom-Booher, C. L. Hart, R. D. Vale; *Cell*, 1997, **90**, 959; (c) A. Yildiz, P. R. Selvin; *Trends in Cell Biology,* 2005, **15**, 112; (d) W. O. Hancock, J. Howard; *Proc. Nat. Acad. Sci. USA.,* 1999, **96**, 13147.

[3] (a) S. S. Rosenfield, P. M. Fordyce, G. M. Jefferson, P. H. King, S. M. Block; *J. Bio. Chem.,* 2003, **278**, 18550; (b) S. Sack, F. J. Kull, E. Mandelkow; *Eur. J. Biochem.,* 1999, **262**, 1; (c) J. Howard, A. J. Huspeth, R. D. Vale; *Nature*, 1989, **342,** 154; (d) S. S. Rosenfield, B. Rener, J. J. Correia, M. S. Mayo, H. C. Cheung; *J. Bio. Chem.,* 1996, **271**, 9473.

[4] (a) E. R. Kay, D. A. Leigh, F. Zerbetto; *Angew. Chem. Int. Ed.,* 2007, **46**, 72; (b) V. Balzani, F. Credi, F. M. Raymon, J. F. Stoddart; *Angew. Chem. Int. Ed.;* 2000, **39**, 3348; (c) Special issue on "Molecular Machines": *Acc. Chem. Res.* 2001*,* **34***,* 409; (d) S. Kottas, L. I. Clarke, D. Horinek, J. Michl, *Chem. Rev.,* 2005, **105**, 1281; (e) A. H. Flood, R. J. A. Ramirez, W. –Q. Deng, R. P. Muller, W. A. Goddard, J. F. Stoddart; *Aust. J. Chem.,* 2004, **57,** 301; (f) W. R. Browne, B. L. Fergina; *Nature Nanotech.,* 2006, **1**, 25.

[5] (a) N. Armaroli, V. Balzani, J. –P. Collin, P. Gavina and J. –P. Sauvage, *Angew. Chem. Int. Ed.,* 2007, **121**, 4397 (b) P. Gavina and J. –P. Sauvage ; *Tetrahedron Lett.,* 1997, **38**, 3521 ; (c) F. Durola, and J. –P. Sauvage, *Angew. Int. Ed. Chem.* 2007, **46**, 3537; (d) J. –P. Collin, F. Durola and J. –P. Sauvage, *Angew. Chem. Int. Ed.* 2009, **48**, 8532. (e) J. –P Collin, V. Heitz, S. Bonnet and J. –P Sauvage, *Inorg. Chem. Comm.* 2005, **8**, 1063; (f) D.

Pomeranc, D. Jouvenot, J. –C. Chambron, J. –P. Collin, V. Heitz, J. –P. Sauvage, *Chem. – Eur. J.,* 2003, **11**, 4247.

[6] (a) R. A. Bissell, E. Córdova, A. E. Kaifer, J. F. Stoddart, *Nature,* 1994, **369**, 133. (b) A. M. Elizarov, S. –H. Chiu, J. F. Stoddart; *J. Org. Chem.,* 2002, **67**, 9175; (c) H. -R Tseng, S. A. Vignon, J. F. Stoddart; *Angew. Chem. Int. Ed.* 2003, **42**, 1491; (d) P. L. Anelli, N. Spencer, J. F. Stoddart; *J. Am. Chem. Soc.,* **113**, 5131; (e) P. R. Ashton**,** M. R. Johnston, J. F. Stoddart; *Chem. Comm.,* 1992, 1128.

[7] (a) A. Altieri, G . Bottari, F. Dehez, D. A. Leigh, J. K. Y. Wong, F. Zerbetto, *Angew. Chem. Int. Ed.,* 2003, **42**, 2296; (b) W. Clegg, C. Gimenez-Saiz, D. A. Leigh, A. Murphy, A. M. Z. Slawin, S. J. Teat; *J. Am. Chem. Soc.,* 1999, **121**, 4124; (c) C. M. Keaveney, D. A. Leigh; *Angew. Chem. Int. Ed.,* 2004, **43**, 1222; (d) A. Altieri, G . Bottari, F. Dehez, D. A. Leigh, J. K. Y. Wong, F. Zerbetto, *Angew. Chem.,* 2003, **115**, 2398; (e) C. M. Keaveney, D. A. Leigh; *Angew. Chem.,* 2004, **116**, 1242; (f) J. V. Hernández, E. R. Kay, D. A. Leigh; *Science*, 2004, **306**, 1532; (g) D. A. Leigh, J. K. Y. Wong, F. Zerbetto, *Nature,* 2003, **424**, 174.

[8] (a) C. A. Steiner, S. J. Alderman, D. W. Claridge, H. L. Anderson; *J. Am. Chem. Soc.,* 2002, **41**, 1769; (b) H. Murakami, A. Kawabuchi, R. Matsumoto, T. Ido, N. Nakashima; *J. Am. Chem. Soc.,* 2005, **127**, 15891; (c) H. Murakami, A. Kawabuchi, M/. Kotoo, M. Kunitake, N. Nakashima; *J. Am. Chem. Soc.,* 1997, **119**, 7605.

[9] (a) A. H. Flood, A. J. Peters, S. A. Vignon, D. W. Steuerman, H. –R. Tseng, S. Kang, J. R. Heath, J. F. Stoddart; *Chem. -Eur. J.,* 2004, **10**, 6558; (b) H. –R. Tseng, S. A. Vignon, J. F. Stoddart; *Angew. Chem. Int. Ed.,* 2003, **42**, 1491.

[10] (a) P. R. Ashton, R. Ballardini, V. Balzani, A. Credi, K. R. Dress, E. Ishow, C. J. KlE. Everlaan, O. Kocian, J. A. Preece, N. Spencer, J. F. Stoddart, M Venturi, S. Wenger; *Chem. –Eur. J.,* 2000, **6**, 3558; (b) V. Balzani, M.

Clemente-León, A. Credi, M. Semeraro, M. Venturi, H. –R. Tseng, S. Wenger, S. Saha, J. F. Stoddart; *Aust. J. Chem.,* 2006, *59*, 193; (c) V. Balzani, M. Clemente-León, A. Credi, B. Ferrer, M. Venturi, A. H. Flood, J. F. Stoddart; *Proc. Natl. Acad, Sci. USA* 2006, **103**, 1178.

[11] (a) J. D. Crowley, K. D. Hanni, D. A. Leigh, A. M. Z. Slawin, *J. Am. Chem. Soc.,* 2010, **132**, 5309; (b) S. M. Goldup, D. A. Leigh, P. J. Lusby, R. T. McBurney, A. M. Z. Slawin; *Angew. Chem. Int. Ed.,* 2008, **47**, 3381; (c) A. M. Fuller, D. A. Leigh, P. J. Lusby, *J. Am. Chem. Soc.,* 2010, **132**, 4954. (d) J. D. Crowley, D. A. Leigh, P. J. Lusby, R. T. McBurney, L.-E. Perret-Aebi, C. Petzold, A. M. Z. Slawin and M. D. Symes, *J. Am. Chem. Soc.* 2007, **129**, 15085; (e) D. A. Leigh, P.J. Lusby, R. T. McBurney and M. D. Symes, *Chem. Commun.*, 2010, **46**, 2382. (f) Y. Furusho, T. Matsuyama, T. Takata, T. Moriuchi, T. Hirao, *Tetrahedron Lett.* 2004, **45**, 9593-9597.

[12] Q. –C. Wang, D. –H. Qu, J. Ren, K. Chen, H. Tian; *Angew. Chem. Int. Ed.,* 2004, **43**, 2661.

[13] For nanomachines composed of artificial DNA which show translational motion see: (a) Y. Tian, C. Mao; *J. Am. Chem. Soc.*, 2004, **126**, 11410; (b) W. B. Sherman, N. C. Seeman; *Nano Lett.*, 2004, **4**, 1203; (c) J. Bath, S. J. Green, A. J. Turberfield; *Angew. Chem. Int. Ed.*, 2005, **44**, 4358; (d) J. –S. Shin, N. A. Pierce; *J. Am. Chem. Soc.*, 2004, **126**, 10834; (e) M. Von Delius, E. M. Geertsema, D. A. Leigh, *Nature Chem.*, 2010, **2**, 96; (f) M. von Delius, E. M. Geertsema, D. A. Leigh, D. –T. D. Tang, *J. Am. Chem. Soc.*, 2010, **132**, 16134; (g) For a recent example of a small molecule that walks down a track see: M. von Delius, E. M. Geertsema, D. A. Leigh, D. –T. D. Tang, *J. Am. Chem. Soc.*, 2010, **132**, 16134; (h) M. J. Barrell, A. G. Campaña, M. von Delius, E. M. Geertsema, D. A. Leigh, D. –T. D. Tang, *Angew. Chem. Int. Ed.*, 2011, **50**, 285.

[14] For systems in which rotary molecular motion is realised through correlated ligand-exchange of silver ions see: (a) S. Hiraoka, K. Harano, T. Tanaka, M. Shiro, M. Shionoya; *Angew. Chem.,* 2003, **115**, 5340; (b) S. Hiraoka, K. Hirata, M. Shionaya; *Angew. Chem.,* 2004, **116**, 3902; (c) S. Hiraoka, K. Harano, T. Tanaka, M. Shiro, M. Shionoya; *Angew. Chem. Int. Ed.,* 2003, **42**, 5182; (d) S. Hiraoka, K. Hirata, M. Shionaya; *Angew. Chem. Int. Ed.,* 2004, **43**, 3814; (e) S. Hiraoka, K. Hirata, M. Shionaya; *J. Am. Chem. Soc.,* 2004, **126**, 1214.

[15] For reports of fluxional ligand exchange processes (metallotrophic shifts) within palladium complexes see: (a) M. A. Alonso, J. A. Casares, P. Espinet, J. M. Martínez-Ilarduya, C. Pérez-Briso; *Eur. J. Inorg. Chem.,* 1998, 1745; (b) R. A. Stockland Jr., G. K. Anderson; *Organometallics*, 1998, **17**, 4694; (c) J. A. Casares, P. Espinet; *Inorg. Chem.,* 1997, **36**, 5428.

[16] For reports of fluxional ligand exchange processes (metallotrophic shifts) within platinum(II) complexes see: (a) A. J. Blake, Y. V. Roberts, M. Schröder, *J. Chem. Soc. Dalton Trans.,* 1996, 1885; (b) M. A. Bennett, A. J. Canty, J. K. Felixberger, L. M. Rendina, C. Sunderland, A. C. Willis; *Inorg. Chem.,* 1993, **32**, 1951; (c) G. J. Grant, J. A. Pool, D. G. VanDerveer; *J. Chem. Soc. Dalton Trans.* 2003, 3981. (d) H. Nikol, H. -B. Bürgi, K. I. Hardcastle, H. B. Gray, *Inorg. Chem.* 1995, **34**, 6319; (e) K. D. Tau, R. Uriarte, T. J. Mazanec, D. W. Meek; *J. Am. Chem. Soc.,* 1979, **101**, 6614; (f) D. E. Jansen, K. N. Patel, D. G. VanDerveer, G. J. Grant; *Chem. Comm.,* 2006, 3540. For reports of fluxional ligand exchange processes (metallotrophic shifts) within palladium and platinum complexes see: (g) D. E. Janzen, D. G. VanDerveer, L. F. Mehne, D. A. De Silva Filho, J. –L. Brédas, G. J. Grant; *Dalton Trans.,* 2007, 1872; (h) G. J. Grant, K. N. Patel, M. L. Helm, L. F. Mehne, D. W. Klinger, D. G. VanDerveer; *Polyhedron*, 2001, 3333.

[17] (a) J. D. Crowley, D. A. Leigh, P. J. Lusby, R. T. McBurney, L.-E. Perret-Aebi, C. Petzold, A. M. Z. Slawin and M. D. Symes, *J. Am. Chem. Soc.* 2007,

129, 15085; (b) D. A. Leigh, P. J. Lusby, R. T. McBurney and M. D. Symes, *Chem. Commun.*, 2010, **46**, 2382.

[18] For platinum(II) terpyridine-based complexes see: (a) S. Kogularaman, A. J. P. White, V. Ramun, *Inorg. Chem.,* 2010, **48**, 9427; (b) S. D. Cummings, *Coordination Chemistry Reviews,* 2009, **253**, 449; (c) W. K. Man-Chung, Y. V. Wing-Wah, *Coordination Chemistry Reviews,* 2007, **251**, 2477; For recent examples of platinum(II)-NCN pincer ligands see (a) K. L. Garner, L. F. Parkes, J. D. Piper, J. A. G. Williams, *Inorg. Chem.,* 2010, **49**, 476; (b) B. Wieczonek, B. Lemcke, H. P. Dijkstra, M. R. Egmond, R. J. M. K. Gebbink, G. van Kolter, *Eur. J. Inorg. Chem.,* 2010, **13**, 1929.

[19] (a) G. W. V. Cave, F. P. Fanizzi, R. J. Deeth, W. Errington, J. P. Rourke, *Organometallics*, 2000, **19**, 1355; (b) J. D. Crowley, I. M. Steele, B. Bosnich, *Inorg. Chem.,* 2005, **44**, 2989.

[20] D. H. Cai, D. L. Hughes, T. R. Verhoeven; *Tetrahedron Lett.,* 1996, **37**, 2537.

[21] K. Sonogashira, Y. Tohda, N. Hagihara, *Tetrahedron Lett.,* 1975, **16**, 4467.

[22] A. Weissberg, A. Dahan, M. Portnoy; *J. Comb. Chem.,* 2001, **3**, 154.

[23] T. Bunlaksananusurn, K. Polburn, P. Knochel; *Angew. Chem. Int. Ed.,* 2003, **42**, 3941.

[24] G. T. Morgan, F. H. Burstall; *J. Chem. Soc.,* 1934, 965.

[25] P. J. Blower, S. R. Cooper; *Inorg. Chem.* 1987, **26**, 2009.

[26] We will estímate the error in calculating the ratio from ^{1}H NMR signals to be ±5%.

[27] (a) L. R. Hanton, K. Lee; *Inorg. Chem.,* 1999, **38**, 1634; (b) C. Viñas, P. Anglès, G. Sánchez, N. Lucena, F. Teixidor, L. Escriche, J. Casabó, J. F.

Piniella, A. Alvarez-Larena, R. Kivekäs, R. Sillanpää, *Inorg. Chem.,* 1998, **37**, 701; (c) P. Chakraborty, S. Kumar Chandra, A. Chakravorty; *Organometallics,* 1993, **12**, 4726; (d) M. A. Bennett, L. Y. Goh, A. C. Willis, *J. Am. Chem. Soc.,* 1996, **118**, 4984.

[28] (a) A. J. Blake, A. J. Holder, T. I. Hyde, T. I. Küppers, H. –J. Schröder, M. Stötzel, K. Wieghardt, *Chem. Comm.,* 1989, 1600.

[29] The freezing point of $[D_2]$-tetrachloroethane is -36 °C and whilst a mixed solvent system of $[D_2]$-tetrachloroethane:CD_2Cl_2 0.4:0.1 was used and it was not possible to acquire data below -39 °C.

[30] It should also be noted that whilst it was clear that the signals corresponding to H_{p+q} at δ 3.8 were observed to augment over time and the concomitant reduction of the resonances for H_i and H_l at δ 7.5 and δ 4.3 respectively was noted, these signals could be used only to qualitatively follow the progress of the substitution reaction. They were however not useful for quantitative interpretation due to the complexity of analysis of the resonances caused by the overlapping of peaks.

[31] R. A. Henderson, *The Mechanisms of Reactions at Transition Metal Sites, Oxford University Press,* **2000**, pp 15-21.

[32] M. Winn, E. B. Reilly, G. Liu, J. R. Huth, H. –S. Jae, J. Freeman, Z. Pei, Z. Xin, J. Lynch, J. Kester, T. W. von Geldern, S. Leitza, P. DeVries, R. Dickinson, D. Mussatto, G. F. Okasinski; *J. Med. Chem.,* 2001, **44**, 4393.

[33] The molecular ion peak for in [Pt(phen)(**L6**)](PF_6) was not observed in the spectrum unlike in the electrospray mass spectroscopy study of the analogous complex, [Pt(phen)(**L5**)](X) (where X = Cl and PF_6), both were present.

[34] R. S. Berry; *J. Chem. Phys.,* 1960, **32**, 933-938.

[35] For examples of reports of possible turnstile mechanisms in palladium(II) complexes see: (a) S. Noda, A. Nakamura, T. Kochi, L. W. Chung, K.

Morokuma, K. Nozaki; *J. Am. Chem. Soc.,* **2009**, *131*, 14088; (b) Casares, J. A.,; Espinet, P.; *Inorg. Chem.* **1997**, *36*, 5428; (c) J. A. Casares, P. Espinet, K. Soulantica, I. Pascual, A. G. Orpen; *Inorg. Chem.* **1997**, *36*, 5251.

[36] I. Ugi, D. Marquarding, H. Klusacek, P. Gillespie, *Acc. Chem. Res.,* 1971, **4**, 288.

[37] For examples of reports of possible turnstile mechanisms in platinum(II) complex (wherein the complex is a dimeric platinum(II) species) see: S. Otto, P. Samuleev, V. A. Polyakov, A. Ryabov, L. I. Elding; *Dalton, Tran.,* 2004, 3662.

[38] I. Ugi, D. Marquarding, H. Klusacek, G. Gokel, P. Gillespie, *Angew. Chem. Int. Ed.,* 1970, **9**, 703.

[39] (a) F. Ramirez, F. Ugi, S. Lin, P. Pfohl, D. Hoffman, D. Marquarding; *Tetrahedron*, 1974, **30**, 371; (b) P. D. Hampton, C. E. Daitch, T. M. Alam, Z. Bencze, M. Rosay; *Inorg. Chem.,* 1994, **33**, 4750.

[40] E. W. Abel, A. Gelling, K. G. Orrell, A. G. Osborne, V. Sik, *Chem. Comm.*, 1996, 2329.

CHAPTER THREE

Dual Stimuli-Responsive Interconvertable Heteroleptic Platinum Coordination Modes

Published as "*Dual Stimuli-Responsive Interconvertable Heteroleptic Platinum Coordination Modes*"

Sarah J. Pike, Paul J. Lusby, *Chem. Comm.* **2010**, *46*, 8338-8340.

Acknowledgements

The following people are gratefully acknowledged for their contribution to this chapter: Dr. Patricia Richardson for her guidance and invaluable advice regarding the TD-DFT calculations and kinetic studies and I would also like to thank the Leigh group for the use of their photoreactor. Professor Alexandra Slawin is gratefully acknowledged for solving the crystal structures of [**L**Pt($PyNMe_2$)] and [*cis*-H**L**Pt($PyNMe_2$)OTs]. Dr. Paul Lusby and Gordon Nimmo-Smith are gratefully thanked for their proof-reading of this chapter.

Synopsis

Synthetic molecular shuttles are systems which are able to display controlled, large amplitude translational motion of their sub-molecular components in response to the application of an external stimulus. The operational basis for these systems is often a non-covalent (supramolecular) or transition metal-ligand motif which undergoes a reversible change. In nearly all reported cases, this stimulus serves to adjust the thermodynamic bias of the equilibrium. However, in order to develop synthetic molecular machines which are more sophisticated than simple molecular switches, control over the kinetics of the reversible event needs to be demonstrated. In this chapter, the switchable behaviour of a metal-ligand coordination motif is reported in which a proton input is employed to modify the overall thermodynamic bias and light is orthogonally utilized to selectively lower the energetic barrier for the binding event to re-equilibration.

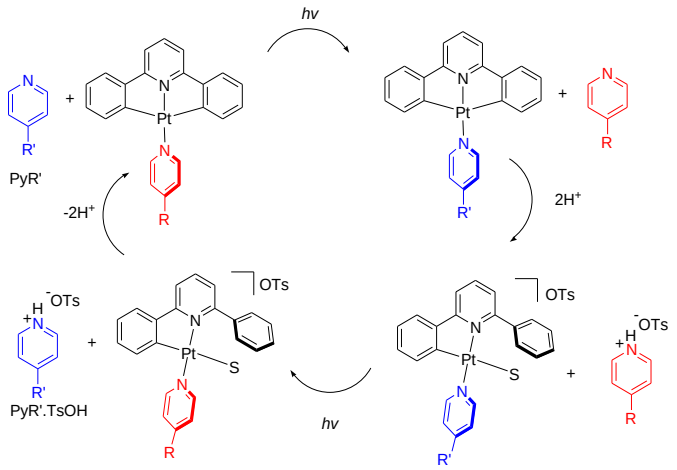

TD-DFT calculations have been undertaken on these cyclometallated platinum(II) complexes, in a range of solvents, to ascertain the low lying singlet and triplet excited states present. Additionally, these calculations have identified electronic transitions which could compliment the dissociative mechanism anticipated for the ligand exchange process under irradiative conditions. Kinetic studies on the selective ligand exchange process have been undertaken with the application of a range of broad band irradiation of differing energies to determine the effect of the light source on the reaction kinetics.

3.1 Introduction

Biological molecular motors, such as kinesin[1] and dynein[2] which are responsible for cellular transport, eloquently demonstrate Natures' ability to accomplish controlled motion at the molecular level in order to perform tasks. They have also provided the inspiration for a generation of synthetic systems; namely artificial devices such as molecular machines[3] in which controlled molecular motion has also been realised. The net positional change in these reported systems is achieved as a result of the reversible modulation of the binding affinity of the sub-molecular components *via* modification of non-covalent or metal-ligand interactions upon application of an external stimulus.[4] In nearly all reported cases,[5] the stimulus functions by adjusting the thermodynamic position of the equilibrium; in systems which rely upon exclusively weak interactions such as hydrogen-bonding,[6] hydrophobic[7] or π-π interactions,[8] re-equilibration often occurs very quickly such that out-of-equilibrium states cannot be easily detected. However, for architectures which utilise transition metal-ligand interactions the relaxation from out-of-equilibrium states often occurs on a much slower timescale, minutes, hours or even days.[9,10] As such, metastable states, which have been shown to be important in molecular electronics[11] and machine ratcheting mechanisms,[12] can be observed or even isolated. These metastable systems require the input of heat to overcome the kinetic barrier of re-equilibration. Nevertheless heat cannot be referred to as a "kinetic stimulus" as it does not adjust the magnitude of this barrier but rather serves to provide surplus energy to attain re-equilibration more rapidly.[9,10,13] However, the development of more sophisticated molecular machines requires systems in which control over the kinetics of exchange and hence transportation pathways can be displayed.

In this chapter, the switchable behaviour of heteroleptic, acceptor-donor-type platinum coordination complexes is reported. The orthogonal use a proton input to adjust the equilibrium position and exploitation of light to selectively lower the energetic barrier to re-equilibration is described. A discussion of the light-promoted ligand exchange reaction will also be presented, supported by a combination of TD-DFT calculations and kinetic studies as a function of wavelength excitations.

3.2 Results and Discussion

3.2.1 [LPt(PyR)] + PyR' ⟹ [LPt(PyR')] + PyR

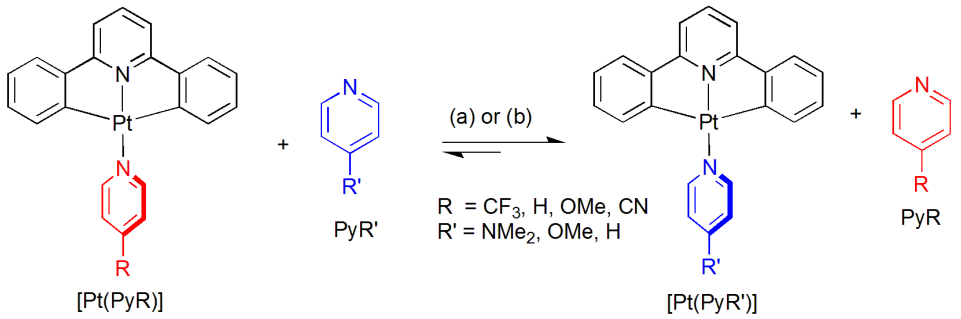

Scheme 3.1 Ligand exchange reaction between Pt coordinated PyR and initially uncoordinated PyR' in the cyclometallated C^N^C complex, [**L**Pt(PyR)]. All reactions carried out at 0.01 M in 1:1 [D_7]-DMF:CD_2Cl_2 at 313 K either in the (a) presence or (b) absence of light (broad band 275-375 nm with λ_{max} = 312 nm).

The system under study aimed to combine the preference of group 10 transition metals to selectively bind heterocycles as a function a basicity,[9,14] a thermodynamic bias that can be reversed by the addition of an equivalent of acid,[9] with the known photochemical lability of 2nd and 3rd row transition metals. While light-promoted ligand exchange is well documented for Ru(II),[15] in particular, it has recently been shown that the rates of Pt(II) substitution can also be increased upon photoirradiation.[16] In order to control the selective exchange of just a single ligand, the neutral platinum motif[17] [**L**Pt(PyR)] (Scheme 3.1) was investigated as it was envisaged that the tridentate, doubly charged $\mathbf{L}^{2-}$ would not undergo dissociation from the platinum centre on exposure to light.

The thermodynamically downhill exchange of $PyNMe_2$ for the 4-trifluoromethylpyridine ligand ($PyCF_3$) of [**L**Pt($PyCF_3$)], (H_2**L** = 2,6-diphenylpyridine) which was prepared from known [**L**Pt(DMSO)],[17] was initially investigated (Table 3.1, Entries 1 and 2). Upon broad band 275-375 nm irradiation (with a λ_{max} of 312 nm, Figure 3.11) of a 0.01 M solution of [**L**Pt($PyCF_3$)] and $PyNMe_2$ in 1:1 [D_7]-DMF:CD_2Cl_2, a steady-state equilibrium

of 11:89 [**L**Pt($PyCF_3$)]:[**L**Pt($PyNMe_2$)] was obtained after 4.5 h (Entry 1). The ligand exchange experiment was followed directly by ^{1}H NMR spectroscopy (Figure 3.1), through the disappearance of the coordinated *ortho* protons of the $PyCF_3$ ligands at δ 9.5 and the concomitant appearance of a signal at δ 8.6 which could be assigned to coordinated $PyNMe_2$. Moreover, the emergence of the peak for the *ortho* protons of liberated $PyCF_3$ at δ 8.9 at the expense of the peak for the *ortho* protons of initially unbound $PyNMe_2$ at δ 8.4 was clearly evident. To assess the effect of light, the reaction was also carried out under identical conditions (0.01 M in 1:1 [D_7]-DMF:CD_2Cl_2, 313 K) but in the dark. The reaction of $PyNMe_2$ with [**L**Pt($PyCF_3$)] took 44 h to reach an equilibrium ratio of 15:85 (Entry 2) which was within error of the ratio obtained under irradiative conditions,[18] indicating that light significantly lowers the activation barrier to exchange without perturbing the relative ground state energies.

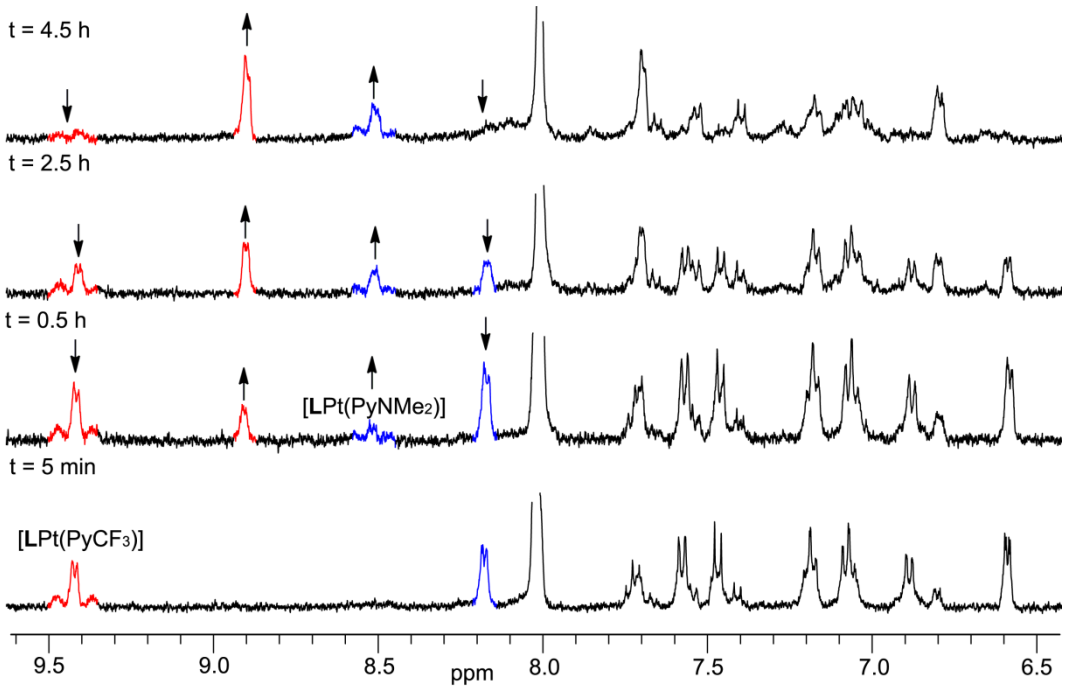

Figure 3.1 Partial ^{1}H NMR spectra (400 MHz, 1:1 [D_7]-DMF:CD_2Cl_2, 300 K) showing the photochemical reaction (upon broad band irradiation 275-375 nm with λ_{max} = 312 nm) between [**L**Pt($PyCF_3$)] and $PyNMe_2$ over time. The *ortho* pyridyl protons of [**L**Pt($PyNMe_2$)] and free $PyNMe_2$ are highlighted in blue and the *ortho* pyridyl protons of [**L**Pt($PyCF_3$)] and free $PyCF_3$ in red.

To investigate the effect of the pK_a difference of the two exchangeable heterocycles on both the thermodynamic bias and the rate of equilibration, the reaction of $PyNMe_2$ and [**L**Pt(PyR)] (where R = H, OMe (PyOMe = 4-methoxypyridine) and CN (PyCN = 4-cyanopyridine)) were also investigated (Table 3.1, Entries 3-8). Under the same conditions (0.01 M, 1:1 [D_7]-DMF:CD_2Cl_2) the exchange between [**L**Pt(PyR)] and initially unbound $PyNMe_2$ upon light irradiation for 10.5 h (R = H), 11 h (R = OMe) and 2.5 h (R = 2.5 h) steady-state equilibria of 17:83 (R = H), 33:67 (R = OMe) and 9:91 (R = CN), [**L**Pt(PyR)]:[**L**Pt($PyNMe_2$)] (Entries 3, 5 and 7) were obtained. In the absence of light, equilibration of [**L**Pt(PyH)] with $PyNMe_2$ at the same temperature (313 K) gave a ratio of 28:72 after 11 days (Entry 4). However, the sluggishness of the thermal exchange process (even at 333 K), coupled with the slow but steady decomposition of the complexes that occurred after further, prolonged heating, meant that this reaction could not be followed to completion. For this reason, the reaction under non-irradiative conditions for the other exchange processes (with differing R substitutents) were not monitored to completion as it was presumed that decomposition would invalidate the results. Instead, the progress of the reaction was followed by ^{1}H NMR spectroscopy for the same amount of time required to reach equilibriation upon irradiation for each individual reaction. Accordingly it was found that after 11 h heating at 313 K (R = OMe) and 2.5 h (R = CN) ratios of 75:25 (R = OMe) and 78:22 (R = CN), for [**L**Pt(PyR)]:[**L**Pt($PyNMe_2$)] (Entries 6 and 8) were attained. As expected for the ligand exchange reaction between $PyNMe_2$ and [**L**Pt(PyR)] (where R = OMe, H, CF_3 and CN) an increase in the pK_a difference between the two interchangeable ligands leads to a larger thermodynamic bias in favour of coordination of the more basic nitrogen donor (Table 3.1, Entries 1-8). This would seem to indicate that the strength of binding of the heterocycle to the platinum is dominated by σ-donation of the pyridyl lone pair and that the π-back bonding nature of the heterocyclic ligand is less important. Additionally, a distinct rate enhancement in the kinetics of this exchange process was observed under irradiative conditions upon an increase in the pK_a difference between the switchable nitrogen donors (Table 3.1 Entries 1-8). However, the relationship between final thermodynamic

bias and reaction rate does not appears to be that straightforward, for instance when R = CF_3 and CN the thermodynamic bias was strikingly similar; (11:89 vs 9:91) (Table 3.1, Entries 1 and 7) but the time taken to attain steady-state equilibrium under irradiative conditions in each case was quite different; 4.5 h for R =CF_3 (Entry 1) and 2.5 h for R = CN (Entry 7).

To further study the influence of the pK_a difference between the exchangeable heterocycles, the reactions between [**L**Pt(PyR)] and PyR' with a range of *N*-donors (where R' = OMe, H and R = CF_3 and CN) were investigated. For the reactions between [**L**Pt($PyCF_3$)] and PyR' (R' = OMe and H) after irradiative equilibration was complete (16.5 h for R' = OMe, 18.5 h for R' = H) steady-state equilibrium ratios of 25:75 (R' = OMe) and 27:73 (R' = H) [**L**Pt($PyCF_3$)]:[**L**Pt(PyR')] (Entries 9 and 11) were obtained. Both reactions, were undertaken under non-irradiative conditions (16.5 h for R' = OMe and 18.5 h for R' = H) to produce ratios of 61:39 (R' = OMe) and 66:34 (R' = CN), [**L**Pt(CF_3)]:[**L**Pt(PyR')] (Entries 10 and 12). The reaction between [**L**Pt(PyCN)] and PyR' (R = OMe and H) gave ratios of 12:88 (R' = OMe) and 20:80 (R' = H) [**L**Pt(PyCN)]:[**L**Pt(PyR')] after irradiation for 6.5 h (R' = OMe) and 8 h (R' = H) (Entries 13 and 15). Under non-irradiative conditions with heating to 313 K for 6.5 h (R' = OMe) and 8 h (R' = H) steady-state equilibria of 72:28 (R' = OMe) and 90:10 (R' = H) [**L**Pt(PyCN)]:[**L**Pt(PyR')] were observed (Entries 14 and 16). These additional results supported the general trend for the reaction thermodynamics wherein an increase in the pK_a difference of the switchable nitrogen donors led to a more pronounced bias in favour of binding the more basic *N*-heterocycle at the platinum centre. Interestingly, the rate of ligand exchange under irradiative conditions clearly displayed a dependence on the nature of the incoming nucleophile, PyR' (where R' = NMe_2, OMe and H) for the studied ligand exchange reactions. This was most notable for the exchange processes with strongly electron-withdrawing groups in the *para* position of the exchangeable heterocycle (i.e. when R = CF_3 and CN) in [**L**Pt(PyR)] (*cf* Entries 1, 9 and 11 for R = CF_3 and Entries 7, 13 and 15 for R = CN). This displayed dependence of the reaction kinetics on the nature of the incoming nucleophile was indicative of the operation of a mechanism under irradiative conditions

which was to some extent associative in nature and not exclusively dissociative for these neutral cyclometallated platinum(II) complexes.

Entry	Starting Complex Pt(PyR)	Heterocycle PyR'	Pt(PyR): Pt(PyR')	Time (h)	Method
1	[**L**Pt($PyCF_3$)]	$PyNMe_2$	11:89	4.5	A
2	[**L**Pt($PyCF_3$)]	$PyNMe_2$	15:85	44	B
3	[**L**Pt(PyH)]	$PyNMe_2$	17:83	10.5	A
4	[**L**Pt(PyH)]	$PyNMe_2$	28:72	265	B
5	[**L**Pt(PyOMe)]	$PyNMe_2$	33:67	11	A
6	[**L**Pt(PyOMe)]	$PyNMe_2$	75:25	11	B
7	[**L**Pt(PyCN)]	$PyNMe_2$	9:91	2.5	A
8	[**L**Pt(PyCN)]	$PyNMe_2$	78:22	2.5	B
9	[**L**Pt($PyCF_3$)]	PyOMe	25:75	16.5	A
10	[**L**Pt($PyCF_3$)]	PyOMe	61:39	16.5	B
11	[**L**Pt($PyCF_3$)]	PyH	27:73	18.5	A
12	[**L**Pt($PyCF_3$)]	PyH	66:34	18.5	B
13	[**L**Pt(PyCN)]	PyOMe	12:88	6.5	A
14	[**L**Pt(PyCN)]	PyOMe	72:28	6.5	B
15	[**L**Pt(PyCN)]	PyH	20:80	8	A
16	[**L**Pt(PyCN)]	PyH	90:10	8	B

Table 3.1 Equilibrium ratios and equilibration times for the reactions between [**L**Pt(PyR)] and PyR' (where R = OMe, H, CF_3 and CN and R' = NMe_2, OMe and H) under irradiative and non-irradiative conditions at 0.01 M in 1:1 [D_7]-DMF:CD_2Cl_2 at 313 K. Method A: Broad band irradiation (275-375 nm with λ_{max} = 312 nm) Method B: Non-irradiative conditions: In absence of light.[18]

3.2.2 [*cis*-HLPt(PyR)(PyR')]OTs ⇌ [*trans*-HLPt(PyR')(PyR)]OTs

Leigh and co-workers have shown that the preferential binding of heterocycles at a Pd(II) centre can be reversed through the addition of an equivalent of acid.[9] Accordingly, it was envisaged that the thermodynamic bias of the interchangeable *N*-heterocycles at Pt(II) could also be reversed upon the addition of a stiochiometric amount of TsOH. However, investigation of the proton-reponsive behaviour of the neutral pseudo-square planar carboplatinum complex, [**L**Pt($PyNMe_2$)], showed that upon treatment with one equivalent or an excess of TsOH the clean and immediate formation of [*cis*-H**L**Pt($PyNMe_2$)OTs] was observed (Scheme 3.2). During this process, TsOH had effectively added across one of the Pt-C bonds.[19] Moreover, the energetics of the protonation process appear finely balanced as simply treating the newly formed [*cis*-H**L**Pt($PyNMe_2$)OTs] with base, either heterogeneously using K_2CO_3 or in solution with the phosphazene base, P_1-^{t}Bu, resulted in rapid conversion back to the starting material, [**L**Pt($PyNMe_2$)] (Scheme 3.2). This process could be easily monitored using ^{1}H NMR spectroscopy and studies in different deuterium labeled solvents indicated that the TsO^- anion of [*cis*-H**L**Pt($PyNMe_2$)OTs] was readily displaced by better ligands such as pyridine and even acetonitrile.[20]

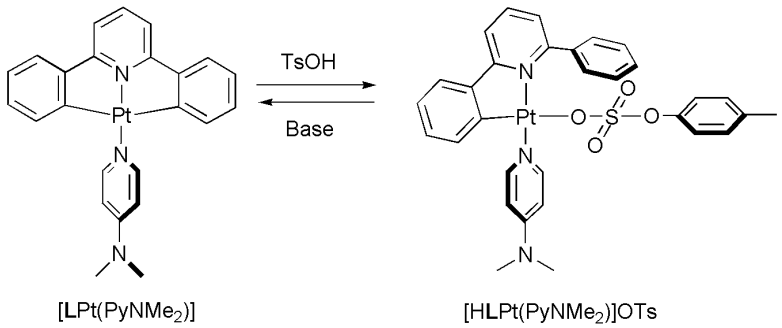

Scheme 3.2 Reversible proton responsive behavior of a platinum coordination mode switching between [**L**Pt($PyNMe_2$)] and [*cis*-H**L**Pt($PyNMe_2$)OTs] upon treatment with acid and base respectively.

The structures of both platinum species, [**L**Pt($PyNMe_2$)] and [*cis*-H**L**Pt($PyNMe_2$)OTs], were confirmed by X-ray crystallography using single crystals grown from hexane and chloroform for [**L**Pt($PyNMe_2$)] and from di-isopropyl ether and chloroform for [*cis*-H**L**Pt($PyNMe_2$)OTs]. It appeared that this process was driven by a slight shortening of the remaining Pt-C bond, from 2.059(11) Å in [**L**Pt($PyNMe_2$)] to 1.955(12) Å in [*cis*-H**L**Pt($PyNMe_2$)OTs], at the expense of the added ligand. The bond between the platinum centre and the monodentate *N*-heterocycle, $PyNMe_2$, was comparable in both complexes; 2.004(11) Å in [*cis*-H**L**Pt($PyNMe_2$)OTs], and 2.044(10) Å in [**L**Pt($PyNMe_2$)]. In [*cis*-H**L**Pt($PyNMe_2$)OTs], unsurprisingly the weakest coordinating group to the metal centre was that of $^{-}$OTs, 2.172(8) Å (Pt-O). Pseudo square planar geometries around the Pt centre were confirmed for both complexes; [**L**Pt($PyNMe_2$)], C1-Pt1-N8 82.1(4), C14-Pt1-N8 81.2(8), C14-Pt1-N19 98.9(4), N19-Pt1-C1 97.8(4) and [*cis*-H**L**Pt($PyNMe_2$)OTs], C1-Pt1-N8 81.8(5), O1-Pt1-N8 99.2(4), O1-Pt1-N19 84.3(4), N19-Pt1-C1 95.6(5).

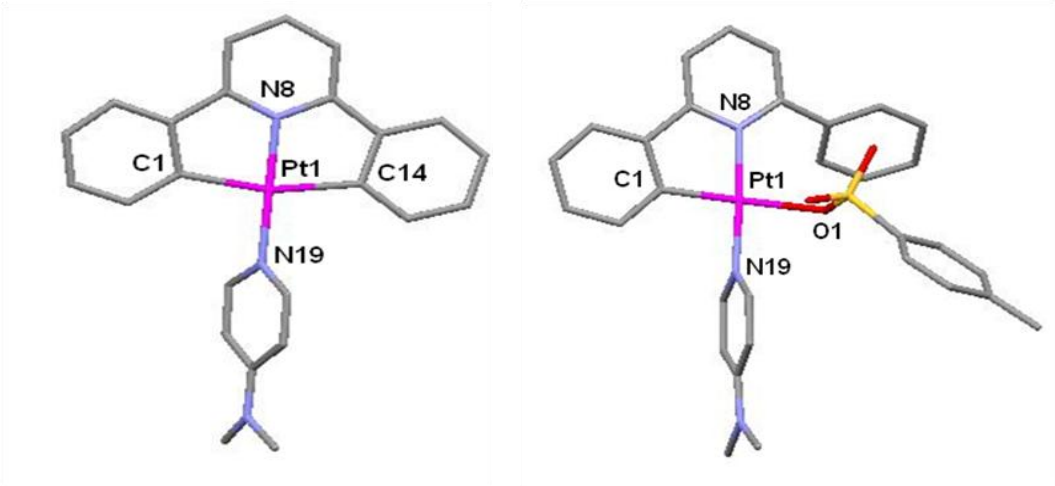

Figure 3.2 a) X-ray crystal structure of [**L**Pt(PyNMe$_2$)]. The carbon atoms of PyNMe$_2$ and **L** in grey, platinum in magenta and nitrogen in pale blue. A chloroform solvent molecule has been removed for clarity. Selected bond lengths [Å] and angles [°]: C1-Pt1 2.059(11), N8-Pt1 1.979(10), C14-Pt1 2.053(10), N19-Pt1 2.044(10), C1-Pt1-N8 82.1(4), C14-Pt1-N8 81.2(8), C14-Pt1-N19 98.9(4), N19-Pt1-C1 97.8(4). b) X-ray crystal structure of [H**L**Pt(PyNMe$_2$)OTs]. The carbon atoms of PyNMe$_2$, **L**, and the tosylate anion are shown in grey, platinum in magenta, nitrogen in pale blue, oxygen in red and sulfur in yellow. Selected bond lengths [Å] and angles [°]: C1-Pt1 1.955(12), N8-Pt1 2.037(12), O1-Pt1 2.172(8), N19-Pt1 2.004(11), C1-Pt1-N8 81.8(5), O1-Pt1-N8 99.2(4), O1-Pt1-N19 84.3(4), N19-Pt1-C1 95.6(5).

The addition of one equivalent of TsOH to a mixture of [**L**Pt(PyR')] and PyR (where PyR' is the more basic heterocycle) did not reverse the coordinative bias of the *N*-heterocycles but instead established an equilibrium (Scheme 3.3) in which [*cis*-H**L**Pt(PyR)(PyR')]OTs was the major species. We reasoned that the stereochemical relationship of the PyR' and PyR ligands with respect to the strong *trans* influence of the phenylato group of H**L**$^-$ would lead to *cis* and *trans* isomers of noticeably different energy. To investigate this, [**L**Pt(PyH)] was initially treated with TsOH and then with PyNMe$_2$[21] to give the presumed higher energy [*cis*-H**L**Pt(PyH)(PyNMe$_2$)]OTs isomer. This existed in equilibrium with [*trans*-H**L**Pt(PyH)(S)]OTs (S = [D$_7$]-DMF) and unbound PyNMe$_2$ as a result of the partial displacement of PyNMe$_2$ by [D$_7$]-DMF in solution. Upon light irradiation of this sample, it could be roughly observed that an increase in [*trans*-H**L**Pt(PyNMe$_2$)(PyH)]OTs was accompanied by a decrease in [*cis*-

H**L**Pt(PyH)(PyNMe$_2$)]OTs (Figure 3.9) with liberation of free PyH also being observed by ^{1}H NMR spectroscopy. However, the complexity of these NMR spectra, caused in part by the unsymmetrical nature of the C^N complexes, prohibited a direct measure of the *cis:trans* complex ratio. Instead, an indirect measure was obtained by treating the samples with P$_1$-^{t}Bu after irradiative equilibration was complete (6.5 h). From this, a ratio of 26:74 [**L**Pt(PyH)]:[**L**Pt(PyNMe$_2$)] was obtained (Table 3.2, Entry 1). For comparison, the non-irradiative reaction produced a ratio of 49:51 after 11 days at 313 K and a further 11 days at 333 K (Table 3.2, Entry 2) however the thermal reaction was stopped before equilibrium due to small amounts of decomposition.

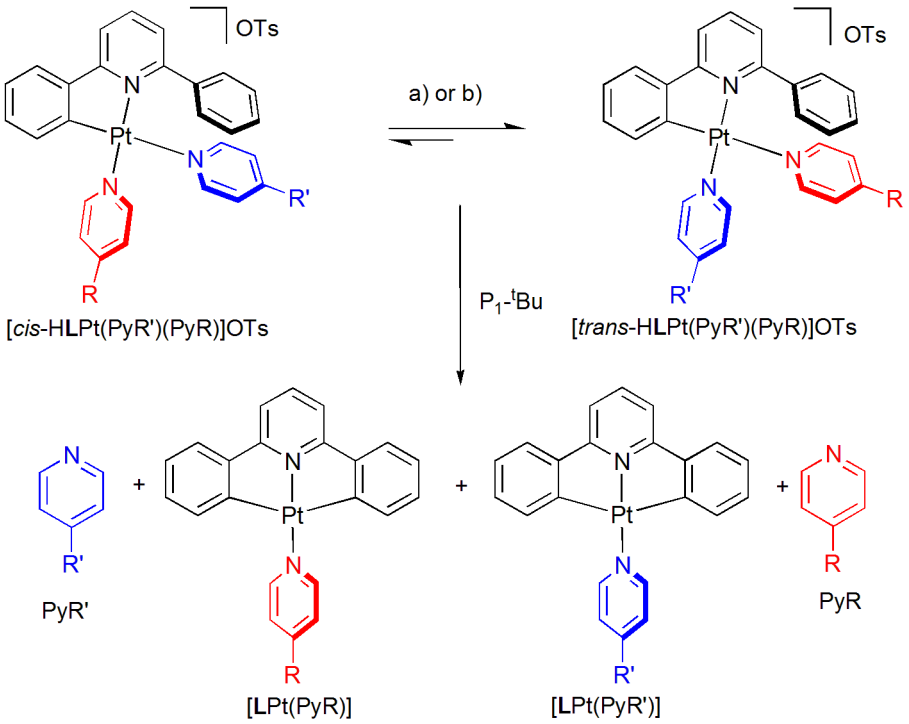

Scheme 3.3 [*cis*-H**L**Pt(PyR)(PyNMe$_2$)]OTs ⇌ [*trans*-H**L**Pt(PyNMe$_2$)(PyR)]OTs followed by base mediated cyclometallation to aid analysis. All reactions carried out at 0.01 M in 1:1 [D$_7$]-DMF:CD$_2$Cl$_2$ at 313 K either in the (a) presence or (b) absence of light (broad band 275-375 nm with λ_{max} = 312 nm).

Having established the success of the ligand exchange process of $PyNMe_2$ for PyH in the charged C^N complex, [*cis*-H**L**Pt(PyH)($PyNMe_2$)]OTs, the exchange reaction for a range of different heterocycles was investigated. Accordingly, the reaction between [**L**Pt(PyR)] (R = OMe, CF_3 and CN) and initially unbound $PyNMe_2$ were investigated following protonation of the initial complex with TsOH (Table 3.2, Entries 3-8). Light irradiation of these samples (9 h for R = OMe, 5 h for R = CF_3 and 4 h for R = CN), followed by the addition of P_1-^{t}Bu to affect cyclometallation, gave steady-state equilibria of 35:65 (R = OMe), 14:86 (R = CN) and 20:80 (R=CF_3) and [**L**Pt(PyR)]:[**L**Pt($PyNMe_2$)] (Entries 3, 5 and 7). The identical protonated thermal reaction, between [**L**Pt($PyCF_3$)] and $PyNMe_2$, gave a ratio of 30:70 [**L**Pt($PyCF_3$)]:[**L**Pt($PyNMe_2$)] after 11 days at 313 K and a further 11 days at 333 K (Entry 8) but the non-irradiative reaction was halted prior to equilibriation due to small amounts of decomposition.[22] Due to this drawback, the exchange processes between $PyNMe_2$ and [**L**Pt(PyR)] (R = OMe and CN) under non-irradiative conditions were not taken to completion but instead were heated at 313 K for the same amount of time taken to reach equilibration under photoirradiation. Hence after 9 h (R = OMe) and 4 h (R = CN) ratios of 84:16 (R = OMe) and 89:11 (R = CN) [**L**Pt(PyR)]:[**L**Pt($PyNMe_2$)] (Entries 4 and 6) were obtained. Clearly, the observed bias reflected the preferential binding of the more basic heterocycle at the stronger coordination site i.e. *trans* to the *N*-donor of H**L**. Unsurprisingly this trend is more pronounced the greater the pK_a difference between the donors. Furthermore, a pronounced rate enhancement was observed under irradiative conditions upon an increase in the pK_a difference between the switchable nitrogen donors (Table 3.2, Entries 1-8).

The reactions of [*cis*-H**L**Pt(PyR')(PyR)]OTs (where R' = OMe, H and R = H, CF_3 and CN) were studied to gain a better understanding of the *cis*-*trans* isomerisation process for these charged systems (Table 3.2, Entries 9-18). The reaction of [*cis*-H**L**Pt(PyH)(PyOMe)]OTs upon broad-band irradiation for 7.5 h, after the addition of base to induce cyclometallation, gave a steady-state equilibrium of 36:64 [**L**Pt(PyH)]:[**L**Pt(PyOMe)] whilst under non-irradiative

conditions for the same length of time gave a ratio of 93:7, [**L**Pt(PyH)]:[**L**Pt(PyOMe)] (Entries 9 and 10). Irradiation of [*cis*-H**L**Pt(PyCF$_3$)(PyR')]OTs (R = OMe and H) for 4.5 h (R' = OMe and H), followed by the addition of P$_1$-^{t}Bu to induce cyclometallation, gave steady-state equilibrium ratios of 21:69 (R' = OMe) and 35:65 (R' = H) [**L**Pt(PyCF$_3$)]:[**L**Pt(PyR')] (Entries 11 and 13). Both reactions, were undertaken under non-irradiative conditions with heating at 313 K, for 4.5 h, to produce ratios of 76:24 (R' = OMe) and 88:12 (R' = H), [**L**Pt(PyCF$_3$)]:[**L**Pt(PyR')] (Entries 12 and 14). Finally, when the reactions between [**L**Pt(PyCN)] and PyR' (R' = OMe and H) were investigated it was found that after irradiation for 4.2 h (R' = OMe) and 4.5 h (R' = H) ratios of 21:79 (R' = OMe) and 23:77 (R' = H), [**L**Pt(PyCN)]:[**L**Pt(PyR')], were obtained (Entries 15 and 17). Meanwhile, ratios of 88:12 (R' = OMe) and 13:87 (R' = H) were observed under non-irradiative conditions with heating at 313 K for 4.2 h (R' = OMe) and 4.5 h (R' = H) (Entries 16 and 18). The thermodynamic bias, to coordinate the most basic heterocycle in the position *trans* to the N of H**L**, is clearly evident and this effect is more pronounced the greater the pK_a difference of the exchangeable donors. Interestingly, the time taken for *cis-trans* isomerisation [*cis*-H**L**Pt(PyR)(PyR')]OTs (where R = CF$_3$ or CN and R' = NMe$_2$, OMe and H) to reach equilibrium under irradiative conditions in each case is comparable, between 4-5 h (Table 3.2, Entries 5, 7, 11, 13, 15 and 17).

Entry	Starting Complex	*cis*:*trans*[a]	Time (h)	Conditions
1	[*cis*-H**L**Pt(PyH)($PyNMe_2$)]OTs	26:74	6.5	A
2	[*cis*-H**L**Pt(PyH)($PyNMe_2$)]OTs	49:51	528[b]	B
3	[*cis*-H**L**Pt(PyOMe)($PyNMe_2$)]OTs	35:65	9	A
4	[*cis*-H**L**Pt(PyOMe)($PyNMe_2$)]OTs	84:16	9	B
5	[*cis*-H**L**Pt(PyCN)($PyNMe_2$)]OTs	14:86	4	A
6	[*cis*-H**L**Pt(PyCN)($PyNMe_2$)]OTs	89:11	4	B
7	[*cis*-H**L**Pt($PyCF_3$)($PyNMe_2$)]OTs	20:80	5	A
8	[*cis*-H**L**Pt($PyCF_3$)($PyNMe_2$)]OTs	30:70	528[b]	B
9	[*cis*-H**L**Pt(PyH)(PyOMe)]OTs	36:64	7.5	A
10	[*cis*-H**L**Pt(PyH)(PyOMe)]OTs	93:7	7.5	B
11	[*cis*-H**L**Pt($PyCF_3$)(PyOMe)]OTs	21:69	4.5	A
12	[*cis*-H**L**Pt($PyCF_3$)(PyOMe)]OTs	76:24	4.5	B
13	[*cis*-H**L**Pt($PyCF_3$)(PyH)]OTs	35:65	4.5	A
14	[*cis*-H**L**Pt($PyCF_3$)(PyH)]OTs	88:12	4.5	B
15	[*cis*-H**L**Pt(PyCN)(PyOMe)]OTs	21:79	4.2	A
16	[*cis*-H**L**Pt(PyCN)(PyOMe)]OTs	88:12	4.2	B
17	[*cis*-H**L**Pt(PyCN)(PyH)]OTs	23:77	4.5	A
18	[*cis*-H**L**Pt(PyCN)(PyH)]OTs	13:87	4.5	B

Table 3.2 Equilibrium ratios and equilibration times for [*cis*-H**L**Pt(PyR)($PyNMe_2$)]OTs $\rightleftharpoons$ [*trans*-H**L**Pt(PyR')(PyR)]OTs under irradiative and non-irradiative conditions. [a]The ratio of *cis:trans* was indirectly measured by converting the corresponding C^N complexes to C^N^C complexes using the base P_1-^{t}Bu, and then by integration of the resultant [**L**Pt(PyR)] and [**L**Pt(PyR')] complexes. [b]264 h at 313 K + 264 h at 333 K. Method A: Broad band irradiation (275-375 nm with λ_{max} = 312 nm) Method B: Non-irradiative conditions: In absence of light.[18]

3.2.3 PyR.TsOH + [*cis*-HLPt(PyR')(S)]OTs $\rightleftharpoons$ PyR'.TsOH + [*cis*-HLPt(PyR)(S)]OTs

To reverse the coordinative bias of the heterocycles, it was anticipated that a second equivalent of acid could be used. Promisingly, the addition of one eq of TsOH to a solution of principally [*trans*-H**L**Pt($PyNMe_2$)(PyH)]OTs resulted in liberation of PyH.TsOH along with formation of a complex we presume to be the solvato complex [*cis*-H**L**Pt($PyNMe_2$)(S)]OTs (where S = [D_7]-DMF). Irradiation of this solution resulted in the emergence of $PyNMe_2$.TsOH and the concomitant reduction of PyH.TsOH (Scheme 3.4). This process was readily monitored by ^{1}H NMR spectroscopy (Figure 3.10). However, due to the complexity of this NMR spectra, a direct measure of the equilibrium position was prohibited, so the sample was treated with P_1-^{t}Bu after equilibration (5.2 h) to affect cyclometallation. From which, the ratio of the steady-state equilibrium was obtained as 70:30 [**L**Pt(PyH)]:[**L**Pt($PyNMe_2$)] (Table 3.3, Entry 1). For comparison, the thermal reaction produced a ratio of 41:59 after 13 days at 313 K and a further 11 days at 333 K but the reaction was impeded from reaching equilibrium due to small amounts of decomposition (Table 3.3, Entry 2).

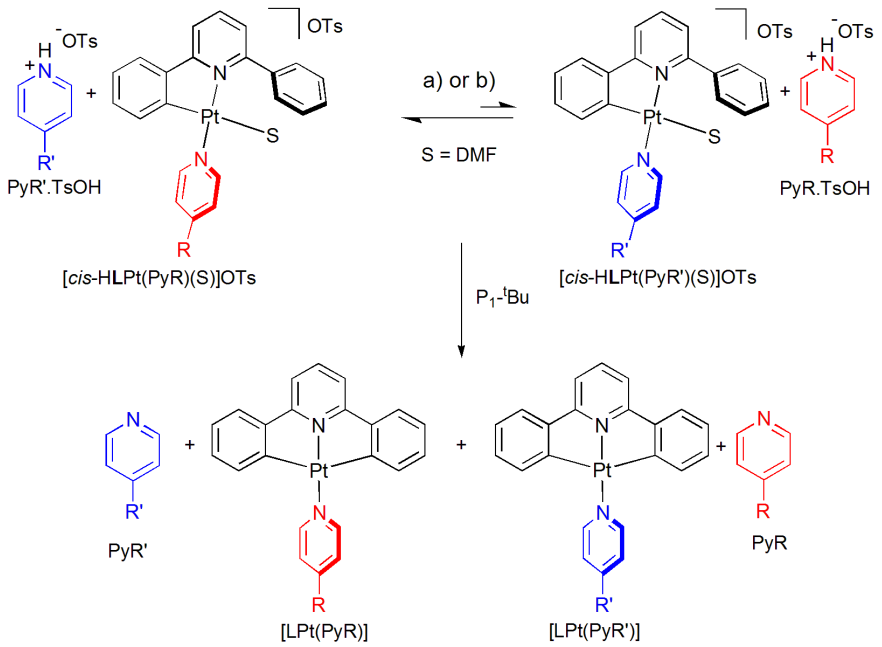

Scheme 3.4 PyR'.TsOH + [*cis*-H**L**Pt(PyR)(S)]OTs ⇌ PyR.TsOH + [*cis*-H**L**Pt(PyR')(S)]OTs followed by base mediated cyclometallation to aid analysis. All reactions carried out at 0.01 M in 1:1 [D_7]-DMF:CD_2Cl_2 at 313 K either in the (a) presence or (b) absence of light (broad band 275-375 nm with λ_{max} = 312 nm).

The reactions between [**L**Pt($PyNMe_2$)] and PyR.TsOH (R = OMe and CF_3) were studied under irradiative and non-irradiative conditions to gain a better understanding of the ligand exchange reaction in these charged systems. Broad band irradiation of these samples, for 5.5 h gave ratios of 85:15 (R = CF_3) and 64:36 (R = OMe), [**L**Pt(PyR)]:[**L**Pt($PyNMe_2$)] (Table 3.3, Entries 5 and 7). The thermal reaction between $PyCF_3$.TsOH and [**L**Pt($PyNMe_2$)] was heated for 13 days at 313 K and a further 11 days at 333 K to give a steady-state equilibrium of 63:37 [**L**Pt($PyCF_3$)]:[**L**Pt($PyNMe_2$)] after base mediated cyclometallation. However, the observation of slight decomposition prevented the reaction from being pushed to equilibrium. Nevertheless, the thermal reaction between PyOMe.TsOH and [**L**Pt($PyNMe_2$)] was undertaken with heating to 313 K for 5.5 h to give a ratio of 14:86 [**L**Pt(PyOMe)]:[**L**Pt($PyNMe_2$)] (Entry 8). Finally, the exchange process between [**L**Pt(PyOMe)] and $PyCF_3$.TsOH was studied with photoirradiation for 5 h after which time the equilibrium was found to be 69:31

[**L**Pt($PyCF_3$)]:[**L**Pt(PyOMe)]. However when the sample was heated in the dark for the same length of time a ratio of 5:95 was obtained (Entry 10). A trend for the thermodynamics of the ligand exchange procedure in these charged species was established. Generally, an increase in the pK_a difference of the interchangeable heterocycles led to a more pronounced bias in favour of the formation of PyR'.TsOH and coordination of the weaker donor at the platinum(II) centre (Entries 1, 3, 5 and 7). Interestingly the time taken to reach equilibrium under irradiative conditions in each case is comparable, between 4-5 h (Table 3.3, Entries 1, 5, 7 and 9). Nonetheless it appears that a distinct rate enhancement is observed under irradiative conditions (compared to non-irradiative reactions) for the studied ligand exchange processes.

Entry	Starting [*cis*-HLPt(PyR')(S)]OTs	Starting PyR.TsOH	Pt(PyR): Pt(PyR)[a]	Time (h)	Method
1	[*cis*-H**L**Pt($PyNMe_2$)(S)]OTs	PyH.TsOH	70:30	5.2	A
2	[*cis*-H**L**Pt($PyNMe_2$)(S)]OTs	PyH.TsOH	41:59	576[b]	B
3	[*cis*-H**L**Pt($PyNMe_2$)(S)]OTs	PyCN.TsOH	71:29	5.3	A
4	[*cis*-H**L**Pt($PyNMe_2$)(S)]OTs	PyCN.TsOH	9:91	5.3	B
5	[*cis*-H**L**Pt($PyNMe_2$)(S)]OTs	$PyCF_3$.TsOH	85:15	5.5	A
6	[*cis*-H**L**Pt($PyNMe_2$)(S)]OTs	$PyCF_3$.TsOH	63:37	576[b]	B
7	[*cis*-H**L**Pt($PyNMe_2$)(S)]OTs	PyOMe.TsOH	64:36	5.5	A
8	[*cis*-H**L**Pt($PyNMe_2$)(S)]OTs	PyOMe.TsOH	14:86	5.5	B
9	[*cis*-H**L**Pt(PyOMe)(S)]OTs	$PyCF_3$.TsOH	69:31	5	A
10	[*cis*-H**L**Pt(PyOMe)(S)]OTs	$PyCF_3$.TsOH	5:95	5	B

Table 3.3 Equilibrium ratios and equilibration times for PyR.TsOH + [*cis*-H**L**Pt(PyR')(S)]OTs $\rightleftharpoons$ PyR'.TsOH + [*cis*-H**L**Pt(PyR)(S)]OTs under irradiative and non-irradiative conditions. [a]The ratio of [*cis*-H**L**Pt(PyR(S)]OTs:[*cis*-H**L**Pt(PyR')(S)]OTs was indirectly measured by converting the C^N complexes to the corresponding C^N^C complexes using the base P_1-^{t}Bu, and then by integration of the resultant [**L**Pt(PyR)] and [**L**Pt(PyR'] complexes. [b]312 h at 313 K + 264 h at 333 K. Method A: Broad band irradiation (275-375 nm with λ_{max} = 312 nm) Method B: Non-irradiative conditions: In absence of light.[18]

3.2.4 Possible Mechanism For Photochemically Induced Rate Enhancement

A likely mechanism for the pronounced rate enhancements observed upon irradiation is through excitation into a MC state with σ-antibonding $d_{x^2-y^2}$ character.[16a,16b] Due to the heavy atom effect, it is probable that this proceeds *via* a ^{3}MLCT state, from which the ^{3}MC state is thermally accessible.[17] However, strong field cyclometallated ligands are known to raise the energy of the MC state, which is why many similar Pt complexes are luminescent, rather than photochemically active, at room temperature.[23] In this current investigation, it could be anticipated that the MC states of [**L**Pt(PyR)] would be less accessible than the corresponding states for either [*cis*-H**L**Pt(PyR)(PyNMe$_2$)]OTs or [*cis*-H**L**Pt(PyNMe$_2$)(S)]OTs. This appears to be supported experimentally as the C^N complexes exhibit greater irradiative rate enhancements in comparison to the thermal reactions (in effect, protonation photochemically activates the C^N^C complexes).[24] Interestingly, it is known that the related C^N^C complex [**L**Pt(CNPh)] is not luminescent at room temperature and a recent theoretical analysis has shown that a likely reason for this is due to significant distortion of the triplet ground state, which reduces the ligand field and brings the MC state into thermal range.[25]

3.2.5 Time Dependent-Density Function Theory Calculations

A series of TD-DFT calculations were carried out on a range of the C^N^C complexes, [**L**Pt(PyR)] (R = NMe$_2$, H and CF$_3$) to determine the first 40 electronic transitions in the singlet and triplet manifolds and also to establish the molecular orbital contributions for each electronic transition. All calculations were performed with the Gaussian 03 software package,[26] running under Linux. The DFT calculations were performed by the Becke three-parameter hybrid exchange functional and Lee–Yang–Parr correlation functional (B3LYP)[27,28] together with the LANL2DZ basis set[29] which was employed for all atoms. The light accelerated ligand exchange for the cyclometallated C^N^C complexes were reported in a 1:1

[D_7]-DMF:CD_2Cl_2 and so accordingly solvent effects were taken into account using the polarisable continuum model (PCM).[30] For each cyclometallated complex, three sets of TD-DFT calculations were performed; the solvent effects of DMF and dichloromethane were taken into account and for comparison no solvent effects were additionally modelled.[31]

3.2.5.1 Singlet Excited State Calculations

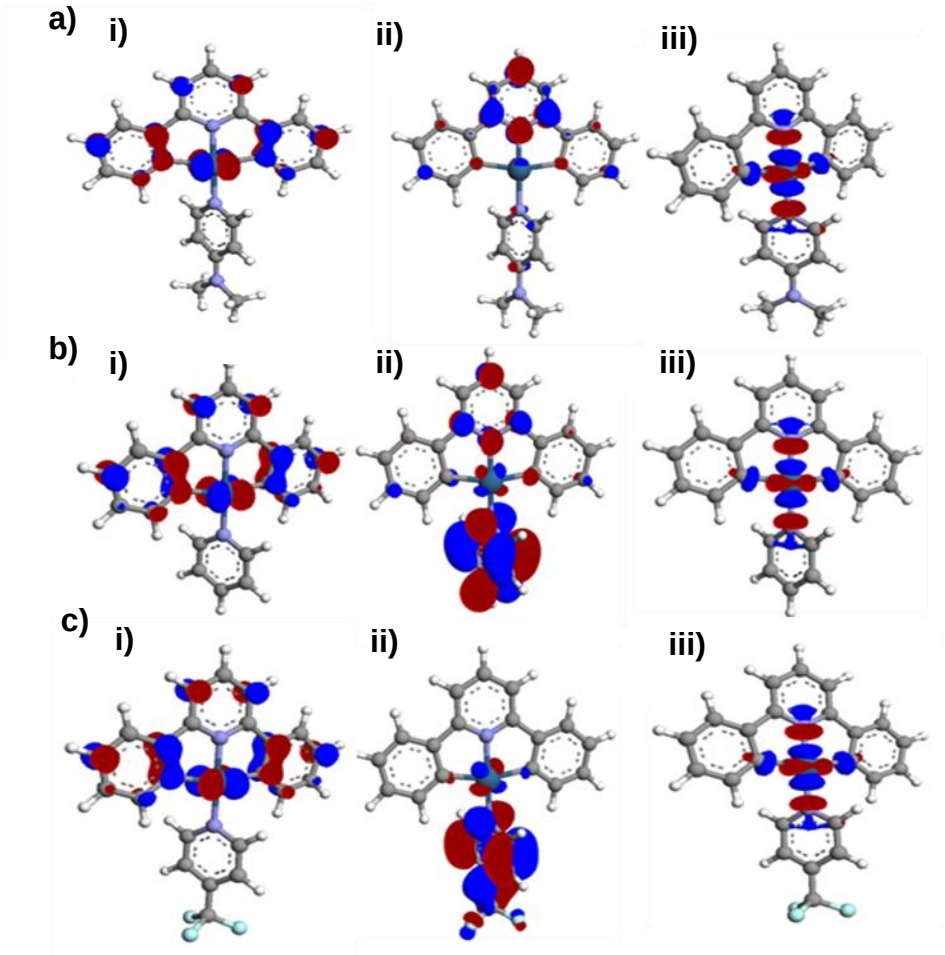

Figure 3.4 Predicted frontier molecular orbitals and selected molecular orbitals for a) [**L**Pt(PyNMe$_2$)], b) [**L**Pt(PyH)] and c) [**L**Pt(PyCF$_3$)] in the singlet manifold using TD-DFT approach with PCM to model the solvent (CH_2Cl_2) effect: i) HOMO ii) LUMO iii) LUMO + 7.

The frontier molecular orbitals (MO) for the cyclometallated complexes, [**L**Pt(PyR)] (where R = NMe_2, H, CF_3) in the singlet manifold were calculated. The HOMOs for all three complexes were observed to be MC states with π-anti-bonding d_{xz} character with the tridentate ligand, $\mathbf{L}^{2-}$ (Figure 3.4i). The LUMO of [**L**Pt($PyNMe_2$)] displayed π-anti-bonding character which was predominantly centred on the pyridine group of **L** (Figure 3.4ai). The LUMO of [**L**Pt(PyR)] (R = H and CF_3) exhibited π-antibonding d_{yz} character with the monodentate heterocycle (Figure 3.4bii and 3.4cii) but in [**L**Pt(PyH)] additional π-antibonding character was observed on **L**, principally centred on the pyridine ligand (Figure 3.6bii). TD-DFT calculations identified relatively high energy ^{1}MC states with σ-antibonding $d_{x^2-y^2}$ character for each of the cyclometallated complexes (Figure 3.4iii) at LUMO + 7. Fujita reported that d-d* dissociation was promoted, under irradiative conditions, in his photoswitchable molecular lock systems as a consequence of direct excitation from the singlet ground state into a ^{1}MC state with σ-antibonding $d_{x^2-y^2}$ character.[16a,16b] This was proposed to lead to the observed photolabilisation of the platinum(II)-pyridyl bond. This mechanistic supposition was supported by TD-DFT calculations (see Section 1.5).[16b]

From the TD-DFT calculations undertaken it was identified that the $S_0 \rightarrow S_1$ transition occurs at 458.20 nm (R = NMe_2), 456.89 nm (H) and 526.29 nm (R = CF_3) and was comprised of exclusively HOMO → LUMO molecular orbital contribution for all three complexes (Table 3.4, Entries 1-3). High energy electronic transitions, which possessed MO contributions directly between the HOMO and the identified ^{1}MC state with σ-antibonding $d_{x^2-y^2}$ character (HOMO → LUMO + 7) were observed for all three of the studied cyclometallated complexes (Table 3.4, Entries 4-9). These electronic transitions appeared at $S_0 \rightarrow S_{31}$ at 249.38 nm (f = 0.0122) and $S_0 \rightarrow S_{34}$ at 247.06 nm (f = 0.0073) (for [**L**Pt($PyNMe_2$)], Entries 4 and 5), $S_0 \rightarrow S_{30}$ at 252.89 nm (f = 0.0709), $S_0 \rightarrow S_{33}$ at 248.48 nm (f = 0.0069) (for [**L**Pt(PyH)], Entries 6 and 7), $S_0 \rightarrow S_{31}$ at 261.29 nm (f = 0.0009) and $S_0 \rightarrow S_{33}$ at 250.74 nm (f = 0.0008) (for [**L**Pt($PyCF_3$)]), Entries 8 and 9). For all three complexes, the described electronic transitions which contain HOMO → LUMO + 7 molecular orbital contributions were of such high energy that they lay outside the range of the light being employed under irradiative conditions (275-375 nm). The electronic

transitions, $S_0 \rightarrow S_{20}$ at 274.59 nm (f = 0.2785), $S_0 \rightarrow S_{27}$ at 254.37 nm (f = 0.0002), $S_0 \rightarrow S_{32}$ at 248.54 nm (f = 0.1346), $S_0 \rightarrow S_{33}$ at 247.16 nm (f = 0.0024) (for [**L**Pt(PyNMe$_2$)], Entries 10-13), $S_0 \rightarrow S_{22}$ at 274.42 nm (f = 0.1968) (for [**L**Pt(PyH)], Entry 14) and $S_0 \rightarrow S_{37}$ at 244.05 nm (f = 0.1580) (for [**L**Pt(PyCF$_3$)], Entry 15) were additionally identified as being responsible for promoting electron density into the desired ^{1}MC state with σ-antibonding $d_{x^2-y^2}$ character (LUMO + 7). However all these high energy transitions, with the exception of $S_0 \rightarrow S_{20}$ at 274.59 nm in [**L**Pt(PyNMe$_2$)] and $S_0 \rightarrow S_{22}$ at 274.74 nm in [**L**Pt(PyH)] (Entries 10 and 14), lay outside the range of the light being employed. Despite the fact that these two aforementioned transitions, $S_0 \rightarrow S_{20}$ in [**L**Pt(PyNMe$_2$)] and $S_0 \rightarrow S_{22}$ in [**L**Pt(PyH)], displayed high oscillator strengths, the MO contribution from the desired ^{1}MC state was low for each electronic transition (with a magnitude of 10% in both [**L**Pt(PyNMe$_2$)] and [**L**Pt(PyH)] Table 3.3). Combined with the fact that singlet lifetimes are generally short-lived it is unlikely that the rate enhancement observed experimentally is a result of direct excitation into these singlet d-d* dissociation states. It is more probable that the mechanism proceeds *via* the triplet state through ISC from the singlet manifold.

Entry	Complex	Wavelength (nm)	Electronic Transition	Osc. Strength (*f*)	Molecular Orbital Contributions*
1	[**L**Pt(PyNMe$_2$)]	458.20	$S_0 \rightarrow S_1$	0.0001	HOMO->LUMO (100%)**
2	[**L**Pt(PyH)]	456.89	$S_0 \rightarrow S_1$	0.0002	HOMO->LUMO (100%)**
3	[**L**Pt(PyCF$_3$)]	526.29	$S_0 \rightarrow S_1$	0.0001	HOMO->LUMO (100%)**
4	[**L**Pt(PyNMe$_2$)]	249.38	$S_0 \rightarrow S_{31}$	0.0122	HOMO->L+7 (11%)
5	[**L**Pt(PyNMe$_2$)]	247.06	$S_0 \rightarrow S_{34}$	0.0073	HOMO->L+7 (73%)
6	[**L**Pt(PyH)]	252.89	$S_0 \rightarrow S_{30}$	0.0709	HOMO->L+7 (17%)
7	[**L**Pt(PyH)]	248.48	$S_0 \rightarrow S_{33}$	0.0069	HOMO->L+7 (69%)
8	[**L**Pt(PyCF$_3$)]	261.29	$S_0 \rightarrow S_{31}$	0.0009	HOMO->L+7 (14%)
9	[**L**Pt(PyCF$_3$)]	250.74	$S_0 \rightarrow S_{33}$	0.0008	HOMO->L+7 (72%)
10	[**L**Pt(PyNMe$_2$)]	274.59	$S_o \rightarrow S_{20}$	0.2785	H-1->L+7 (-10%)
11	[**L**Pt(PyNMe$_2$)]	254.37	$S_0 \rightarrow S_{27}$	0.0546	H-1->L+7 (8%)
12	[**L**Pt(PyNMe$_2$)]	248.54	$S_0 \rightarrow S_{32}$	0.1346	H-1->L+7 (-9%)
13	[**L**Pt(PyNMe$_2$)]	247.16	$S_0 \rightarrow S_{33}$	0.0024	H-1->L+7(12%)
14	[**L**Pt(PyH)]	274.42	$S_0 \rightarrow S_{22}$	0.1968	H-1->L+7 (10%)
15	[**L**Pt(PyCF$_3$)]	244.05	$S_0 \rightarrow S_{37}$	0.1580	H-1->L+7 (-15%)

Table 3.4 Selected calculated singlet-singlet electronic transitions containing HOMO → LUMO + 7 molecular orbital contributions for each of the complexes, [**L**Pt(PyR)] (where R = NMe_2, H, CF_3), using the data obtained from the TD-DFT calculations with PCM to model the solvent(CH_2Cl_2) effect. *For a more comprehensive list of the major molecular orbitals contributing to the described transitions see Section 3. 5. 4. **$S_o \rightarrow S_1$ electronic transition which contains exclusively HOMO → LUMO molecular orbital contributions for all three studied complexes.

3.2.5.2 Triplet Excited State Calculations

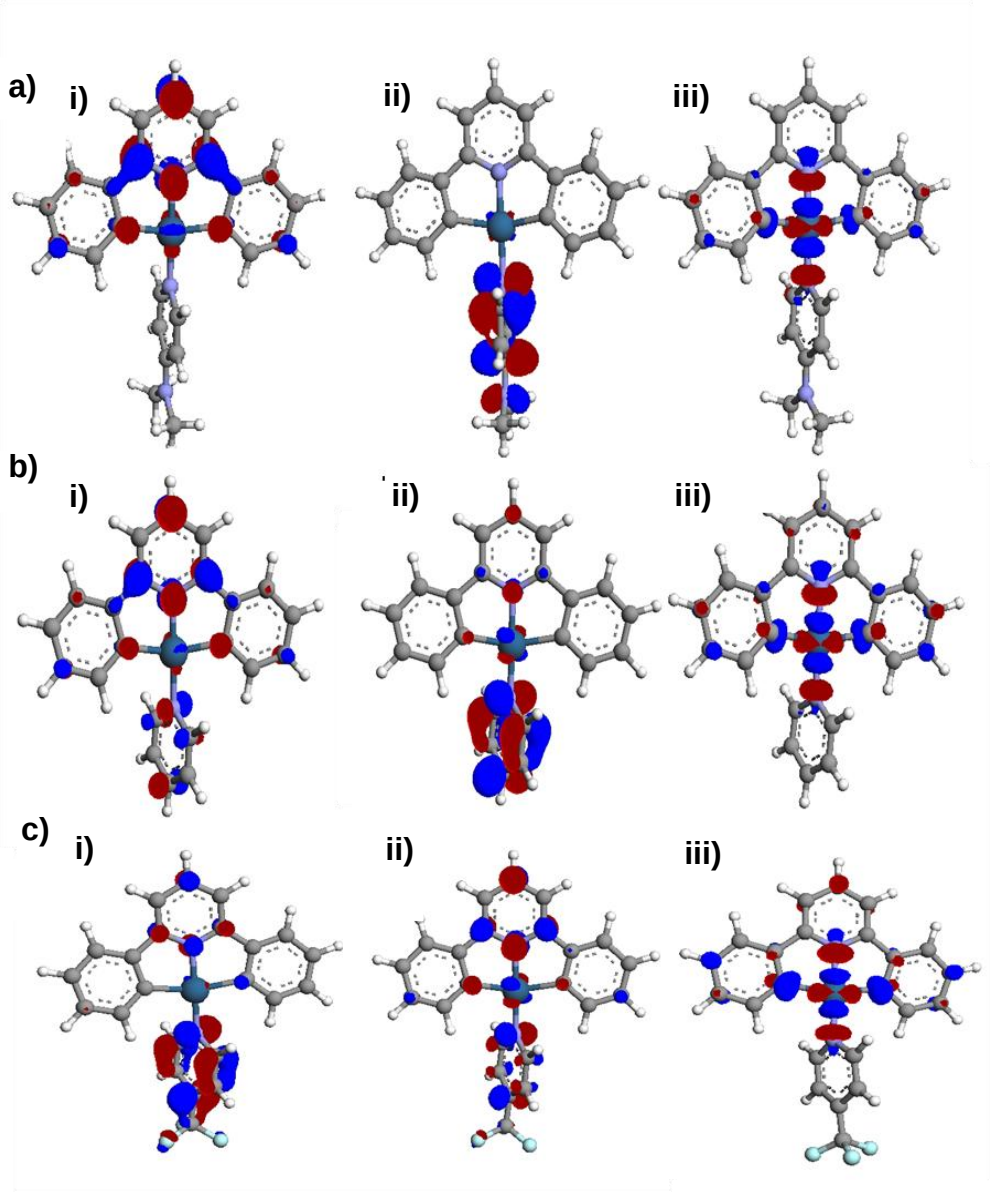

Figure 3.5 Predicted frontier molecular orbitals and selected molecular orbitals for a) [**L**Pt(PyNMe$_2$)], b) [**L**Pt(PyH)] and c) [**L**Pt(PyCF$_3$)] in the triplet manifold using TD-DFT approach with PCM to model the solvent (CH_2Cl_2) effect: i) HOMO ii) LUMO iii) LUMO + 6.

The frontier molecular orbitals for the cyclometallated complexes, [**L**Pt(PyR)] (where R = NMe_2, H, CF_3), in the triplet manifold were calculated. The HOMO of [**L**Pt(PyR)] (R = NMe_2 and H) were observed to display π-anti-bonding character principally centred on the pyridine group of **L** (Figures 3.5ai and 3.5bi). For [**L**Pt(PyH)] additional slight π-anti-bonding d_{xy} character was observed on the monodentate heterocycle (Figures 3.5bi). The HOMO calculated for [**L**Pt($PyCF_3$)] possessed π-antibonding character which was largely centred on the monodentate ligand, $PyCF_3$ (Figure 3.5ci). The LUMOs of [**L**Pt(PyR)] (R = NMe_2, H and CF_3) predominantly exhibit π-anti-bonding character localised on the monodentate ligand, PyR (Figure 3.5ii). However, the LUMOs of [**L**Pt(PyR)] (R = H and CF_3) also displayed π-antibonding d_{yz} character with the monodentate ligand, PyH or $PyCF_3$, but to differing degrees with greater prominence in [**L**Pt($PyCF_3$)] and to a lesser extent in [**L**Pt(PyH)]. In each of the three complexes, ^{3}MC states with σ-antibonding $d_{x^2-y^2}$ character were identified as relatively high energy MOs (LUMO + 6).

The photoresponsive Ru(II)catenane and rotaxane based systems published by Sauvage and co-workers[32] also reportedly function by utilising d-d* dissociative states. In these systems it has been proposed that excitation into a ^{1}MLCT state is followed by ISC into a ^{3}MLCT state, from which the dissociative ^{3}MC state is thermally accessible (see Section 1.4). As such, the mechanism for the pronounced rate enhancement observed experimentally (Section 3.1) was proposed to proceed *via* indirect excitation into a ^{3}MC state with σ-antibonding $d_{x^2-y^2}$ character (*vide supra*). Jablonski diagrams[33] (Figures 3.6-3.8) were constructed for each of the cyclometallated complexes, [**L**Pt(PyR)] (where R = NMe_2, H, CF_3), based on the data obtained from the TD-DFT calculations. From these diagrams (Figures 3.6–3.8) it can be clearly seen that upon broad band irradiation at 275-375 nm (36363-26667 cm^{-1}) excitation into the desired ^{1}MC state with σ-antibonding $d_{x^2-y^2}$ character is unlikely. However, following ISC from the singlet into the triplet manifold the desired d-d* dissociative ^{3}MC states can be readily populated for all three complexes. The triplet excited states, T_7 and T_{11} (for [**L**Pt($PyNMe_2$)]) T_8 and T_{11} (for [**L**Pt(PyH)] and [**L**Pt($PyCF_3$)]) contained MO contributions from the target ^{3}MC state with σ-antibonding $d_{x^2-y^2}$ character. Clearly, population of these excited triplet

states (most particularly T_7 (for [**L**Pt(PyNMe$_2$)]) and T_8 (for [**L**Pt(PyH)] and [**L**Pt(PyCF$_3$)]) could readily occur upon broad band irradiation (275-375 nm) of the relevant cyclometallated complex (Figures 3.6-3.8). Triplet states as high as T_{13} in [**L**Pt(PyNMe$_2$)] and [**L**Pt(PyH)]) and T_{15} in [**L**Pt(PyCF$_3$)] could theoretically be populated under the irradiative conditions employed (375-275 nm) if no energy was lost from the system *via* radiationless decay (i.e. heat) in the singlet manifold. Once ISC has taken place, non-irradiative decay *via* relaxation in the triplet manifold would permit population of the identified excited ^{3}MC states with σ-antibonding $d_{x^2-y^2}$ character. As such, selective labilization of the Pt-py bond under the described irradiative conditions would be achieved to generate the observed rate enhancement of the ligand exchange reaction.

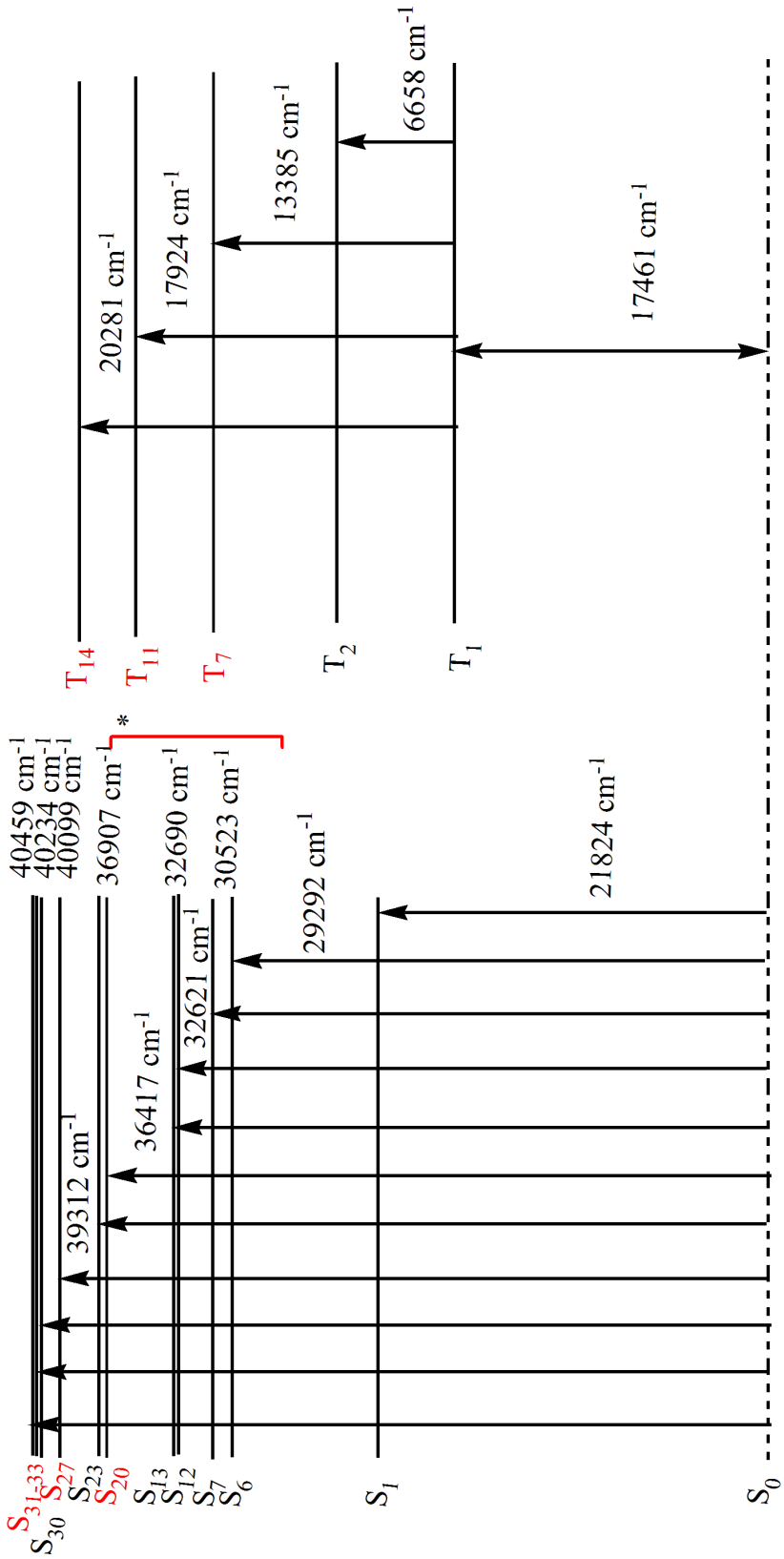

Figure 3.6 Jablonski diagram for [**L**PyNMe$_2$] constructed from the data obtained from the TD-DFT calculations. Electronic transitions which either have an oscillator strength ≥ 0.1 (shown in black) or possess molecular orbital contributions from states with σ-antibonding $d_{x^2-y^2}$ character (LUMO + 7 in singlet state and LUMO + 8 in triplet state) (shown in red) are depicted. * Denotes the range in which excitation occurred upon the application of broad band irradiation (275-375 nm).

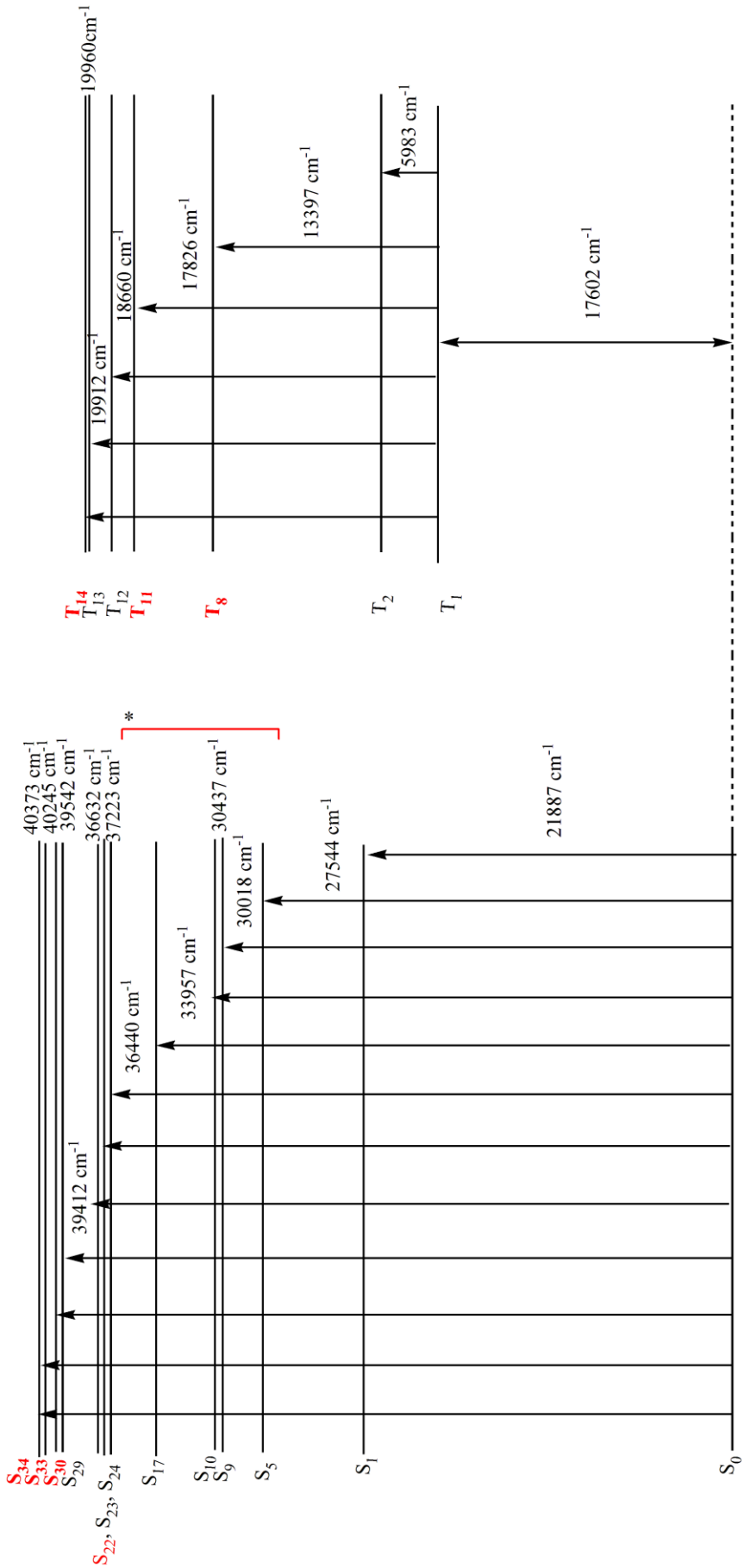

Figure 3.7 Jablonski diagram for [**L**PyH] constructed from the data obtained from the TD-DFT calculations. Electronic transitions which either have an oscillator strength ≥ 0.1 in singlet state or ≥ 0.04 in triplet state (shown in black) or possess molecular orbital contributions from states with σ-antibonding $d_{x^2-y^2}$ character (LUMO + 7 in singlet state and LUMO + 6 in triplet state) (shown in red) are depicted. * Denotes the range in which excitation occurred upon the application of broad band irradiation (275-375 nm).

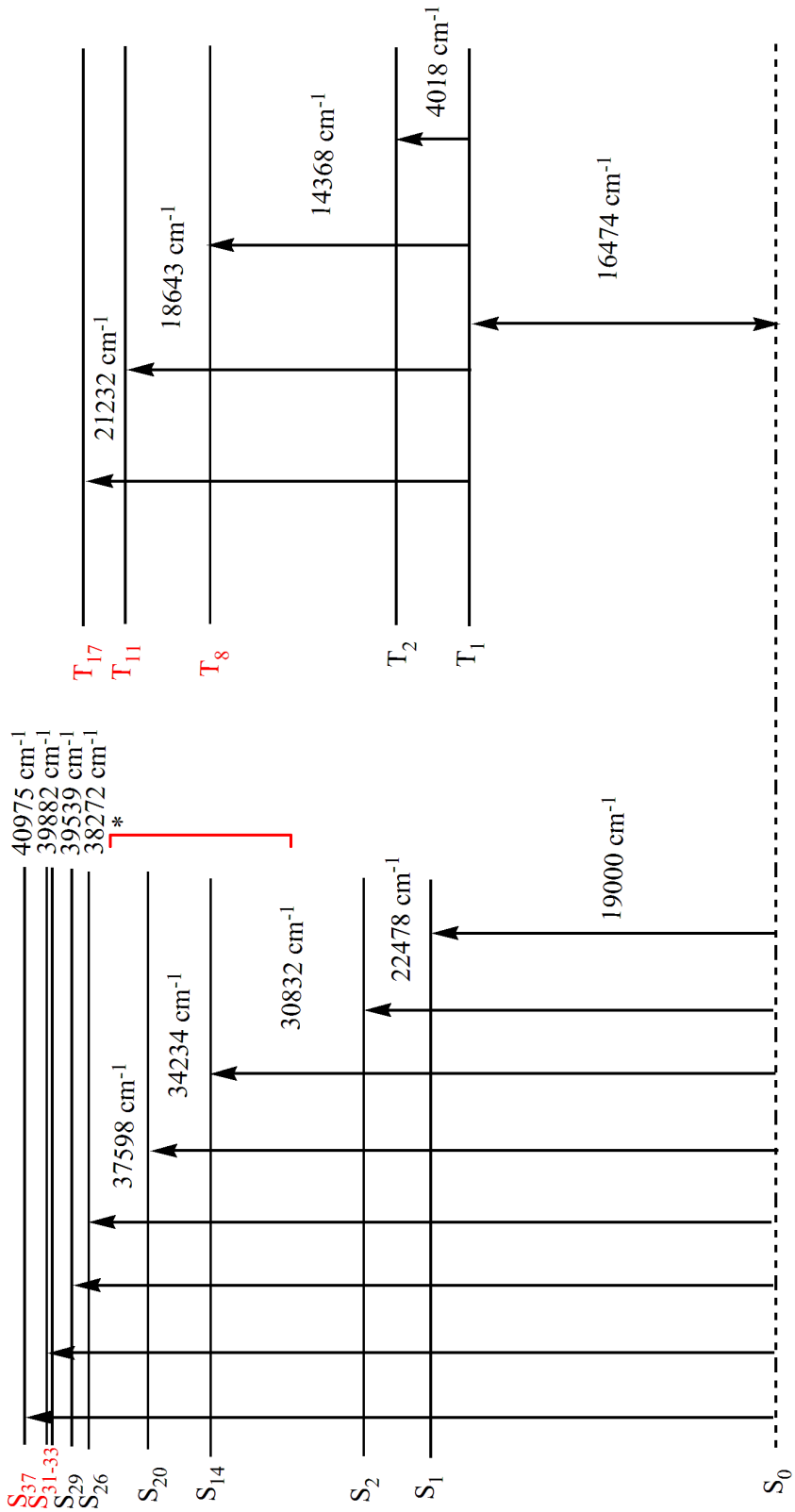

Figure 3.8 Jablonski diagram for [**L**PyCF$_3$] constructed from the data obtained from the TD-DFT calculations. Electronic transitions which either have an oscillator strength ≥ 0.1 (shown in black) or possess molecular orbital contributions from states with σ-antibonding $d_{x^2-y^2}$ character (LUMO + 7 in singlet state and LUMO + 6 in triplet state) (shown in red) are depicted. * Denotes the range in which excitation occurred upon the application of broad band irradiation (275-375 nm).

3.2.6 Kinetic Studies

Kinetic studies for the ligand exchange reaction between [**L**Pt(PyH)] and $PyNMe_2$ in a 0.01 M solution of 1:1 [D_7]-DMF:CD_2Cl_2, at 313 K were undertaken to determine values for the rate of the ligand substitution process at a series of different wavelengths of light, 260-290 nm, 290-320 nm, 320-350 nm and 350-380 nm (Table 3.5). ^{1}H NMR spectroscopy was employed to monitor the rate of the ligand exchange process and determine the ratio of [**L**Pt(PyH)]:[**L**Pt($PyNMe_2$)] at regular time intervals.[18] Upon broad band 260-290 nm irradiation, a value of $2.0x10^{-5}$ s^{-1} was determined for the rate constant (*k*) (Table 3.5, Entry 1). The value was obtained from a straight line plot of ln[**L**Pt(PyH)] *vs* time (Section 3.5.2) which additionally established first order (or pseudo-first order) reaction kinetics for the ligand exchange process.[33] Following the exchange process with broad band irradiation between 290-320 nm, 320-350 nm and 350-380 nm at 313 K gave the rate constant of $1.0x10^{-5}$ s^{-1} (Table 3.5 Entries 2-4) in each case whilst for comparison in the absence of light at 313 K it was determined that $k = 9.0x10^{-6}$ s^{-1} (Table 3.5, Entry 5). Clearly, a distinct rate enhancement was observed upon irradiation with 260-290 nm, double that which was seen under non-irradiative conditions or at longer wavelengths, which implies that excitation within this range is responsible for the electronic transitions that lead to the increased reaction kinetics.[34] The observed dependence on the energy of the light source was consistent with the proposed mechanism (Section 3.2.5) for the rate enhancement which suggested an orbital dependent process. Interestingly, from the TD-DFT calculations undertaken on [**L**Pt(PyH)] (see Section 3.5.5) it can be seen that irradiation between 260-290 nm (38462-34483 cm^{-1}) would lead to excitation into S_{18}-S_{26} states (Figure 3.7). As such, triplet excited states as high as T_{12} could be populated if direct ISC was observed (Figure 3.7). The triplet excited states containing contributions from the desired MO with σ-antibonding $d_{x^2-y^2}$ character were identified as T_{11} and T_8 (*vide supra*) so population of these excited states upon irradiation between 260-290 nm would feasibly promote the desired d-d* dissociation. Although, a slight rate enhancement was observed upon irradiation between 290-320 nm, 320-350 nm and

350-380 nm compared to that obtained under non-irradiative conditions (*cf* Entries 2-4 and Entry 5), this was probably within error of the thermal reaction and the experimental procedure. As different accessible states will cause different levels of dissociation it is likely that the observed increase in *k* at shorter wavelengths (when light between 260-290 nm was employed), is caused by the population of excited states which are more dissociative in character combined with a cumulative effect of populating more ^{3}MC d-d* states.

Entry	Excited Wavelength/nm*	$k/10^{-5}s^{-1}$
1	260-290	2.0
2	290-320	1.0
3	320-350	1.0
4	350-380	1.0
5	/[a]	0.9

Table 3.5 Tabulated data to show the rate for the ligand exchange process between [**L**Pt(PyH)] and $PyNMe_2$ in 0.01 M solution of [D_7]-DMF:CD_2Cl_2; 1:1 upon broad band irradiation with light sources of wavelength ranges. [a]Under non-irradiative conditions, with heating at 313 K in the absence of light.*Fluoromax-P spectrofluorimeter (Horiba-Jobin-Yvon) was employed with band filters as specified and with heating at 313 K.

3.3 Conclusions

The ligand exchange reaction of *N*-heterocycle PyR' (R'=NMe_2, OMe, H) for PyR (R = OMe, H, CF_3 and CN) at the platinum(II) centre of a series of neutral cyclometallated and charged complexes, [**L**Pt(PyR)] and [*cis*-H**L**Pt(PyR)(PyR')]OTs respectively, under irradiative and non-irradiative conditions has been investigated. It has been established that a rate enhancement is observed upon the application of photochemical stimulus in both the neutral and protonated states compared to the analogous reactions under non-irradiative conditions. Futhermore, the observed increase in the kinetics in the charged systems is much more pronounced than that which is observed in neutral complexes such that protonation appears to

photochemically activate the C^N^C complexes. Reversal of the coordinative bias of the exchangeable heterocycles at a platinum(II) centre has been investigated in a series of charged complexes, [*trans*-H**L**Pt(PyR')(PyR)]OTs (R' = NMe_2, OMe, H and R = OMe, H, CF_3 and CN) under irradiative and non-irradiative conditions. As before, a distinct acceleration in the kinetics upon the application of photochemical stimulus was observed for this ligand exchange process. Overall, the exchange between different equilibrium and out-of-equilibrium platinum coordination modes has been demonstrated to be orthogonally controlled; thermodynamically with a proton input and kinetically using light has been established. TD-DFT calculations have been undertaken on [**L**Pt(PyR)] (where R = NMe_2, H, CF_3) to determine the frontier molecular orbitals for each complex in the singlet and triplet state. From this data, Jablonski diagrams have been constructed for [**L**Pt(PyR)] (where R = NMe_2, H, CF_3). It has been determined that the dissociative pathway operating under irradiative conditions, which leads to the observed increase in ligand exchange reaction, most probably does not proceed *via* direct excitation into a ^{1}MC state with σ-antibonding $d_{x^2-y^2}$ character. Instead, it is more plausible that the dissociative mechanism proceeds through population of d-d* states within the triplet manifold. Kinetic studies for the ligand exchange process between [**L**Pt(PyH)] and $PyNMe_2$, with different wavelengths of excitation and for comparison under non-irradiative conditions, have been carried out. A distinct increase in the reaction kinetics for the exchange reaction was observed when light between 260-290 nm was employed. The observed dependence on the energy of the light source was consistent with the proposed mechanism for rate enhancement which suggested an orbital dependent process.

3.4 References and Notes

[1] (a) R. D. Vale, T. S. Reese, M. P. Sheetz; *Cell*, 1985, **42**, 39; (b) K. Svoboda, C. F. Schmidt, B. J. Schnapp, S. M. Block; *Nature*, 1993, **365**, 721; (c) M. C. Alonso, D. R. Drummond, S. Kain, J. Hoeng, L. Amos, R. A. Cross; *Science*, 2007, **316**, 120; (c) R. B. Case, D. W. Pierce, N. Hom-Booher, C. L. Hart, R. D. Vale; *Cell*, 1997, **90**, 959; (d) W. Hua, E. C. Young, M. L. Fleming, J. Gelles; *Nature*, 1997, **388**, 390; (e) S. S. Rosenfield, P. M. Fordyce, G. M. Jefferson, P. H. King, S. M. Block; *J. Bio.Chem.* 2003, **278**, 18550. (f) J. Howard, A. J. Huspeth, R. D. Vale, *Nature*, 1989, **342**, 154. (g) W. O. Hancock, J. Howard; *Proc. Nat. Aca. Sci.*, 1999, **96**, 13147.

[2] S. Toba, T. M. Watanabe, L. Yamaguchi-Okimoto, Y. Y. Toyoshima, H. Higuchi, *Proc. Natl. Acad. Sci. USA* 2006, **103**, 5741.

[3] For recent reviews on molecular machines see: (a) V. Balzani, A. Credi, M. Venturi; *Chem. Soc. Rev.*, 2009, **38**, 1542; (b) S. Bonnet, J. –P. Collin; *Chem. Soc. Rev.*, 2008, **37**, 1207; (c) S. Bonnet, M. Koizumi, P. Mobien; *Adv. Mater.*, 2006, **18**, 1239; (d) V. Balzani, A. Credi, F. M. Raymo, J. F. Stoddart, *Angew. Chem. Int. Ed*., 2000, **39**, 3348; (e) V. Balzani, M. Venturi, A. Credi, *Molecular Devices and Machines: A Journey into the Nanoworld*, Wiley-VCH, Weinheim (2003) (f) V. Balzani; *Photochem. Photobiol. Sci.*, 2003, **2**, 459; (g) W. R. Browne, B. L. Feringa, *Nature Nanotech*. 2006, **1**, 25.

[4] D. A. Leigh, F. Zerbetto, E. R. Kay; *Angew. Chem. Int. Ed.*, 2007, **46**, 72.

[5] (a) M. Alvarez-Perez, S. M. Goldup, D. A. Leigh, A. M. Z. Slawin, *J. Am. Chem. Soc.*, 2008, **130**, 1836; (b) V. Serreli, C.-F. Lee, E. R. Kay, D. A. Leigh, *Nature*, 2007, **445**, 523.

[6] (a) A. Altieri, G . Bottari, F . Dehez, D. A. Leigh, J. K. Y. Wong, F. Zerbetto, *Angew. Chem. Int. Ed.*, 2003, **42**, 2296; (b) A. S. Lane, D. A. Leigh, A. Murphy, *J. Am. Chem. Soc.*, 1997, **119**, 11092; (c) A. M. Brouwer, C. Frochot, F. G. Gatti, D. A. Leigh, L. Mottier, F. Pailucci, S. Roffia, G. W. H. Wurpel, *Science*, 2001, **291**, 2124.

[7] (a) H. Murakami, A. Kawabuchi, R. Matsumoto, T. Ido, N. Nakashima, *J. Am. Chem. Soc.*, 2005, **127**, 15891; (b) C. A. Steiner, S. J. Alderman, D. W. Claridge, H. L. Anderson, *J. Am. Chem. Soc.*, 2002, **41**, 1769.

[8] (a) R. A. Bissell, E. Córdova, A. E. Kaifer, J. F. Stoddart, *Nature*, 1994, **369**, 133; (b) H. –R Tseng, S. A. Vignon, J. F. Stoddart; *Angew. Chem. Int. Ed.*, 2003, **42**, 1491; (c) P. L. Anelli, N. Spencer, J. F. Stoddart, *J. Am. Chem. Soc.*, 1991, **113**, 5131.

[9] (a) J. D. Crowley, D. A. Leigh, P. J. Lusby, R. T. McBurney, L.-E. Perret-Aebi, C. Petzold, A. M. Z. Slawin, M. D. Symes; *J. Am. Chem. Soc.*, 2007, **129**, 15085. (b) D. A. Leigh, P. J. Lusby, R. T. McBurney, M. D. Symes; *Chem. Comm.*, 2010, **46**, 2382.

[10] (a) A. Livoreil, C. O. Dietrich-Buchecker, J.-P. Sauvage; *J. Am. Chem. Soc.*, 1994, **116**, 9399; (b) U. Letinois-Halbes, D. Hanss, J. M. Beierle, J. –P. Collin, J. –P. Sauvage; *Org. Lett.* 2005, **7**, 5753; (c) J. –P Collin, V. Heitz, S. Bonnet, J. –P Sauvage, *Inorg. Chem. Comm.* 2005, **8**, 1063; (d) D. J. Cárdenas, A. Livoreil, J.-P. Sauvage, *J. Am. Chem. Soc.*, 1996, **118**, 11980; (c) A. Livoreil, J.-P. Sauvage, N. Armaroli, V. Balzani, L. Flamigni, B. Ventura, *J. Am. Chem. Soc.*,1997, **119**, 12114; (d) N. Armaroli, V. Balzani, J.-P. Collin, P. Gaviña, J. -P. Sauvage, B. Ventura, *J. Am. Chem. Soc.*, 1999, **121**, 4397. For a muscle-like Cu(I)/Zn(II) based dimer in which stretching and contraction processes are achieved through Cu(I)-Zn(II) exchange C.

Jimenez, C. Dietrich-Buchecker, J. –P. Sauvage, *Angew. Chem. Int. Ed.,* 2000, **39**, 3284.

[11] (a) D. W. Steuerman, H. –P. Tseng, A. J. Flood, J. O. Jeppesen, K. A. Neilsen, J. F. Stoddart, J. R. Heath, *Angew. Chem. Int. Ed.*, 2004, **43**, 6486. (b) H. –R. Tseng, D. Wu, N. X. Fang, X. Zhang, J. F. Stoodart, *ChemPhysChem*, 2004, **5**, 111; (c) J. W. Choi, A. H. Flood, D .W. Steuerman, S. Nygaard, A. B. Braunschweig, N. N. P. Moonen, B. W. Laursen, Y. Luo, E. DeIonno, A. J. Peters, J . O. Jeppesen, K. Xu, J. F. Stoddart, J. R. Heath, *Chem. Eur. J.*, 2006, **12**, 261.

[12] M. N. Chatterjee, E. R. Kay and D. A. Leigh, *J. Am. Chem. Soc.*, 2006, **128**, 4058.

[13] (a) N. Koumura, R. W. J. Zijlstra, R. A. van Delden, N. Harada , B. L. Feringa, *Nature*, 1999, **401**, 152; (b) H. Murakami, A. Kawabuchi, R. Matsumoto, T. Ido, N. Nakashima, *J. Am. Chem. Soc.*, 2005, **127**,15891.

[14] D. M. Loveless, S. L. Jeon, S. L. Craig, *J. Mater. Chem.* 2007, **17**, 56.

[15] For photochemical lability in Ru(II) ligand exchange reactions see: (a) J. Van Houten, R. J. Watts, *Inorg. Chem.*, 1978, **17**, 3381; (b) B. Durham, J. V. Caspar, J. K. Nagle, T. J. Meyer, *J. Am. Chem. Soc.*,1982, **104**, 4803.

[16] For photochemical lability in Pt(II) substitution reactions see: (a) K. Yamashita, M. Kawano, M. Fujita, *J. Am. Chem. Soc.*, 2007, **129**, 1850; (b) K. Yamashita, K. Sato, M. Kawano, M. Fujita, *New J. Chem*., **2009**, *33*, 264. However, photoinduced *cis-trans* isomerisation of Pt complexes was first shown during the 1960s, see: (c) P. C. Haake, T. A. Hylton, *J. Am. Chem. Soc*., 1962, **84**, 3774.

[17] (a) J. D. Crowley, I. M. Steele, B. Bosnich, *Inorg. Chem.* 2005**, 44**, 2989-2991; (b) G. W. V. Cave, F. P. Fanizzi, R. J. Deeth, W. Errington, J. P. Rourke, *Organometallics*, 2000**, 19**, 1355.

[18] We estimate the error in calculating the ratio from ^{1}H NMR integrals to be ±5%.

[19] P. J. Lusby, P. Muller, S. J. Pike, A. M. Z. Slawin, *J. Am. Chem. Soc.* 2009, **131**, 16398.

[20] S. J. Pike, P. J. Lusby, *Chem. Comm.* 2010, **46**, 8338.

[21] The sequential addition of TsOH and followed by $PyNMe_2$ is required for the ligand exchange reaction between [**L**Pt(PyR)] (R = OMe, H, CF_3 and CN) and initially unbound $PyNMe_2$ as direct addition of the salt $PyNMe_2$.TsOH caused no protonation event of the C^N^C complex, [**L**Pt(PyR)].

[22] The ratios of [**L**Pt(PyR)]:[**L**Pt(PyR')] for the reaction of [**L**Pt(PyR)] + PyR' →[**L**Pt(PyR')] + PyR were measured directly by integration of the ^{1}H NMR spectra. The ratios of [*cis*-H**L**Pt(PyR)(PyR')]OTs:[*trans*-H**L**Pt(PyR')(PyR)]OTs and [*cis*-H**L**Pt(PyR)(S)]OTs:[*cis*-H**L**Pt(PyR')(S)]OTs were measured indirectly by converting the corresponding C^N complexes to C^N^C complexes using the base P_1-^{t}Bu, and then by integration of the resultant [**L**Pt(PyR)] and [**L**Pt(PyR')] complexes. This cyclometallation reaction is fast in comparison to the ligand exchange processes; at room temperature it is complete within the 5 minutes it takes to acquire a ^{1}H NMR spectrum. As control experiments, when samples of pure [*cis*-H**L**Pt(PyR)($PyNMe_2$)]OTs and [*trans*-H**L**Pt($PyNMe_2$)(PyR)]OTs are treated with P_1-^{t}Bu, they exclusively yield [**L**Pt(PyR)] and [**L**Pt($PyNMe_2$)], respectively.

[23] (a) T. –C. Cheng, K. –K. Cheung, S. –M. Peng, C. –M. Che, *J. Chem. Soc., Dalton Trans.*, 1996, 1645; (b) J. A. G. Williams, A. Beeby, E. S. Davies, J. A. Weinstein, C. Wilson, *Inorg. Chem.*, 2003, **42**, 8609; (c) J. A. G. Williams, *Top. Curr. Chem.*, 2007, **281**, 205.

[24] It is possible that the mechanism of light-promoted ligand exchange in the C^N complexes also involves tetrahedral distortion of an excited ^{3}MC state, see V. Balzani, V. Carassiti, *J. Phys. Chem*., 1969, **72**, 383.

[25] G. S.-M. Tong, C.-M. Che; *Chem. Eur. J.*, 2009, **15**, 7225.

[26] Gaussian 03, Revision B.05; M. J. Frisch, G. W. Trucks, H. B. Schlegel, G. E. Scuseria; M. A. Robb, J. R. Cheeseman, J. J. A. Montgomery, T. Vreven, K. N. Kudin, J. C. Burant, J. M. Millam, S. S. Iyengar, J. Tomasi, V. Barone, B. Mennucci, M. Cossi, G. Scalmani, N. Rega, G. A. Petersson, H. Nakatsuji, M. Hada, M. Ehara, K. Toyota, R. Fukuda, J. Hasegawa, M. Ishida, T. Nakajima, Y. Honda, O. Kitao, H. Nakai, M. Klene, X. Li, J. E. Knox, H. P. Hratchian, J. J. B. Cross, V. Bakken, C. Adamo, J. Jaramillo, R. Gomperts, R. E. Stratmann, O. Yazyev, A. J. Austin, R. Cammi, C. Pomelli, J. W. Ochterski, P. Y. Ayala, K. Morokuma, G. A. Voth, P. Salvador, J. J. Dannenberg, V. Zakrzewski, S. Dapprich, A. D. Daniels, M. C. Strain, O. Farkas, D. K. Malick, A. D. Rabuck, K. Raghavachari, J. B. Foresman, J. V. Ortiz, Q. Cui, A. G. Baboul, S. Clifford, J. Cioslowski, B. B. Stefanov, G. Liu, A. Liashenko, P. Piskorz, I. Komaromi, R. L. Martin, D. J. Fox, T. Keith, M. A. Al-Laham, C. Y.; Peng, A. Nanayakkara, M. Challacombe, P. M. W. Gill, B. Johnson, W. Chen, M. W. Wong, C. Gonzalez, J. A. Pople, C. T. Wallingford.

[27] A. D. Becke; *J. Chem. Phys.* 1993, **98**, 1372.

[28] P. J. Stephens, F. J. Devlin, C. F. Chabalowski, M. J. Frisch; *J. Chem. Phys.*, 1994, **100**, 11623.

[29] Dolg, M.; Stoll, H.; Preuss, H.; Pitzer, R. M., *J. Phys. Chem.* 1993, **97**, 5852.

[30] Cossi, M.; Scalmani, N.; Rega, N.; Barone, V., *J. Chem. Phys.* 2002, **117**, 43.

[31] The data obtained from all three sets of TD-DFT calculations (where DMF, dichloromethane and no solvent effects were accounted for) gave very similar results for all three cyclometallated complexes. As such, the data obtained for the dichloromethane studies were used to plot the Jablonski diagrams are reported in Tables 3.11 – 3.14.

[32] (a) P. Mobian, J. –M. Kern, J. –P. Sauvage, *J. Am. Chem. Soc.*, 2003, **125**, 2016; (b) P. Mobian, J. –M. Kern, J. –P. Sauvage, *Angew. Chem. Int. Ed.*, 2004, **43**, 2392.

[33] The values for the R^2 value of the regression line of plots of ln[H(Pt(PyH)] *vs* time (Section 7), as calculated by the Mircosoft Office Excel package, all show good correlation and fit of the data to linear straight line plots with the values of R^2 ranging between 0.9959-0.9729. (where 1 = perfect correlation and 0 = no correlation).

[34] The rate enhancement observed with irradiation between 260-290 nm not as pronounced as that which was observed when broad band irradiation (275-375 nm) was employed (Section 3.1). However, this was most likely a consequence of the differing experimental set-ups and the use of different photoreactors (and equipment) rather than the different wavelength of light being employed.

CHAPTER FOUR

Stimuli-Responsive Reversible Assembly of 2D and 3D Metallosupramolecular Architectures

Published as "*Stimuli-Responsive Reversible Assembly of 2D and 3D Metallosupramolecular Architectures*"

Paul J. Lusby, Peter Müller, Sarah J. Pike, Alexandra M. Z. Slawin,
J. Am. Chem. Soc. **2009**, *131*, 16398.

Acknowledgements

The following people are gratefully acknowledged for their practical contribution to this chapter: Peter Muller for undertaking preliminary studies with the molecular square complex, $[(H\mathbf{L}Pt)_4(4,4'\text{-bipy})_4](PF_6)_4$ and trigonal prism, $[(H\mathbf{L}Pt)_6(4,4'\text{-bipy})_3(tpt)_2](PF_6)_6]$ and Professor Alexandra Slawin who solved the X-ray crystal structure of the molecular square. Dr. Martin De Cecco and Dr. Perdita Barran who undertook the electrospray mass spectrometry on $[(H\mathbf{L}Pt)_4(4,4'\text{-bipy})_4](PF_6)_4$ and $[(H\mathbf{L}Pt)_6(4,4'\text{-bipy})_3(tpt)_2](PF_6)_6]$.

Synopsis

The discovery of interconvertible platinum coordination modes, which reveals/masks cis coordinating groups upon addition of acid and base respectively, has been exploited to facilitate stimuli-responsive assembly and disassembly of both two and three-dimensional metallosupramolecular architectures. By treating a binuclear platinum complex with acid and either a ditopic or a tritopic donor ligand, both a molecular square and a trigonal prism have been generated in good to high yield. These complexes have been unambiguously identified using electrospray mass spectrometry, ^{1}H NMR spectroscopy and X-ray crystallography. Both assemblies can be disassembled into their constituent parts by simply treating with base and the prism cycled between assembled and disassembled states by the alternate addition of base and acid.

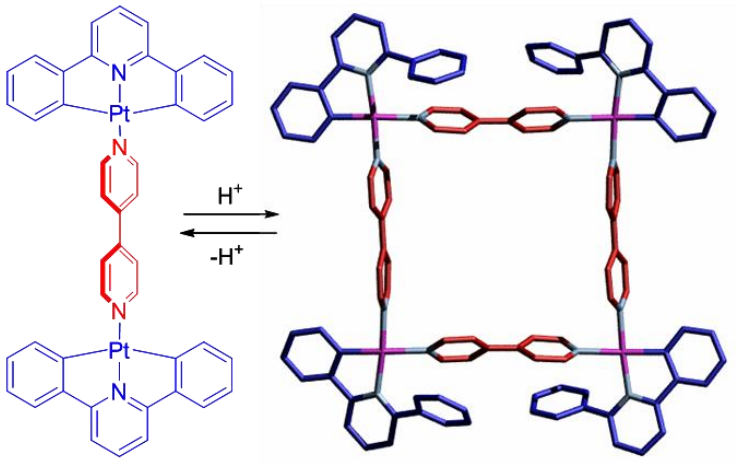

4.1 Introduction

Over the past two decades, remarkable advances in coordination driven self-assembly has led to the creation of an abundance of discrete supramolecules,[1-11] such as molecular cages[9,10] and capsules.[7,11] The rational systematic design approach, pioneered by Fujita[3] and Stang,[4] in which the encoding of information, such as coordination directionality and geometry, within carefully designed building blocks has been extensively exploited for the formation of intricate preprogrammed architectures of well defined shape and structure. These complex artificial architectures are of great particular interest due to their widespread applications in molecular sensing[12] and catalysis.[13-17] Nonetheless, many of these artificial systems lack the ability possessed by their biological counterparts to self-assemble in response to the application of an external stimulus or to a change in the local environment (e.g. a pH change).[18] This self assembly (or disassembly) process is often an allosteric process in which regulation of a discrete molecular change is brought about by the masking or revelation of a relevant functional group. The demonstration of stimuli-responsive dynamic function in metallosupramolecular systems, for instance reversible switching between assemblies in solution, remain rare.[19]

This chapter describes how a switchable platinum coordination mode has been exploited to facilitate the proton-driven self-assembly of the two and three-dimensional metallosupramolecular architectures which can be subsequently disassembled into their constituent components simply by treating with base.

4.2 Results and Discussion

4.2.1 Stimuli-Responsive Reversible Assembly of Molecular Square

The pH-switchable molecular event, in which neutral [**L**Pt(PyNMe$_2$)] (H_2**L** = 2,6-diphenylpyridine) was readily and reversibly interconverted into charged [H**L**Pt(PyNMe$_2$)OTs], has been studied using ^{1}H NMR spectroscopy.[20] These studies have shown that in different deuterium-labelled solvents the TsO^- anion is readily displaced by better ligands such as pyridine or acetonitrile.[21] In effect, this protonation/deprotonation event reveals/masks *cis* coordinating groups at a square planar Pt(II) center, a process which it was reasoned could be used to reversibly assemble metallosupramolecular architectures, similar to those previously reported by Fujita[3] and Stang.[4]

To explore this concept, [(**L**Pt)$_2$(4,4'-bipy)] (4,4'-bipy = 4,4'-bipyridine) was prepared by stirring two equivalents of the known complex [**L**Pt(DMSO)][22] with 4,4′-bipy in dichloromethane for 18 h at ambient temperature. [(**L**Pt)$_2$(4,4'-bipy)] showed relatively low solubility which facilitated its isolation as an orange solid in 77% yield through simple filtration. In spite of the low solubility, the addition of a dichloromethane solution of (+)-camphor-10-sulfonic acid ((+)-CSA) to the dimer led to formation of a pale yellow solution within minutes of treatment, after which time a second equivalent of 4,4′-bipy was added (Scheme 4.1). The ^{1}H NMR spectrum of the resulting solution indicated the rapid formation of a predominantly single species, which did not appear to change over time. As well as sequential addition, treating [(**L**Pt)$_2$(4,4'-bipy)] directly with the CSA salt of 4,4'-bipy, i.e. 4,4'-bipy·2CSA, gave the same ^{1}H NMR spectrum. To aid isolation, NH_4PF_6 was added to the solution and following recrystallization from nitromethane and diethyl ether the product was obtained as a yellow solid in 56% yield.

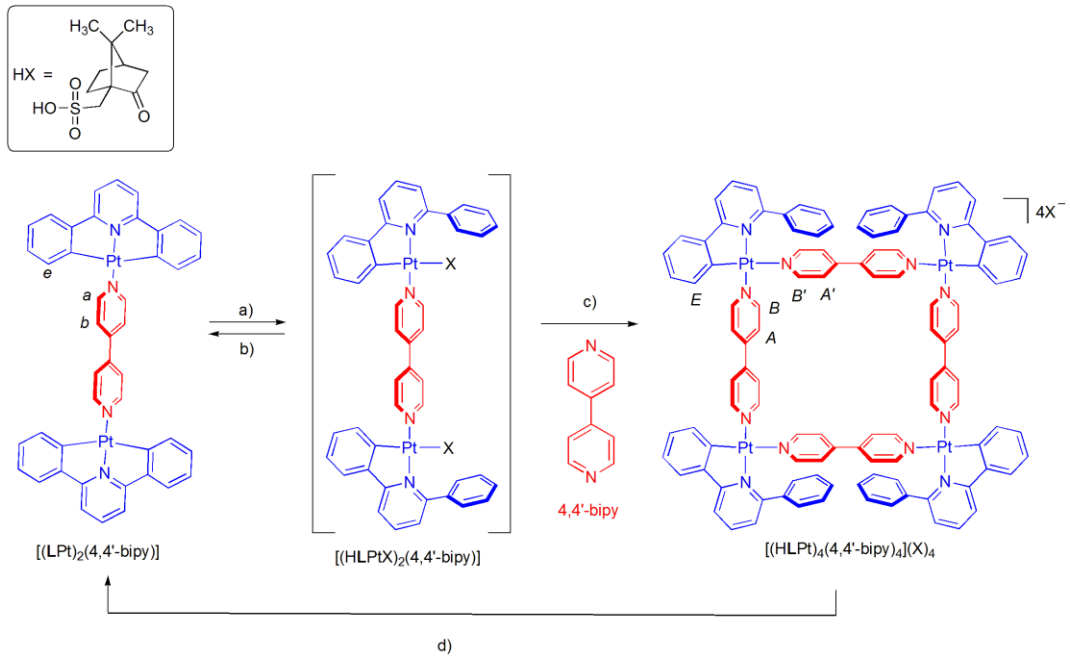

Scheme 4.1 Stimuli-responsive assembly and disassembly of the two dimensional metallosupramolecular architecture; $[(\mathbf{H}LPt)_4(4,4'\text{-bipy})_4](PF_6)_4$. Reagents and conditions: a) (+)-CSA, CH_2Cl_2, 298 K, 15 min, quantitative; b) P_1-^{t}Bu, CH_2Cl_2, 298 K, quantitative; c) i) 4,4'-bipy, CH_2Cl_2, 298 K, 45 min, ii) NH_4PF_6, acetone, 56%; d) P_1-^{t}Bu, CH_2Cl_2, 298 K, 18 h, 59%.

The electrospray mass spectrum of this sample (Figure 4.1) showed several peaks between 500-1500 *m/z* units but a closer inspection of the peak at 823 *m/z* (Figure 4.2a) revealed a third of a unit peak separation and compared well to the predicted isotopic distribution (Figure 4.2b) for the tricationic molecular square[23] $[[(\mathbf{H}LPt)_4(4,4'\text{-bipy})_4](PF_6)]^{3+}$. The peak at 1307 *m/z* (Figure 4.3a) showed half unit separation and although this was consistent with the 2+ molecular square ($[(\mathbf{H}LPt)_4(4,4'\text{-bipy})_4](PF_6)_2]^{2+}$) it overlapped with the singly charged half-molecular square fragment ($[(\mathbf{H}LPt)_2(4,4'\text{-bipy})_2](PF_6)]^{+}$) (Figure 4.3b) and thus prohibited further predicted isotope comparison (Figure 4.3c). Virtually all the peaks within the 500-1500 *m/z* region could be readily assigned to fragments of $[(\mathbf{H}LPt)_4(4,4'\text{-bipy})_4](PF_6)_4$.

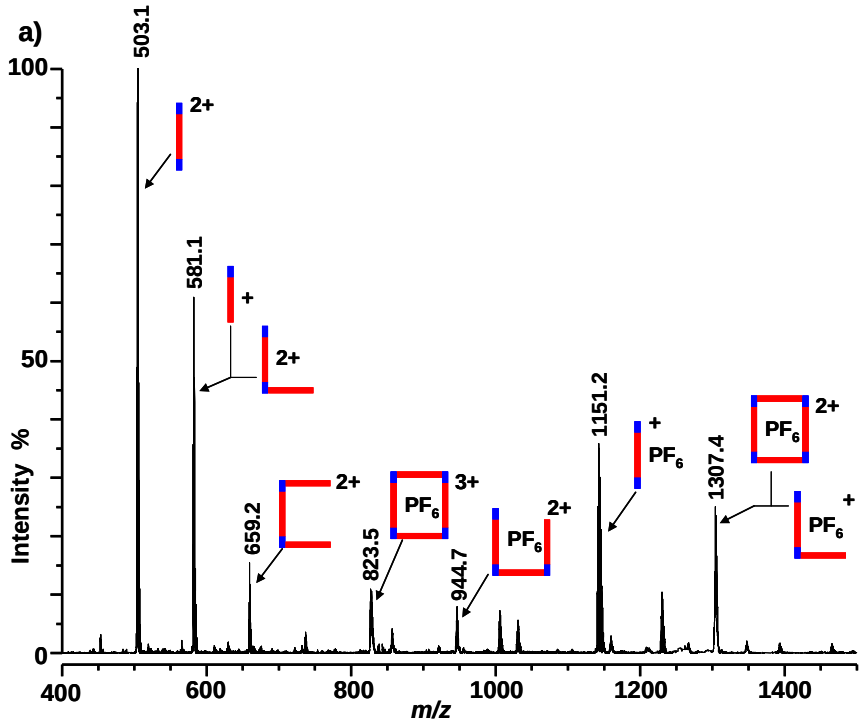

Figure 4.1 Electrospray mass spectrum of $[(HLPt)_4(4,4'\text{-bipy})_4](PF_6)_4$ between 400-1500 *m/z* units. Labeling of peaks are diagrammatic representations of molecular square in accordance with the colouring of $[(HLPt)_4(4,4'\text{-bipy})_4](PF_6)_4$ in Scheme 4.1; consisting of blue Pt corner pieces and red 4,4'-bipy units.

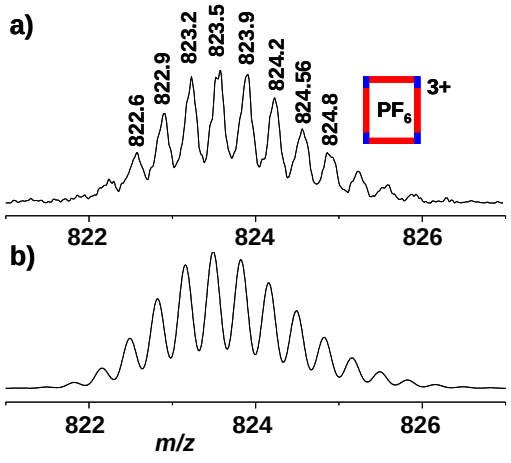

Figure 4.2 a) Observed isotope pattern for tricationic molecular square $[(HLPt)_4(4,4'\text{-bipy})_4](PF_6)]^{3+}$ and b) predicted isotope distribution for tricationic molecular square $[(HLPt)_4(4,4'\text{-bipy})_4](PF_6)]^{3+}$.

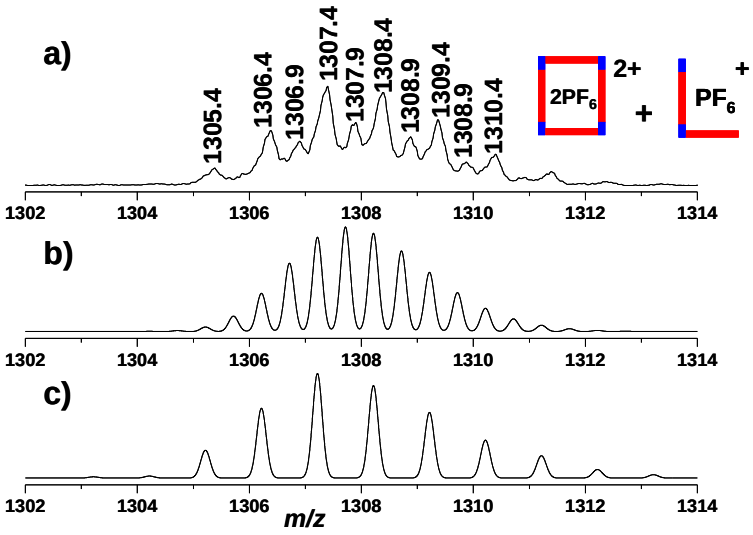

Figure 4.3 a) Observed isotope pattern for dicationic molecular square $[(H\mathbf{L}Pt)_4(4,4'\text{-bipy})_4](PF_6)_2]^{2+}$ overlapped with monocationic half molecular-square fragment $[(H\mathbf{L}Pt)_2(4,4'\text{-bipy})_2](PF_6)]^{+}$; b) Predicted isotopic distribution for dicationic molecular square $[(H\mathbf{L}Pt)_4(4,4'\text{-bipy})_4](PF_6)_2]^{2+}$; c) Predicted isotopic distribution for monocationic half molecular-square fragment $[(H\mathbf{L}Pt)_2(4,4'\text{-bipy})_2](PF_6)]^{+}$.

$[(H\mathbf{L}Pt)_4(4,4'\text{-bipy})_4](PF_6)_4$ could potentially adopt several different isomeric forms. However, the ^1H NMR spectrum of $[(H\mathbf{L}Pt)_4(4,4'\text{-bipy})_4](PF_6)_4$ in CD_3NO_2 (Figure 4.4) indicated a single product with fourteen different proton environments which eliminated lower symmetry isomers and suggested that the product was one of two possibilities – either the D_{2h} symmetric isomer shown in Scheme 4.1, or the C_{4h} isomer in which the Pt corner pieces all point in a clockwise direction. Further NMR analysis revealed an NOE (Nuclear Overhauser Effect) cross signal between the different *ortho* 4,4'-bipy protons (H_B and $H_{B'}$) but not between the *meta* 4,4'-bipy protons (H_A and $H_{A'}$), which eliminated the C_{4h} isomer.[24] In effect, the formation of the D_{2h} metallocycle in dichloromethane at room temperature is a kinetically controlled, four-component, self assembly process between two acceptor and two donor components and explains the absence of any entropically favored triangular species.[25]

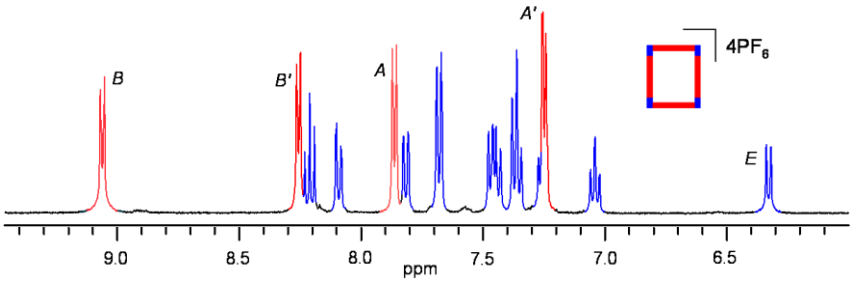

Figure 4.4 ^{1}H NMR spectrum (CD_3NO_2, 400 MHz, 300 K) of molecular square $[(H\mathbf{L}Pt)_4(4,4'\text{-bipy})_4](PF_6)_4$ The assignments correspond to the lettering and colouring shown in Scheme 4.1.

Single crystals of $[(H\mathbf{L}Pt)_4(4,4'\text{-bipy})_4](PF_6)_4$ suitable for analysis by X-ray crystallography were grown from nitromethane and diethyl ether. The solid state structure (Figure 4.5) confirmed a tetrameric molecular square arrangement and also the connectivity of the kinetic D_{2h} product. However, when viewed along the plane of the square it can clearly be observed that the product adopts a lower symmetry arrangement in the solid state due to quite different 4,4'-bipy conformations. The 4,4'-bipy units which lie *trans* to the nitrogen donor of H**L** adopt an essentially planar conformation (torsion angle = 9°) and lie perpendicular to the plane of the four platinum ions. In contrast, the other 4,4'-bipy units adopt a non-planar orientation (torsion angle = 46°) such that two hydrogen atoms from each constituent pyridine moiety point slightly towards the centre of the square. The adoption of this conformation appears to be caused by π-π interactions between these constituent pyridine groups and the non-coordinating phenyl moiety of H**L** (centroid-centroid distances of between 3.41 and 3.52 Å).[26] In addition, the non-coordinating phenyl groups of H**L** are oriented either above or below the plane of the four platinum ions, presumably to avoid unfavorable steric interactions between adjacent sites.

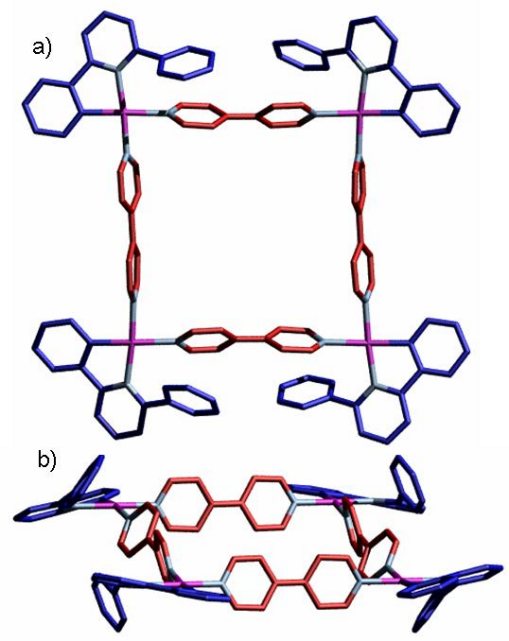

Figure 4.5 X-ray crystal structure of molecular square $[(H\mathbf{L}Pt)_4(4,4'\text{-bipy})_4](PF_6)_4$ viewed from a) above the plane and b) a tilted side-on perspective. The carbon atoms of 4,4'-bipy are shown in red, the carbon atoms of H**L** in blue, platinum in magenta and nitrogen in pale blue. The PF_6 counter anions and five nitromethane solvent molecules have been removed for clarity.

To explore the stimuli-responsive disassembly process, a dichloromethane solution of phosphazene base, P_1-^{t}Bu, was added to $[(\mathbf{L}Pt)_4(4,4'\text{-bipy})_4](PF_6)_4$ (Scheme 4.1). Almost immediately, a darkening of the solution was observed and after stirring overnight at room temperature an orange solid was filtered off, which showed identical spectroscopic properties to the material already assigned as $[(\mathbf{L}Pt)_2(4,4'\text{-bipy})]$. Unsurprisingly this base-induced disassembly of the tetramer is slow in comparison to the reaction of the mononuclear complex ($[H\mathbf{L}Pt(PyNMe_2)OTs] \rightarrow [\mathbf{L}Pt(PyNMe_2)]$) which under similar conditions is complete by the time an NMR spectrum can be recorded (less than five minutes).

4.2.2 Stimuli-Responsive Reversible Assembly of Trigonal Prism

To take this chemistry from two to three dimensions, the switchable self-assembly with the triazine ligand, tpt,[27] has also been investigated, both by sequential addition of CSA and tpt to [(**L**Pt)$_2$(4,4'-bipy)] (Scheme 4.2) and by direct addition of the salt, tpt.3CSA. Again, formation of the metallosupramolecular architecture was rapid at room temperature and after exchange of the counter anions by treatment with NH_4PF_6, a yellow solid was isolated in 97% yield.

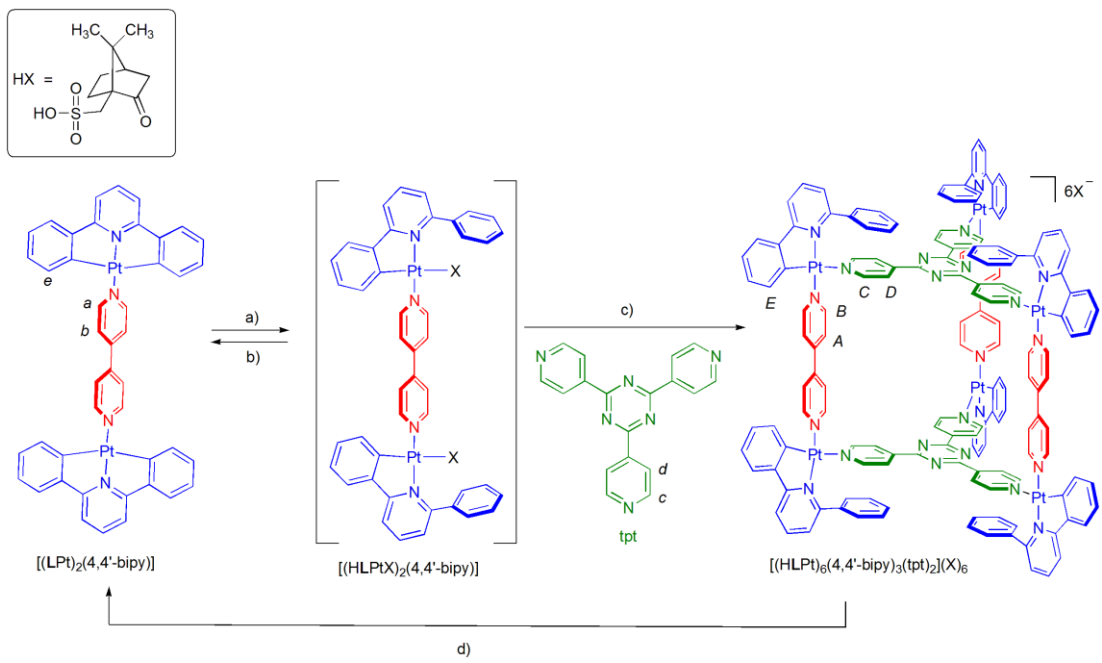

Scheme 4.2 Stimuli-responsive assembly and disassembly of the three dimensional metallosupramolecular architecture; [(H**L**Pt)$_6$(4,4'-bipy)$_3$(tpt)$_2$](PF$_6$)$_6$. Reagents and conditions: a) (+)-CSA, CH_2Cl_2, 298 K, 15 min, quantitative; b) P_1-^{t}Bu, CH_2Cl_2, 298 K, quantitative; c) i) tpt, CH_2Cl_2, 298 K, 45 min, ii) NH_4PF_6, acetone, 97%; d) P_1-^{t}Bu, CD_2Cl_2, 298 K, 3 h, quantitative.

The electrospray mass spectrum of this product (Figure 4.6) showed several peaks between 400-2200 *m/z* units but a closer inspection of the peak at 1359 *m/z* (Figure 4.7a) revealed a third of a unit peak separation and compared well to the predicted isotopic distribution (Figure 4.7b) for the tricationic trigonal prism [(H**L**Pt)$_6$(4,4′-bipy)$_3$(tpt)$_2$](PF$_6$)$_3$]$^{3+}$. The peak at 2112 *m/z* (Figure 4.8a) showed half unit separation

and compared well to the predicted isotopic distribution (Figure 4.8b) for the 2+ triangular prism $[(H\mathbf{L}Pt)_6(4,4'\text{-bipy})_3(tpt)_2](PF_6)_4]^{2+}$. Virtually all the peaks within the 400-2200 *m/z* region could be readily assigned to fragments of $[(H\mathbf{L}Pt)_6(4,4'\text{-bipy})_3(tpt)_2](PF_6)_6]$.

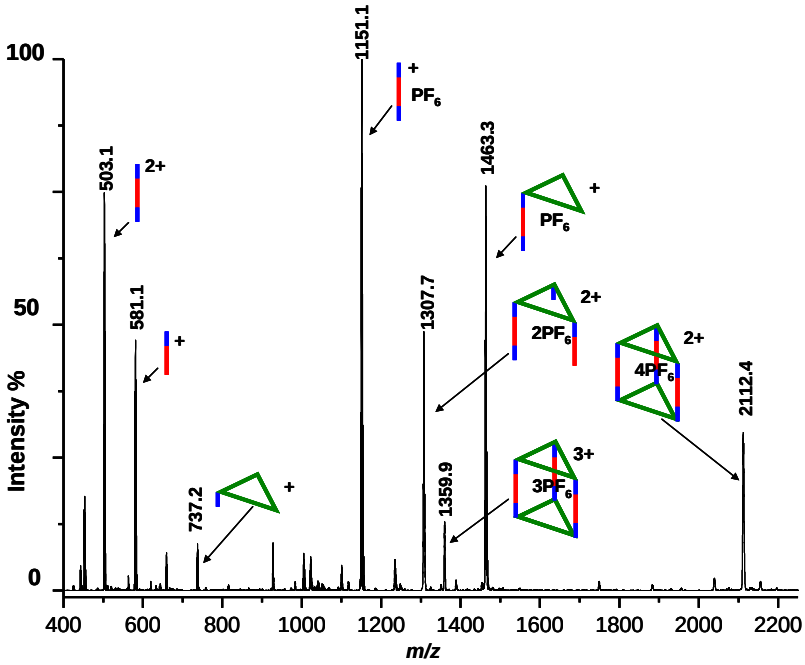

Figure 4.6 Electrospray mass spectrum of $[(H\mathbf{L}Pt)_6(4,4'\text{-bipy})_3(tpt)_2](PF_6)_6]$ between 400-2200 *m/z* units. Labeling of peaks are diagrammatic representations of the trigonal prism and its fragments in accordance with the colouring of $[(H\mathbf{L}Pt)_6(4,4'\text{-bipy})_3(tpt)_2](PF_6)_6]$ in Scheme 4.2.

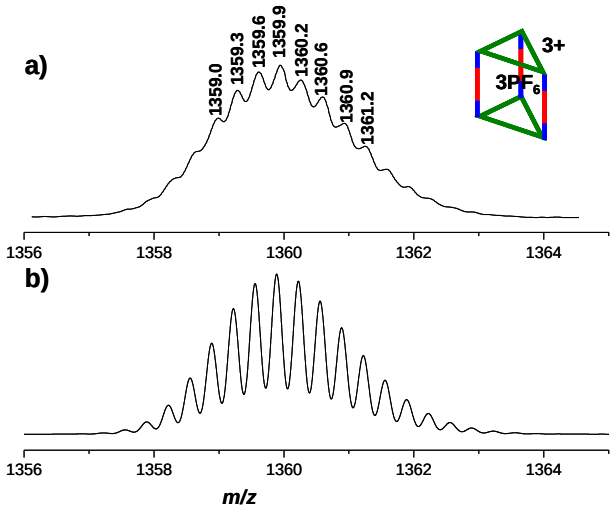

Figure 4.7 a) Observed isotope pattern for tricationic trigonal prism $[(H\mathbf{L}Pt)_6(4,4'\text{-bipy})_3(tpt)_2](PF_6)_3]^{3+}$ and b) Predicted isotopic distribution for tricationic trigonal prism $[[(H\mathbf{L}Pt)_6(4,4'\text{-bipy})_3(tpt)_2](PF_6)_3]^{3+}$.

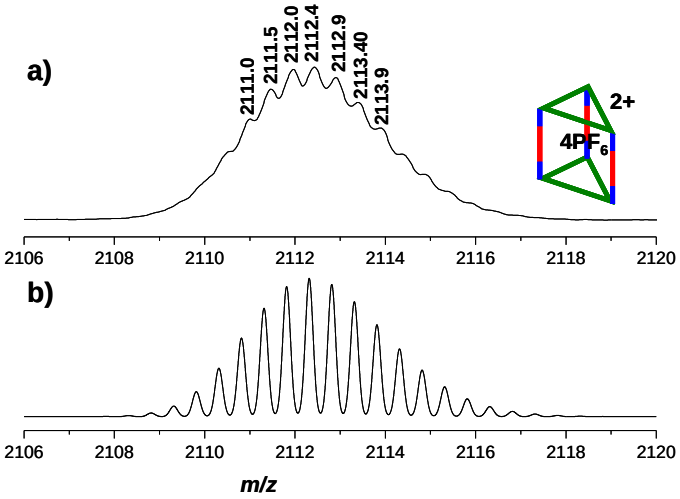

Figure 4.8 a) Observed isotope pattern for dicationic trigonal prism $[(H\mathbf{L}Pt)_6(4,4'\text{-bipy})_3(tpt)_2](PF_6)_4]^{2+}$ and b) Predicted isotopic distribution for tricationic trigonal prism $[(H\mathbf{L}Pt)_6(4,4'\text{-bipy})_3(tpt)_2](PF_6)_4]^{2+}$.

The ^{1}H NMR of this product (Figure 4.9a) showed the correct ratio of triazine signals (H_C and H_D), 4,4'-bipy signals (H_A and H_B) and those of H**L** (e.g. H_e) and the NOE spectrum showed a cross peak between H_B and H_C. The large upfield shifts of the triazine pyridyl signals (H_C and H_D) compared to the free triazine ligand are

likely caused by π-π interactions with the non-coordinating phenyl group of H**L**, which further supports the formation of a single product isomer from what is in effect a kinetically-controlled, five-component self-assembly process between three ditopic acceptors and two tritopic donor units.

The increased solubility of the prism $[(H\mathbf{L}Pt)_6(4,4'\text{-bipy})_3(tpt)_2](PF_6)_6$ in dichloromethane, in comparison to the square, has allowed the stimuli-responsive switching to be monitored in solution using ^{1}H NMR spectroscopy (Figure 4.9). This experiment was initiated by the addition of 12 eq of P_1-^{t}Bu (2 eq per Pt ion) to a CD_2Cl_2 solution of $[(H\mathbf{L}Pt)_6(4,4'\text{-bipy})_3(tpt)_2](PF_6)_6$. After 2 h, complete disappearance of the signals assigned to $[(H\mathbf{L}Pt)_6(4,4'\text{-bipy})_3(tpt)_2](PF_6)_6$ ($H_{A\text{-}E}$) and the emergence of new resonances which correspond to the disassembled components tpt (H_c and H_d) and $[(\mathbf{L}Pt)_2(4,4'\text{-bipy})]$ (H_a, H_d, H_e) was observed. Addition of 12 eq of CSA to the same sample resulted in the disappearance of the signals due to free tpt and $[(\mathbf{L}Pt)_2(4,4'\text{-bipy})]$ and the appearance of a new set of signals (Figure 4.9c). This spectrum showed a striking similarity to the spectrum of $[(H\mathbf{L}Pt)_6(4,4'\text{-bipy})_3(tpt)_2](PF_6)_6$ (Figure 4.9a) indicating that the addition of CSA causes the re-assembly of the trigonal prism in solution. The subtle differences and slight broadening in the spectrum of the CSA re-assembled species are likely caused by a mixture of different counter anions present in solution, e.g. $[(H\mathbf{L}Pt)_6(4,4'\text{-bipy})_3(tpt)_2](PF_6)_m(CSA)_{6\text{-}m}$. A second addition of 12 eq of P_1-^{t}Bu (Figure 4d) followed by 12 eq of CSA (Figure 4.9e) indicate these metallosupramolecular architectures can be efficiently cycled between assembled and disassembled states in solution by simply alternating the addition of base and acid.

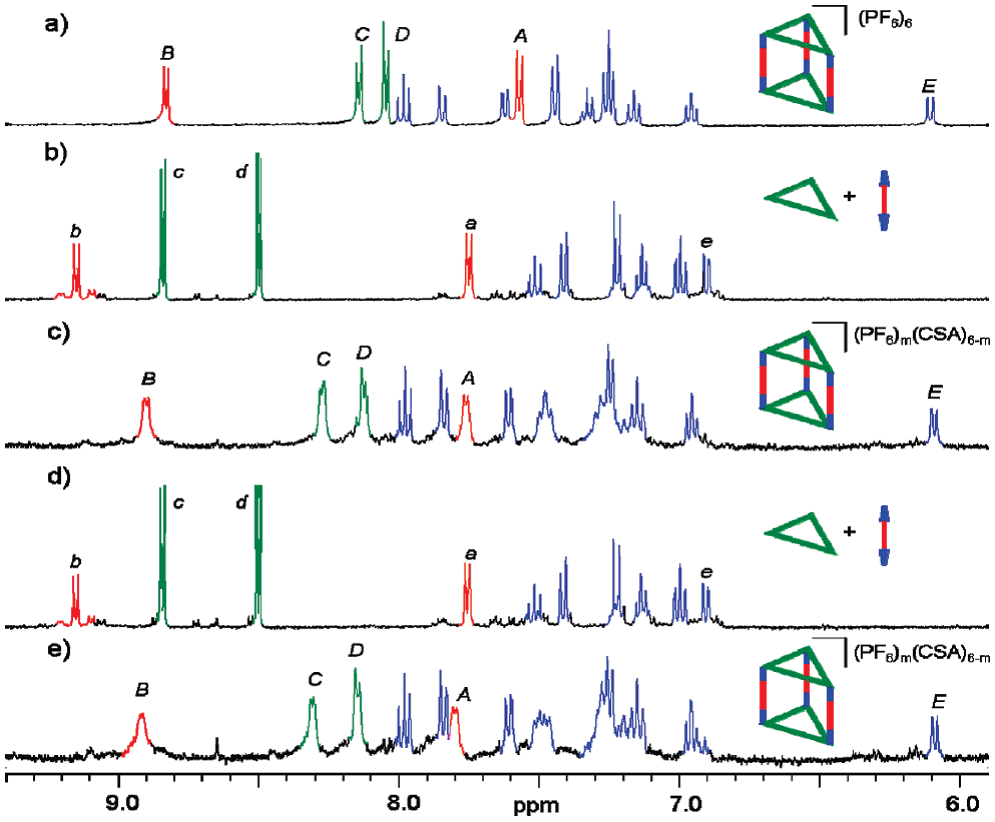

Figure 4.9 a) ^{1}H NMR spectra (400 MHz, CD_2Cl_2, 298 K) showing solution switching between assembled and disassembled states of trigonal prism $[(HLPt)_6(4,4'\text{-bipy})_3(tpt)_2](PF_6)_6$: a) spectrum of $[(HLPt)_6(4,4'\text{-bipy})_3(tpt)_2](PF_6)_6$; spectra recorded b) 2 h after the addition of 12 eq of P_1-^{t}Bu to $[(HLPt)_6(4,4'\text{-bipy})_3(tpt)_2](PF_6)_6$; c) 30 min after subsequent addition of 12 eq of CSA; d) 2 h after subsequent addition of 12 eq of P_1-^{t}Bu; and e) 30 mins after subsequent addition of 12 eq of CSA. The assignments correspond to the lettering and colouring shown in Scheme 4.2.

4.3 Conclusions

In conclusion, the discovery of a pH switchable platinum coordination mode has been exploited to switch on the self- assembly of two and three dimensional metallosupramolecular architectures. The efficacy of this self-asssembly process was demonstrated through the formation of single species in good to excellent yields and in both cases the self-assembly process could be simply reversed in full by treating with a slight excess of base.

4.4 References and Notes

[1] (a) J. –M. Lehn, *Supramolecular Chemistry*, VCH, Weinheim, 1995; (b) J. L. Atwood, J. E. D. Davies, D. D. Macnicol, F. Vögtle, *Comprehensive Supramolecular Chemistry*, Pergamon, Oxford, 1996, vol 9.

[2] R. W. Saafrand, H. Maid, A. Scheurer, *Angew. Chem. Int. Ed.* 2008, **47**, 8794.

[3] For the first example of first rationally designed molecular square metallacycle see: (a) M. Fujita, J. Yazaki, K. Ogura; *J. Am. Chem. Soc.* 1990, **112**, 5645. For other examples of kinetically controlled coordination driven self assembly of group 10 transition metal based molecular squares see: (b) M. Fujita, F. Ibukuro, K. Yamaguchi, K. Ogura; *J. Am. Chem. Soc.* 1995, **117**, 4175; (c) M. Fujita, Y. J. Kwon, S. Washizu, K. Ogura; *J. Am. Chem. Soc.* 1994, **116**, 1151; (d) M. Fujita, O. Sasaki, T. Mitsuhashi, T. Fujita, J. Yazaki, K. Yamaguchi, K. Ogura; *Chem. Comm.* 1996, **14**, 1535; (e) M. Yoshizawa, M. Nagao, K. Kumazawa, M. Fujita; *J. Organometallic Chem.* 2005, **690**, 5383; (f) K-I. Yamashita, K-I Sato, M. Kawano, M. Fujita; *New J. Chem.*, 2009, **33**, 264. For the first example of guest-host encapsulation/molecular recognition in group 10 transition metal based metallocycle see: (g) M. Fujita, J. Yazaki, K. Ogura; *Tetrahedron Lett.* 1991, **32**, 5589; For other examples of metal-mediated self assembly of Pt(II) and Pd(II)-based molecular cages which display guest-host encapsulation see: (i) M. Fujita, D. Ogura, M. Miyazawa, H. Oka, K. Yamaguchi, K. Ogura; *Nature*, 1995, **378**, 469; (j) T. Kusukawa, M. Fujita; *Angew. Chem. Int. Ed.* 2001, **40**, 1879; For examples of coordination-driven self-assembly of spherical frameworks; (k) S. Sato, Y. Ishido, M. Fujita; *J. Am. Chem. Soc.* 2009, **131**, 6064; (l) S. Sato, J. Iida, K. Suzuki, M. Kawano, T. Ozeki, M, Fujita; *Science*, 2006, **313**, 1273; (m) K. Suzuki, J. Iida, S. Sato, M. Kawano, M. Fujita; *Angew. Chem. Int. Ed.* 2008, **47**, 5780; For some recent examples of metal-mediated self assembly of Pt(II) and Pd(II)-based molecular

polyhedron and capsules see: (m) S. –Y. Yu, T. Kusukawa, K. Biradha, M. Fujita; *J. Am. Chem. Soc.* 2000, 122, 7150; (n) K. Kumazawa, K. Biradha, T. Kusukawa, T. Okano, M. Fujita; *Angew. Chem. Int. Ed.* 2003, **42**, 3909; For reviews of supramolecular architectures whose directed self-assembly rely upon transition metal-ligand bonds see: (o) M. Fujita, M. Tominaga, A. Hori, B. Therrien; *Acc. Chem. Res.*, 2005, ***38***, 371; (p) M Fujita; *Coord. Chem. Rev.*, 1998, **27**, 417.

[4] (a) L. Zhao, B. H. Northrop, P. J. Stang; *J. Am. Chem. Soc.*, 2008, **130**, 11886; (b) D. C. Caskey, T. Yamamoto, C. Addicott, R. K. Shoemaker, J. Vacek, A. M. Hawkridge, D. C. Muddiman, G. S. Kottas, J. Michl, P. J. Stang; *J. Am. Chem. Soc.*, 2008, **130**, 7620; (c) J. Fan, J. A. Whiteford, B. Olenyuk, M. D. Levin, P. J. Stang, E. B. Fleischer; *J. Am. Chem. Soc.*, 1999, **121**, 2741; (e) G. Tárkányi, H. Jude, G. Pálinkas, P. J. Stang; *Org. Lett.*, 2005, **7**, 4971; (f) M. Wang, Y-R. Zheng, K. Ghosh, P. J. Stang; *J. Am. Chem. Soc.*, 2010, **132**, 6282; (g) H. –B. Yang, K. Gnosh, B. H. Northrop, Y. –R. Zheng, M. M. Lyndon, D. C. Muddiman, P. J. Stang, *J. Am. Chem. Soc.*, 2007, **129**, 14187; (h) K. Gnosh, H. –B. Yang, B. H. Northrop, M. M. Lyndon, Y. –R. Zheng, D. C. Muddiman, P. J. Stang, *J. Am. Chem. Soc.*, 2008, **130**, 5320; (i) K. Gnosh, J. Hu, H. S. White, P. J. Stang; *J. Am. Chem. Soc.*, 2009, **131**, 6695; (j) L. Zhao, K. Gnosh, Y. Zheng, M. M. Lyndon, T. I. Williams, P. J. Stang; *Inorg. Chem.*, 2007, *48*, 5590; (k) Z. Zhao, Y. –R. Zheng, M. Wang, J. B. Pollock, P. J. Stang; *Inorg. Chem.*, 2010, **49**, 8653; For recent examples of supramolecular-to-supramolecular transformations see; (l) L. Zhao, B. H. Northrop, P. J. Stang; *J. Am. Chem. Soc.*, 2008, **130**, 11886; (m) T. Yamamoto, A. Arif, P. J. Stang; *J. Am. Chem. Soc.*, 2003, **125**, 12309.

[5] A. Shivanyuk, J. Jr. Rebek; *J. Am. Chem. Soc.*, 2003, **125**, 3432; (b) O. Hayashida, L. Seho, J. Jr. Rebek; *J. Org. Chem.*, 2002, **67**, 8291; (c) A. Scarso, L. Trembleau, J. Jr. Rebek; *J. Am. Chem. Soc.*, 2004, **126**, 13512; (d) A. Shivanyuk, J. Jr. Rebek; *J. Am. Chem. Soc.*, 2002, **124,** 12074; (e) T.

Heinz, D. M. Rudkevich, J. Jr. Rebek; *Nature*, 1994, **394**, 764; (f) T. Iwasawa, E. Mann, J. Jr. Rebek; *J. Am. Chem. Soc.,* 2006, **129**, 8818.

[6] B. J. Holliday, C. A. Mirkin, *Angew. Chem. Int. Ed.* 2001, **40**, 2022.

[7] (a) A. J. Terpin, M. Ziegler, D. W. Johnston, K. N. Raymond; *Angew. Chem. Int. Ed.,* 2001, **40**, 157; (b) J. L. Brumaghim, M. Michls, D. Pagliero, K. N. Raymond; *Eur. J. Org. Chem.,* 2004, **24**, 5115; (c) T. Beissel, R. E. Powers, K. N. Raymond; *Angew. Chem. Int. Ed.,* 1996, **35**, 1084; (d) S. M. Biros, R. M. Yeh, K. N. Raymond; *Angew. Chem. Int. Ed.,* 2008, **47**, 6062; (e) C. Bruckner, R. E. Powers, K. N. Raymond; *Angew. Chem. Int. Ed.,* 1998, **37**, 1837; (f) M. D. Pluth, R. G. Bergman, K. N. Raymond, *Angew. Chem. Int. Ed.,* 2008, **46**, 8587; (g) D. Fiedler, D. H. Leung, R. G. Bergman, K. N. Raymond; *Acc. Chem. Res.,* 2005, **38**, 349.

[8] (a) A. M. Najar, I. S. Tidmarsh, H. Adams, M. D. Ward; *Inorg. Chem.,* 2009, **48**, 11871; (b) T. K. Ronson, H. Adams, M. D. Ward; *CrystEngComm*., 2006, **8**, 497; (c) I. S. Tidmarsh, T. B. Faust, H. Adams, L. P. Harding, L. Russo, W. Clegg, M. D. Ward; *J. Am. Chem. Soc.*, 2008, **130**, 15167; (d) R. L. Paul, S. P. Argent, J. C. Jeffrey, L. P. Harding, J. M. Lynam, *Dalton Trans.*, 2004, **21**, 3453.

[9] (a) P. Mal, B. Breiner, K. Rissanen, J. R. Nitschke; *Science*, **2009**, *324*, 1697; (b) J. R. Nitschke, *Acc. Chem. Res.* **2007**, *40*, 103.

[10] For other recent examples of the coordination-driven, self-assembly of metal based cages see: (a) D. Zuccaccia, L. Pirondini, R. Pinalli, E. Dalcanale, A. Macchioni, *J. Am. Chem. Soc.* 2005, **127**, 7025; (b) R. Pinalli, B. Cristini, B. Sottili, S. Geremia, J. Campagnolo, *J. Am. Chem. Soc.* 2004, **126**, 6516; (c) J. Mattson, P. Govindaswamy, J. Furrer, Y. Sei, K. Yamaguchi, G. Süss-Fink, B. Therrien; *Organometallics*, 2008, **27**, 4346; (d) K. Kobayashi, Y. Yamada, M. Yamanaka, Y. Sei, K. Yamaguchi; *J. Am. Chem. Soc.* 2006, **126,** 13896;

(e) M. Yamanaka, Y. Yamada, Y. Sei, K. Yamaguchi, K. Kobayashi; *J. Am. Chem. Soc.* 2006, **128**, 1531; (f) D. C. Caskey, J. Michl; *J. Org. Chem.* 2005, **70**, 5442; (g) T. K. Ronson, J. Fisher, L. P. Harding, M. J. Hardie; *Angew. Chem., Int. Ed.* 2007, **46**, 9086; (h) R. W. Saalfrank, H. Maid, A. Scheurer, F. W. Heinemann, R. Puchta, W. Bauer, D. Stern, D. Stalke; *Angew. Chem. Int. Ed.* 2008, **47**, 8941.

[11] For some recent examples of the self-assembly of molecular capsules; (a) K. Kobayashi, R. Kitagawa, Y. Yamada, M. Yamanaka, T. Suematsu, Y. Sei, K. Yamaguchi; *J. Org. Chem.*, 2007, **72**, 3242; (b) N. P. Power, S. J. Dalgarno, J. L. Atwood, *Angew. Chem. Int. Ed.,* 2007, **46**, 8601; (c) N. P. Power, S. J. Dalgarno, J. L. Atwood, *Angew. Chem. Int. Ed.*, 2007, **45**, 8522.

[12] (a) Y. Liu, X. Wu, C. He, Y. Jiao, C. Duan, *Chem. Comm.*, 2009, **48**, 7554; (b) M. R. Ams, D. Ajami, L. Craig, J. –S. Yang, J. Jr. Rebek; *J. Am. Chem. Soc.*, 2009, **131,** 13190; (c) H. Dube, M. R. Ams, J. Jr. Rebek; *J. Am. Chem. Soc.*, 2010, **132**, 9984.

[13] (a) M. Yoshizawa, J. K. Klosterman, M. Fujita, *Angew. Chem. Int. Ed.*, 2009, **48**, 3418; (b) D. Fiedler, H. van Halbeek, R. G. Bergman, K. N. Raymond; *J. Am. Chem. Soc.*, 2006, **128**, 10240; (c) M. Yoshizawa, M. Tamura, M. Fujita; *Science,* 2006, **312**, 251; (d) D. Fiedler, R. G. Bergman, K. N. Raymond; *Angew. Int. Ed. Chem.*, 2004, **43**, 6748; (e) M. D. Pluth, R. G. Bergman, K. N. Raymond; *Science.*, 2007, **316**, 85.

[14] For some recent examples of stoichiometric reactions carried out in metal-mediated coordination driven, self-assembled, supramolecular architectures see: (a) D. H. Leung, R. G. Bergman, K. N. Raymond, *J. Am. Chem. Soc.*, **2006**, *128*, 10240; (b) M. Yoshizawa, Y. Takeyama, T. Kusukawa, M. Fujita, *Angew. Chem. Int. Ed.*, **2002**, *41*, 1347; (c) D. H. Leung, D. Fiedler, R. G. Bergman, K. N. Raymond, *Angew. Chem. Int. Ed.,* **2002**, *43,* 963; (d) Y.

Nishioka, T. Yamaguchi, M. Yoshizawa, M. Fujita, *J. Am. Chem. Soc.*, **2007**, *129*, 7000. (e) H. Ito, T. Kusukawa, M. Fujita; *Chem. Lett.*, **2000**, 598.

[15] For recent examples of highly stereoselective [2+2] photodimerisation reactions achieved upon self-assembly of a coordination cage see; (a) M. Yoshiwawa, Y. Takeyama, T. Kusukawa, M. Fujita; *Angew. Chem. Int. Ed.*, **2002**, *41*, 1347; (b) M. Yoshizawa, Y. Takeyama, T. Okano, M. Fujita; *J. Am. Chem. Soc.*, **2003**, *125*, 3243; (c) J. –L Hou, D. Ajami, J. Jr. Rebek; *J. Am. Chem. Soc.*, **2008,** *130*, 7810.

[16] For recent examples of trapping of reactive intermediates in metal-mediated, self-assembled, supramolecular architectures see: (a) J. L. Brumaghim, M. Michels, D. Pagliero, K. N. Raymond; *Eur. J. Org. Chem.*, 2004, **22**, 5115; (b) V. M. Dong, D. Fiedler, B. Carl, R. G. Bergman, K. N. Raymond; *J. Am. Chem. Soc.*, 2006, **128,** 14464; (c) J. L. Brumaghim, M. Michels, K. N. Raymond; *Eur. J. Org. Chem.*, 2004, **22**, 4552; (d) M. Yoshizawa, T. Kusukawa, M. Fujita, K. Yamaguchi; *J. Am. Chem. Soc.*, 2000, **122**, 6311; (e) M. Yoshizawa, T. Kusukawa, M. Fujita, S. Sakamoto, K. Yamagichi; *J. Am. Chem. Soc.*, 2001, **123**, 10454.

[17] M. Kawano, M. Fujita; *Coord. Chem. Rev.*, 2007, **251**, 2592.

[18] (a) P. Mal, D. Schultz, K. Beyeh, K. Rissanen, J. R. Nitschke; *Angew. Chem., Int. Ed.*, 2008, **47**, 8297; (b) M. Balboiu, L. Prodi, M. Montalti, N. Zaccheroni, N. Kyritsakas, J. –M. Lehn; *Chem -.Eur. J.*, 2004, **10,** 2953.

[19] (a) S. Hiraoka, T. Yi, M. Shiro, M. Shionoya; *J. Am. Chem. Soc.*, 2002, **124**, 14510; (b) K. Harano, S. Hiraoka, M. Shionoya, *J. Am. Chem. Soc.*, 2007, **129**, 5300; (c) S. Hiraoka, Y. Sakata, M. Shionoya; *J. Am. Chem. Soc.*, 2008, **130**, 10058; (d) A. M. Brown, M. V. Ovchinnikov, C. L. Stern, C. A. Mirkin; *J. Am. Chem. Soc.*, 2004, **126**, 14316.

[20] P. J. Lusby, P. Müller, S. J. Pike, A. M. Z. Slawin, *J. Am. Chem. Soc.* 2009, **131**, 16398.

[21] S. J. Pike, P. J. Lusby, *Chem. Comm.* 2010, **46**, 8338.

[22] (a) G. W. V. Cave, F. P. Fanizzi, R. J. Deeth, W. Errington, J. P. Rourke; *Organometallics*, 2000, **19**, 1355. (b) J. D. Crowley, I. M. Steele, B. Bosnich; *Inorg. Chem.*, 2005, **44**, 2989.

[23] M. Fujita, J. Yazaki, K. Ogura, *J. Am. Chem. Soc.*, 1990, **112**, 5645.

[24] Formation of the D_{2h} isomer was additionally supported by the observed dominance of the fragments of $[(H\mathbf{L}Pt)_2(4,4'\text{-bipy})]^{2+}$ and $[(HLPt)_2(4,4'\text{-bipy})](PF_6)]^{+}$ in the electrospray mass spectrum for the molecular square, $[(H\mathbf{L}Pt)_4(4,4'\text{-bipy})_4](PF_6)_4$ which occur at m/z 503 and 1151, respectively.

[25] T. Weilandt, R. W. Troff, H. Saxell, K. Rissanen, C. A. Schalley, *Inorg. Chem.*, 2008, **47**, 7588.

[26] (a) A. Rang, M. Engeser, N. M. Maier, M. Nieger, W. Lindner, C. A. Schalley; *Chem.- Eur. J.* 2008, **14**, 3855. (b) A. Rang, M. Nieger, M. Engeser, A. Lützen, C. A. Schalley; *Chem. Commun.* 2008, **39**, 4789.

[27] M. Yoshizawa, J. Nakagawa, K. Kumazawa, M. Nagao, M. Kawano, T. Ozeki, M. Fujita, *Angew. Chem. Int. Ed.*, 2005, **44**, 1810.

CHAPTER FIVE

Towards a Stimuli-Responsive Bistable [2]Rotaxane Which Switches Between "3+1" and "2+2" Square Planar Pt Coordination Modes

Acknowledgements

Professor Alexandra Slawin is gratefully acknowledged for solving the crystal structures of [**L**Pt(3,5-Lut)], [**L**Pt(PPh_3)] and [H**L**Pt(dmbipy)]OTs. Dr. Paul Lusby and Dr. Martin DeCecco are gratefully thanked for their proof-reading of this chapter.

Synopsis

*In Chapter Three, it was revealed how the serendipitous discovery of a reversible platinum coordination cyclometallation reaction had been used to create stimuli-responsive multimetallic architectures. This responsiveness is faciliated by changes to the way 2,6-diphenylpyridine (H_2**L**) coordinates to platinum, either through doubly anionic tridentate C^N^C ligating mode or via a bidentate C^N donor set. The acid-induced change from tridentate to a bidentate ligand permits the cis-coordination of monodentate ligands and thus the formation of metallosupramolecular assemblies from suitable rigid exotopic donors. In this chapter, the same reversible change to H_2**L** is investigated to determine if it can be employed to drive the exchange of the partner ligand – from a monodentate donor when H_2**L** coordinates in a η^3 fashion to a bidentate chelate when H_2**L** is coordinated in a η^2 mode. In effect, it is possible to swap between "3+1" and "2+2" square planar donor sets in response to subtle pH changes. In addition to investigating the scope of this reaction, this chapter will outline the design of a stimuli-responsive bistable [2]rotaxane based on this switchable coordination chemistry and some preliminary synthesis towards this goal.*

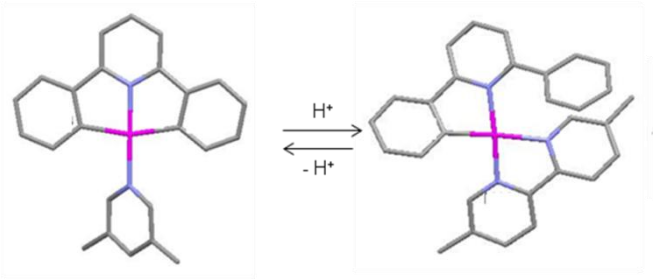

5.1 Introduction

The redox-responsive Cu(I)/Cu(II) rotaxane and catenane systems[1,2] developed by Sauvage demonstrated the versatility of stimuli-responsive switchable metal-ligand coordination motifs as an operational basis to achieve molecular motion in synthetic machines.[3] The metastability often presented by Sauvage's early systems, where switching times can vary from minutes to hours and even days,[1,2,4] are of great interest in molecular electronics[5] and ratcheting machines.[6] Despite this, most reported stimuli-responsive molecular shuttles depend on manipulation of exclusively weak non-covalent interactions,[7-9] including π-π interactions and hydrogen bonding, to induce a reversible change in the architecture. Whilst molecular switches that exploit metal-ligand interactions between components are known;[1,2,4,10,11] the operational basis for these systems relies upon changes in the binding affinity of the thread/stations whilst the macrocycle-metal component itself remains passive. For example, the palladium-based molecular shuttles reported by Leigh and co-workers,[4] in which translocation of a Pd(II)-macrocycle between 4-dimethylaminopyridine and pyridine monodentate stations was achieved *via* reversible protonation, relied upon manipulation of the binding affinities of the *N*-heterocycles for the metal centre. However, throughout operation the metal centre remained coordinated to the macrocycle component to constantly retain its square planar geometry. In effect, this system displays molecular switching between two different "3+1" square planar donors sets. The electrochemically driven copper-based molecular machines[1,2] therefore are the only reported examples in which a distinct change in the coordination geometry of the metal ion is employed to achieve net positional change of the system.

Here it is reported how the previously described acid-base switching between a C^N^C-Pt and a C^N-Pt motif can be used to bring about the exchange of the accompanying ligand from a monodentate donor, when $\mathbf{L}^{2-}$ coordinates in a η^3 fashion, to a bidentate chelate, when $H\mathbf{L}^{-}$ is coordinated in a η^2 mode. This molecular switching between "3+1" and "2+2" square planar coordination modes has been investigated with a range of different monodentate and bidentate ligands to

determine the tolerance of the system. In addition, the preliminary steps towards a bistable [2]rotaxane based on this switchable chemistry is described.

5.2 Results and Discussion

5.2.1 Model Studies: Switching from "3+1" to "2+2" donor sets

Cyclometallated complexes, [**L**Pt(**L**`)] (where **L**` = DMSO, PyH, $PyNMe_2$, benzyl sulfoxide ($S(O)(CH_2Ph)_2$), 3,5-lutidine (3,5-Lut) and triphenylphosphine (PPh_3)) were investigated to determine if the acid-induced change in the coordination mode of H_2**L** could be exploited to induce the substitution of the monodentate ligand, **L**`, for the bidentate 5,5'-dimethyl-2,2'-bipyridyl (dmbipy) ligand (Schemes 5.1, 5.2 and 5.3). Previous studies on [*cis*-HPt($PyNMe_2$)(OTs)] have shown that in solution the $^-$OTs anion undergoes rapid displacement by better donors, namely monodentate *N*-heterocycles or even by coordinating solvent molecules such as [D_7]-DMF.[12,13] It was reasoned, therefore, that the addition of a chelating ligand, such as dmbipy, to a protonated C^N complex of this nature would result in either simultaneous or stepwise displacement of both monodentate ligands. In effect, this process would be switching from a "3+1" to a "2+2" platinum coordination mode.

The cyclometallated complex [**L**Pt(DMSO)] was prepared accordingly to literature procedures[14] and [**L**Pt(PyH)], [**L**Pt($PyNMe_2$)] prepared as discussed previously (see Chapter Two). [**L**Pt$S(O)(CH_2Ph)_2$], [**L**Pt(3,5-Lut)] and [**L**Pt(PPh_3)] were all prepared in a similar fashion, through displacement of DMSO from the known precursor complex, [**L**Pt(DMSO)], at ambient temperature. The desired carboplatinum complexes were isolated in excellent yields after flash column chromatography, with silica as the stationary phase and dichloromethane as the eluent. The formation of [**L**Pt$S(O)(CH_2Ph)_2$], [**L**Pt(3,5-Lut)] and [**L**Pt(PPh_3)] were confirmed by mass spectrometry, ^{1}H and ^{13}C NMR spectroscopy. Additionally, the structures [**L**Pt(3,5-Lut)] and [**L**Pt(PPh_3)] were confirmed by X-ray crystallography using single crystals grown *via* slow diffusion of di-isopropyl ether into a saturated solution of the [**L**Pt(3,5-Lut)] or [**L**Pt(PPh_3)] in chloroform (Figure 5.1a and 5.1b). The solid state structures confirmed the pseudo square planar geometry around the Pt(II) centre in both complexes; C1-Pt1-N8 81.25(16)°, C14-Pt1-N8 80.80(5)°, C14-Pt1-N19 99.33(15)°, N19-Pt1-C1 98.60(16)° for [**L**Pt(3,5-Lut)] (Figure 5.1a) and

C1-Pt1-N8 80.30(14)°, C14-Pt1-N8 80.14(14)°, C14-Pt1-P1 102.26(11)°, P1-Pt1-C1 97.53(11)° for [**L**Pt(PPh_3)] (Figure 5.1b). The bond lengths between the Pt centre and the N atom in **L** slightly increase from 1.977(4) Å ([**L**Pt(3,5-Lut)]) to 2.022(3) Å ([**L**Pt(PPh_3)]). This slight bond lengthening probably results from the labilising *trans* effect of the PPh_3 ligand. The bond length between the platinum centre and the monodentate ligand, unsurprisingly, differs significantly between the cyclometallated complexes; N19-Pt1 = 2.030(4) Å ([**L**Pt(3,5-Lut)]) and Pt1-P1 = 2.2145(11) Å ([**L**Pt(PPh_3)]).

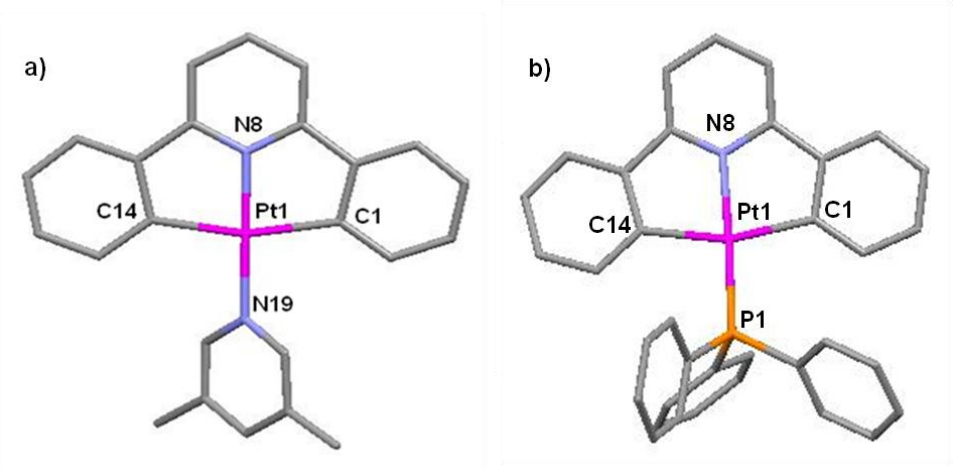

Figure 5.1 X-ray crystal structures of a) [**L**Pt(3,5-Lut)] and b) [**L**Pt(PPh_3)]. For a) the carbon atoms of 3,5-Lut and **L** are shown in grey, platinum in magenta and nitrogen in pale blue. The H atoms have been removed for clarity. Selected bond lengths [Å] and angles [°]: C1-Pt1 2.070(4), N8-Pt1 1.977(4), C14-Pt1 2.073(4), N19-Pt1 2.030(4), C1-Pt1-N8 81.25(16), C14-Pt1-N8 80.80(5), C14-Pt1-N19 99.33(15), N19-Pt1-C1 98.60(16). For b) the carbon atoms of PPh_3 and **L** are shown in grey, platinum in magenta, nitrogen in pale blue and phosphine in orange. The H atoms have been removed for clarity. Selected bond lengths [Å] and angles [°]: C1-Pt1 2.078(4), N8-Pt1 2.022(3), C14-Pt1 2.080(4), P1-Pt1 2.2145(11), C1-Pt1-N8 80.30(14), C14-Pt1-N8 80.14(14), C14-Pt1-P1 102.26(11), P1-Pt1-C1 97.53(11).

Switching between a "3+1" and "2+2" Pt(II) complex was initially investigated with [**L**Pt(DMSO)] and dmbipy (Scheme 5.1). As a control experiment, one equivalent of dmbipy was added to a solution of [**L**Pt(DMSO)] in [D_7]-DMF at 298 K. The resultant ^{1}H NMR spectrum, which remained unchanged after 3 h, revealed a coordinated DMSO signal and several peaks which were identical to those of free dmbipy. However the reaction between [**L**Pt(DMSO)] and dmbipy in the presence of one equivalent of TsOH (Scheme 5.1) resulted in an initial lightening of the solution followed by darkening after agitation for one minute, which ^{1}H NMR spectroscopy appeared to indicate was due to quantitative formation of [H**L**Pt(dmbipy)]OTs. As an alternative method, the direct addition of dmbipy.TsOH gave an identical spectrum with the same colour changes being observed. Finally, when an excess of di-isopropyl ether was added either of the reaction mixtures, [H**L**Pt(dmbipy)]OTs was isolated as a bright yellow solid in 78% yield.

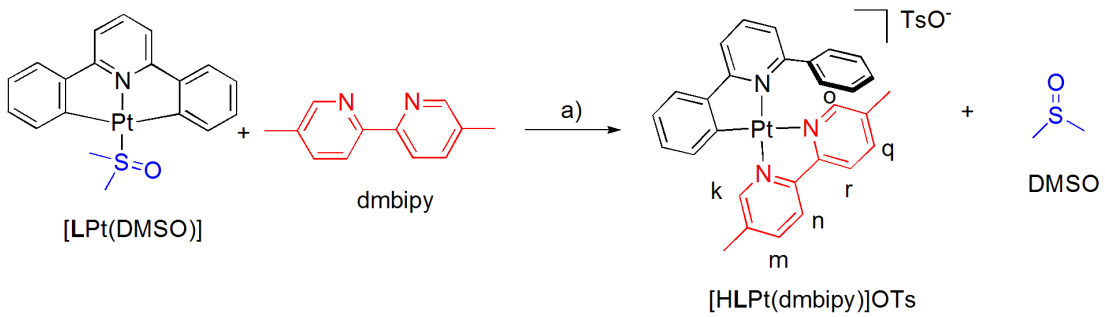

Scheme 5.1 Acid-driven formation of [H**L**Pt(dmbipy)]OTs from [**L**Pt(DMSO)] and dmbipy. Reagents and conditions: a) TsOH, CH_2Cl_2, 298 K, 5 min, 78%.

The ^{1}H NMR spectrum of pure [H**L**Pt(dmbipy)]OTs revealed, as expected, a characteristic desymmetrisation of the dmbipy moiety (Figure 5.2). For instance, the *ortho* protons of dmbipy appeared at δ 9.5 and δ 8.7, which correspond to H_k and H_o respectively where the pronounced difference in these two signals is most probably caused by shielding of H_o by the non-coordinating phenyl group of H**L**. In addition to ^{1}H NMR spectroscopy, the formation of [H**L**Pt(dmbipy)]OTs has been confirmed using ^{13}C NMR spectroscopy, electrospray mass spectrometry and X-ray crystallography (Figure 5.3).

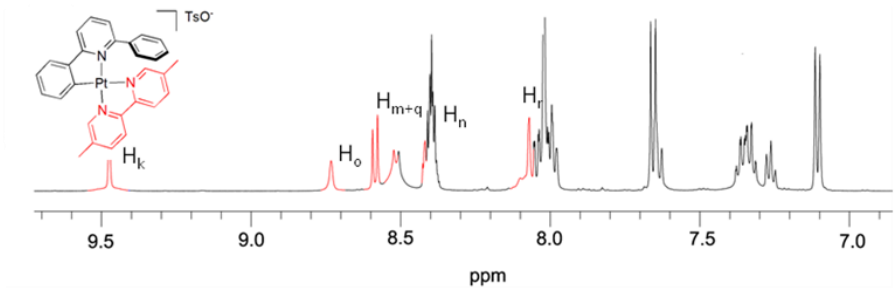

Figure 5.2 Partial ^{1}H NMR spectrum (400 MHz, [D_7]-DMF, 300 K) of pure [H**L**Pt(dmbipy)]OTs. The assignments correspond to the lettering in Scheme 5.1.

As expected, the solid state structure showed that the platinum ion adopts a pseudo square planar geometry; C1-Pt1-N8 79.6(3), C1-Pt1-N19 98.2(3), N27-Pt1-N19 77.6(3), N8-Pt1-N27 104.3(3). The bond lengths between the Pt centre and the C and N atoms of H**L** were 1.997(9) Å and 2.063(7) Å, respectively. A noticeable difference in the bond lengths between the Pt centre and the N atoms of dmbipy was also observed, Pt1-N19; 2.027(7) Å and Pt1-N27; 2.137(7) Å, where the latter bond is presumably longer, and hence weaker, due to the strong *trans* effect of the phenylato group of H**L**. Interestingly, in the solid state [H**L**Pt(dmbipy)]OTs appears chiral where the non-coordinating phenyl group sits either above or below the plane of the dmbipy ligand thus creating an axis of helical chirality. The packing diagram for [H**L**Pt(dmbipy)]OTs, meanwhile, shows the presence of four molecules in which two display M helicity whilst the other two molecules possess P helicity.

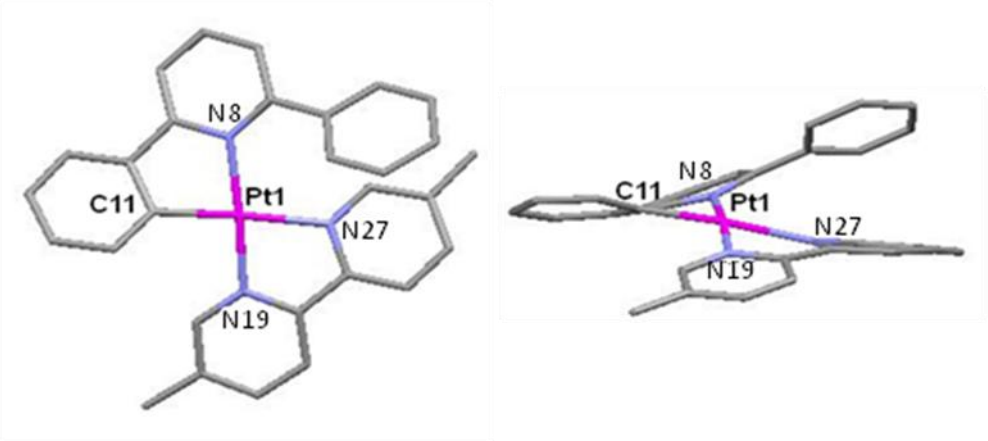

Figure 5.3 Two views of the X-ray crystal structure of [H**L**Pt(dmbipy)]OTs. The carbon atoms of H**L** and dmbipy are shown in grey, nitrogen atoms in light blue and the platinum atom in magenta. The H atoms, two chloroform solvent molecules and the OTs counter anion have been removed for clarity. (a) Front view of [H**L**Pt(dmbipy)]OTs (b) Side view of [H**L**Pt(dmbipy)]OTs. Selected bond lengths [Å] and angles [°]: C1-Pt1 1.997(9), N19-Pt1 2.027(7), N27-Pt1 2.137(7), N8-Pt1 2.063(7), C1-Pt1-N8 79.6(3), C1-Pt1-N19 98.2(3), N27-Pt1-N19 77.6(3), N8-Pt1-N27 104.3(3).

The exchange between the monodentate nitrogen donors in [**L**Pt(PyH)] and [**L**Pt($PyNMe_2$)] and the substituted bidentate ligand, dmbipy, were then undertaken to establish the tolerance of the system for switching from "3+1" and "2+2" donor sets. To a solution of [**L**Pt(PyR)] (where R = H or NMe_2) in [D_6]-acetone:CD_2Cl_2 1:1 at 298 K was sequentially added, one equivalent of TsOH and subsequently one equivalent of dmbipy. This resulted in the quantitative formation of [H**L**Pt(dmbipy)]OTs by ^{1}H NMR spectroscopy.[15] In both cases, no exchange of dmbipy for PyH or $PyNMe_2$ was observed in the absence of TsOH.

To continue the trend of exchange of increasingly stronger monodentate donors (i.e. $PyNMe_2$>PyH>DMSO) for dmbipy, the reaction of [**L**Pt(PPh_3)] with dmbipy was also investigated through the addition of one equivalent of dmbipy.TsOH to a solution of the cyclometallated complex at 298 K in [D_7]-DMF. Analysis of the ^{1}H NMR spectrum showed that whilst a distinct change in the coordination mode at the platinum centre had been achieved, [H**L**Pt(dmbipy)]OTs had not been formed. The sequential addition of TsOH and dmbipy to [**L**Pt(PPh_3)] gave the same spectrum.

Further investigation of this system would be necessary in order to establish the nature of the coordinating groups at the platinum centre.

To create a stimuli-responsive [2]rotaxane based on this switchable metal-ligand chemistry would require the monodentate and bidentate ligand units be incorporated into the thread component. Thus dmbipy was chosen as the bidentate ligand as it was anticipated that it would better represent (in comparison to unsubstituted dmbipy) the steric demands of a rotaxane architecture. In order to accurately model the sterics of a potential monodentate station, further exchange experiments were undertaken using 3,5-Lut and dibenzylsulfoxide. As well as replicating the steric demands of an interlocked architecture, these ligands were chosen with potential synthetic routes to a rotaxane in mind.

As before, the addition of one equivalent of the salt, dmbipy.TsOH, to a solution of [**L**PtS(O)$(CH_2Ph)_2$] in [D_7]-DMF at 298 K gave the quantitative formation of [H**L**Pt(dmbipy)]OTs (Scheme 5.2) by ^{1}H NMR spectroscopy (Figure 5.4a). The spectrum of the reaction mixture showed peaks identical to those of previously prepared [H**L**Pt(dmbipy)]OTs (Figure 5.2. *cf* 5.2a and 5.2b). Most notably the *ortho* protons of dmbipy, H_k and $H_{o,}$ at δ 9.5 and δ 8.7 and additionally the aromatic protons H_{m+q}, H_n and H_r were present at δ 8.6, δ 8.4 and δ 8.1 respectively. The complete displacement of S(O)$(CH_2Ph)_2$ was also observed, as evidenced by the absence of the peaks at δ 7.6 and δ 7.3, which corresponded to $H_{i\text{-}k}$ and the disappearance of the ^{195}Pt-split benzylic signals (not shown). Sequential addition of TsOH and dmbipy to [**L**PtS(O)$(CH_2Ph)_2$] gave the same spectrum.

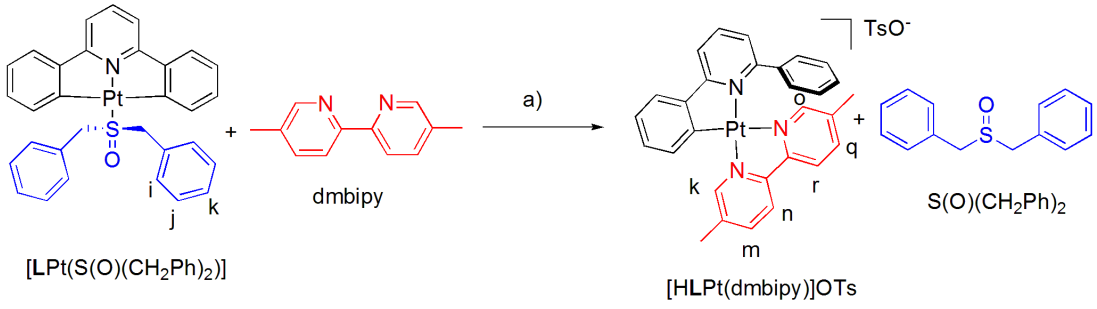

Scheme 5.2 Acid-driven formation of [H**L**Pt(dmbipy)]OTs from [**L**Pt(S(O)$(CH_2Ph)_2$)] and dmbipy. Reagents and conditions: a) TsOH, [D_7]-DMF, 298 K, 5 min, quantitative.

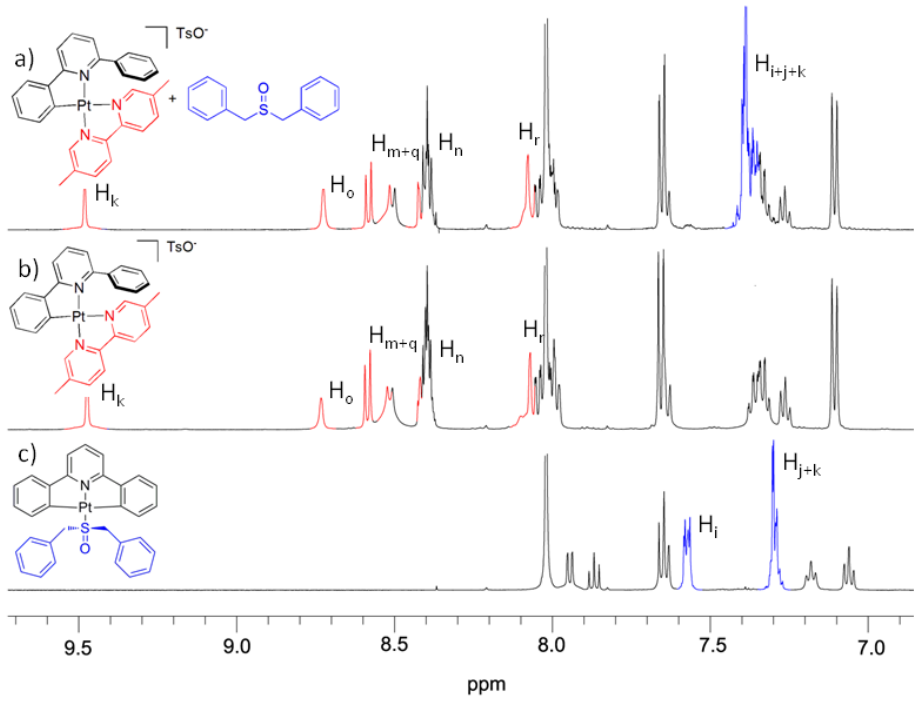

Figure 5.4 ^{1}H NMR spectra (400 MHz, [D_7]-DMF, 298 K) of a) the reaction mixture 5 min after the direct addition of one eq of the salt dmbipy.TsOH to [**L**PtS(O)(CH_2Ph)$_2$]; b) [H**L**Pt(dmbipy)]OTs and c) [**L**PtS(O)(CH_2Ph)$_2$]. The bound dmbipy ligand of [H**L**Pt(dmbipy)]OTs is shown in red and S(O)(CH_2Ph)$_2$, both as [**L**PtS(O)(CH_2Ph)$_2$] and free, is shown in blue. The assignments correspond to the lettering and colouring shown in Scheme 5.2.

Finally the reaction of [**L**Pt(3,5-Lut)] with dmbipy.TsOH in [D_7]-DMF at 298 K (Scheme 5.3) was undertaken. The ^{1}H NMR spectrum of the reaction mixture taken 5 min after the addition of the salt showed that a new species which bore a striking similarity to [H**L**Pt(dmbipy)]OTs (*cf* Figure 5.5a and 5.5b) had been formed. In particular, the peaks which correspond to H_k, H_n and H_r at δ 9.4, δ 8.4 and δ 8.1 respectively, could be clearly observed. However, whilst the symmetry of the C^N^C complex had been broken, a slight shifting and broadening of the peaks H_o and $H_{m/q}$ in [H**L**Pt(dmbipy)]OTs (*cf* Figure 5.5a and 5.5b) was observed. A possible explanation of this could be the occurrence of some dynamic process involving the partial displacement of the dmbipy ligand in [H**L**Pt(dmbipy)]OTs at the labilised coordination site by 3,5-Lut. As an alternative method, the sequential addition of TsOH and dmbipy gave the same spectrum.

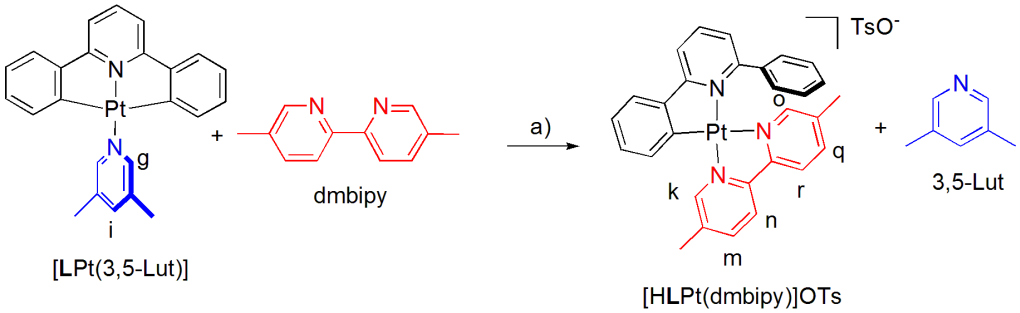

Scheme 5.3 Acid-driven formation of [H**L**Pt(dmbipy)]OTs from [**L**Pt(3,5-Lut)] and dmbipy. Reagents and conditions: a) TsOH, [D_7]-DMF, 298 K, 5 min, quantitative.

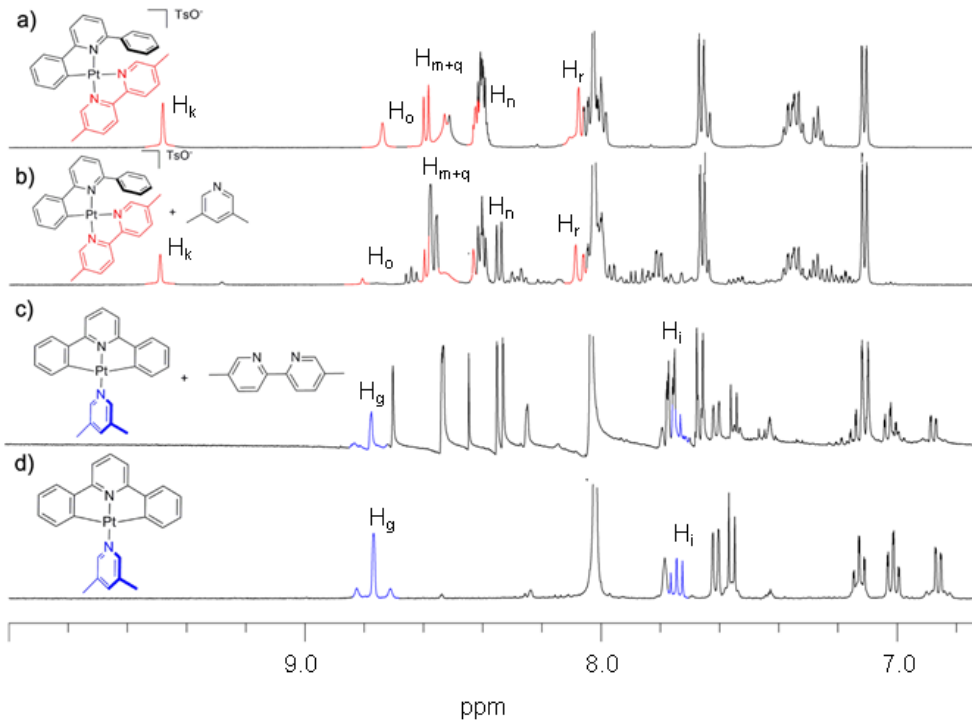

Figure 5.5 ^{1}H NMR spectra (400 MHz, [D_7]-DMF, 298 K) of a) [H**L**Pt(dmbipy)]OTs; b) the reaction mixture 5 min after the sequential addition of one equivalent of TsOH and one equivalent of dmbipy to[**L**Pt(3,5-Lut)]; c) reaction mixture 18 h after the addition of five equivalents of phosphazene base, P_1-^{t}Bu, to [H**L**Pt(dmbipy)]OTs and free 3,5-Lut, d) [**L**Pt(3,5-Lut)]. The bound 3,5-Lut ligand of [**L**Pt(3,5-Lut)] is highlighted in blue and the bound dmbipy ligand of [H**L**Pt(dmbipy)]OTs in red. The assignments correspond to the lettering and colouring shown in Scheme 5.3.

5.2.2 Model Studies: Switching "2+2" for "3+1" donor sets

As the phosphazene base, P_1-^{t}Bu, had previously been used to affect the cyclometallation of H**L**Pt to **L**Pt[12,13] (see Chapters Three and Four) and also because it has been observed that monodentate ligands are not displaced by dmbipy in the absence of TsOH (*vide supra*), it was envisaged that simply adding base to the mixture of [H**L**Pt(dmbipy)]OTs and **L`** would reverse the coordinative bias of dmbipy and **L`**. Accordingly, five equivalents of P_1-^{t}Bu was added to [H**L**Pt(dmbipy)]OTs and 3,5-Lut in [D_7]-DMF at 298 K. Analysis of this reaction, using ^{1}H NMR spectroscopy, indicated that this ligand exchange reaction was signficantly slower than the acid-activated conversion of [**L**Pt(3,5-Lut)] to [H**L**Pt(dmbipy)]OTs, taking 12 h until no further change was observed. Nonetheless, the resulting ^{1}H NMR spectrum (Figure 5.5c) clearly showed that the desired cyclometallation had occurred with a concomitant re-coordination of 3,5-Lut. Comparison of the resulting spectrum to authentic [**L**Pt(3,5-Lut)] (*cf* Figure 5.5c and 5.5d) revealed the distinctive ^{195}Pt satellite peaks of the *ortho* pyridyl protons, H_g, of [**L**Pt(3,5-Lut)] at δ 8.8 and aromatic proton, H_i, of the monodentate *N*-heterocycle, was also clearly evident at δ 7.7. In addition, the displacement of free dmbipy was observed. The addition of five equivalents of P_1-^{t}Bu to a solution of [H**L**Pt(dmbipy)]OTs and $S(O)(CH_2Ph)_2$ in [D_7]-DMF at 298 K was also carried out. However, while change to the appearance of the ^{1}H NMR spectrum was observed after leaving for 18 h, the desired complex, [**L**Pt$S(O)(CH_2Ph)_2$], was observed only as a minor product (wherein ratio of bound to free $S(O)(CH_2Ph)_2$ was 14:86). Further investigation is required to determine the nature of the coordinating groups at the metal centre for this reaction.

5.2.3 Towards the Target Interlocked Molecular Architecture

Based on the criteria of the discussed model studies, it was envisaged that a stimuli-responsive bistable [2]rotaxane, **L7**Pt, could be created (Scheme 5.4). Translocation of the macrocycle-metal complex between the monodentate pyridine (*Py*) station and the bidentate pyridyl-triazole station (*Py-triazole*) would be achieved using acid-base switching. Under neutral conditions, a "3+1" square planar coordination mode about the metal centre is anticipated, wherein $\mathbf{L}^{2-}$ binds in a η^3 fashion, and as a result the cyclometallated Pt(II)-macrocycle coordinates in a monodentate fashion to the *Py* station to give *Py*-**L7**Pt. Upon the addition of TsOH, a change in the coordination mode at the metal centre would be induced, where H**L** binds as a bidentate C^N chelate. Shuttling of the bidentate macrocycle component would permit coordination of the metal centre to the pyridyl-triazole station to generate the "2+2" rotaxane *Py-triazole*-[**L7**HPt]OTs. The addition of P_1-^{t}Bu to this charged species, *Py-triazole*-[**L7**HPt]OTs, would affect cyclometallation to complete the cycle and regenerate *Py*-**L7**Pt.

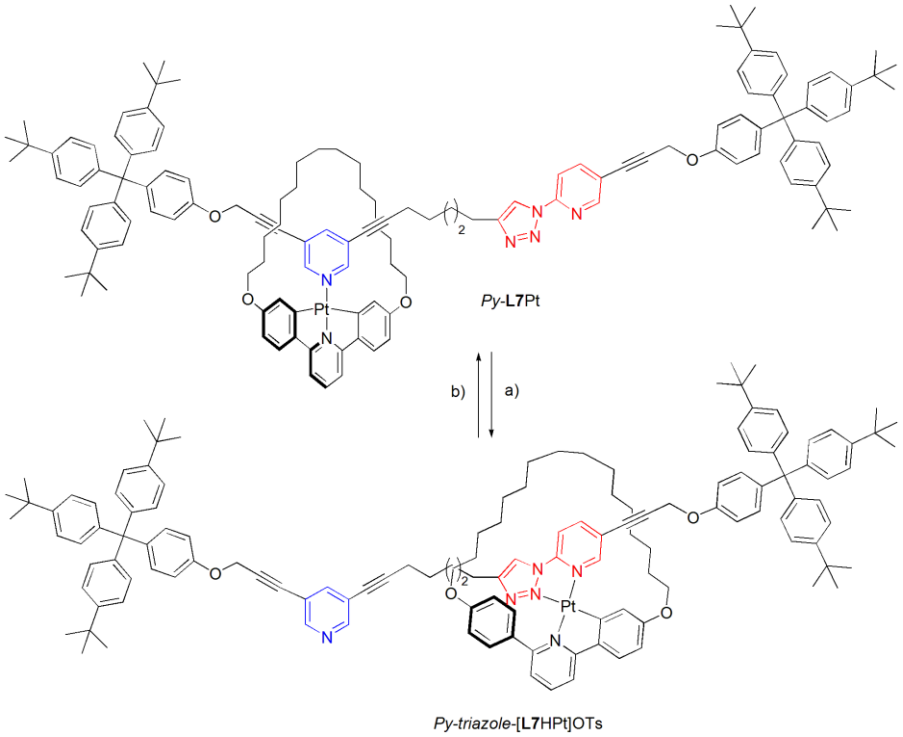

Scheme 5.4 Under neutral conditions *Py*-**L7**Pt will be formed in which the Pt(II)-macrocycle is bound to the monodentate *Py* station. Reagents and conditions: a) TsOH; b) P_1-^{t}Bu.

Scheme 5.5 outlines the synthetic strategy which will be employed for the assembly of the interlocked architecture, **L7**Pt. Square planar, Pd(II), "passive" metal templates have been extensively used to construct [2]rotaxanes using a "3+1" approach.[4,16,17] It has been shown, however, that the use of 3,5-substituted pyridine ligands at the monodentate coordination site in this "passive" metal template leads to formation of non-interlocked products.[18] Meanwhile, the use of 2,6-substituted, monodentate pyridine ligands in Pd(II) "3+1" template assemblies have been shown to afford interlocked architectures.[18] However, such substitution patterns are not appropriate in the described system as 2,6-disubstituted pyridine-based ligands do not coordinate to platinum(II) centres. Alternatively, it has been reported that an "active" metal template strategy employing the Cu(I) catalyzed azide-alkyne 1,3-cycloaddition reaction[19] (the CuAAC "click" reaction)[20] in the presence of the macrocycle, H_2**L8**, and appropriate terminal alkyne and azide "half-threads" afforded a [2]rotaxane.[20e] As such, it is proposed that the assembly of metal free [2]rotaxane, **L7**, would be realised using a "Click" reaction between **78** and **79** in the presence of H_2**L8** and an appropriate Cu(I) source (Scheme 5.5). Insertion of the platinum(II) centre into the C^N^C scaffold would then be realised using a modified Rourke's procedure[14] to generate, *Py*-**L7**Pt. Furthermore, incorporation of the platinum(II) centre into the macrocycle after the "Click" reaction has been performed avoids any potential problems involving coordination of the platinum(II) centre to the terminal alkyne group. Reports on the dual use of a triazole unit to both complete the mechanically interlocked structure and form a fundamental element of the system (i.e. a station) are rare.[21]

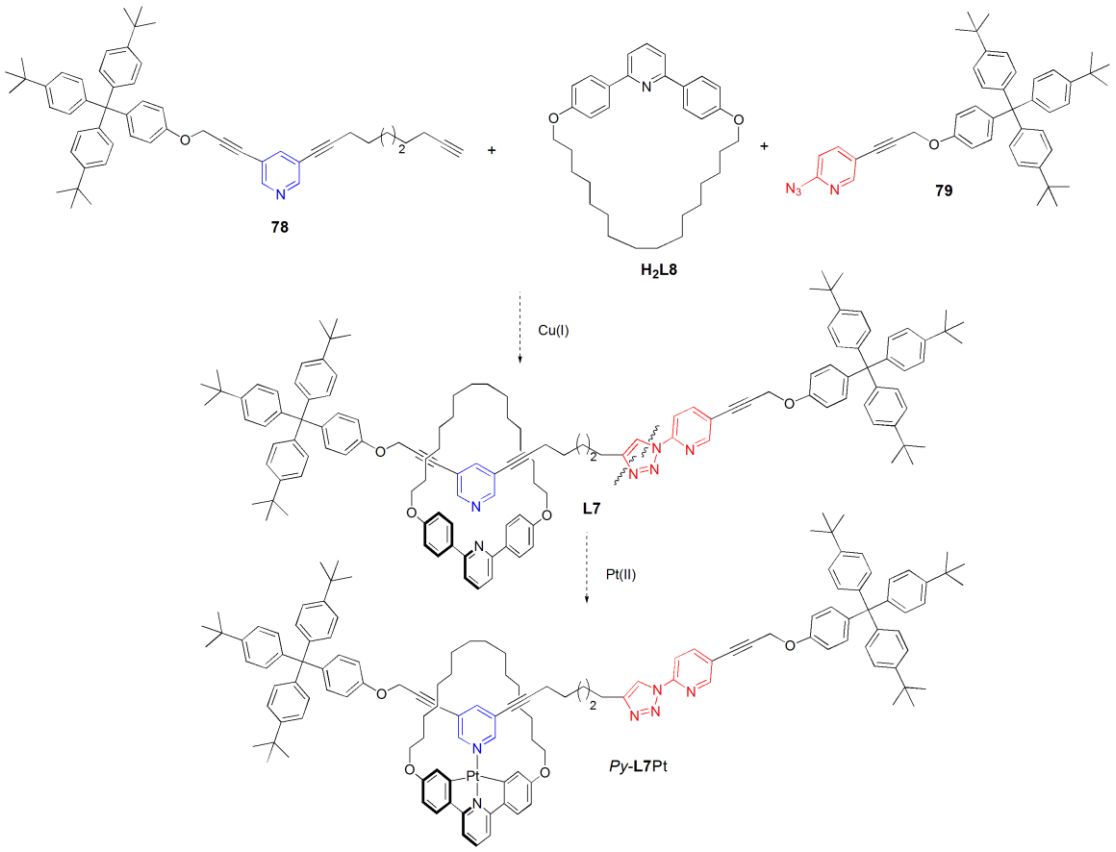

Scheme 5.5 Proposed scheme for the synthesis of Py-**L7**Pt. Formation of the demetallated [2]rotaxane, **L7**, using a "Click" reaction between **78** and **79** in the presence of H_2**L8**, followed by insertion of the Pt(II) centre into the macrocycle.

5.3.2.1 Synthesis of Platinum(II)-Macrocycle Complex, L8Pt

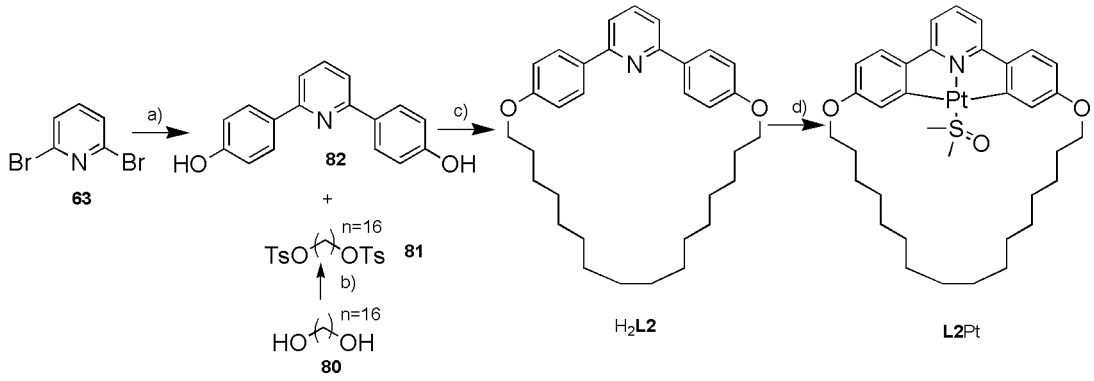

Scheme 5.6 Synthesis of platinum(II)-macrocycle, **L8**Pt, *via* single macrocyclisation of **81** and **82** followed by insertion of platinum into H_2**L8**. Reagents and conditions (a) PEPPSI-IPr,[22-25] 4-hydroxylphenyl-boronic acid, ^{i}PrOH, 298 K, 12 h, 53%; (b) *para*-tosylchloride, NMP, THF, 298 K, 5 days, 63%; (c) K_2CO_3, DMF, 398 K, 2 days, 41%; (d) AcOH, $K_2[PtCl_4]$, H_2O, reflux, 3 days, K_2CO_3, DMSO, 388 K, 3 h, 12%.

H_2**L8** was prepared in four steps from commercially available materials (Scheme 5.6). Treatment of 2,6-dibromopyridine with 4-hydroxylphenyl-boronic acid and a catalytic amount of PEPPSI-IPr[22-25] in isopropanol at room temperature for 12 h gave the desired palladium mediated cross coupled product, **82**, in 53%. Conversion of 1,16-decanediol to the corresponding ditosylate was achieved in a 63% yield using an excess of *para*-tosylchloride (*p*-TsCl) and *N*-methylmorpholine (NMP). Formation of the H_2**L8** was accomplished by simply stirring the precursors, **81** and **82**, in DMF for 2 days at 398 K, under high dilution conditions in the presence of K_2CO_3, to give the macrocycle in a respectable 41% yield (which is comparable with the reported literature procedure).[10a] Introduction of platinum(II) into the C^N^C scaffold of the macrocycle was undertaken using a modified Rourke procedure.[14] The desired product, **L8**Pt, was obtained as a bright yellow solid in 12% yield after flash column chromatography. Formation of the Pt(II)-macrocycle complex, **L8**Pt, was confirmed unambiguously by electrospray mass spectrometry and ^{1}H and ^{13}C NMR spectroscopy. The low yield (12%) observed for the reaction is most likely due to the fact that the reaction proceeds *via* a chloride bridged dimeric platinum

species,[14] whose formation would almost certainly be inhibited by the steric bulk of the macrocyclic scaffold.

5.2.3.2 Synthesis of the Pyridyl-TriAzole "Half-Thread"

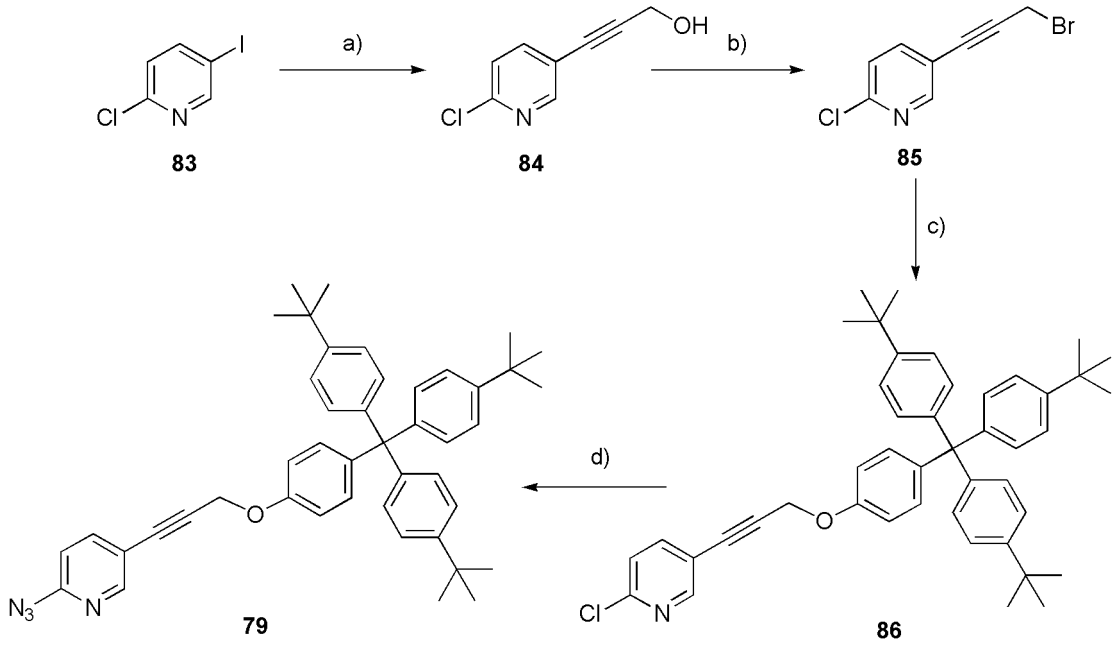

Scheme 5.7 Four step procedure for the synthesis of azide station, **79**, from commercially available materials. Reagents and conditions (a) propargyl alcohol, NEt_3, $Pd(Ph_3)_4$, CuI, 298 K, absence of light, 20 h, 91%; (b) CBr_4, CH_2Cl_2, PPh_3, 298 K, 18 h, 23%; (c) 4-[tris-(4-*tert*-butylphenyl)methyl]phenol, K_2CO_3, butanone, reflux, 36 h, 79%; (d) NaN_3, DMF, 418 K, 18 h, 41%.

A four step procedure was employed for the synthesis of **79** from readily available materials (Scheme 5.7). Firstly, a Sonogashira cross-coupling reaction[26] between 2-chloro-5-iodo-pyridine and propargyl alcohol under standard conditions gave **84** in 91% yield. The hydroxyl functionality of **84** was then converted into a bromide group in 23% following a reported procedure.[4a] Refluxing a solution of **85** and 4-[tris-(4-*tert*-butylphenyl)methyl]phenol,[27] in the presence of an excess of K_2CO_3 for 36 h afforded **86** as an off-white solid in 79%. Interconversion of the chloride group

of **86** for an azide moiety was accomplished in 41% yield through reaction of **86** with NaN_3 in DMF over 18 h.

5.2.3.3 Proposed Synthetic Route to Pyridine "Half Thread"

Scheme 5.8 outlines a proposed synthetic route to **80** from commercially available materials. A Sonogashira reaction between 3,5-dibromopyridine, **87**, and propargyl alcohol would afford **88**. Installation of the "stopper" at the hydroxyl group would be achieved using a known Williamson alkylation procedure to generate **89**.[4] Finally, a second Sonogashira reaction between **89** and 1,9-decadiyne would afford **86**.

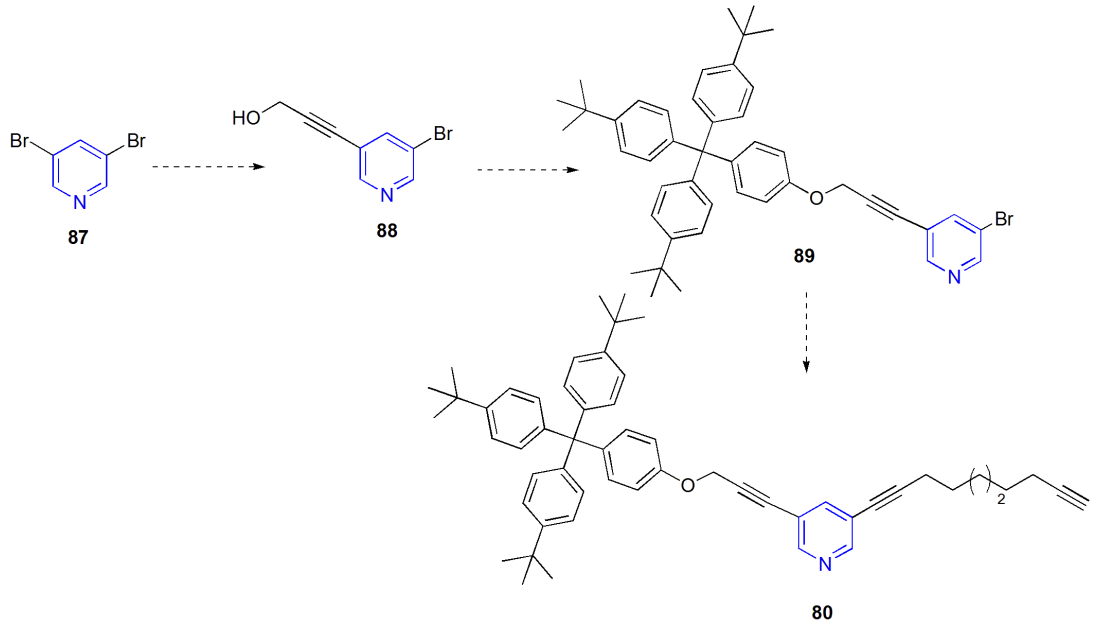

Scheme 5.8 Proposed scheme for the formation of half thread **80** in three steps from commerically available materials.

5.3 Conclusions

In conclusion, it has been shown that a series of monodentate ligands, **L`**, undergo acid-activated exchange for dmbipy in the cyclometallated C^N^C complex, [**L**Pt(**L`**)]. Moreover, this switching between "3+1" and "2+2" square planar Pt coordination modes has been shown to take place rapidly at room temperature with a variety of substituted and unsubstituted sulfoxides and *N*-heterocycles (of both *para*- and *meta*-substitution patterns). However, it was shown that PPh_3 cannot be displaced from the Pt centre in the same fashion. Reverse of the coordinative bias of dmbipy and the substituted monodentate ligands, 3,5-Lut and $S(O)(CH_2Ph)_2$, at the platinum(II) centre was achieved through the addition of excess base. This reverse reaction was found however to be much slower than the corresponding forward reaction and whilst exchange between the *N*-heterocycles pleasingly gave the desired cyclometallated species as the major product it was observed that when **L`** = $S(O)(CH_2Ph)_2$ the desired C^N^C complex was seen only as a minor product.

Molecular switching based on metal-ligand motifs that can be employed towards the creation of molecular machines are rare and furthermore systems in which the macrocycle component induces the motion are even rarer. Preliminary work towards a stimuli-responsive bistable [2]rotaxane based on this switchable metal-ligand coordination motif has been described with the "half thread" pyridyl-azole station, **2**, and the platinum(II)-macrocycle complex, **L8**Pt, being synthesised and fully characterized using ^{1}H and ^{13}C NMR spectroscopy and mass spectrometry.

5.4. References and Notes

[1] For macrocycle rotation in stimuli-responsive Cu(I)/Cu(II)molecular shuttles see: (a) N. Weber, C. Hamann, J. –M. Kern, J. –P. Sauvage, *Inorg. Chem.*, 2003, **42**, 6780; (b) U. Letinois-Halbes, D. Hanss, J. M. Beierle, J. –P. Collin, J. –P. Sauvage; *Org. Lett.* 2005, **7**, 5753; (c) L. Raehm, J. –M. Kern, J. –P. Sauvage; *Chem. –Eur. J.*, 1999, **5**, 3310; For macrocycle translocation in stimuli-responsive Cu(I)/Cu(II) molecular shuttles see: (d) N. Armaroli, V. Balzani, J. –P. Collin, P. Gavina, J. –P. Sauvage, *Angew. Chem. Int. Ed.*, 2007, **121**, 4397 ; (e) P. Gavina, J. –P. Sauvage, *Tetrahedron Lett.*, 1997, **38**, 3521; (f) F. Durola, J. –P. Sauvage, *Angew. Int. Ed. Chem.* 2007, **46**, 3537; For a stimuli-responsive Cu(I)/Cu(II) molecular shuttle which exhibits fast submolecular dynamics see : (g) J. –P. Collin, F. Durola, J. –P. Sauvage, *Angew. Chem. Int. Ed.* 2009, **48**, 8532. For large amplitude macrocycle translation in stimuli-responsive Cu(I)/Cu(II) [2]catenanes see: (h) A. Livoreil, C. Dietrich-Buchecker, J. –P. Sauvage, *J. Am. Chem. Soc.*, 1994, **116**, 9399; (i) F. Baumann, A. Livoreil, W. Kaim, J. –P. Sauvage, *Chem. Comm.*, 1997, **1**, 35; (j) D. Cardenas, A. Livoreil, J. –P. Sauvage, *J. Am. Chem. Soc.*, 1996, **118**, 11980; (k) A. Livoreil, J. –P. Sauvage, N. Armaroli, V. Balzani, L. Flamigni, B. Ventura, *J. Am. Chem. Soc.*, 1997, **119**, 12114; For reviews of transitions metal-ligand complexed molecular machines see: (l) J. –P. Collin, V. Heitz, J. –P. Sauvage, *Top. Curr. Chem.*, 2005, **262**, 29; (m) S. Bonnet, J. –P. Collin, M. Koizumi, P. Mobian, J. –P. Sauvage, *Adv. Mat.*, 2006, **18**, 1239; (n) J. –P Collin, V. Heitz, S. Bonnet, J. –P Sauvage, *Inorg. Chem. Comm.* 2005, **8**, 1063.

[2] For a muscle-like Cu(I)/Zn(II) based dimer in which stretching and contraction processes are achieved through Cu(I)-Zn(II) exchange (a) C. Jimenez, C. Dietrich-Buchecker , J. –P. Sauvage, *Angew. Chem. Int. Ed.*, 2000, **39**, 3284; (b) C. Jimenez, C. Dietrich-Buchecker, J. –P. Sauvage, *Chem. Eur. J.*, 2002, **8**, 1456.

[3] E.R. Kay, D. A. Leigh, F. Zerbetto, *Angew. Chem. Int. Ed.*, 2007, **46**, 72.

[4] (a) J. D. Crowley, D. A. Leigh, P. J. Lusby, R. T. McBurney, L.-E. Perret-Aebi, C. Petzold, A. M. Z. Slawin, M. D. Symes, *J. Am. Chem. Soc.*, 2007, **129**, 15085; (b) D. A. Leigh, P.J. Lusby, R. T. McBurney, M. D. Symes, *Chem. Commun.*, 2010, **46**, 2382.

[5] (a) A. H. Flood, A. J. Peters, S. A. Vignon, D. W. Steuerman, H. –R Tseng, S. Kang, J. R. Heath, J. F. Stoddart, *Chem. -Eur. J.*, 2004, **10**, 6558; (b) D. W. Steuerman, H. –R Tseng, A. J. Peters, A. H. Flood, J. O. Jeppeson, K. A. Nielsen, J. F. Stoddart, J. R. Heath, *Angew. Chem. Int. Ed.*, 2004, **43**, 6486; (c) J. W. Choi, A. H. Flood, D .W. Steuerman, S. Nygaard, A. B. Braunschweig, N. N. P. Moonen, B. W. Laursen, Y. Luo, E. DeIonno, A. J. Peters, J . O. Jeppesen, K. Xu, J. F. Stoddart, J. R. Heath, *Chem. Eur. J.*, 2006, **12**, 261.

[6] M. N. Chatterjee, E. R. Kay, D. A. Leigh, *J. Am. Chem. Soc.*, 2006, **128**, 4058.

[7] For examples of stimuli-reponsive [2]rotaxanes whose shuttling dynamics are controlled through manipulation of π-π interactions see: (a) R. A. Bissell, E. Córdova, A. E. Kaifer, J. F. Stoddart, *Nature*, 1994, **369**, 133. (b) A. M. Elizarov, S. –H. Chiu, J. F. Stoddart; *J. Org. Chem.*, 2002, **67**, 9175; (c) H. -R Tseng, S. A. Vignon, J. F. Stoddart; *Angew. Chem. Int. Ed.* 2003, **42**, 1491. For an example of a degenerate shuttle which demonstrated temperature dependent shuttling dynamics see:(d) P. L. Anelli, N. Spencer, J. F. Stoddart, *J. Am. Chem. Soc.*, 1991, **113**, 5131. For an example of a molecular elevator see: (e) J. D. Badjic, A. Credi, S. Silvi, J. F. Stoddart, *Science*, 2004, **303**, 1845; (f) J. D. Badjic, C. M. Ronconi, J. F. Stoddart, V. Balzani, S. Silvi, A. Credi, *J. Am. Chem. Soc.*, 2006, **128**, 1489.

[8] For examples of stimuli-reponsive [2]rotaxanes whose shuttling dynamics are controlled through manipulation of hydrophobic interactions see: (a) C. A. Steiner, S. J. Alderman, D. W. Claridge, H. L. Anderson; *J. Am. Chem. Soc.,* 2002, **41**, 1769; (b) H. Murakami, A. Kawabuchi, K. Kotoo, M. Kunitake, N. Nakashima, *J. Am. Chem. Soc.,* 1997, **119**, 7605; (c) H. Murakami, A. Kawabuchi, R. Matsumoto, T. Ido, N. Nakashima, *J. Am. Chem. Soc.,* 2005, **127**, 15891.

[9] For examples of stimuli-reponsive [2]rotaxanes whose shuttling dynamics are controlled through manipulation of hydrogen- bonding see; (a) Q. – C. Wang, D. –H. Qu, J. Ren, K. Chen, H. Tian, *Angew, Chem. Int. Ed.,* 2004, **43**, 2661; (b) A. Altieri, G . Bottari, F. Dehez, D. A. Leigh, J. K. Y. Wong, F. Zerbetto, *Angew. Chem. Int. Ed.,* 2003, **42**, 2296; (c) C. M. Keaveney, D. A. Leigh, *Angew. Int. Ed. Chem.,* 2004, **43**, 1222; (d) A. M. Brouwer, C. Frochot, F. G. Gatti, D. A. Leigh, L. Mottier, F. Pailucci, S. Roffia, G. W. H. Wurpel, *Science,* 2001, **291**, 2124; (e) A. Altieri, F. G. Gatti, E. R. Kay, D. A. Leigh, D. Martel, F. Paolucci, A. M. Z. Slawin, J. K. Y. Wong *J. Am. Chem. Soc.,* 2003, **125**, 8644. For a degenerate molecular shuttle which displayed rapid inherent dynamics at room temperature; (f) A. S. Lane, D. A. Leigh, A. Murphy, *J. Am. Chem. Soc.*,1997, **119**, 11092.

[10] (a) V. Aucagne, J. Berna, J. D. Crowley, S. M. Goldup, K. D. Hanni, D. A. Leigh, P. J. Lusby, V. E. Ronaldson, A. M. Z. Slawin, A. Viterisi, D. B. Walker, *J. Am. Chem. Soc.,* 2007, **129**, 11950; (b) M. J. Barrell, D. A. Leigh, P. J. Lusby, A. M. Z. Slawin, *Angew. Chem. Int. Ed.,* 2008, **47**, 8036. (c) J. D. Crowley, K. D. Hanni, D. A. Leigh, A. M. Z. Slawin, *J. Am. Chem. Soc.,* 2010, **132**, 5309; (d) A. M. Fuller, D. A. Leigh, P. J. Lusby, *J. Am. Chem. Soc.,* 2010, **132**, 4954.

[11] For other types of rotaxanes and catenanes which feature intercomponent metal-ligand coordination see: (a) J. D. Crowley, S. M. Goldup, N. D. Gowans, D. A. Leigh, V. E. Ronaldson, A. M. Z. Slawin, *J. Am. Chem. Soc.,*

2010, **132**, 6243; (b) A. M. Rijs, N. Sandig, M. Blom, J. Oomens, J. S. Hannam, D. A. Leigh, F. Zerbetto, W. J. Buma, *Angew. Chem. Int. Ed.*, 2010, **49**, 3896; (c) S. M. Goldup, D. A. Leigh, P. J. Lusby, R. T. McBurney, A. M. Z. Slawin, *Angew. Int. Ed. Chem.*, 2008, **47**, 6999; (d) J. D. Crowley, K. D. Hanni, A. Lee, D. A. Leigh, *J. Am. Chem. Soc.*, 2007, **129**, 12092; (e) S. M. Goldup, D. A. Leigh, P. R. McGonigal, V. E. Ronaldson, A. M. Z. Slawin, *J. Am. Chem. Soc.*, 2010, **132**, 315; (f) B. A. Blight, J. A. Wisner, M. C. Jennings, *Angew. Int. Ed. Chem.*, 2007, **46**, 2835; (g) M. Hutin, C. A. Schalley, G. Bernardinelli, J. R. Nitschke, *Chem. –Eur. J.*, 2006, **12**, 4069; For ruthenium-coordinated pseudo-rotaxanes, rotaxanes and catenanes which undergo photo-induced decomplexation of the components see: (h) D. Pomeranc, D. Jouvenot, J. –C. Chambron, J. –P. Collin, V. Heitz, J. –P. Sauvage, *Chem. – Eur. J.*, 2003, **11**, 4247; (i) J. –P. Collin, D. Jouvenot, M. Koizumi, J. –P. Sauvage, *Eur. J. Inorg. Chem.*, 2005, 1850. (j) P. Mobain, J. –M. Kern, J. –P. Sauvage, *J. Am. Chem. Soc.*, 2003, **125**, 2016. (k) P. Mobian, J. –M. Kern, J. –P. Sauvage, *Angew. Chem. Int. Ed.*, 2004, **43**, 2392.

[12] P. J. Lusby, P. Müller, S. J. Pike, A. M. Z. Slawin, *J. Am. Chem. Soc.*, 2009, **131**, 16398.

[13] S. J. Pike, P. J. Lusby, *Chem. Comm.* 2010, **46**, 8338.

[14] (a) G. W. V. Cave, F. P. Fanizzi, R. J. Deeth, W. Errington, J. P. Rourke, *Organometallics*, 2000, **19**, 1355; (b) J. D. Crowley, I. M. Steele, B. Bosnich, *Inorg. Chem.*, 2005, **44**, 2989.

[15] The same colour changes were observed as for the analogous reaction with [LPt(DMSO)]and dmbipy in the presence of one equivalent of TsOH.

[16] For examples of the assembly of mechanically interlocked molecular shuttles which employ a "3+1" donor set about a square planar Pd(II) metal centre, see: (a) C. Hamann, J.-M. Kern, J.-P. Sauvage, *Dalton Trans.* 2003, 3770-

3775; (b) Y. Furusho, T. Matsuyama, T. Takata, T. Moriuchi, T. Hirao, *Tetrahedron Lett.*, 2004, **45**, 9593; (c) D. A. Leigh, P. J. Lusby, A. M. Z. Slawin, D. B. Walker, *Angew. Chem. Int. Ed.*, 2005, **44**, 4557.

[17] For an example of an assembly of a [*n*]-rotaxane using a Pd(II) template, see: A.-M. L. Fuller, D. A. Leigh, P. J. Lusby, *Angew. Chem.* 2007, **119**, 5103; *Angew. Chem. Int. Ed.* 2007, **46**, 5015.

[18] A.-M. Fuller, D. A. Leigh, P. J. Lusby, I. D. H. Oswald, S. Parsons, D. B. Walker, *Angew. Chem. Int. Ed.*, 2004, **43**, 3914.

[19] For some recent examples of the CuAAC reaction see; (a) M. A. White, J. A. Johnson, J. T. Koberstein, N. J. Turro, *J. Am. Chem. Soc.*, 2006, **128**, 11356; (b) B. Helms, J. L. Mynar, C. J. Hawker, J. M. Frechet, *J. Am. Chem. Soc.*, 2004, **126**, 15020; (c) P. Wu, M. Malkoch, J. N. Hunt, R. Vestberg, E. Kaltgrad, M. G. Finn, V. V. Fokin, K. B. Sharpless, C. J. Hawker, *Chem. Comm.* 2005, 5775; (d) V. Aucagne, D. A. Leigh, *Org. Lett.* 2006, **8**, 4505; (e) M. B. Steffensen, E. E. Simanek, *Angew. Chem. Int. Ed.*, 2004, **43**, 5178.

[20] For reviews and discussion of the "click chemistry" concept, see: (a) H. C. Kolb, M. G. Finn, K. B. Sharpless, *Angew. Chem. Int. Ed.*, 2001, **40**, 2004; (b) H. C. Kolb, K. B. Sharpless, *Drug Discovery Today*, 2003, **8**, 1128. (c) D. A. Leigh, K. Hanni; *Chem. Soc. Rev.*, 2010, **39**, 1240. For examples of interlocked molecular shuttles which are assembled using an active metal templating strategy Cu(I) catalysed azide-alkyne 1,3-cycloadditions, see: (d) V. Aucagne, K. D. Hanni, D. A. Leigh, P. J. Lusby, D. B. Walker, *J. Am. Chem. Soc.*, 2006, **128**, 2186; (e) V. Aucagne, J. Berna, J. D. Crowley, S. M. Goldup, K. D. Hanni, D. A. Leigh, P. J. Lusby, V. E. Ronaldson, A. M. Z. Slawin, A. Viterisi, D. B. Walker, *J. Am. Chem. Soc.*, 2007, **129**, 11950.

[21] (a) M. J. Barrell, D. A. Leigh, P. J. Lusby, A. M. Z. Slawin, *Angew. Chem. Int. Ed.*, 2008, **47**, 8036; (b) S. M. Goldup, D. A. Leigh, P. J. Lusby, R. T.

McBurney, A. M. Z. Slawin, *Angew. Chem.* **2008**, *120*, 3429; *Angew. Chem. Int. Ed.* **2008**, *47*, 3381.

[22] H. W. Gibson, S. H. Lee, P. T. Engen, P. Lecavalier, J. Sze, Y. X. Shen, M. Bheda, *J. Org. Chem.*, 1993, **58**, 3748.

[23] E. A. B. Kantchev, C. J. O'Brien, M. G. Organ, *Aldrichchimica Acta,* 2006, **39**, 97.

[24] C. J. O'Brien, E. A. B. Kantchev, C. Valente, N. Hadei, G. A. Chass, A. Lough, A. C. Hopkinson, M. G. Organ, *Chem. Eur. J.*, 2006, **12**, 4743.

[25] M. G. Organ, M. Abdel-Hadi, S. Avola, N. Hadei, J. Nasielski, C. J. O'Brien, C. Valente, *Chem. Eur. J.*, 2006, **13**, 150.

[26] K. Sonogashira, Y. Tohda, N. Hagihara, *Tetrahedron Lett.*, 1975, **16**, 4467.

[27] M. G. S. Avola, I. Dubovyk, N. Hadei, E. A. B. Kantchev, C. J. O'Brien, C. Valente, *Chem. Eur. J.* 2007, **12**, 4749.

CHAPTER SIX

Conclusions and Future Work

6.1 Conclusions

A series of simple metal-ligand motifs have been employed to synthesis an array of dynamic, platinum(II)-based metallosupramolecular architectures. These systems range from non-interlocked molecular assemblies, capable of processive motion to the self-assembly of multimetallic structures, and extend to the study of model studies of reversible metal-ligand switchable motifs for future application as molecular switching mechanisms in interlocked molecular machines.

In Chapter Two, a series of prototype molecular machines capable of demonstrating processive rotary and translational motion have been identified in coordinating solvents and in one case in a non-coordinating solvent. The kinetic parameters for the observed fluxional intramolecular molecular exchange processes in each of the complexes have been determined using a series of VT NMR experiments. Chapter Three outlines the discovery of a pH driven reversible molecular switch in which dual control over the kinetics and thermodynamics of a binding event at a metal centre is achieved using pH and light stimuli for a series of platinum(II) heteroleptic complexes.

Chapter Four details the successful exploitation of the discovered pH switchable platinum(II) coordination mode to induce the stimuli-responsive reversible assembly of two and three dimensional metallosupramolecular architectures in good to excellent yields. In Chapter Five, model studies on the same acid-activated metal-ligand motif are detailed wherein molecular switching between “3+1” and “2+2” square planar platinum coordination modes is successfully demonstrated with a series of monodentate ligands and a substituted bidentate ligand.

6.2 Future Work

To extend upon the work undertaken on non-interlocked molecular machines, outlined in Chapter Two, a VT NMR study of [Pt(phen)(**L5**)]$(BPh_4)_2$ in CD_2Cl_2 should be undertaken to determine values for the kinetic parameters, *k* and $\Delta G^{\ddagger}$, for the ligand exchange reaction in a non-coordinating solvent. A ligand exchange reaction between [Pt(phen)(**L6**)]$(PF_6)_2$ and a deuterated analogue of **L6** (similar to those studies described with [Pt(phen)([9]aneS_3)]$[PF_6]_2$ and [Pt(phen)(**L5**)]$(PF_6)_2$) should be undertaken to determine the relative rates of the intra- and intermolecular ligand substitution reactions in both coordinating and non-coordinating solvents. A pairs experiment between [Pt(phen)(**L5**)]$(PF_6)_2$ and [Pt(phen`)([$D_4$]-[9]ane$S_3$)]$[PF_6]_2$ (where phen` = an analogue of phen) should be conducted to gain a better reflection of the relative rates of the intra- and intermolecular ligand exchange processes. Complexation of the precursor, [Pt(phen)Cl_2] to pentadentate ligand, **L3**, should be undertaken to generate [Pt(phen)(**L3**)]$^{2+}$. A series of VT NMR experiments should then be carried out on this complex to determine the kinetic parameters of the anticipated intramolecular ligand exchange process. Finally, ligand exchange reactions with a suitable deuterated analogue of **L3** should be undertaken in both coordinating and non-coordinating solvents to determine the relative rates of the intra- and intermolecular ligand substitution reactions.

To expand upon the studies described in Chapter Three, concerning the dual-stimuli responsive interconvertable heteroleptic platinum(II) coordination modes, the photophysics of the cyclometallated complexes, [**L**Pt($PyNMe_2$)], [**L**Pt(PyH)] and [**L**Pt($PyCF_3$)], should be investigated in order to determine the fluorescence and phosphorescence properties of these complexes. From this data, information about the existence, lifetime and quantum yields of the triplet excited state of these structures can be obtained to provide further detail into the possible mechanism operating under irradiative conditions.

To complete the work undertaken towards the synthesis of a stimuli-responsive bistable [2]rotaxane, which switches between "3+1" and "2+2" square planar platinum coordination modes, model studies for molecular switching between a 3,5-methyl-substituted monodentate pyridine ligand and a bidentate ligand at the metal centre of **L7**Pt should be investigated. The synthesis outlined for the pre-rotaxane pyridine station, **78**, should be undertaken. Reaction conditions for the Cu(I) catalysed azide-alkyne 1,3-cycloaddition reaction should be investigated where the Pt(II)-macrocycle complex is coordinated to the pyridine station of **78**. Upon formation of the bistable [2]rotaxane, **L7**Pt, translocation of the Pt(II)-macrocycle complex between the monodentate pyridine and bidentate pyridyl-triazole stations needs to be demonstrated using acid-base switching

CHAPTER SEVEN

Experimental Section

7.1 General Comments on Experimental Data

Unless otherwise stated, all reagents and solvents were purchased from Aldrich Chemicals and used without further purification. Tetrahydrofuran, dichloromethane, chloroform, acetonitrile and *N*,*N*`-dimethylformamide were dried using a solvent purification system manufactured by Innovative Technology, Newburyport, MA, USA. Unless stated otherwise, all reactions were carried out under an atmosphere of nitrogen at room temperature. Column chromatography on silica was carried out using Kiesegel C69 (Merck, Germany) as the stationary phase and TLC was performed on precoated silica 60 gel plates (0.20 mm thick, $60F_{254}$. Merck Germany) and observed under UV light. Column chromatography on alumina was carried out using Brockmann activity II, basic; pH 10 ± 0.5 (Fluka) as the stationary phase and TLC was performed on precoated aluminium oxide 60 gel plates (0.25 mm thick, $60F_{254}$. Merck Germany) and observed under UV light. By petrol is meant the fraction of petroleum ether boiling between 40 ºC - 60 ºC. All ^{1}H NMR and ^{13}C NMR spectra were recorded on a Bruker AV 400 and Bruker DMX 500 instruments at a constant temperature of 298 K (unless otherwise stated). Chemical shifts are reported in parts per million (ppm) from low to high field and referenced to the residual solvent resonance. Coupling constants (*J*) are reported in hertz (Hz) and refer to coupling through three bonds i.e. ^{3}J, unless otherwise stated. Standard abbreviations indicating multiplicity were used as follows: m = multiplet, br = broad, d = doublet, t = triplet, s = singlet and dd (doublet of doublets). All melting points (m.p.) were determined using Sanyo Gallenkamp apparatus. Mass spectrometry of $[(H\mathbf{L}Pt)_4(4,4'\text{-bipy})_4](PF_6)_4$ and $[(H\mathbf{L}Pt)_6(4,4'\text{-bipy})_3(tpt)_2](PF_6)_6$ was performed on a Q-Tof 2 (MicromassWaters Corporation, Manchester, UK) mass spectrometer using a nano-electrospray ionization source. The samples were dissolved in nitromethane and made up to a concentration 100 μmol dm^{-3}. Ions were produced by positive nano-electrospray ionisation (Z-spray source) within a spray voltage range of 1.0-1.2 kV and source temperature range of 80 °C. Sample and extractor cone voltages were maintained as low as possible so as to avoid in-source dissociation and to maintain stable signal. Nanospray tips were prepared in-house from borosilicate glass capillaries (Kwik-Fil, World Precision Instruments Inc., Sarasota, FL, USA) using a

Flaming/Brown Micropipette puller (Model P-97, Sutter Instrument Co., Novato, USA). Platinum wire (0.125mm, 99.95% purity, Goodfellow Cambridge Ltd., Huntingdon, UK) was used to apply the potential to solutions. Data were analysed using MassLynx software (version 4.0 Waters Corporation) and Origin 7.5 SR2. Predicted isotopic distributions were calculated using Molecular Weight Calculator Version 6.45. FAB and EI mass spectrometry was carried out by the services at the University of Edinburgh. The absorption spectra were recorded using a PerkinElmer Lambda 9 spectrometer controlled using UV/Winlab software. Photochemical reactions were carried out in quartz NMR tubes using a multilamp photoreactor (model MLU18, manufactured by Photochemical Reactors Ltd, Reading, UK) or Fluoromax-P spectrofluorimeter (Horiba-Jobin-Yvon) was employed with band filters as specified.

7.2 Experimental Data

64 was prepared according to a modified literature procedure.[1] H_2**L4**,[2] [**L4**Pt(DMSO)],[3] [Pt(phen)Cl_2],[4] [Pt(phen)([9]aneS_3)][PF_6]$_2$,[5] H_2**L8**[6] were prepared according to literature procedures.

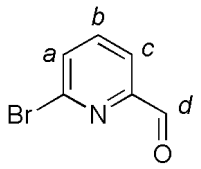

64[1]

To a solution of *n*-BuLi (13 mL, 21 mmol) in THF (50mL) at -78 ºC was added 2,6-dibromopyridine, (5.0 g, 21 mmol), in THF (50 mL), dropwise maintaining a temperature below -70 ºC to initially generate a bright yellow solution. Upon complete addition, the solution was stirred at -78 ºC for a further 30 min. After this time, DMF (2.5 mL, 32 mmol) was then added to the reaction mixture and the solution was removed from the dry ice bath and allowed to warm to room temperature. The reaction was quenched through the addition of methanol (20 mL). Saturated aqueous sodium bicarbonate (50 mL) was then added and the aqueous phase was extracted with diethyl ether (3 x 50 mL). The organic phases were collected and combined, dried over Na_2SO_4, and the solvent removed *in vacuo*. After flash column chromatography (dichloromethane) and crystallisation from dichloromethane and ether the product was obtained as a white solid. (3.2 g, 83%). ^{1}H NMR (400 MHz, $CDCl_3$): 9.86 (1H, s, H_d), 7.82 (1H, d, J = 7.6 Hz, H_c), 7.71 (1H, t, J = 7.6 Hz, H_b), 7.65 (1H, d, J = 7.6 Hz, H_a); ^{13}C NMR (100 MHz, $CDCl_3$): 191.6, 153.3, 142.4, 139.3, 132.6, 120.3; LRESI-MS *m/z*: 185.5, 187.8 ($[MH]^+$).

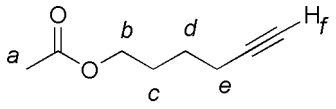

66

To a solution of 5-hexyn-1-ol (1.6 mL, 14 mmol) in pyridine (1.1 mL, 1.4 mmol) was added acetic anhydride (1.3 mL, 14 mmol) and the mixture stirred at room temperature for 3 h. The reaction was then quenched through the addition of 1M HCl (20 mL) and the aqueous phase extracted using EtOAc (3 x 20 mL). Saturated aqueous sodium bicarbonate (25 mL) was then added to the solution and the aqueous phase was again extracted with EtOAc (2 x 20 mL). The organic washings were combined, washed with brine, dried over $MgSO_4$ and concentrated under reduced pressure to give the desired product as a pale yellow oil. (7.1 g, 96%). ^{1}H NMR (400 MHz, $CDCl_3$): 3.96 (2H, t, J = 6.4 Hz, H_b), 2.11 - 2.09 (2H, m, H_e), 1.90 (3H, s, H_a), 1.87 (1H, t, ^4J = 2.7 Hz, H_f), 1.65 – 1.58 (2H, m, H_c), 1.49 – 1.42 (2H, m, H_d); ^{13}C NMR (100 MHz, $CDCl_3$): 170.3, 83.1, 68.4, 63.2, 27.0, 24.3, 20.2, 17.4; LRESI-MS *m/z*: 141. 2 ($[MH]^+$).

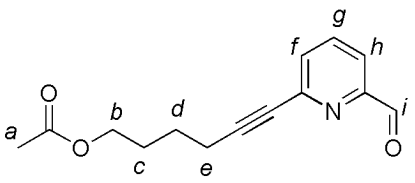

67

To a solution of **64** (3.9 g, 21 mmol) in THF/ NEt_3 (120/60 mL) was added CuI (0.41 g, 2.2 mmol), $PdCl_2(PPh_3)_2$ (0.76 g, 1.1 mmol) and **66** (8.9 g, 63 mmol) to generate a black solution. The reaction mixture was stirred at room temperature for 18 h and then saturated aqueous NH_4Cl (100 mL) was added and the aqueous phase extracted with dichloromethane (3 x 100 mL). The organic extracts were combined, washed with brine, dried over $MgSO_4$ and concentrated down *in vacuo.* The resulting residue was subjected to flash column chromatography (3:97, EtOAc:CH_2Cl_2) to yield the desired product as a yellow oil. (4.0 g, 87%). ^{1}H NMR (400 MHz, $CDCl_3$): 9.82 (1H, s, H_i), 7.65 – 7.62 (2H, m, H_{f+h}), 7.41 (1H, m, H_g), 3.93 (2H, t, J = 6.4 Hz, H_b), 2.35 (2H, t, J = 7.2 Hz, H_e), 1.84 (3H, s, H_a), 1.65 – 1.60 (2H, m, H_c), 1.56 – 1.49 (2H, m, H_d) ^{13}C NMR (100 MHz, $CDCl_3$): 192.3, 170.4, 152.2, 143.7, 136.8, 130.5, 119.5, 91.3, 79.4, 63.2, 27.3, 24.2, 20.4, 18.5; LRESI-MS *m/z*: 246.23 ($[MH]^+$).

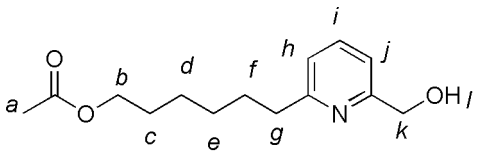

68

$Pd(OH)_2$ 15-205 dispersion on charcoal (0.41 g, 2.9 mmol) was added to a solution of **67** (1.3 g, 5.8 mmol) in THF (60 mL). H_2 gas was bubbled through the stirred solution for 32 h at room temperature. The reaction mixture was then filtered over celite and the excess solvent removed *in vacuo* to generate the product as a yellow oil. (1.3 g, 99%).^{1}H NMR (400 MHz, $CDCl_3$): 7.44 (1H, t, J = 7.6 Hz, H_i), 7.01 (1H, d, J = 7.6 Hz , H_j), 6.87 (1H, d, J = 7.6 Hz, H_h), 4.86 (1H, s, br, H_l), 4.57 (2H, s, H_k), 3.88 (2H, t , J = 6.6 Hz, H_b), 2.61 (2H, t, J = 7.7 Hz, H_g), 1.86 (3H, s, H_a), 1.55 - 1.52 (2H, m, H_c), 1.46 - 1.43 (2H, m, H_f), 1.20 – 1.16 (4H, m, H_{d+e}); LRESI-MS *m/z*: 252.15 ($[MH]^+$).

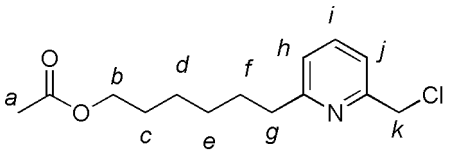

69

Thionyl chloride (0.64 mL, 8.8 mmol) was added to a solution of **68** (0.39 g, 1.8 mmol) in dichloromethane (20 mL) in a dropwise manner. The reaction mixture was then stirred at room temperature for 18 h. The excess solvent was evaporated off under reduced pressure and the resulting residue diluted with saturated aqueous Na_2CO_3 and extracted with dichloromethane (3 x 50 mL). The organic fractions were combined and washed with brine, dried over Na_2SO_4 and concentrated under vacuum to afford the desired product as an orange oil. (0.41 g, 96%). ^{1}H NMR (400 MHz, $CDCl_3$): 7.49 (1H, t, J = 7.6 Hz, H_i), 7.15 (1H, d, J = 7.6 Hz, H_j), 6.94 (1H, d, J = 7.6 Hz, H_h), 4.50 (2H, s, H_k), 3.92 (2H, t , J = 7.0 Hz, H_b), 2.65 (2H, t, J = 7.6 Hz, H_g), 1.88 (3H, s, H_a), 1.60 – 1.56 (2H, m, H_c), 1.50 - 1.45 (2H, m, H_f), 1.27 – 1.23 (4H, m, H_{d+e}); ^{13}C NMR (100 MHz, $CDCl_3$):171.0, 162.0, 155.8, 137.1, 121.8, 119.8, 64.3, 46.8, 38.0, 29.6, 28.8, 28.3, 25.6, 20.8; LRESI-MS *m/z*: 292.7 ($[MNa]^+$), 270.9 ($[MH]^+$).

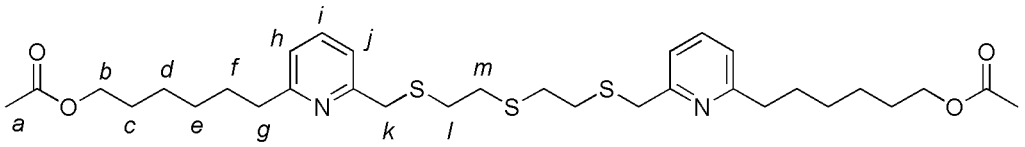

L3

To a solution of **7** (1.0 g, 3.8 mmol) in butanone (40 mL) there was added K_2CO_3 (2.1 g, 7.5 mmol) and 2,2-thiodiethanolthiol (0.24 mL, 1.9 mmol) and the mixture was refluxed for 48 h. The excess solid was removed by filtration. Water (25 mL) added to the resulting solution and the aqueous phase extracted with dichloromethane (3 x 25 mL). The organic fractions were combined and washed with brine, dried over Na_2SO_4 and concentrated down *in vacuo.* The resulting residue was subjected to flash column chromatography (ethyl acetate:dichloromethane; 1:1) to give the desired product as a yellow oil. (0.53 g, 23%). ^{1}H NMR (400 MHz, $CDCl_3$): 7.53 (2H, t, J = 7.6 Hz, H_i), 7.13 (2H, d, J = 7.6 Hz, H_j), 6.99 (2H, d, J = 7.6 Hz , H_h), 4.01 (4H, t, J = 6.8 Hz, H_b), 3.77 (4H, s, H_k), 2.73 (4H, t, J = 7.6 Hz, H_g), 2.63 (8H, s, br, H_{l+m}), 1.99 (6H, s, H_a), 1.68 - 1.64 (4H, m, H_c), 1.56 – 1.36 (4H, m, H_f), 1.34 – 1.33 (8H, m, H_{d+e}); ^{13}C NMR (100 MHz, $CDCl_3$): 171.3, 161.9, 157.9, 137.0, 120.9, 120.1, 64.4, 45.1, 38.0, 31.5, 30.9, 29.8, 29.0, 28.5, 25.8, 21.2; LRESI-MS *m/z*: 621.9 ($[MH]^+$).

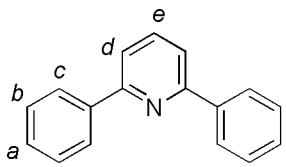

H_2**L4**[2]

A solution of 2,6-dibromopyridine (2.0 g, 8.4 mmol) and $Pd(PPh_3)_4$ (0.39 g, 0.34 mmol) in toluene (28 mL) was treated with a solution of Na_2CO_3 (3.6 g, 34 mmol) in water (17 mL). A solution of 4-phenylboronic acid (4.1 g, 34 mmol) in methanol (35 mL) was then added to this two phase system and the reaction mixture stirred at 85 ^{o}C for 16 h. Upon cooling to room temperature concentrated aqueous NH_3 (4 mL) and saturated Na_2CO_3 (40 mL) was added and the aqueous phase extracted with dichloromethane (3 x 30 mL). The organic washings were combined and washed with brine, dried over $MgSO_4$ and concentrated down under reduced pressure. The

crude residue was subjected to flash column chromatography (Et_2O:ether; 2:98) and the desired product isolated as a white solid after crystallisation from methanol and ether. (1.6 g, 81%). ^{1}H NMR (400 MHz, $CDCl_3$): 8.17 (4H, m, H_c), 7.85 (H, t, J = 7.2 Hz, H_e), 7.71 (2H, m, H_d), 7.53 (4H, m, H_b), 7.45 (2H, m, H_a); LRESI-MS *m/z*: 232.1 ($[MH]^+$). The ^{1}H NMR spectra and mass spectroscopy data of H_2**L4** were consistent with the published data.[2]

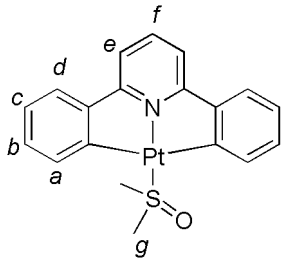

[L4 Pt(DMSO)]^3

To a solution of H_2**L4** (2.2 g, 9.6 mmol) in acetic acid (400 mL) was added a solution of $K_2[PtCl_4]$ (4.0 g, 9.6 mmol) in H_2O (25 mL) in a dropwise manner to generate a light rose coloured inhomogeneous solution. The mixture was refluxed for 18 h upon which time the red colour of the Pt salt had disappeared. The yellow precipitate which had formed was filtered off and washed with water (30 mL), acetone (30 mL), Et_2O (30 mL) and hexane (15 mL). The yellow solid was then dissolved in DMSO (20 mL) and K_2CO_3 (5.5g, 39 mmol) and H_2O (20 mL) were added and the mixture heated to 90 ºC for 1 h. Upon the addition of water (100 mL) the product precipitated out as a bright yellow solid. Flash column chromatography (dichloromethane) and crystallisation from ether and dichloromethane gave the product as a bright yellow solid. (2.1 g, 43%). ^{1}H NMR (400 MHz, $CDCl_3$): 7.85 (2H, d, J = 7.4, J (^{195}Pt) = 29.7 Hz, H_a), 7.63 (H, t, J = 8.0, H_f), 7.50 – 7.47 (2H, m, H_d), 7.32 – 7.27 (4H, m, H_{b+e}), 7.15 (2H, m, H_c), 3.69 (6H, s, J(^{195}Pt) = 26.6 Hz, H_g). ^{13}C NMR (100 MHz, $CDCl_3$): 166.8, 166.0, 149.7, 141. 2, 136.2 (J(^{195}Pt) = 92 Hz),130.8 (J(^{195}Pt) = 56 Hz), 125.0 , 124.5 (J(^{195}Pt) = 56 Hz), 115.0 (J(^{195}Pt) = 64 Hz), 48.3 (J(^{195}Pt) = 144 Hz); LRESI-MS *m/z*: 524.1 ($[MNa]^+$), 503.1 ($[MH]^+$).

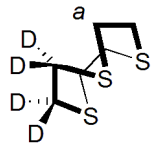

[D_4]-[9]aneS_3

To a solution of Cs_2CO_3 (3.7 g, 11 mmol) in DMF (112 mL) at 100 °C was simultaneously added solutions of 2,2-thiodiethanolthiol (1.6 g, 10 mmol) in DMF (50 mL) and at the same time a solution of 1,2-dichloroethane-d_4 (1.0 g, 10 mmol) in DMF (50 mL), both at a rate of 5 mL/h. After the additions were complete, the reaction mixture was stirred at 100 °C for a further 12 h after which time the excess solvent was removed under reduced pressure. The residual white solid was extracted with dichloromethane (3 x 100 mL) and washed with brine (100 mL), dried over Mg_2SO_4 and concentrated down under reduced pressure. The desired product was isolated as a white solid after crystallisation from hexane and dichloromethane. (22 mg, 1 %) ^{1}H NMR (400MHz, $CDCl_3$); δ = 3.03 – 2.94 (8H, m, H_a); ^{13}C NMR (100MHz, $CDCl_3$); 31.9, 31.2; LRESI-MS: *m/z* = 184 $[MH]^+$; HRESI-MS; *m/z* = 184.03537 (calc. for $C_6H_8{}^2H_4S_3$, 184.03577).

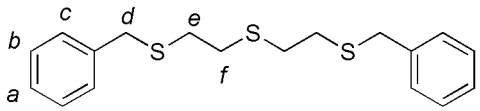

L5

To a solution of 2,2-thiodiethanolthiol (2.0 g, 13 mmol) and K_2CO_3 (5.4 g, 39 mmol) in DMF (60 mL) was added benzyl bromide (22 g, 130 mmol) and the reaction mixture was stirred at room temperature for 3 h. H_2O (50 mL) was then added to the reaction mixture and the aqueous phase extracted using dichloromethane (3 x 50 mL). The organic phases were combined and washed with brine (2 x 50 mL) and then dried over Mg_2SO_4 and concentrated down under reduced pressure. The resulting residue was subjected to flash column chromatography (hexane:dichloromethane 9:1) and recrystallisation from ethanol to give the desired product as a white solid (3.0 g, 69%). m.p. 32-35°C; ^{1}H NMR (400MHz, $CDCl_3$); δ

= 7.34 – 7.22 (10H, m, H_{a-c}), 3.73 (4H, s, H_d), 2.62 – 2.53 (8H, m, H_{e+f}); ^{13}C NMR (100MHz, $CDCl_3$); 138.1, 128.8, 128.6, 127.2, 36.4, 31.8, 31.3; LRESI-MS: *m/z* = 334 $[MH]^+$; HRESI-MS *m/z* = 334.08892 (calc. for $C_{18}H_{22}S_3$, 334.08891).

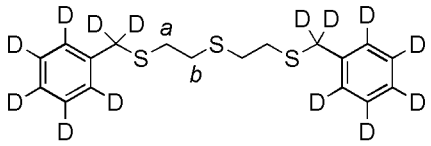

[D_{14}]-L5

To a solution of 2,2-thiodiethanolthiol (0.38 g, 2.5 mmol) and K_2CO_3 (1.0 g, 7.5 mmol) in DMF (7 mL) was added benzyl chloride-d_7 (1.0 g, 7.5 mmol) and the reaction mixture was stirred at room temperature for 18 h. H_2O (50 mL) was then added to the reaction mixture and the aqueous phase extracted using dichloromethane (3 x 50 mL). The organic phases were combined and washed with brine (2 x 50 mL) and then dried over Mg_2SO_4 and concentrated down under reduced pressure. The resulting residue was subjected to flash column chromatography (hexane:dichloromethane; 8:2) and recrystallisation from ethanol to give the desired product as a white solid. (0.81 g, 94%). m.p. 31-34 °C; ^1H NMR (400MHz, $CDCl_3$); δ = 2.74 – 2.63 (8H, m, H_{a+b}); ^{13}C NMR (100MHz, $CDCl_3$); 31.9, 31.3; LRESI-MS: *m/z* = 349 $[MH]^+$; HRESI-MS; *m/z* = 348.17629 (calc. for $C_{18}H_8{}^2H_{14}S_3$, 348.17679).

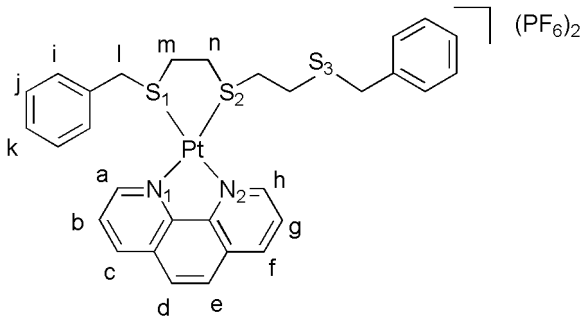

[Pt(phen)(L5)](PF$_6$)$_2$

To a solution of **L5** (0.26 g, 0.78 mmol) in MeCN:H_2O:MeOH; 20 mL:20 mL:20 mL was added [Pt(phen)Cl_2][4] (0.34 g, 0.78 mmol) and the reaction mixture was refluxed for 3 h until a homogenous bright yellow solution was obtained. Upon the addition of NH_4PF_6 (1.3 g, 7.8 mmol) the product precipitated out of solution as a bright yellow solid, when it was filtered off and collected. The resulting bright yellow solid was subjected to column chromatography (acetonitrile:dichloromethane; 10:90) and crystals were grown *via* slow diffusion of Et_2O into a saturated solution of the complex in acetone to give the desired product as a yellow solid. (0.40 g, 53%). m.p. 136-140 °C; ^{1}H NMR (400MHz, [D_6]-acetone); δ = 9.70 (1H, dd, *J* = 5.6 Hz, ^4J = 1.2 Hz, *J* (^{195}Pt) = 33.6 Hz, H_a), 9.31 (1H, dd, *J* = 8.4 Hz, ^4J = 1.2 Hz, H_c), 9.14 (1H, dd, *J* = 8.4 Hz, ^4J = 0.8 Hz, H_f), 8.83 (1H, dd, *J* = 5.6 Hz, ^4J = 0.8 Hz, *J* (^{195}Pt) = 32.0 Hz, H_h), 8.50 – 8.44 (2H, m, H_{d+e}), 8.40 – 8.36 (1H, m, H_b), 7.99 – 7.95 (1H, m, H_g), 7.46 – 7.45 (4H, m, $H_{i/}$), 7.10 – 7.08 (6H, m, H_{j+k}), 4.40 – 4.29 (4H, m, br, H_l), 3.90 – 3.74 (4H, m, br, $H_{m/n}$), 3.54 – 3.41 (4H, m, br, $H_{m/n}$); ^{13}C NMR (100MHz, [D_6]-acetone); 154.5, 154.2, 148.5, 144.6, 143.9, 143.7, 133.7, 133.0, 131.8, 131.2, 131.0, 130.6, 130.5, 130.1 (2C), 129.5, 129.2, 37.9, 30.6; LRESI-MS: *m/z* = 854 [MPF_6]$^+$, 745 [MCl]$^+$, 618 [M-$PhCH_2$]$^+$, 558 [M-$PhCH_2SCH_2CH_2$]$^+$; HRESI-MS; *m/z* = 854.08569 (calc. for $C_{30}H_{30}N_2F_6PPtS_3$, 854.08552).

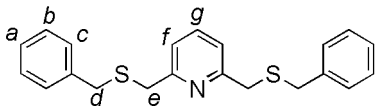

L6

To a solution of 2,6-bis(bromomethyl)pyridine (1.0 g, 3.8 mmol) and K_2CO_3 (5.2 g, 38 mmol) in DMF (40 mL) was added benzyl mercaptan (5.1 g, 38 mmol) and the reaction mixture stirred at room temperature for 3 h. After which time, H_2O (100 mL) was added to the reaction mixture and the aqueous phase extracted using dichloromethane (3 x 100 mL). The organic phases were combined and washed with brine (2 x 100 mL) and then dried over Mg_2SO_4 and concentrated down under reduced pressure. The resulting residue was subjected to flash column chromatography (1:1 dichloromethane:hexane) to give the desired product as a yellow oil. (1.2 g, 93%). ^{1}H NMR (400MHz, $CDCl_3$); δ = 7.61 (1H, t, J = 6.0, H_g), 7.35 – 7.18 (12H, m, $H_{a+b+c+f}$), 3.75 (4H, s, H_e), 3.72 (4H, s, H_d); ^{13}C NMR (100MHz, $CDCl_3$); 158.2, 138.1, 137.3, 129.1, 128.5, 127.0, 121.2, 37.3, 35.9; LRESI-MS: *m/z* = 352 $[MH]^+$; HRESI-MS; *m/z* = 352.12020 (calc. for $C_{21}H_{22}NS_2$, 352.11991).

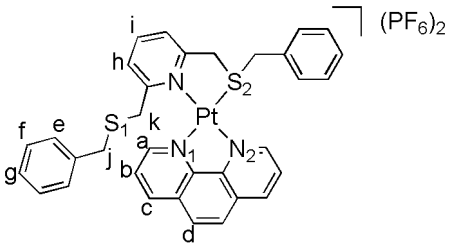

[Pt(phen)(L6)](PF$_6$)$_2$

To a solution of **L6** (0.28 g, 0.78 mmol) in MeCN:H_2O:MeOH; 20 mL:20 mL: 20 mL was added [Pt(phen)Cl_2] (0.35 g, 0.78 mmol) and the reaction mixture was refluxed for 20 min until a homogenous bright orange solution was obtained. Upon the addition of NH_4PF_6 (1.3 g, 0.78 mmol) a bright yellow solid precipitated from solution which was then subjected to flash column chromatography (acetonitrile:dichloromethane; 10:90) to isolate the desired product bright orange solid. (0.22 g, 41%). ^{1}H NMR (400MHz, [D_6]-acetone); δ = 9.61 (2H, d, J = 8.0 Hz,

H_a), 8.81 (2H, d, *J* = 8.0 Hz, H_c), 8.34 (1H, t, *J* = 8.0 Hz, H_i), 8.22 (2H, s, H_d), 8.00 (2H, t, br, H_h), 7.93 (2H, d, *J* = 8.0 Hz, H_b), 7.25 – 7.23 (4H, m, H_e), 7.11 – 7.02 (6H, m, H_{f+g}), 5.07 (4H, s, br, H_j), 4.40 (4H, s, *J* (^{195}Pt) = 39.2 Hz, H_k); ^{1}H NMR (400MHz, 4:1; [D_2]-tetrachloroethane:CD_2Cl_2); δ = 9.43 (2H, d, *J* = 8.0 Hz, H_a), 8.51 (2H, d, *J* = 8.0 Hz, H_c), 8.18 (1H, t, *J* = 8.0 Hz, H_i), 7.99 (2H, s, H_d), 7.86 (2H, t, br, H_h), 7.69 (2H, d, *J* = 8.0 Hz, H_b), 7.10-7.03 (4H, m, H_{e+f+g}), 4.71 (4H, s, br, H_j), 4.12 (4H, s, *J* (^{195}Pt) = 37.2 Hz, H_k); ^{13}C NMR (100MHz, 4:1; [D_2]-tetrachloroethane:CD_2Cl_2); 160.8, 142.2, 141.3, 131.4, 130.6 (2C), 129.6, 129.2, 129.1 (2C), 129.0 (2C), 128.9, 44.9, 44.3; LRESI-MS: *m/z* = 761 $[MCl]^+$; HRESI-MS; *m/z* = 761.11375 (calc. for $C_{33}H_{29}N_3ClPtS_2$, 761.11337).

7.2.1 Ligand Exchange Reactions

a) [Pt(phen)([9]aneS_3)]$(PF_6)_2$ + [D_4]-[9]aneS_3 ⇌ [Pt(phen)([D_4]-[9]aneS_3)]$(PF_6)_2$ + [9]aneS_3

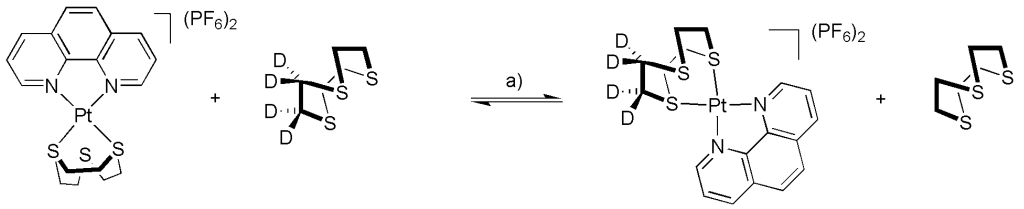

Scheme 7.1 Ligand exchange reaction between [Pt(phen)([9]aneS_3)]$(PF_6)_2$ and [D_4]-[9]aneS_3 in [D_6]-acetone. Reagent and conditions: (a) [D_6]-acetone, 298 K, 0.01 M.

To a 0.01 M solution of [Pt(phen)([9]aneS_3)]$(PF_6)_2$ (4.4 mg, 5.2 μmol) in [D_6]-acetone (0.52 mL) was added one equivalent of [D_4]-[9]aneS_3 (0.96 mg, 5.2 μmol) at 298 K and the substitution of [9]aneS_3 for [D_4]-[9]aneS_3 in [Pt(phen)([9]aneS_3)]$(PF_6)_2$ was monitored by ^{1}H NMR spectroscopy over nine days with spectra recorded at various time intervals.

b) [Pt(phen)(**L5**)]$(PF_6)_2$ + $[D_{14}]$-**L5** ⇌ [Pt(phen)($[D_{14}]$-**L5**)]$(PF_6)_2$ + **L5**

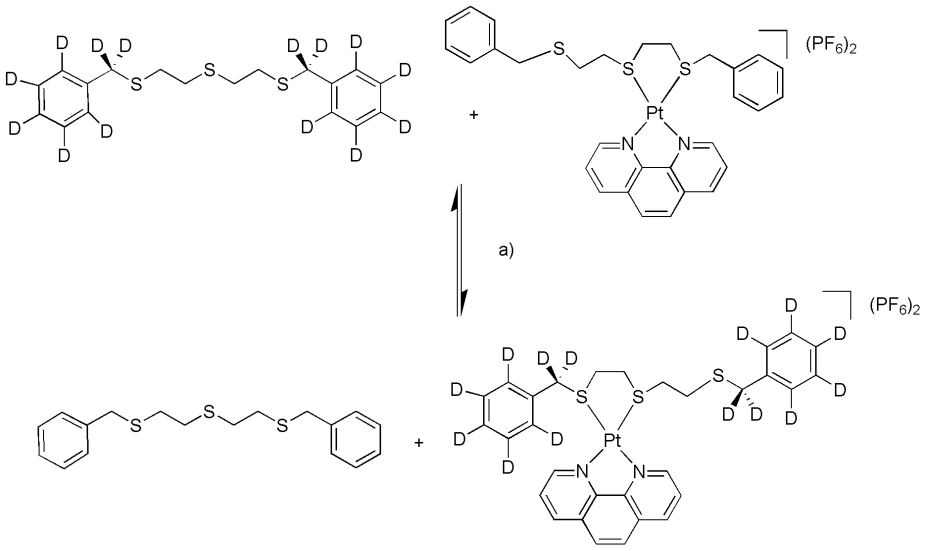

Scheme 7.2 Ligand exchange reaction between [Pt(phen)(**L5**)]$(PF_6)_2$ and $[D_{14}]$-**L5** in $[D_6]$-acetone. Reagent and conditions: (a) $[D_6]$-acetone, 298 K, 0.01 M.

To a 0.01 M solution of [Pt(phen)(**L5**)]$(PF_6)_2$, (4.4 mg, 4.4 µmol) in $[D_6]$-acetone (0.45 mL) was added one equivalent of $[D_{14}]$-**L5** (1.5 mg, 4.4 µmol) at 298 K and the substitution of $[D_{14}]$-**L5** for **L5** in [Pt(phen)(**L5**)]$(PF_6)_2$ was monitored by ^{1}H NMR spectroscopy over 150 min with spectra recorded at regular intervals.

c) [Pt(phen)(**L5**)](BPh$_4$)$_2$ + [D$_{14}$]-**L5** $\rightleftharpoons$ [Pt(phen)([D$_{14}$]-**L5**)](BPh$_4$)$_2$ + **L5**

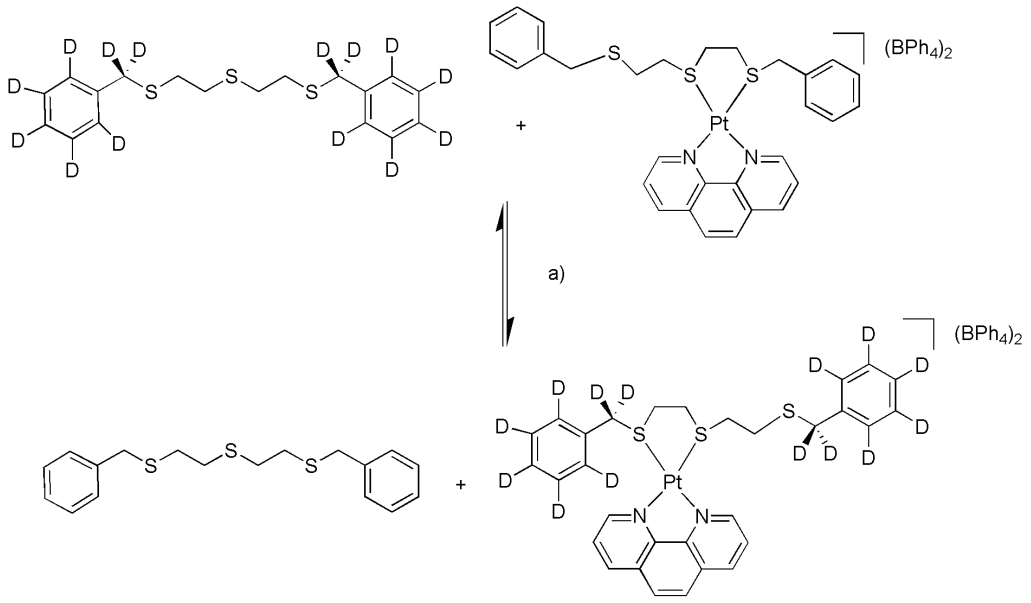

Scheme 7.3 Ligand exchange reaction between [Pt(phen)(**L5**)](BPh$_4$)$_2$ and [D$_{14}$]-**L5** in CD_2Cl_2. Reagents and conditions: (a) CD_2Cl_2, 298 K, 0.01 M.

To a 0.01 M solution of [Pt(phen)(**L5**)](BPh$_4$)$_2$, (5.0 mg, 3.7 µmol) in CD_2Cl_2 (0.37 mL) was added one equivalent of [D$_{14}$]-**L5** (1.3 mg, 3.7 µmol) at 298 K and the NMR tube wrapped in foil and the substitution of [D$_{14}$]-**L5** for **L5** in [Pt(phen)(**L5**)](BPh$_4$)$_2$ was monitored by ^{1}H NMR spectroscopy over 40 h.

7.2.2 Calculations for Number of Rotations/Steps Taken By [Pt(phen)([9]aneS$_3$)](PF$_6$)$_2$ and [Pt(phen)(L5)](PF$_6$)$_2$.

a) [Pt(phen)([9]aneS$_3$)](PF$_6$)$_2$

The Eyring equation:

$$k = \frac{k_B T}{h} e^{-K^{\ddagger}} \quad (1)$$

and $\Delta G^{\ddagger} = -RT.\ln K^{\ddagger}$ (2)

therefore $$k = \frac{k_B T}{h} e^{-\frac{\Delta G^{\ddagger}}{RT}} \quad (3)$$

(k_B = 1.381x10^{-23} JK^{-1}, R = 8.314 JK^{-1}mol^{-1}, T = 298 K , h = 6.634x10^{-34} Js, $\Delta G^{\ddagger}$ = 38 000 J.)

therefore k = 1.35x10^6 s^{-1}

In a second therefore [9]aneS$_3$ takes 1.35x10^6 steps around the platinum(II)-phen stator. For one full rotation to occur [9]aneS$_3$ must take six steps around the platinum(II)-phen stator (see Scheme 2.6).

b) [Pt(phen)(**L5**)](PF$_6$)$_2$

Using $$k = \frac{k_B T}{h} e^{-\frac{\Delta G^{\ddagger}}{RT}}$$

when R = 1.9872 cal K^{-1} mol^{-1}, k_B = 3.30 x 10^{-24} cal K^{-1}, h = 1.58 x 10^{-34} cal s, $\Delta G^{\ddagger}$ = 10 823 calmol^{-1}.

therefore $k = 71903\ s^{-1}$

Hence in one second [Pt(phen)(**L5**)](PF$_6$)$_2$ takes 71903 steps. The distance between the S12 and S18 sulfur donors in [Pt(phen)(**L5**)](PF$_6$)$_2$ is 0.663 nm (data extracted from the X-ray crystal structure of [Pt(phen)(**L5**)](PF$_6$)$_2$) hence the maximum distance travelled in an intramolecular manner in one step in [Pt(phen)(**L5**)](PF$_6$)$_2$ is 0.663 nm.

7.2.3 Variable Temperature ^{1}H NMR Studies

a) Variable Temperature ^{1}H NMR investigation of Degenerate Shuttling Process in [Pt(phen)(L5)](PF$_6$)$_2$ in [D$_6$]-acetone.

Variable temperature ^{1}H NMR experiments allow the estimation of the activation for the shuttling process in [Pt(phen)(**L5**)](PF$_6$)$_2$ in [D$_6$]-acetone. Using a Bruker AVA 400 M Hz spectrometer, ^{1}H NMR spectra were taken every 2-3 K increments from 225 K to 243 K, a stacked plot of ^{1}H NMR obtained at 298 K and every 20 K from 273 K to 213 K is shown in Figure 2.5. Upon cooling the spectra became more complicated as the peaks in the aliphatic region coalesced but only the proton resonance, H$_i$, was useful for interpretation. The coalescence temperature, T$_c$, along with the maximum peak separation, $\Delta\nu_o$ and an estimation of the observed k_{obs} and the activation free energy, $\Delta G^{\ddagger}$, are listed below in Table 7.1. The value for $\Delta G^{\ddagger}$ was estimated using a modified Eyring equation.

$$k_{coalsence} = (\pi\ \Delta\nu_o) / \sqrt{2}$$

$$\Delta G^{\ddagger} = - RT \ln K^{\ddagger} \qquad \text{where } K^{\ddagger} = (k_{coalsence} h / k_B T)$$

$$\Delta G^{\ddagger} = - RT \ln (k_{obs} h / k_B T)$$

(R = 1.9872 cal K^{-1} mol^{-1}, k_B = 3.30 x 10^{-24} cal K^{-1}, h = 1.58 x 10^{-34} cal s)

Resonance	T_c (K)	$\Delta\nu_o$ (Hz)	k_{obs} (s^{-1})	$\Delta G^{\ddagger}$ (kcal mol^{-1})
H_e	235	190 ± 9.5	422 ± 21	$10.8 \pm 2.5x10^{-4}$

Table 7.1 Estimation of kinetic parameters for the fluxional ligand exchange process in [Pt(phen)(**L5**)]$(PF_6)_2$ in [D_6]-acetone from VT ^{1}H NMR studies.

b) Variable Temperature ^{1}H NMR investigation of Degenerate Shuttling Process in [Pt(phen)(L6)]$(PF_6)_2$ in [D_6]-acetone.

Variable temperature ^{1}H NMR experiments allow the estimation of the activation for the shuttling process in [Pt(phen)(**L6**)]$(PF_6)_2$ in [D_6]-acetone. Using a Bruker AVA 400 M Hz spectrometer, ^{1}H NMR spectra were taken every 2 – 3 K increments from 225 K to 257 K, a stacked plot of ^{1}H NMR obtained at every 20 K from 293 K to 213 K is shown in Figure 2.5. Upon cooling the spectra became more complicated as the peaks coalesced but only four resonances, H_a, H_c, H_d, H_e and H_f were useful for interpretation. The coalescence temperature, T_c, for those protons along with the maximum peak separation, $\Delta\nu_o$, and an estimation of both k_{obs}, and the activation free energy, $\Delta G^{\ddagger}$, are listed in Table 2.3.

c) Variable Temperature ^{1}H NMR investigation of Degenerate Shuttling Process in [Pt(phen)(L6)]$(PF_6)_2$ in 4:1 CD_2Cl_2:[D_2]-tetrachloroethane

Variable temperature ^{1}H NMR experiments allow the estimation of the activation for the shuttling process in [Pt(phen)(**L6**)]$(PF_6)_2$ in 4:1 CD_2Cl_2:[D_2]-tetrachloroethane. Using a Bruker AVA 400 M Hz spectrometer, ^{1}H NMR spectra were taken every 2 K increments from 230 K to 248 K, a stacked plot of ^{1}H NMR spectra obtained at every 10 K from 298 K to 248 K and at 232 K is shown in Figure 2.8. Upon cooling the spectra became more complicated as the peaks in the aliphatic region coalesced; two resonances, H_a and H_g were useful for interpretation. The coalescence

temperature, T_c, for those protons along with the maximum peak separation, $\Delta\nu_o$, and an estimation of both k_{obs}, and the activation free energy, $\Delta G^{\ddagger}$, are listed in Table 2.4.

Crystal data and structure refinement for [Pt(phen)(L5)](PF$_6$)$_2$.

Structural data were collected at 93 K using a Rigaku Mercury diffractometer (MM007 high-flux RA/MoKa radiation, confocal optic). All data collection employed narrow frames (0.3-1.0) to obtain at least a full hemisphere of data. Intensities were corrected for Lorentz polarisation and absorption effects (multiple equivalent reflections). The structures were solved by direct methods, non-hydrogen atoms were refined anisotropically with CH protons being refined in riding geometries (SHELXTL) against F^2.

Table 7.2 Crystal data and structure refinement for [Pt(phen)(**L5**)](PF$_6$)$_2$.

Identification code	[Pt(phen)(**L5**)](PF$_6$)$_2$	
Empirical formula	C33 H36 F12 N2 O P2 Pt S3	
Formula weight	1057.85	
Temperature	93(2) K	
Wavelength	0.71073 Å	
Crystal system	Monoclinic	
Space group	P2(1)/c	
Unit cell dimensions	a = 13.025(2) Å	α = 90°.
	b = 21.211(3) Å	β = 108.06(4)°.
	c = 14.688(3) Å	γ = 90°.
Volume	3858.0(11) Å^3	
Z	4	
Density (calculated)	1.821 Mg/m^3	
Absorption coefficient	3.972 mm^{-1}	
F(000)	2080	
Crystal size	0.1200 x 0.1000 x 0.0800 mm^3	
Theta range for data collection	2.07 to 25.35°.	
Index ranges	-15<=h<=14, -25<=k<=25, -12<=l<=17	

Reflections collected	24125
Independent reflections	7012 [R(int) = 0.0585]
Completeness to theta = 25.00°	99.4 %
Absorption correction	Multiscan
Max. and min. transmission	1.0000 and 0.7823
Refinement method	Full-matrix least-squares on F^2
Data / restraints / parameters	7012 / 0 / 488
Goodness-of-fit on F^2	1.086
Final R indices [I>2sigma(I)]	R1 = 0.0415, wR2 = 0.0909
R indices (all data)	R1 = 0.0517, wR2 = 0.0970
Largest diff. peak and hole	1.213 and -0.986 e.Å

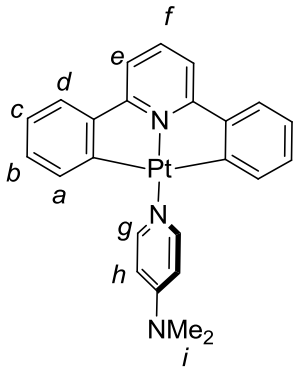

[**L**Pt(PyNMe$_2$)]

To a yellow solution of [**L**Pt(DMSO)] (0.094 g, 0.19 mmol) in CH_2Cl_2 (4 mL) was added PyNMe$_2$ (0.028 g, 0.19 mmol), which resulted in a darkening of the solution colour to orange within 5 mins. The reaction was monitored by TLC (alumina, 90.5:9:0.5 EtOAc:CH_2Cl_2:NEt_3) until complete (1.5 h), after which time the excess solvent was removed under reduced pressure. Purification of the crude product using column chromatography on alumina (90.5:9:0.5 EtOAc:CH_2Cl_2:NEt_3) and subsequent recrystallisation (CH_2Cl_2/hexane) gave an orange solid (0.10 g, 98%). m.p. 292 ºC (dec.); ^{1}H NMR (400 MHz, [D_7]-DMF:CD_2Cl_2; 1:1): 8.58 (2H, d, J = 7.2 Hz, J (^{195}Pt) = 42.0 Hz, H_g), 7.69 – 7.65 (1H, m, H_f), 7.55 (2H, d, J = 7.2 Hz, H_d), 7.43 – 7.40 (2H, m, H_e), 7.20 – 7.17 (2H, m, H_h), 7.10 – 7.02 (4H, m, H_{b+c}), 6.81 – 6.79 (2H, m, H_a), 3.26 (6H, s, H_i); ^{13}C NMR (100 MHz, [D_7]-DMF:CD_2Cl_2; 1:1): 172.8, 167.6, 151.7, 148.9, 138.8, 133.1, 129.5, 123.1, 122.4, 121.9, 113.7, 107.9, 38.4; UV/Vis ([D_7]-DMF:CD_2Cl_2; 1:1): λ_{max} / nm (ε / M^{-1} cm^{-1}): 386 (2944), 285 (33618), 336 (8939); LR-FABMS (3-NOBA matrix): *m/z* = 547 $[MH]^+$; HR-FABMS (3-NOBA matrix); *m/z* = 547.1457 (calc. for $C_{24}H_{22}N_3Pt$, 547.1461).

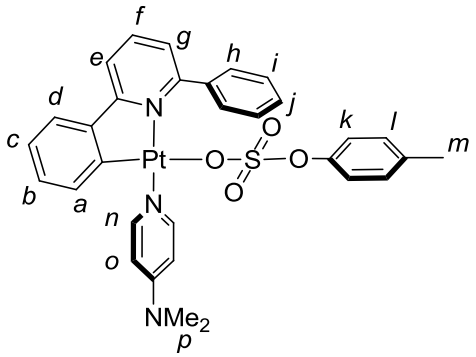

[*cis*-H**L**Pt(PyNMe$_2$)OTs]

To a solution of [**L**Pt(PyNMe$_2$)] (10.0 mg, 0.018 mmol) in 1:1 CH_2Cl_2/acetone (2 mL) was added TsOH·H_2O (3.5 mg, 0.018 mmol). After stirring for 5 min. the excess solvent was removed under reduced pressure to give the product as a pale yellow solid (9.7 mg, 72%). ^{1}H NMR (400 MHz, [D_7]-DMF:CD_2Cl_2; 1:1): 8.32 – 8.17 (4H, m, H_{e+f+n}), 8.09 – 8.07 (1H, d, H_g), 7.76 – 7.71 (3H, m, H_{d+k}), 7.60 – 7.59 (4H, m, H_{h+i}), 7.55 (1H, m, H_j), 7.21 – 7.18 (3H, m, H_{c+l}), 7.04 – 7.00 (1H, m, H_b), 6.73 (2H, d, J = 7.2 Hz, H_o), 6.53 – 6.41 (1H, m, H_a), 3.17 (6H, s, H_p), 2.38 (3H, s, H_m); ^{13}C NMR (100 MHz, [D_7]-DMF:CD_2Cl_2; 1:1): 166.0, 161.5, 161.4, 157.1, 157.0, 153.8, 150.4, 145.0, 143.3, 138.9, 138.4, 131.2, 128.4, 128.3, 128.2, 127.6, 127.4, 125.1, 123.5, 123.3, 116.7, 107.5, 38.2, 20.0; LR-FABMS (3-NOBA matrix): *m/z* = 547 [M-OTs]$^+$; HR-FABMS (3-NOBA matrix); *m/z* = 547.1457 (calc. for $C_{24}H_{22}N_3Pt$, 547.1461).

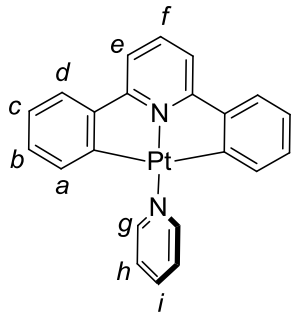

[**L**Pt(PyH)]

To a yellow solution of [**L**Pt(DMSO)] (0.050 g, 0.10 mmol) in CH_2Cl_2 (20 mL) was added PyH (0.0080 mL, 0.10 mmol). The reaction was monitored by TLC (alumina, 90.5:9:0.5 EtOAc:CH_2Cl_2:NEt_3) until complete (3 h), after which time the excess solvent was removed under reduced pressure. Purification of the crude product using column chromatography on alumina (90.5:9:0.5 EtOAc:CH_2Cl_2:NEt_3) and subsequent recrystallisation (CH_2Cl_2/hexane) gave an orange solid (0.042 g, 84%). m.p. 201-203 ºC; ^{1}H NMR (400 MHz, [D_7]-DMF:CD_2Cl_2; 1:1): 9.16 (2H, d, J = 6.8 Hz, J (^{195}Pt) = 43.6 Hz, H_g), 8.12 – 8.08 (1H, m, H_i), 7.72 – 7.65 (3H, m, H_{f+h}), 7.57 (2H, d, J = 6.8 Hz, H_d), 7.45 – 7.43 (2H, m, H_e), 7.19 – 7.16 (2H, m, H_b), 7.08 – 7.03 (2H, m, H_c), 6.94 – 6.89 (2H, m, H_a); ^{13}C NMR (100 MHz, [D_7]-DMF:CD_2Cl_2; 1:1): 172.1, 167.5, 153.2, 148.8, 139.4, 136.3, 132.5, 129.7, 126.2, 123.3, 122.7, 113.9; UV/Vis ([D_7]-DMF:CD_2Cl_2; 1:1); λ_{max} / nm (ε / M^{-1} cm^{-1}): 393 (999), 344 (3237), 280 (7266), 251 (8953); LR-FABMS (3-NOBA matrix); *m/z* = 504 $[M]^+$; HR-FABMS (3-NOBA matrix); *m/z* = 504.10469 (calc. for $C_{22}H_{17}N_2Pt$, 504.10340).

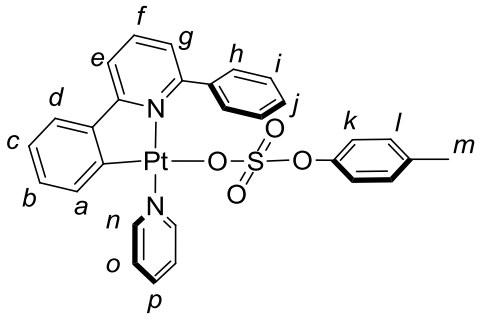

[*cis*-H**L**Pt(PyH)OTs]

To a solution of [**L**Pt(PyH)] (20 mg, 0.040 mmol) in 1:1 CH_2Cl_2/acetone (3/1 mL) was added TsOH.H_2O (7.6 mg, 0.040 mmol). After stirring for 5 min. the excess solvent was removed under reduced pressure to give the product as a pale yellow solid and the desired product was recrystallised from hexane and $CHCl_3$ (19 mg, 71%). ^{1}H NMR (400 MHz, [D_7]-DMF:CD_2Cl_2; 1:1): 9.01 (2H, *J* = 6.4 Hz, *J* (^{195}Pt) = 38.8 Hz, H_n), 8.23 – 8.10 (3H, m, H_{e+h}), 7.78 – 7.55 (10H, m, $H_{d+f+g+i+k+o+p}$), 7.24 – 7.16 (4H, m, H_{c+j+l}), 7.03 – 6.99 (1H, m, H_b), 6.38 – 6.22 (1H, m, H_a), 2.34 (3H, s, H_m); ^{13}C NMR (100 MHz, [D_7]-DMF:CD_2Cl_2; 1:1): 176.9, 157.6, 157.6, 153.5, 140.0, 139.7, 139.3, 135.6, 132.1, 131.6, 129.4, 129.3, 128.5 (2C), 128.3, 127.0, 125.9 (2C), 124.5, 117.6, 115.9, 114.9, 107.9; LR-FABMS (3-NOBA matrix): *m/z* = 504 [M-OTs]$^+$; HR-FABMS (3-NOBA matrix); *m/z* = 504.10397 (calc. for $C_{22}H_{17}N_2Pt$, 504.10340).

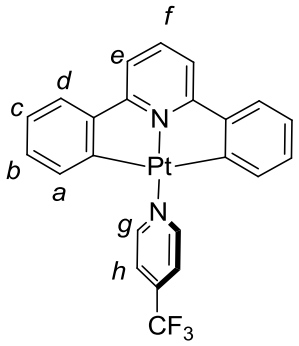

[**L**Pt(PyCF$_3$)]

To a yellow solution of [**L**Pt(DMSO)] (0.067 g, 0.13 mmol) in CH_2Cl_2 (10 mL) was added PyCF$_3$ (0.020 g, 0.13 mmol), which resulted in a darkening of the solution to orange. The reaction was stirred overnight at room temperature and the excess solvent was removed under reduced pressure. Purification of the crude product using column chromatography on alumina (90.5:9:0.5 EtOAc:CH_2Cl_2:NEt_3) and subsequent recrystallisation (CH_2Cl_2/hexane) gave an orange solid (0.062 g, 83%). m.p. 228-232 ºC (dec); ^{1}H NMR (400 MHz,[D_7]-DMF:CD_2Cl_2; 1:1): 9.48 (2H, d, J = 6.0 Hz, J (^{195}Pt) = 45.6 Hz, H$_g$), 8.02 – 7.99 (2H, m, H$_h$), 7.74 (1H, t, J = 8.0 Hz, H$_f$), 7.58 (2H, d, J = 6.8 Hz, H$_d$), 7.47 (2H, d, J = 8.0 Hz, H$_e$), 7.23 – 7.18 (2H, m, H$_b$), 7.13 – 7.07 (2H, m, H$_c$), 6.95 – 6.86 (2H, m, H$_a$); ^{13}C NMR (100 MHz, [D_7]-DMF:CD_2Cl_2; 1:1): 171.6, 167.5, 154.5, 148.7, 139.7, 132.3, 129.8, 127.9, 125.0, 123.5, 123.0, 122.3, 114.1; UV/Vis ([D_7]-DMF:CD_2Cl_2; 1:1); λ_{max} / nm (ε / M^{-1} cm^{-1}): 392 (2717), 340 (6584), 270 (18991); LR-FABMS (3-NOBA matrix): *m/z* = 572 $[MH]^+$; HR-FABMS (3-NOBA matrix); *m/z* = 572.0916 (calc. for $C_{23}H_{16}N_2F_3Pt$, 572.09078).

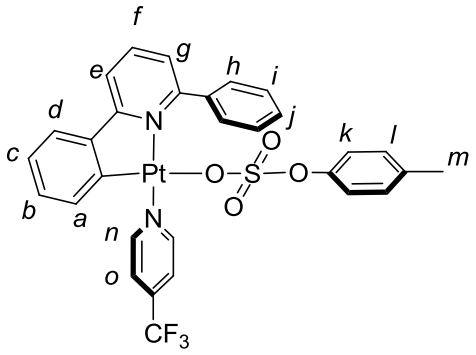

[*cis*-H**L**Pt(PyCF$_3$)OTs]

To a solution of [**L**Pt(PyCF$_3$)] (12 mg, 0.022 mmol) in 1:1 CH_2Cl_2/acetone (4 mL) was added TsOH.H_2O (4.1 mg, 0.022 mmol). After stirring for 5 min the excess solvent was removed under reduced pressure to give the product as a pale yellow solid (16 mg, 98%). ^{1}H NMR (400 MHz, [D_7]-DMF:CD_2Cl_2; 1:1): 9.39 – 9.22 (2H, m, H_n), 8.20 (1H, t, *J* = 7.6 Hz, H_f), 8.10 (1H, d, *J* = 7.6 Hz, H_e), 7.97-7.92 (2H, m, H_o), 7.78 – 7.54 (8H, m, $H_{d+k+h+i+j}$), 7.25 – 7.22 (2H, m, H_{c+g}), 7.13 (2H, d, *J* = 6.4 Hz, H_l), 7.04 – 7.00 (1H, m, H_b), 6.36 – 6.25 (1H, m, H_a), 2.35 (3H, s, H_m); ^{13}C NMR (100 MHz, [D_7]-DMF:CD_2Cl_2; 1:1): 171.4, 167.7, 161.5, 155.7, 154.7, 152.4, 142.7, 142.2, 139.6, 131.3, 128.8, 128.7, 128.4, 127.7, 127.5, 125.2, 124.6, 124.0, 123.9, 122.4, 122.3, 115.1 (2C), 20.1; LR-FABMS (3-NOBA matrix): *m/z* = 572[M-OTs]$^+$; HR-FABMS (3-NOBA matrix); *m/z* = 572.08949 (calc. for $C_{23}H_{16}N_2F_3Pt$, 572.09078).

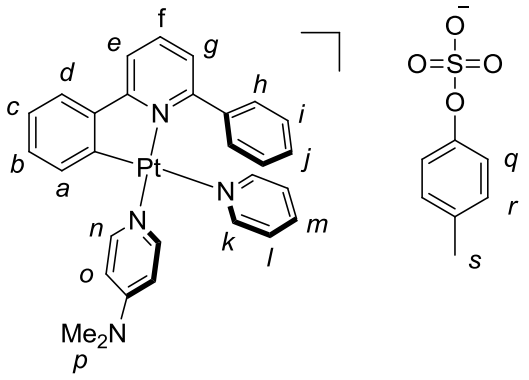

[*trans*-H**L**Pt(PyNMe$_2$)(PyH)]OTs

To a bright yellow solution of [**L**Pt(PyNMe$_2$)] (7.3 mg, 0.013 mmol) in 1:1 CH_2Cl_2/acetone (6 mL) was added pyridinium tosylate (3.3 mg, 0.013 mmol) and the pale yellow solution was stirred at RT for 5 min. The excess solvent was removed under reduced pressure to give the product as a bright yellow solid (10 mg, 90%). ^{1}H NMR (400 MHz, [D$_7$]-DMF:CD_2Cl_2; 1:1): 8.31 – 8.14 (6H, m, $H_{e+f+k+n}$), 7.85 (1H, d, J = 7.6 Hz, H_d), 7.74 – 7.66 (3H, m, H_{m+q}), 7.60 – 7.58 (2H, m, H_h), 7.46 (1H, dd, J = 7.6 Hz, ^4J = 1.2 Hz, H_g), 7.27 – 7.20 (4H, m, H_{c+j+l}), 7.17 – 7.13 (4H, m, H_{i+r}), 7.09 – 7.05 (1H, m, H_b), 6.66 – 6.65 (2H, d, J = 7.2 Hz, H_o), 6.55 – 6.45 (1H, m, H_a), 3.12 (6H, s, H_p), 2.35 (3H, s, H_s); ^{13}C NMR (100 MHz, [D$_7$]-DMF:CD_2Cl_2; 1:1): 167.1, 161.5, 153.7, 150.0, 149.5, 145.8, 145.5, 139.8, 139.1, 139.0, 137.2, 137.0, 136.8, 132.1, 128.7, 128.3, 127.9, 127.7, 127.4, 125.2, 124.9, 123.7, 116.9, 108.1, 102.2, 38.3, 20.0; UV/Vis ([D$_7$]-[DMF:CD_2Cl_2; 1:1); λ_{max} / nm (ε / M^{-1} cm^{-1}): 342 (2407), 285 (7897); LR-FABMS (3-NOBA matrix): *m/z* = 547 [M-PyH]$^+$; HR-FABMS (3-NOBA matrix); *m/z* = 547.14537 (calc. for $C_{24}H_{22}N_3Pt$, 547.14560).

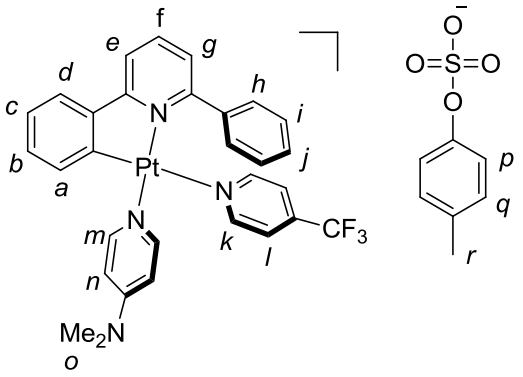

[*trans*-H**L**Pt(PyNMe$_2$)(PyCF$_3$)]OTs

To a bright yellow solution of [**L**Pt(PyNMe$_2$)] (8.4 mg, 0.015 mmol) in 1:1 CH_2Cl_2/acetone (6 mL) was added trifluoromethylpyridinium tosylate (5.2 mg, 0.015 mmol) and the pale yellow solution was stirred at RT for 5 mins. The excess solvent was removed under reduced pressure to give the product as a bright yellow solid (12 mg, 81%). ^{1}H NMR (400 MHz, [D$_7$]-DMF:CD_2Cl_2; 1:1): 8.40 – 8.21 (3H, m, H$_{f+m}$), 8.15 (1H, d, *J* = 6.4 Hz, H$_e$), 7.84 (1H, d, *J* = 6.4 Hz, H$_j$), 7.74 – 7.71 (4H, m, H$_{i+q}$), 7.59 (2H, d, *J* = 6.4 Hz, H$_k$), 7.49 – 7.44 (3H, m, H$_{g+h}$), 7.29 – 7.22 (4H, m, H$_{c+d+l}$), 7.18 (2H, d, *J* = 6.4 Hz, H$_p$), 7.09 (1H, t, *J* = 6.8 Hz, H$_b$), 6.66 (2H, d, *J* = 6.0 Hz, H$_n$), 6.51 – 6.40 (1H, m, H$_a$), 3.11 (6H, s, H$_o$), 2.37 (3H, s, H$_r$); ^{13}C NMR (100 MHz,[D$_7$]-DMF:CD_2Cl_2; 1:1): 167.07, 153.9, 151.4, 150.2, 150.1, 145.8, 144.5, 139.4, 139.1, 138.7, 137.9, 132.2, 129.0, 128.5, 128.2, 127.9, 127.6, 125.3, 124.1, 124.0, 123.9, 120.9, 120.9, 118.8, 117.1, 108.3, 38.4, 20.1; UV/Vis ([D$_7$]-DMF:CD_2Cl_2; 1:1); λ_{max} / nm (ε / M^{-1} cm^{-1}): 386 (2943), 336 (8939), 285 (33618); LR-FABMS (3-NOBA matrix): *m/z* = 548 [MH-PyCF$_3$]$^+$; HR-FABMS (3-NOBA matrix); *m/z* = 548.15420 (calc. for $C_{24}H_{23}N_3Pt$, 548.15452).

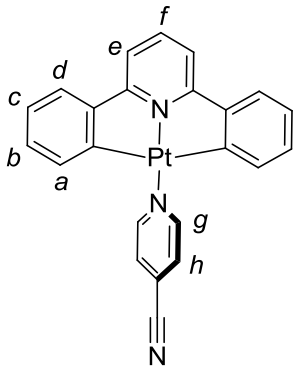

[**L**Pt(PyCN)]

To a yellow solution of [**L**Pt(DMSO)] (0.20 g, 0.40 mmol) in CH_2Cl_2 (15 mL) was added 4-cyanopyridine (0.083 g, 0.80 mmol), and the reaction mixture was refluxed for 2 h after which time a darkening of the solution to orange was observed. The excess solvent was removed under reduced pressure and purification of the crude product using column chromatography on alumina (90.5:9:0.5 EtOAc:CH_2Cl_2:NEt_3) and subsequent recrystallisation (CH_2Cl_2/hexane) gave an orange solid (0.20 g, 93%). ^{1}H NMR (400 MHz, [D_7]-DMF:CD_2Cl_2; 1:1): 9.43 (2H, d, J = 6.4 Hz, J (^{195}Pt) = 46.0 Hz, H_g), 8.05 – 8.01 (2H, m, H_h), 7.73 (1H, t, J = 7.6 Hz, H_f), 7.57 (2H, d, J = 7.2 Hz, H_d), 7.46 (2H, d, J = 7.6 Hz, H_e), 7.20 – 7.17 (2H, m, H_b), 7.08 – 7.04 (2H, m, H_c), 6.91 – 6.83 (2H, m, H_a); ^{13}C NMR (400 MHz, [D_7]-DMF:CD_2Cl_2; 1:1): 171.2, 167.2, 157.0, 153.9, 148.4, 139.5, 132.0, 131.7, 129.6, 128.2, 123.3, 122.9, 113.9; UV/Vis ([D_7]- DMF:CD_2Cl_2; 1:1); λ_{max} / nm (ε / M^{-1} cm^{-1}): 395 (5987), 343 (12429), 264 (23756); LR-FABMS (3-NOBA matrix): *m/z* = 529 $[MH]^+$; HR-FABMS (3-NOBA matrix); *m/z* = 529.09776 (calc. for $C_{23}H_{16}N_3Pt$, 529.09921).

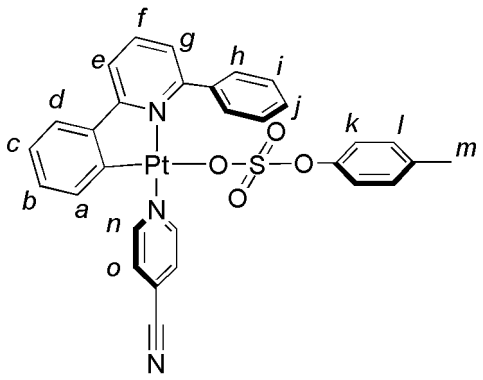

[*cis*-H**L**Pt(PyCN)OTs]

To a solution of [**L**Pt(PyCN)] (12.2 mg, 0.023 mmol) in 1:1 CH_2Cl_2/acetone (2 mL) was added $TsOH{\cdot}H_2O$ (4.4 mg, 0.018 mmol). After stirring for 5 min the excess solvent was removed under reduced pressure to give the product as a pale yellow solid (12.6 mg, 76%). ^{1}H NMR (400 MHz, [D_7]-DMF:CD_2Cl_2; 1:1): 9.33 – 9.22 (2H, m, H_n), 8.25 (1H, t, J = 7.6 Hz, H_f), 8.15 – 8.12 (3H, m, H_{e+o}), 7.81 (1H, d, J = 7.6 Hz, H_d), 7.73 – 7.72 (3H, m, H_{j+k}), 7.61 – 7.57 (3H, m, H_{g+h}), 7.25 – 7.21 (1H, m, H_c), 7.17 – 7.15 (4H, m, H_{i+l}), 7.04 – 7.00 (1H, m, H_b), 6.37 – 6.24 (1H, m, H_a), 2.36 (3H, s, H_m); ^{13}C NMR (400 MHz, [D_7]-DMF:CD_2Cl_2; 1:1): 166.8, 155.0, 140.2, 136.8, 132.7, 131.9, 130.3, 129.5, 129.4, 129.3, 129.2 (2C), 128.9, 128.5, 128.3, 128.1, 125.9, 124.7, 124.6 (2C), 124.0, 122.7, 115.4, 20.8; LR-FABMS (3-NOBA matrix): *m/z* = 530 $[M\text{-}OTs]^+$; HR-FABMS (3-NOBA matrix); *m/z* = 530.10699 (calc. for $C_{23}H_{17}N_3Pt$, 530.10647).

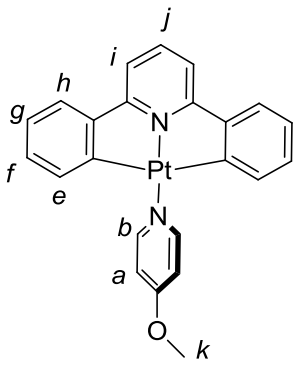

[**L**Pt(PyOMe)]

To a yellow solution of [**L**Pt(DMSO)] (0.22 g, 0.43 mmol) in CH_2Cl_2 (15 mL) was added 4-methoxypyridine (0.047 g, 0.43 mmol). The reaction was monitored by TLC (alumina, 90.5:9:0.5 EtOAc:CH_2Cl_2:NEt_3) until complete (1 h), after which time the excess solvent was removed under reduced pressure. The excess solvent was removed under reduced pressure and purification of the crude product using column chromatography on alumina (90.5:9:0.5 EtOAc:CH_2Cl_2:NEt_3) and subsequent recrystallisation (CH_2Cl_2/hexane) gave an orange solid (0.19 g, 81%). ^{1}H NMR (400 MHz, [D_7]-DMF:CD_2Cl_2; 1:1): 8.95 (2H, d, J = 7.2 Hz, J (^{195}Pt) = 48.0 Hz, H_b), 7.70 (1H, t, J = 8.0 Hz, H_j), 7.55 (2H, d, J = 7.2 Hz, H_h), 7.42 (2H, d, J = 8.0 Hz, H_i), 7.22 - 7.17 (4H, m, H_{a+f}), 7.08 – 6.95 (4H, m, H_{e+g}), 4.09 (3H, s, H_k); ^{13}C NMR (400 MHz, [D_7]-DMF:CD_2Cl_2; 1:1): 172.2, 171.1, 153.7, 148.7, 139.0, 132.7, 129.5, 123.1, 122.5, 113.6, 112.0, 55.5; UV/Vis ([D_7]- DMF:CD_2Cl_2; 1:1); λ_{max} / nm (ε / M^{-1} cm^{-1}): 394 (2966), 345 (10012), 268 (19758); LR-FABMS (3-NOBA matrix): *m/z* = 534 $[MH]^+$; HR-FABMS (3-NOBA matrix); *m/z* = 534.11435 (calc. for $C_{23}H_{19}N_2PtO$, 534.11452).

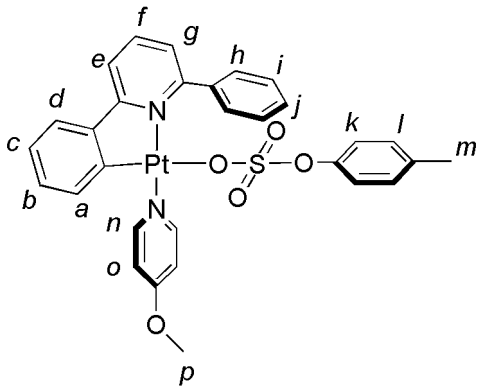

[*cis*-H**L**Pt(PyOMe)OTs]

To a solution of [LPt(OMe)] (9.7 mg, 0.018 mmol) in 1:1 CH_2Cl_2/acetone (2 mL) was added $TsOH{\cdot}H_2O$ (3.5 mg, 0.018 mmol). After stirring for 5 min. the excess solvent was removed under reduced pressure to give the product as a pale yellow solid (9.3 mg, 71%). ^{1}H NMR (400 MHz, [D_7]-DMF:CD_2Cl_2; 1:1): 8.76 (2H, d, *J* = 7.2 Hz, *J* (^{195}Pt) = 36.4 Hz, H_n), 8.22 (1H, t, *J* = 8.0 Hz, H_f), 8.10 (1H, d, *J* = 8.0 Hz, H_e), 7.77 – 7.72 (5H, m, H_{d+i+k}), 7.62 – 7.54 (4H, m, H_{g+h+j}), 7.21 – 7.17 (5H, m, H_{c+l+o}), 7.04 – 6.99 (1H, m, H_b), 6.45 – 6.21 (1H, m, H_a), 4.05 (3H, s, H_p), 2.37 (3H, s, H_q); ^{13}C NMR (400 MHz, [D_7]-DMF:CD_2Cl_2; 1:1): 171.9, 161.2, 153.0, 140.1, 138.9, 137.9, 137.8, 135.5, 132.7, 131.3, 129.2, 128.3 (2C), 128.0, 127.3 (2C), 124.9, 123.5, 123.4, 116.5, 115.2, 111.9, 55.6, 19.8; LR-FABMS (3-NOBA matrix): m/z = 534 $[M\text{-}OTs]^+$; HR-FABMS (3-NOBA matrix); m/z = 535.12142 (calc. for $C_{23}H_{20}ON_2Pt$, 535.12179).

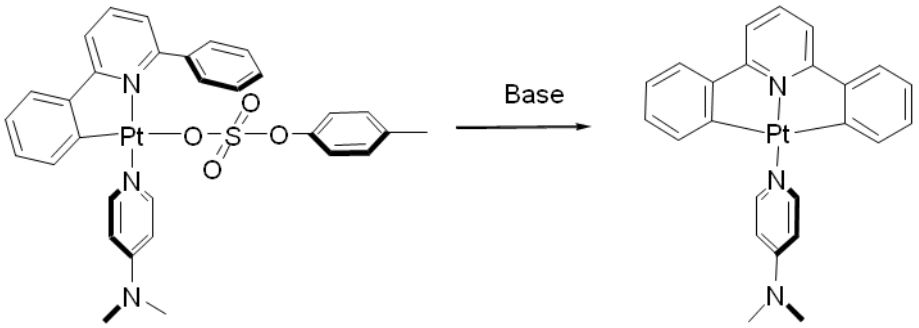

[H**L**Pt(DMAP)OTs] [**L**Pt(DMAP)]

Conversion of [H**L**Pt(DMAP)OTs] to [**L**Pt(DMAP)]

(a) Using K_2CO_3

To a pale yellow solution of [H**L**Pt(DMAP)OTs] (10.8 mg, 0.015 mmol) in CH_2Cl_2 (20 mL) was added K_2CO_3 (20.7 mg, 0.15 mmol) and the reaction mixture stirred at RT for 5 min. The K_2CO_3 was filtered off and washed with CH_2Cl_2 (20 mL) to give a bright orange solution. Removal of the solvent under reduced pressure gave [**L**Pt(DMAP)] as an orange solid. (9.7 mg, 89%). Characterisation as previously reported.

(b) UsingP_1-^{t}Bu

To a pale yellow solution of [H**L**Pt(DMAP)OTs] (11.3 mg, 0.015 mmol) in CD_2Cl_2 (1 mL) was added P_1-^{t}Bu (5.9 µL, 0.023 mmol) and immediately a darkening of the solution was observed. The reaction was monitored by ^{1}H NMR spectroscopy which indicated quantitative conversion of [H**L**Pt(DMAP)OTs] to [**L**Pt(DMAP)] within 5 minutes.

7.2.4 Theoretical and Experimental UV-Vis Spectra

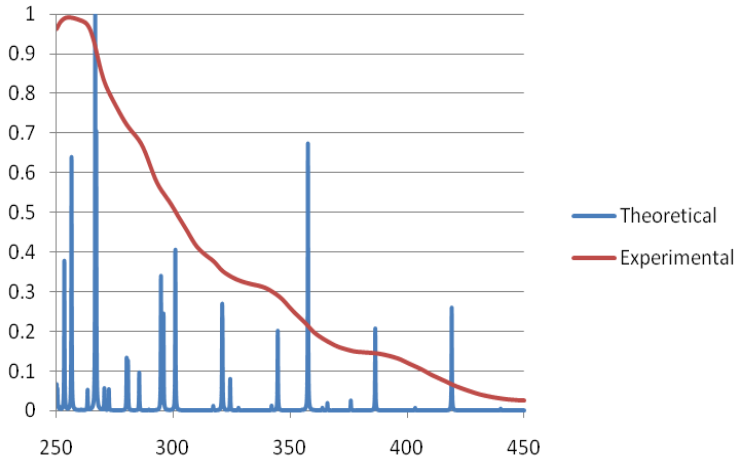

Graph 7.1 Experimental and calculated UV/Vis absorbance spectra of [**L**Pt(PyH)] in [D_7]-DMF:DCM-d_2 for experimental data and CH_2Cl_2 for theoretical data showing good overall agreement with transitions.

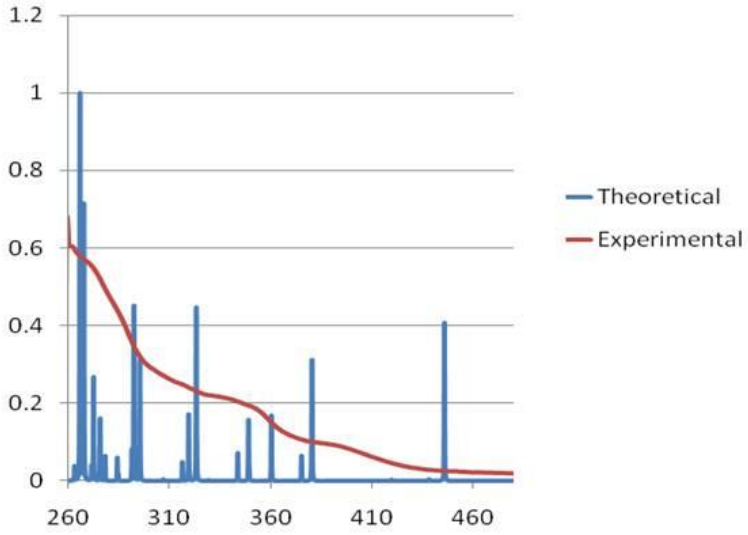

Graph 7.2 Experimental and calculated UV/Vis absorbance spectra of [**L**Pt(PyCF$_3$)] in [D_7]-DMF:DCM-d_2 for experimental data and CH_2Cl_2 for theoretical data showing good overall agreement with transitions

7.2.5 Kinetic Studies: Tabulated Data and Graphs

a) $PyNMe_2$ + [**L**Pt(PyH)] $\rightleftharpoons$ [**L**Pt($PyNMe_2$)] + PyH under non-irradiative conditions.

Time(s)	[LPt(PyH)]	ln[LPt(PyH)]
1200	98	4.58
3900	95	4.55
5400	94	4.54
6600	93	4.53
7500	92	4.52

Table 7.3 Values for time (s), [**L**Pt(PyH)] and ln[**L**Pt(PyH)] for the exchange reaction $PyNMe_2$ + [**L**Pt(PyH)] $\rightleftharpoons$ [**L**Pt($PyNMe_2$)] + PyH under non-irradiative conditions with heating at 313 K.

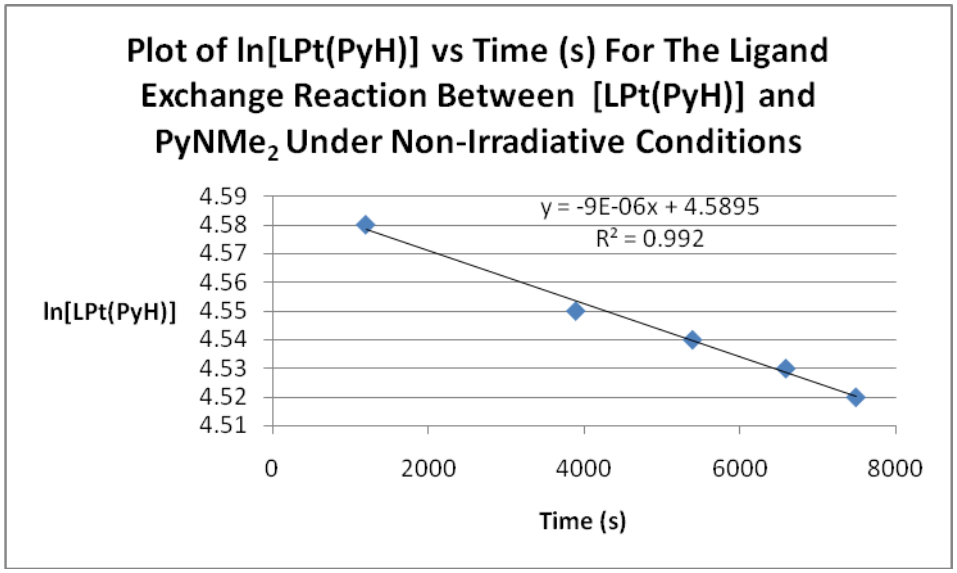

Graph 7.3 Plot of ln[**L**Pt(PyH)] vs Time (s) for the exchange reaction $PyNMe_2$ + [**L**Pt(PyH)] $\rightleftharpoons$ [**L**Pt($PyNMe_2$)] + PyH under non-irradiative conditions showing first order reaction kinetics.

b) $PyNMe_2$ + [**L**Pt(PyH)] $\rightleftharpoons$ [**L**Pt($PyNMe_2$)] + PyH under irradiative conditions between 260-290 nm.

Time(s)	[LPt(PyH)]	ln[LPt(PyH)]
900	96	4.56
1500	95	4.55
2220	94	4.54
2700	92	4.52
4200	90	4.50

Table 7.4 Values for time (s), [**L**Pt(PyH)] and ln[**L**Pt(PyH)] for the exchange reaction $PyNMe_2$ + [**L**Pt(PyH)] $\rightleftharpoons$ [**L**Pt($PyNMe_2$)] + PyH under irradiative conditions between 260-290 nm.

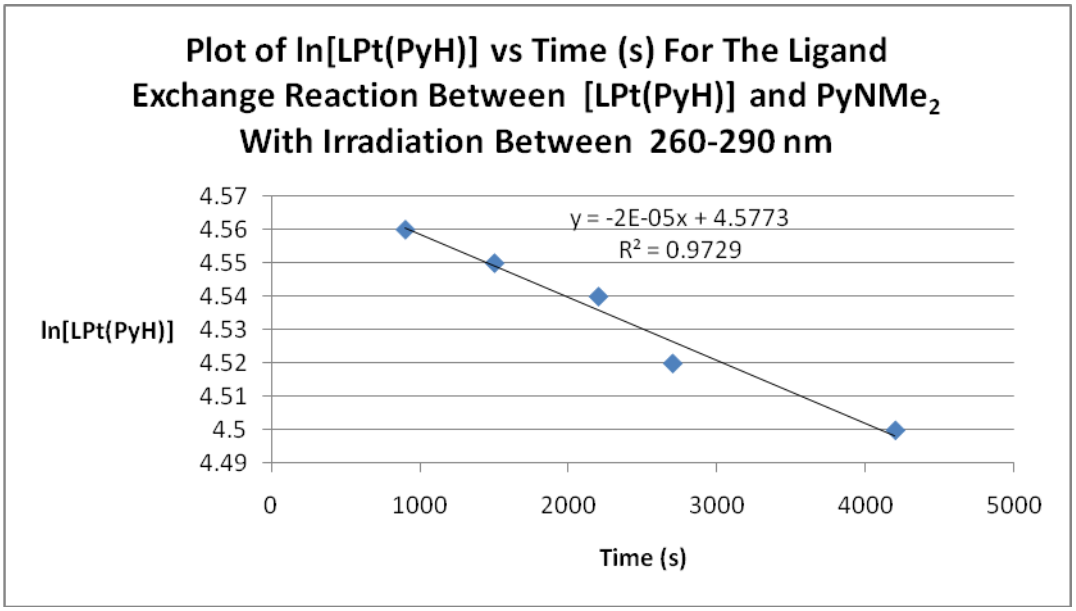

Graph 7.4 Plot of ln[**L**Pt(PyH)] vs Time (mins) for the exchange reaction $PyNMe_2$ + [**L**Pt(PyH)] $\rightleftharpoons$ [**L**Pt($PyNMe_2$)] + PyH under irradiative conditions between 260-290 nm showing first order reaction kinetics.

c) $PyNMe_2$ + [**L**Pt(PyH)] $\rightleftharpoons$ [**L**Pt($PyNMe_2$)] + PyH under irradiative conditions between 290-320 nm.

Time(s)	[LPt(PyH)]	ln[LPt(PyH)]
900	99	4.60
2400	97	4.57
4200	96	4.56
6300	93	4.53
7500	92	4.52

Table 7.5 Values for time (s), [**L**Pt(PyH)] and ln[**L**Pt(PyH)] for the exchange reaction $PyNMe_2$ + [**L**Pt(PyH)] $\rightleftharpoons$ [**L**Pt($PyNMe_2$)] + PyH under irradiative conditions between 290-320 nm.

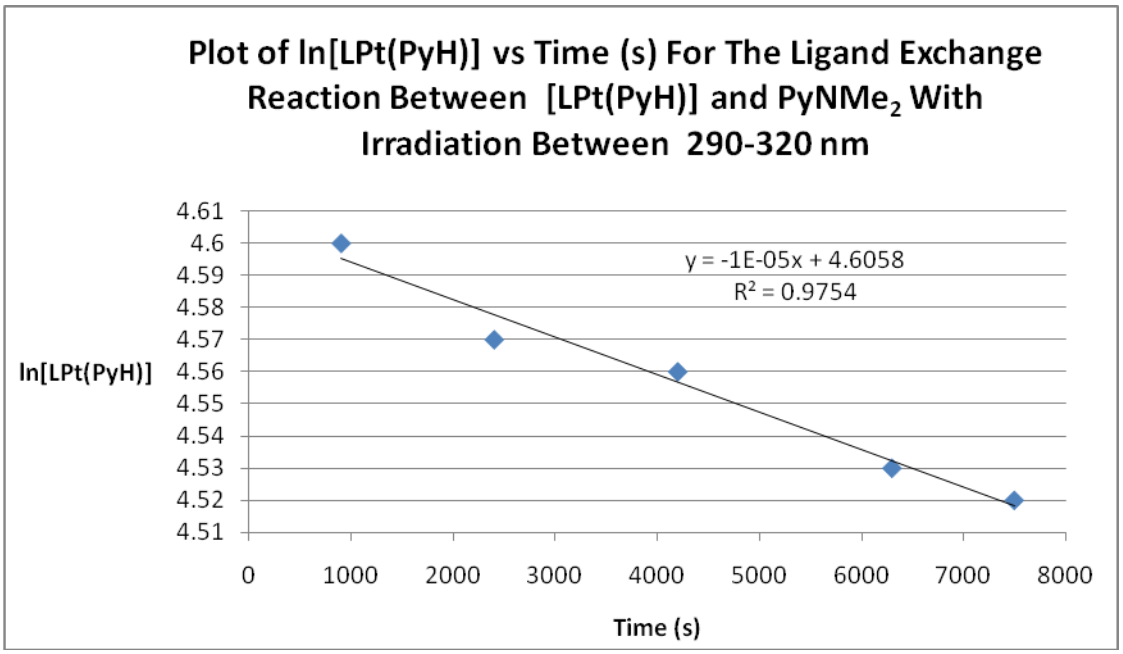

Graph 7.5 Plot of ln[**L**Pt(PyH)] vs Time (s) for the exchange reaction $PyNMe_2$ + [**L**Pt(PyH)] $\rightleftharpoons$ [**L**Pt($PyNMe_2$)] + PyH under irradiative conditions between 290-320 nm showing first order reaction kinetics.

d) $PyNMe_2$ + [**L**Pt(PyH)] $\rightleftharpoons$ [**L**Pt($PyNMe_2$)] + PyH under irradiative conditions between 320-350 nm.

Time(s)	[LPt(PyH)]	ln[LPt(PyH)]
1800	98	4.58
3600	96	4.56
4800	95	4.55
6300	93	4.53
7500	92	4.52

Table 7.6 Values for time (s), [**L**Pt(PyH)] and ln[**L**Pt(PyH)] for the exchange reaction $PyNMe_2$ + [**L**Pt(PyH)] $\rightleftharpoons$ [**L**Pt($PyNMe_2$)] + PyH under irradiative conditions between 320-350 nm.

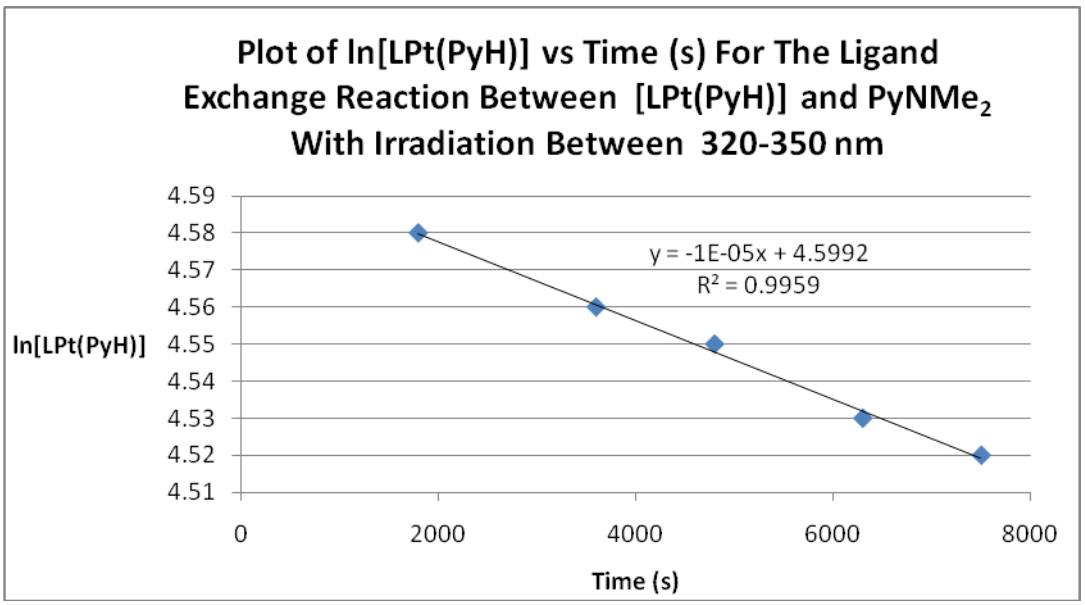

Graph 7.6 Plot of ln[**L**Pt(PyH)] vs Time (s) for the exchange reaction $PyNMe_2$ + [**L**Pt(PyH)] $\rightleftharpoons$ [**L**Pt($PyNMe_2$)] + PyH under irradiative conditions between 320-350 nm showing first order reaction kinetics.

e) $PyNMe_2$ + [**L**Pt(PyH)] $\rightleftharpoons$ [**L**Pt($PyNMe_2$)] + PyH under irradiative conditions between 350-380 nm.

Time(s)	[LPt(PyH)]	ln[LPt(PyH)]
1800	98	4.58
3600	96	4.56
4800	95	4.55
6300	93	4.53
7500	90	4.52

Table 7.7 Values for time (s), [**L**Pt(PyH)] and ln[**L**Pt(PyH)] for the exchange reaction $PyNMe_2$ + [**L**Pt(PyH)] $\rightleftharpoons$ [**L**Pt($PyNMe_2$)] + PyH under irradiative conditions between 350-380 nm.

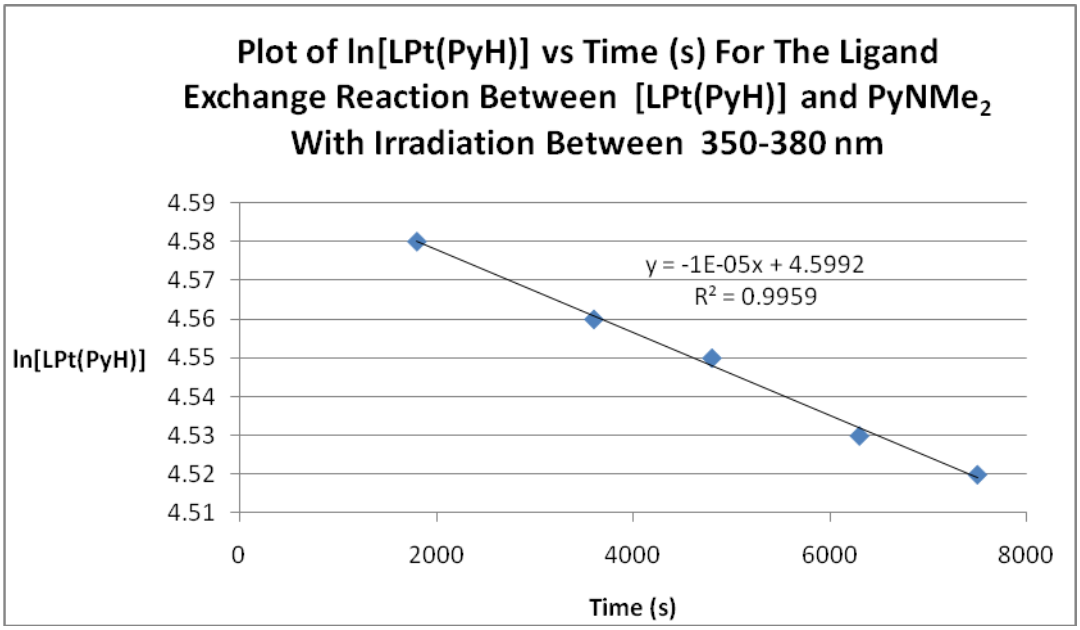

Graph 7.7 Plot of ln(A) vs Time (mins) for the exchange reaction $PyNMe_2$ + [**L**Pt(PyH)] $\rightleftharpoons$ [**L**Pt($PyNMe_2$)] + PyH under irradiative conditions between 350-380 nm showing first order reaction kinetics.

7.2.6 Ligand Exchange Reactions for Chapter Three

a) PyR'+ [**L**Pt(PyR)] $\rightleftharpoons$ [**L**Pt(PyR')] + PyR

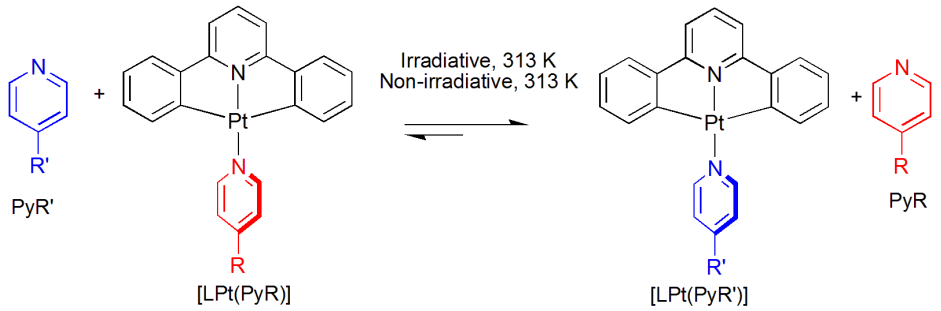

Scheme 7.4 Equilibrium between PyR' + [**L**Pt(PyR)] $\rightleftharpoons$ [**L**Pt(PyR')] + PyR under irradiative and non-irradiative conditions.

Experimental procedure under irradiative and non-irradiative conditions

(i) Irradiative conditions

To a 0.01 M solution of [**L**Pt(PyR)] (7.95 μmol) in 1:1 v/v [D_7]DMF:CD_2Cl_2 (0.35 mL:0.35 mL) was added PyR' (7.95 μmol). The mixture was agitated for one minute to give a clear solution and then placed in a quartz NMR tube. The sample was irradiated with broad band 275-375 nm light at 313 K until no further changes could be detected by ^{1}H NMR spectroscopy.

(ii) Non-irradiative conditions

To a 0.01 M solution of [**L**Pt(PyR)] (7.95 μmol) in 1:1 v/v [D_7]DMF:CD_2Cl_2 (0.35 mL:0.35 mL) was added PyR'(7.95 μmol). The mixture was agitated for one minute to give a clear solution and then placed in a darkened NMR tube and wrapped in aluminium foil. The sample was maintained at 313 K until no further changes could be detected by ^{1}H NMR spectroscopy.

b) [*cis*-H**L**Pt(PyR)(S)]OTs $\rightleftharpoons$ PyR.TsOH + [*cis*-H**L**Pt(PyR')(S)]OTs

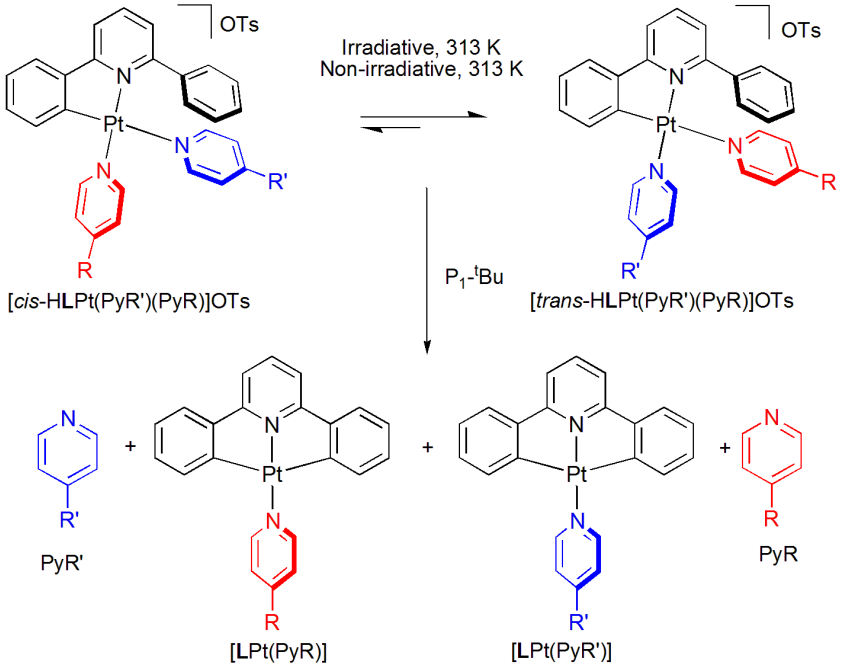

Scheme 7.5 [*cis*-H**L**Pt(PyR)(PyNMe$_2$)]OTs $\rightleftharpoons$ [*trans*-H**L**Pt(PyR')(PyR)]OTs followed by base mediated cyclometallation to aid analysis.

Experimental procedure under irradiative and non-irradiative conditions

(i) Irradiative conditions

To a 0.01 M solution of [H**L**Pt(PyR)OTs] (7.95 μmol) in 1:1 v/v [D_7]DMF:CD_2Cl_2 (0.35 mL:0.35 mL) was added PyR' (7.95 μmol). The mixture was agitated for one minute to give a clear solution and then placed in a quartz NMR tube. The sample was irradiated with broad band 275-375 nm light at 313 K until no further changes could be detected by ^{1}H NMR spectroscopy. P_1-^{t}Bu (10.1 μL, 39.75 μmol) was added directly to the NMR tube and then the sample was vigorously shaken for 30 seconds before a final ^{1}H NMR spectrum was recorded.

(ii) Non-irradiative conditions

To a 0.01 M solution of [H**L**Pt(PyR)OTs] (7.95 μmol) in 1:1 v/v [D_7]DMF:CD_2Cl_2 (0.35 mL:0.35 mL) was added PyR' (7.95 μmol). The mixture was agitated for one minute to give a clear solution and then placed in a darkened NMR tube and

wrapped in aluminium foil. The sample was maintained at 313 K until no further changes could be detected by ^{1}H NMR spectroscopy. P_1-^{t}Bu (10.1 μL, 39.75 μmol) was added directly to the NMR tube and then the sample was vigorously shaken for 30 seconds before a final ^{1}H NMR spectrum was recorded.

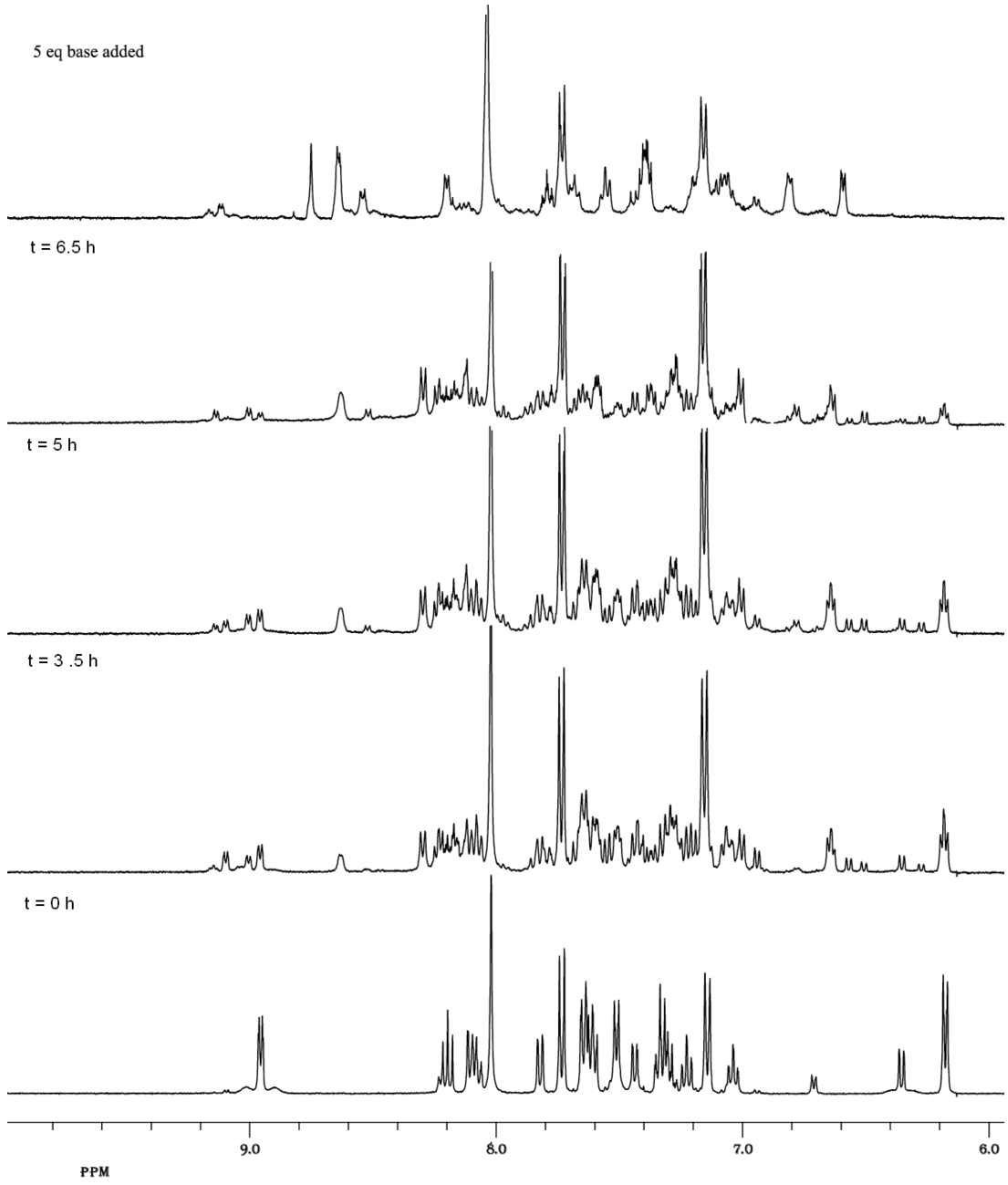

Figure 7.1 Representative ^{1}H NMR spectra to show the equilibration of $PyNMe_2$.TsOH + [*cis*-H**L**Pt(PyH)(S)]OTs $\rightleftharpoons$ PyH.TsOH + [*cis*-H**L**Pt($PyNMe_2$)(S)]OTs under irradiative conditions, followed by base mediated cyclometallation to aid analysis.

c) PyR'.TsOH + [*cis*-H**L**Pt(PyR)(S)]OTs ⇌ PyR.TsOH + [*cis*-H**L**Pt(PyR')(S)]OTs

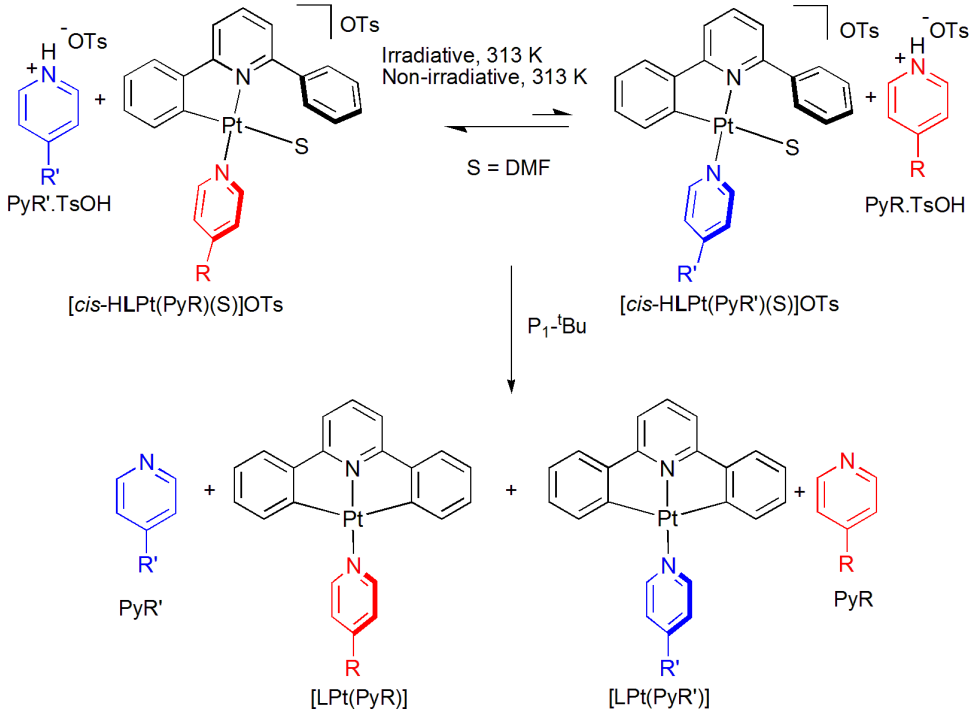

Scheme 7.6 PyR'.TsOH + [*cis*-H**L**Pt(PyR)(S)]OTs ⇌ PyR.TsOH + [*cis*-H**L**Pt(PyR')(S)]OTs followed by base mediated cyclometallation to aid analysis.

Experimental procedure under irradiative and non-irradiative conditions

(i) Irradiative conditions

To a 0.01 M solution of [H**L**Pt(PyR')OTs] (7.95 µmol) in 1:1 v/v [D_7]DMF:CD_2Cl_2 (0.35 mL:0.35 mL) was added PyR.TsOH (7.95 µmol). The mixture was agitated for one minute to give a clear solution and then placed in a quartz NMR tube. The sample was irradiated with broad band 275-375 nm light at 313 K until no further changes could be detected by ^{1}H NMR spectroscopy. P_1-^{t}Bu (10.1 µL, 39.75 mmol) was added directly to the NMR tube and then the sample was vigorously shaken for 30 seconds before a final ^{1}H NMR spectrum was recorded.

(i) Non-irradiative conditions

To a 0.01 M solution of [H**L**Pt(PyR')OTs] (7.95 µmol) in 1:1 v/v [D_7]DMF:CD_2Cl_2 (0.35 mL:0.35 mL) was added PyR.TsOH (7.95 µmol). The mixture was agitated for

one minute to give a clear solution and then placed in a darkened NMR tube and wrapped in aluminium foil. The sample was maintained at 313 K until no further changes could be detected by ^{1}H NMR spectroscopy. P_1-^{t}Bu (10.1 μL, 39.75 mmol) was added directly to the NMR tube and then the sample was vigorously shaken for 30 seconds before a final ^{1}H NMR spectrum was recorded.

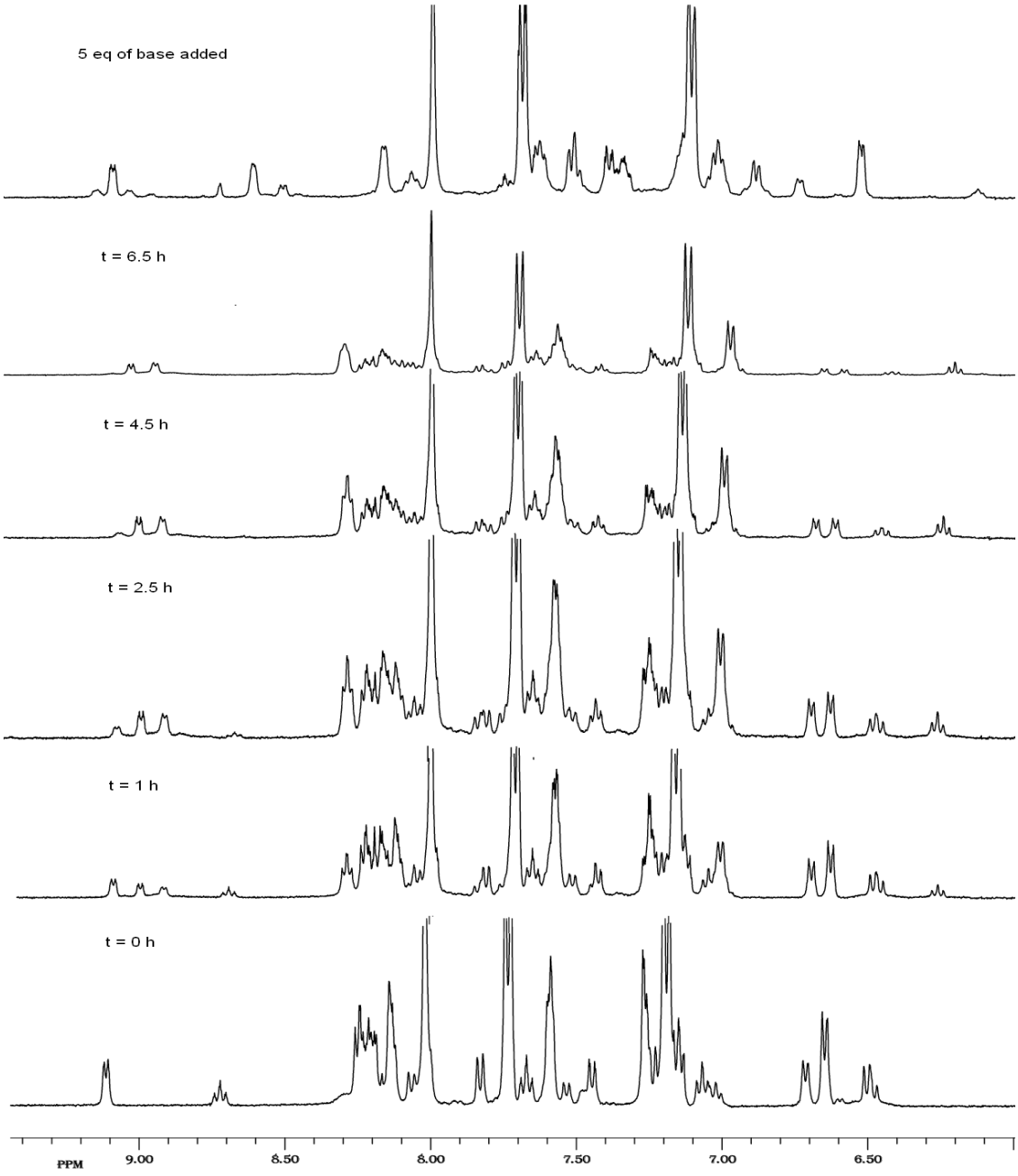

Figure 7.2 Representative ^{1}H NMR spectra to show the equilibration of $PyNMe_2$.TsOH + [*cis*-H**L**Pt($PyCF_3$)(S)]OTs $\rightleftharpoons$ $PyCF_3$.TsOH + [*cis*-H**L**Pt($PyNMe_2$)(S)]OTs under irradiative conditions, followed by base mediated cyclometallation to aid analysis.

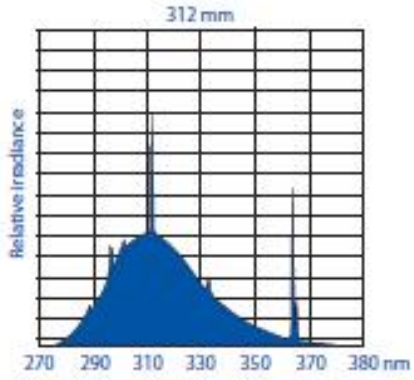

Figure 7.3 Emission spectrum for the broad band 275-375 nm light used for the irradiative studies.

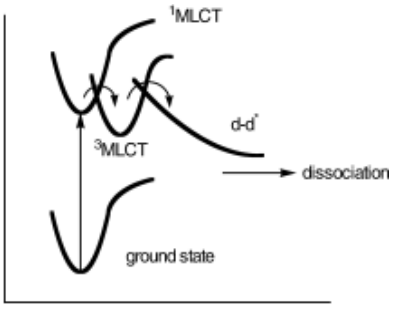

Figure 7.4 Energy diagram to show relationship between the metal centre states (d-d), in relation to the metal-ligand charge transfer states (MLCT) both singlet and triplet and the ground state.

7.2.7 TD-DFT Calculations for [LPt(PyNMe$_2$)]

a) Singlet Excited State Calculations

Wavelength (nm)	Electronic Transition	Osc. Strength (*f*)	Major Contributions
458.20	$S_o \rightarrow S_1$	0.0001	HOMO->LUMO (100%)
341.38	$S_o \rightarrow S_6$	0.1806	H-5->LUMO (12%), H-3->LUMO (67%), HOMO->L+2 (21%)
327.62	$S_o \rightarrow S_7$	0.1178	H-5->L+1 (11%), H-4->LUMO (59%), H-3->L+1 (26%)
306.55	$S_o \rightarrow S_{12}$	0.1102	H-4->LUMO(16%), H-5->LUMO (-10%), H-3->L+2 (-13%), H-1->L+2 (52%)
274.59	$S_o \rightarrow S_{20}$	0.2785	H-6->L+1(36%), H-1->L+7 (-10%), H-1->L+4 (35%)
270.95	$S_o \rightarrow S_{23}$	0.1384	H-8->LUMO(21%), H-7->LUMO (34%), H-4->L+1 (14%), H-2->L+3 (-31%)
268.89	$S_o \rightarrow S_{24}$	0.1900	H-7->L+1(15%), H-6->L+1 (39%), H-2->L+3 (-37%)
254.37	$S_o \rightarrow S_{27}$	0.0546	H-7->LUMO (19%), H-5->L+1 (-28%), H-2->L+2 (36%), H-1->L+7 (8%)
249.38	$S_o \rightarrow S_{30}$	0.0122	H-5->L+3 (13%), H-1->L+5 (55%), HOMO->L+7 (10%)
248.54	$S_o \rightarrow S_{32}$	0.1346	H-9->LUMO (-21%), H-7->L+1 (-17%), H-5->L+3 (30%), H-1->L+7 (-9%)
247.16	$S_o \rightarrow S_{33}$	0.0024	H-8->L+2 (-28%), H-1->L+6 (60%), H-1->L+7 (-12%)
247.06	$S_o \rightarrow S_{34}$	0.0073	H-9->L+7 (12%), H-1->L+5 (15%), HOMO->L+7 (73%)

Table 7.7 Selected calculated singlet-singlet transitions (those with oscillator strength ≥ 0.1 omitted for clarity apart from the HOMO → LUMO transition and selected transitions which include excitation into L+7 states wherein any additional excitations for these transitions which contribute <10% have been omitted for clarity) in the UV/Vis spectra from TD-DFT calculations of [**L**Pt(PyNMe$_2$)] with PCM to model the solvent (CH_2Cl_2) effect.

b) Triplet Excited State Calculations

Wavelength (nm)	Electronic Transition	Osc. Strength (*f*)	Major Contributions
1524.78	$T_0 \rightarrow T_1$	0.0238	HOMO->LUMO (87%), H-3->L-2 (-13%)
747.10	$T_0 \rightarrow T_6$	0.0423	HOMO->L+3 (67%), HOMO->L+6 (9%), H-5->L-2 (8%), H-4->L-2 (15%)
557.92	$T_0 \rightarrow T_{10}$	0.0357	HOMO->L+5 (73%), HOMO->L+6 (27%)
493.08	$T_0 \rightarrow T_{13}$	0.0251	HOMO->L+5 (-24%), HOMO->L+6 (67%)

Table 7.8 Selected calculated triplet-triplet transitions (those with oscillator strength ≥ 0.1 omitted for clarity apart from those transitions including excitation into L+8 states wherein any additional excitations for these transitions which contribute ≤10% have been omitted for clarity) in the UV/Vis spectra from TD-DFT calculations on [**L**Pt($PyNMe_2$)] with PCM to model the solvent (CH_2Cl_2) effect.

7.2.8 TD-DFT Calculations for [LPt(PyH)]

a) Singlet Excited State Calculations

Wavelength (nm)	Electronic Transition	Osc. Strength (*f*)	Major Contributions
456.89	$S_0 \rightarrow S_1$	0.0002	HOMO->LUMO (100%)
363.05	$S_0 \rightarrow S_5$	0.1297	H-6->LUMO (11%), H-4->LUMO (14%), H-1->L+1 (16%), HOMO->L+2 (58%)
333.13	$S_0 \rightarrow S_9$	0.1068	H-4->LUMO (82%), HOMO->L+2 (18%)
328.55	$S_0 \rightarrow S_{10}$	0.1527	H-4->L+2 (23%), H-3->LUMO (66%)
294.49	$S_0 \rightarrow S_{17}$	0.1127	H-4->L+2 (-40%), H-3->L+1 (45%), HOMO->L+4 (15%)
274.42	$S_0 \rightarrow S_{22}$	0.1968	H-8->LUMO (16%), H-5->L+2 (48%), H-1->L+7 (10%), HOMO-L+4 (-23%)
272.98	$S_0 \rightarrow S_{23}$	0.2051	H-3->LUMO (17%), H-6->LUMO (46%), H-3->L+2 (24%)
268.65	$S_0 \rightarrow S_{24}$	0.2625	H-6->L+2 (17%), H-5->L+2 (26%), HOMO->L+4 (46%)
253.73	$S_0 \rightarrow S_{29}$	0.1252	H-8->LUMO (28%), H-6->L+2 (49%)
252.89	$S_0 \rightarrow S_{30}$	0.0709	H-7->L+1 (59%), HOMO->L+7 (17%)
248.83	$S_0 \rightarrow S_{32}$	0.1803	H-8->LUMO (22%), HOMO->L+5 (56%)
248.48	$S_0 \rightarrow S_{33}$	0.0069	H-8->L+7 (12%), H-7->L+1 (-19%), HOMO->L+7 (69%)
247.69	$S_0 \rightarrow S_{34}$	0.1003	H-8->LUMO (28%), H-7->L+2 (-22%), H-6->L+2 (21%), HOMO->L+5 (19%)

Table 7.9 Selected calculated singlet-singlet transitions (those with oscillator strength ≥ 0.1 omitted for clarity apart from the HOMO → LUMO transition and those transitions including excitation into L+7 states wherein any additional excitations for these transitions which contribute ≤10% have been omitted for clarity) in the UV/Vis spectra from TD-DFT calculations on [**L**Pt(PyH)] with PCM to model the solvent (CH_2Cl_2) effect.

b) Triplet Excited State Calculations

Wavelength (nm)	Electronic Transition	Osc. Strength (*f*)	Major Contributions
1671.26	$T_0 \rightarrow T_1$	0.0135	HOMO->LUMO (100%)
746.45	$T_0 \rightarrow T_7$	0.0327	HOMO->L+3 (68%), HOMO->L+6 (10%), H-5->L-2 (8%)
560.98	$T_0 \rightarrow T_{10}$	0.0226	HOMO->L+4 (19%), HOMO->L+5 (54%), HOMO->L+6 (26%)
535.92	$T_0 \rightarrow T_{11}$	0.0713	HOMO->L+4 (35%), HOMO->L+5 (13%), H-7->L-2 (-14%), H-6->L-2 (22%), H-3->L-2 (-23%)
502.20	$T_0 \rightarrow T_{12}$	0.0403	HOMO-L+4 (18%), H-7->L-2 (50%), H-4->L-2 (-23%)
500.99	$T_0 \rightarrow T_{13}$	0.0409	HOMO->L+5 (-25%), HOMO->L+6 (64%)

Table 7.10 Selected calculated triplet-triplet transitions (those with oscillator strength ≥ 0.04 omitted for clarity apart from those transitions including excitation into L+6 states wherein any additional excitations for these transitions which contribute ≤10% have been omitted for clarity) in the UV/Vis spectra from TD-DFT calculations on [**L**Pt(PyH)] with PCM to model the solvent (CH_2Cl_2) effect.

7.5.8 TD-DFT Calculations for [LPt($PyCF_3$)]

a) Singlet Excited State Calculations

Wavelength (nm)	Electronic Transition	Osc. Strength (*f*)	Major Contributions
526.29	$S_0 \rightarrow S_1$	0.0001	HOMO->LUMO (100%)
444.87	$S_0 \rightarrow S_2$	0.1496	H-1-> LUMO(100%)
324.34	$S_0 \rightarrow S_{14}$	0.1553	H-4->L+2 (15%), H-3->L+1 (50%), H-2->L+1 (18%)
292.11	$S_0 \rightarrow S_{20}$	0.1387	H-4->L+2 (69%), H-3->L+1 (-15%), HOMO->L+7 (-16%)
268.42	$S_0 \rightarrow S_{28}$	0.2550	H-7->L+1 (20%), H-6->L+1 (51%), H-3->L+2 (12%), H-3-L+3 (14%)
265.97	$S_0 \rightarrow S_{29}$	0.3193	H-6->L+2 (13%), H-5->L+2 (24%), H-5->L+3 (-13%), H-3->L+2 (10%), H-1->L+4 (39%)
261.29	$S_0 \rightarrow S_{31}$	0.0009	H-7->L+1 (-12%), H-1->L+4 (74%), H-1->L+7 (14%)
252.91	$S_0 \rightarrow S_{32}$	0.1718	H-8->L+1 (17%), H-8->L+2 (59%), H-5->L+2 (-13%), HOMO->L+4 (-10%)
250.74	$S_0 \rightarrow S_{33}$	0.0008	H-8->L+7 (14%), H-1->L+4 (-15%), HOMO->L+7 (72%)
244.05	$S_0 \rightarrow S_{37}$	0.1580	H-8->L+1 (40%), H-6->L+2 (-11%), H-6->L+3 (-11%), H-1->L+7 (13%), HOMO->L+4 (10%)

Table 7.11 Selected calculated singlet-singlet transitions (those with oscillator strength ≥ 0.1 omitted for clarity apart from the HOMO → LUMO transition and those transitions including excitation into L+7 states wherein any additional excitations for these transitions which contribute ≤10% have been omitted for clarity) in the UV/Vis spectra from TD-DFT calculations on [**L**Pt($PyCF_3$)] with PCM to model the solvent (CH_2Cl_2) effect.

b) Triplet Excited State Calculations

Wavelength (nm)	Osc. Strength	Major Contributions
2488.23	0.0687	HOMO->LUMO (88%), H-2->L-2 (-12%)
696.01	0.0005	HOMO->L+2 (55%), H-4->H-1 (-16%)
670.91	0.0015	HOMO->L+2 (16%), H-5->H-1 (-19%), H-4->H-1 (30%), H-4->H-1 (17%)
536.39	0.0004	HOMO->L+2 (7%), HOMO->L+4 (32%), HOMO->L+5 (30%), HOMO->L+6 (-20%)
470.98	0.0091	HOMO->L+2 (-6%), HOMO->L+4 (17%), HOMO->L+5 (18%), HOMO->L+6 (52%)

Table 7.12 Selected calculated singlet-triplet transitions (those with oscillator strength ≥ 0.1 omitted for clarity apart from the HOMO → LUMO transition and those transitions including excitation into L+6 states wherein any additional excitations for these transitions which contribute ≤10% have been omitted for clarity) in the UV/Vis spectra from TD-DFT calculations on [**L**Pt($PyCF_3$)] with PCM to model the solvent (CH_2Cl_2) effect.

Crystal data and structure refinement for [LPt(PyNMe$_2$)] and [cis-HLPt(PyNMe$_2$)OTs].

Structural data were collected at 93 K using a Rigaku Mercury diffractometer (MM007 high-flux RA/MoKa radiation, confocal optic). All data collection employed narrow frames (0.3-1.0) to obtain at least a full hemisphere of data. Intensities were corrected for Lorentz polarisation and absorption effects (multiple equivalent reflections). The structures were solved by direct methods, non-hydrogen atoms were refined anisotropically with CH protons being refined in riding geometries (SHELXTL) against F^2.

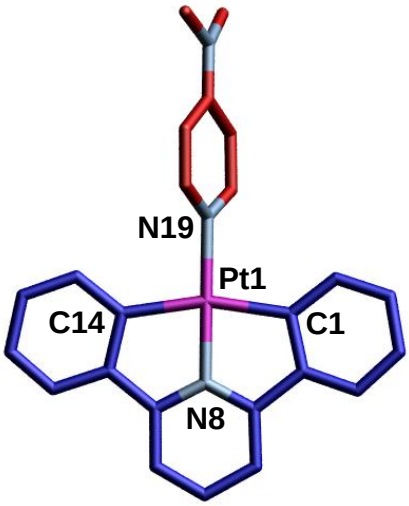

Figure 7.5 X-ray crystal structure of [**L**Pt(DMAP)]. The carbon atoms of DMAP are shown in red, the carbon atoms of **L** in blue, platinum in magenta and nitrogen in pale blue. A chloroform solvent molecule has been removed for clarity. Selected bond lengths [Å] and angles [°]: C1-Pt1 2.07, N8-Pt1 1.98, C14-Pt1 2.06, N19-Pt1 2.04, C1-Pt1-N8 82.1, C14-Pt1-N8 81.2, C14-Pt1-N19 98.9, N19-Pt1-C1 97.8, C1-Pt1-C14 163.2.

Table 7.13 Crystal data and structure refinement for [**L**Pt(DMAP)]·$CHCl_3$.

Identification code	LPtDMAP	
Empirical formula	C25 H22 Cl3 N3 Pt	
Formula weight	665.90	
Temperature	93(2) K	
Wavelength	0.71073 Å	
Crystal system	Orthorhombic	
Space group	Pbca	
Unit cell dimensions	a = 9.0828(18) Å	α= 90°.
	b = 20.691(4) Å	β= 90°.
	c = 25.599(5) Å	γ = 90°.
Volume	4810.8(17) $Å^3$	
Z	8	
Density (calculated)	1.839 Mg/m^3	
Absorption coefficient	6.185 mm^{-1}	
F(000)	2576	
Crystal size	0.1500 x 0.0300 x 0.0300 mm^3	
Theta range for data collection	1.97 to 25.33°.	
Index ranges	-10<=h<=10, -24<=k<=23, -30<=l<=21	
Reflections collected	28543	
Independent reflections	4393 [R(int) = 0.1190]	
Completeness to theta = 25.00°	100.0 %	
Absorption correction	Multiscan	
Max. and min. transmission	1.0000 and 0.4512	
Refinement method	Full-matrix least-squares on F^2	
Data / restraints / parameters	4393 / 0 / 292	
Goodness-of-fit on F^2	1.088	
Final R indices [I>2sigma(I)]	R1 = 0.0648, wR2 = 0.1437	
R indices (all data)	R1 = 0.1012, wR2 = 0.1620	
Largest diff. peak and hole	3.301 and -2.211 $e.Å^{-3}$	

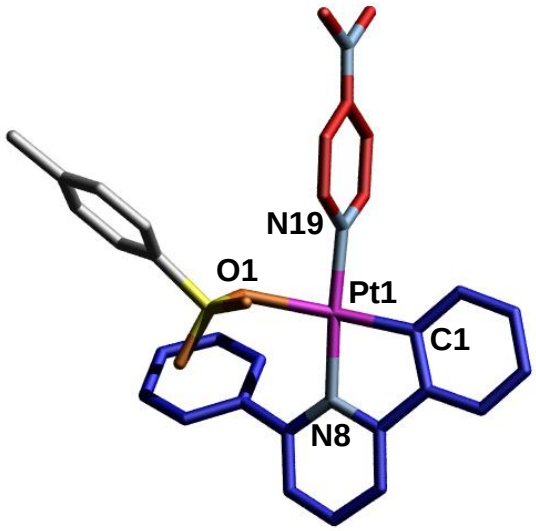

Figure 7.6 X-ray crystal structure of [H**L**Pt(DMAP)OTs]. The carbon atoms of DMAP are shown in red, the carbon atoms of **L** in blue, the carbon atoms of the tosylate anion in grey, platinum in magenta, nitrogen in pale blue, oxygen in orange and sulfur in yellow. Selected bond lengths [Å] and angles [°]: C1-Pt1 1.95, N8-Pt1 2.04, O1-Pt1 2.17, N19-Pt1 2.00, C1-Pt1-N8 81.7, O1-Pt1-N8 99.2, O1-Pt1-N19 84.3, N19-Pt1-C1 95.6.

Table 7.14 Crystal data and structure refinement for [H**L**Pt(DMAP)OTs].

Identification code	HLPtDMAPOTs	
Empirical formula	C31 H29 N3 O3 Pt S	
Formula weight	718.72	
Temperature	93(2) K	
Wavelength	0.71073 Å	
Crystal system	Monoclinic	
Space group	C2/c	
Unit cell dimensions	a = 28.995(6) Å	α= 90°.
	b = 11.188(2) Å	β= 129.933(5)°.
	c = 22.014(5) Å	γ = 90°.
Volume	5475.6(19) $Å^3$	
Z	8	
Density (calculated)	1.744 Mg/m^3	
Absorption coefficient	5.240 mm^{-1}	
F(000)	2832	
Crystal size	0.100 x 0.100 x 0.050 mm^3	
Theta range for data collection	3.58 to 25.35°.	
Index ranges	-34<=h<=33, -13<=k<=10, -17<=l<=26	
Reflections collected	14351	
Independent reflections	4956 [R(int) = 0.1898]	
Completeness to theta = 25.00°	99.3 %	
Absorption correction	Multiscan	
Max. and min. transmission	1.0000 and 0.6295	
Refinement method	Full-matrix least-squares on F^2	
Data / restraints / parameters	4956 / 0 / 356	
Goodness-of-fit on F^2	1.135	
Final R indices [I>2sigma(I)]	R1 = 0.0707, wR2 = 0.1651	
R indices (all data)	R1 = 0.1100, wR2 = 0.1906	
Largest diff. peak and hole	4.161 and -3.710 $e.Å^{-3}$	

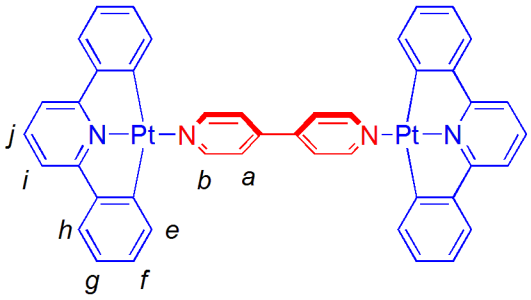

[(**L**Pt)$_2$(4,4'-bipy)]

To a solution of [**L**Pt(DMSO)] (0.40 g, 0.80 mmol) in CH_2Cl_2 (16 mL) was added 4,4'-bipyridine (0.060 g, 0.40 mmol). The reaction was stirred at room temperature for 18 h during which time a bright orange solid precipitated from solution. This was subsequently collected by filtration and then washed with CH_2Cl_2 (15 mL) to give the product as an orange solid (0.31 g, 77%). m.p. 358 ºC (dec.); ^{1}H NMR (400 MHz, $(CD_3)_2SO$): 8.73 (4H, d, J = 6.0 Hz, H_b), 7.84 (6H, m, H_{a+j}), 7.78 (4H, dd, ^3J = 7.2 Hz, ^4J = 0.8 Hz, H_e), 7.66 – 7.63 (8H, m, H_{h+i}), 7.21 (4H, m, H_f), 7.10 (4H, m, H_g); ^{13}C NMR (100 MHz, $(CD_3)_2SO$): 166.3, 166.0, 150.5, 149.4, 144.3, 142.8, 136.3, 130.3, 124.6, 124.5, 121.2, 115.5; LREI-MS (CH_2Cl_2): m/z = 1005 $[MH]^+$.

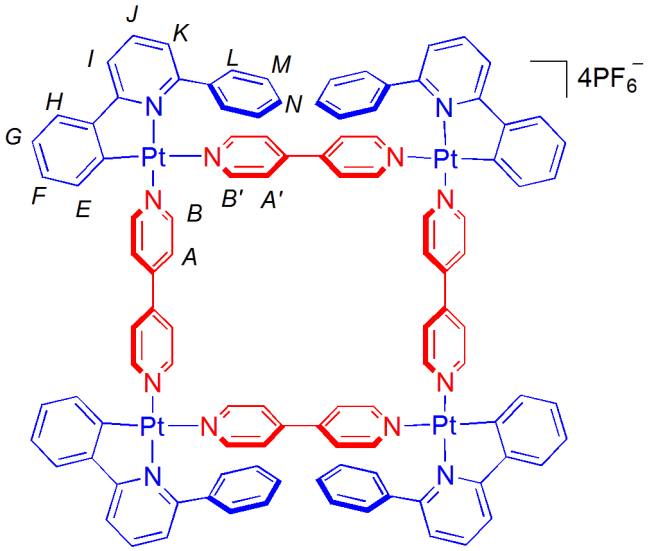

$[(H\mathbf{L}Pt)_4(4,4'\text{-bipy})_4](PF_6)_4$

Method (a) sequential addition of CSA and 4,4'-bipy.

To a suspension of $[(\mathbf{L}Pt)_2(4,4'\text{-bipy})]$ (0.10 g, 0.1 mmol) in CH_2Cl_2 (5 mL) was added (+)-CSA (0.046 g, 0.2 mmol) in CH_2Cl_2 (5mL). Upon complete dissolution (15 min) 4,4'-bipy (0.016 g, 0.1 mmol) in CH_2Cl_2 (5 mL) was added and the solution stirred for a further 45 min.

Method (b) direct addition of 4,4'-bipy·2CSA.

To a suspension of $[(\mathbf{L}Pt)_2(4,4'\text{-bipy})]$ (0.10 g, 0.10 mmol) in CH_2Cl_2 (15 mL) was added 4,4'-bipy.2CSA (0.062g, 0.10 mmol). The reaction mixture was stirred at room temperature for 1 h to give a pale yellow solution.

Common isolation procedure from routes (a) and (b)

The volume of solvent was reduced to *ca.* 5 mL under reduced pressure, followed by the addition of NH_4PF_6 (0.049 g, 0.30 mmol) in acetone (5 mL). The resulting yellow solid was filtered off and subjected to recrystallization from CH_3NO_2 and Et_2O to give the desired product as a pale yellow solid (0.090 g, 56%). Single crystals of $[(H\mathbf{L}Pt)_4(4,4'\text{-bipy})_4](PF_6)_4$ suitable for X-ray crystallography were grown from CH_3NO_2 and Et_2O. m.p. 310 ºC (dec.); ^{1}H NMR (400 MHz, CD_3NO_2): 9.07 (8H, d, J = 7.2 Hz, H_B), 8.26 (8H, d, J = 6.4 Hz, $H_{B'}$), 8.23 (4H, m, H_J), 8.10 (4H, dd, ^3J = 8.0 Hz, ^4J = 1.2 Hz, H_I), 7.87 (8H, d, J = 7.2 Hz, H_A), 7.82 (4H, d, J = 6.8 Hz, H_H), 7.69 (8H, d, J = 6.8 Hz, H_L), 7.48 (8H, m, H_{K+N}), 7.38 (8H, m, H_M), 7.27 (12H,

m, $H_{G+A'}$), 7.06 (4H, m, H_F), 6.34 (4H, d, J = 7.6 Hz, H_E); ESI-MS *m/z*: 1307.4 $[(H\mathbf{L}Pt)_4(4,4'\text{-bipy})_4(PF_6)_2]^{2+}$ + $[(H\mathbf{L}Pt)_2(4,4'\text{-bipy})_2(PF_6)]^{+}$, 1151.2 $[(H\mathbf{L}Pt)_2(4,4'\text{-bipy})(PF_6)]^{+}$, 944.7 $[(H\mathbf{L}Pt)_3(4,4'\text{-bipy})_3(PF_6)]^{2+}$, 823.5 $[(H\mathbf{L}Pt)_4(4,4'\text{-bipy})_4(PF_6)]^{3+}$, 737.6 $[(H\mathbf{L}Pt)(4,4'\text{-bipy})_2]^{+}$, 659.2 $[(H\mathbf{L}Pt)_2(4,4'\text{-bipy})_3]^{2+}$, 581.1 $[(H\mathbf{L}Pt)(4,4'\text{-bipy})]^{+}$ + $[(H\mathbf{L}Pt)_2(4,4'\text{-bipy})_2]^{2+}$, 503.1 $([H\mathbf{L}Pt]_2(4,4'\text{-bipy})]^{2+}$.

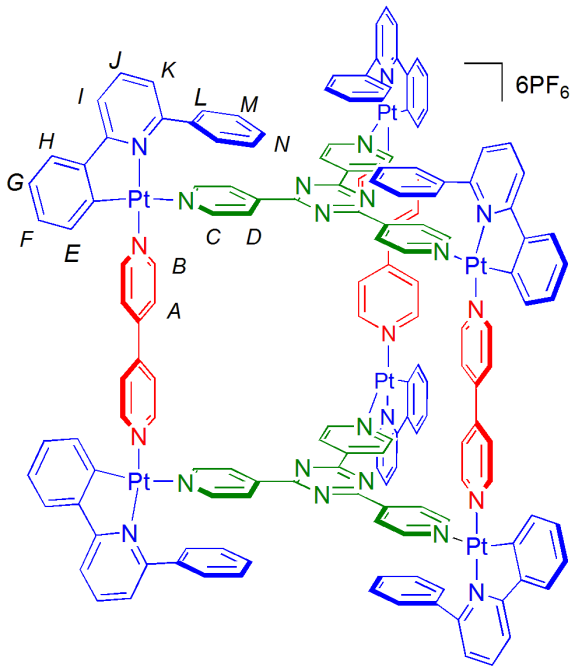

$[(H\mathbf{L}Pt)_6(4,4'\text{-bipy})_3(tpt)_2](PF_6)_6$

Method (a) sequential addition of CSA and tpt.

To a suspension of $[(\mathbf{L}Pt)_2(4,4'\text{-bipy})]$ (0.10 g, 0.1 mmol) in CH_2Cl_2 (10 mL) was added (+)-CSA (0.046 g, 0.2 mmol) in CH_2Cl_2 (5mL). Upon complete dissolution (15 min), tpt (0.021 g, 0.066 mmol) was added and the mixture stirred for a further 45 min to give a pale yellow solution.

Method (b) direct addition of tpt·3CSA.

To a suspension of $[(\mathbf{L}Pt)_2(4,4'\text{-bipy})]$ (0.10 g, 0.1 mmol) in CH_2Cl_2 (15 mL) was added tpt·3CSA (0.067g, 0.066 mmol). The reaction mixture was stirred at room temperature for 1 h to give a pale yellow solution.

Common isolation procedure from routes (a) and (b)

The volume of solvent was reduced to ca. 5 mL under reduced pressure, followed by the addition of NH_4PF_6 (0.073 g, 0.45 mmol) in acetone (5 mL). The product was then evaporated to dryness, acetone added (10 mL) and the yellow solid filtered off and washed with diethyl ether (0.146 g, 97%). m.p. 222 ºC (dec.); ^{1}H NMR (400 MHz, CD_2Cl_2): 8.93 (12H, d, J = 6.8 Hz, H_B), 8.25 (12H, d, J = 6.4 Hz, H_C), 8.15 (12H, d, J = 6.4 Hz, H_D), 8.08 (6H, t, ^3J = 8.0 Hz, H_J), 7.93 (6H, m, H_I), 7.70 (18H, m, H_{H+A}), 7.54 (12H, d, J = 7.6 Hz, H_L), 7.42 (6H, m, H_N), 7.35 (18H, m, H_{K+M}), 7.26 (6H, m, H_G), 7.06 (6H, m, H_F), 6.19 (6H, d, J = 7.2 Hz, H_E); ESI-MS *m/z:* 2112.4 $[(H\mathbf{L}Pt)_6(4,4'\text{-bipy})_3(tpt)_2(PF_6)_4]^{2+}$, 1463.3 $[(H\mathbf{L}Pt)_2(4,4'\text{-bipy})(tpt)(PF_6)]^{+}$, 1359.9 $[(H\mathbf{L}Pt)_6(4,4'\text{-bipy})_3(tpt)_2(PF_6)_3]^{3+}$, 1307.7 $[(H\mathbf{L}Pt)_4(4,4'\text{-bipy})_2(tpt)(PF_6)_2]^{2+}$, 1151.1 $[(H\mathbf{L}Pt)_2(4,4'\text{-bipy})(PF_6)]^{+}$, 737.2 $[(H\mathbf{L}Pt)(tpt)]^{+}$, 581.1 $[(H\mathbf{L}Pt)(\ 4,4'\text{-bipy})]^{+}$, 503.1 $[(H\mathbf{L}Pt)_2(4,4'\text{-bipy})]^{2+}$.

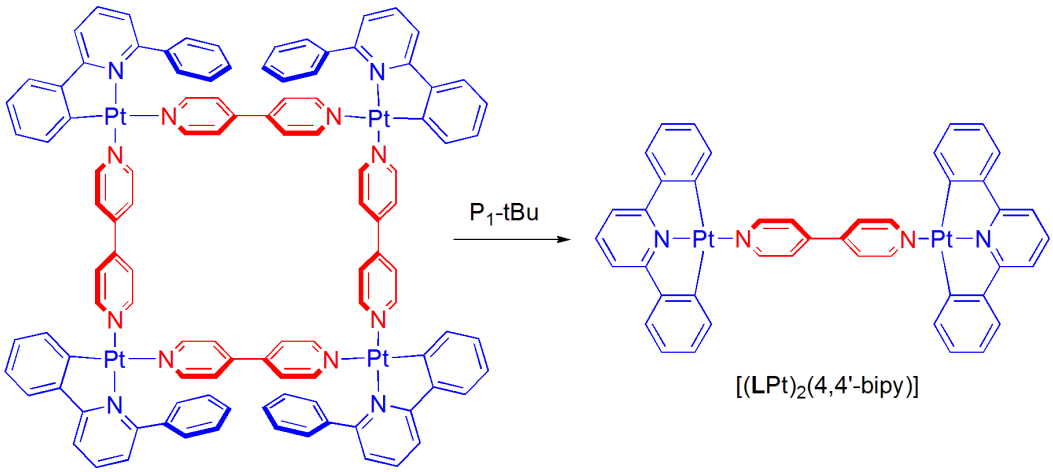

To a solution of $[(H\mathbf{L}Pt)_4(4,4'\text{-bipy})_4](PF_6)_4$(18.5 mg, 3.3 mmol) in CH_2Cl_2 (3 mL) was added P_1-^{t}Bu (18.8 µL, 74 mmol) and the reaction stirred overnight at RT. The bright orange precipitate, $[(\mathbf{L}Pt)_2(4,4'\text{-bipy})]$, was filtered off and dried under vacuum (6.8 mg, 59%).

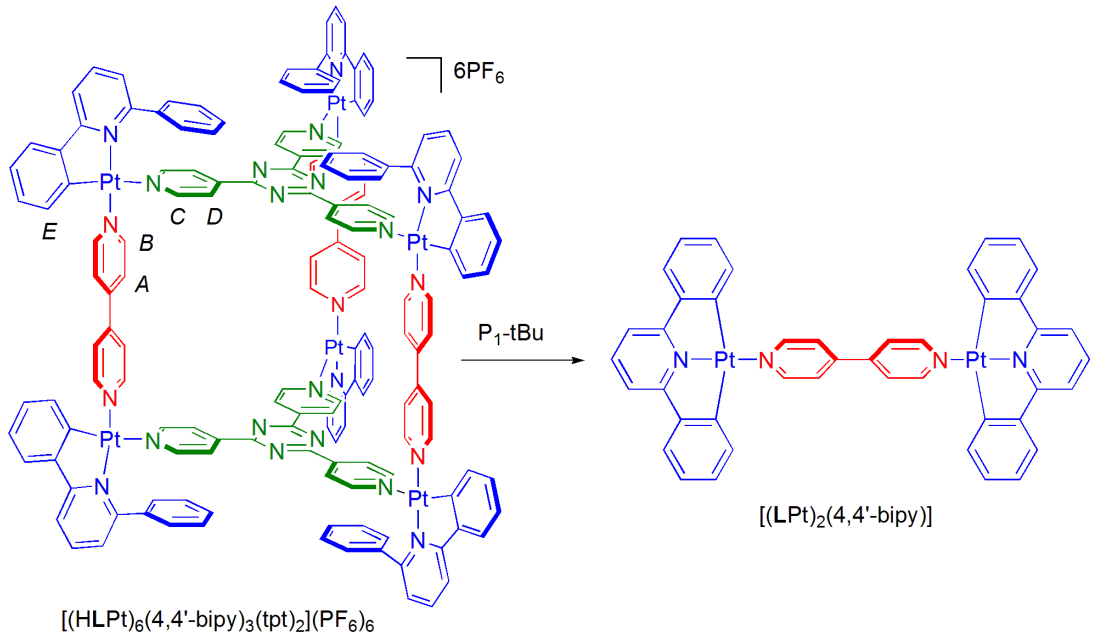

To a solution of $[(H\mathbf{L}Pt)_6(4,4'\text{-bipy})_3(tpt)_2](PF_6)_6$ (2.59 mg, 0.057 mmol) in CD_2Cl_2 (1 mL) was added P_1-^{t}Bu (1.32 µL, 0.52 mmol). The reaction was monitored *via* ^{1}H NMR spectroscopy, which showed quantitative conversion to $[(\mathbf{L}Pt)_2(4,4'\text{-bipy})]$ and tpt after 3 h at ambient temperature.

Crystal data and structure refinement for $[(HLPt)_4(4,4'\text{-bipy})_4](PF_6)_4$.

Structural data were collected at 93 K using a Rigaku Mercury diffractometer (MM007 high-flux RA/MoKa radiation, confocal optic). All data collection employed narrow frames (0.3-1.0) to obtain at least a full hemisphere of data. Intensities were corrected for Lorentz polarisation and absorption effects (multiple equivalent reflections). The structures were solved by direct methods, non-hydrogen atoms were refined anisotropically with CH protons being refined in riding geometries (SHELXTL) against F^2.

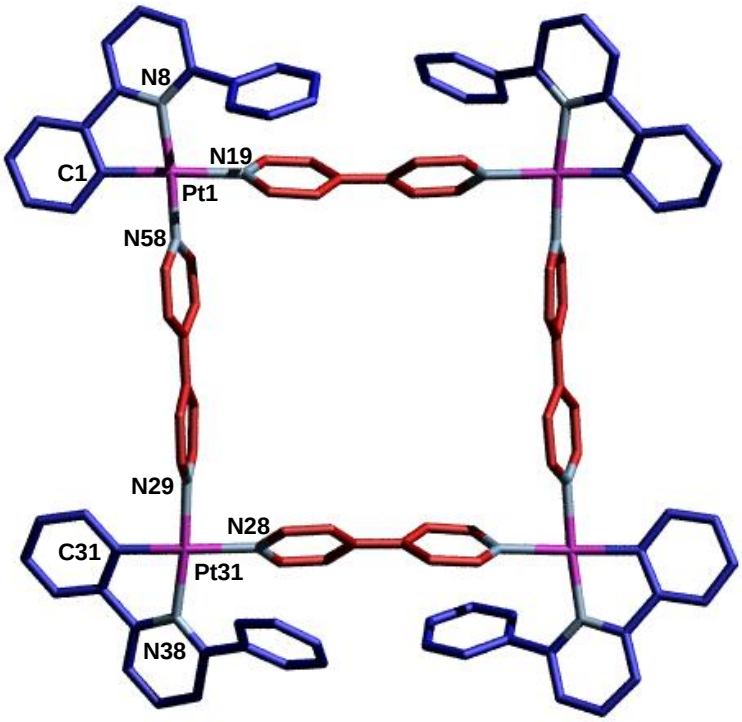

Figure 7.7 X-ray crystal structure of molecular square $[(\mathbf{L}Pt)_4(4,4'\text{-bipy})_4](PF_6)_4$. The carbon atoms of 4,4'-bipy are shown in red, the carbon atoms of H**L** in blue, platinum in magenta and nitrogen in pale blue. The PF_6 counter anions and five nitromethane solvent molecules have been removed for clarity. Selected bond lengths [Å] and angles [°]: C1-Pt1 2.02, N8-Pt1 2.06, N19-Pt1 2.15, N58-Pt1 2.04, C1-Pt1-N8 82.2, N8-Pt1-N19 99.8, N19-Pt1-N58 84.6, N58-Pt1-C1 93.3, C31-Pt31 2.00, N29-Pt31 2.04, N28-Pt31 2.16, N38-Pt31 2.05, C31-Pt31-N29 93.1, N29-Pt31-N28 87.2, N28-Pt31-N38 98.1, N38-Pt31-C31 81.3.

Table 7.14 Crystal data and structure refinement for $[(HLPt)_4(4,4'\text{-bipy})_4](PF_6)_4]\cdot 5CH_3NO_2$.

Identification code	square	
Empirical formula	C113 H95 F24 N17 O10 P4 Pt4	
Formula weight	3211.30	
Temperature	93(2) K	
Wavelength	0.71073 Å	
Crystal system	Triclinic	
Space group	P-1	
Unit cell dimensions	a = 13.5137(17) Å	α= 97.384(7)°.
	b = 13.8563(18) Å	β= 100.261(7)°.
	c = 21.010(2) Å	γ = 116.076(7)°.
Volume	3380.6(7) $Å^3$	
Z	1	
Density (calculated)	1.577 Mg/m^3	
Absorption coefficient	4.262 mm^{-1}	
F(000)	1560	
Crystal size	0.1800 x 0.1800 x 0.1200 mm^3	
Theta range for data collection	2.63 to 25.30°.	
Index ranges	-16<=h<=15, -16<=k<=16, -21<=l<=25	
Reflections collected	33698	
Independent reflections	12098 [R(int) = 0.0521]	
Completeness to theta = 25.00°	99.2 %	
Absorption correction	Multiscan	
Max. and min. transmission	1.0000 and 0.8007	
Refinement method	Full-matrix least-squares on F^2	
Data / restraints / parameters	12098 / 18 / 905	
Goodness-of-fit on F^2	1.046	
Final R indices [I>2sigma(I)]	R1 = 0.0673, wR2 = 0.1857	
R indices (all data)	R1 = 0.0729, wR2 = 0.1944	
Extinction coefficient	0.0033(2)	
Largest diff. peak and hole	3.011 and -1.804 $e.Å^{-3}$	

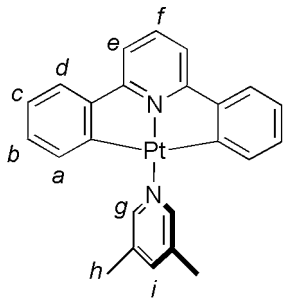

[**L**Pt(3,5-Lut)]

To a yellow solution of [**L**Pt(DMSO)] (0.093 g, 0.19 mmol) in CH_2Cl_2 (10 mL) was added 3,5-lutidine (0.040 g, 0.37 mmol), which resulted in a darkening of the solution to orange. The reaction was stirred for 18 h at room temperature and the excess solvent was removed under reduced pressure. Purification of the crude product using column chromatography (1:1:0.01; CH_2Cl_2:hexane:NEt_3). Crystals suitable for X-ray crystallography were grown *via* slow diffusion of di-isopropyl ether into a saturated solution of the desired complex in chloroform to give bright orange crystals. (0.052 g, 53 %). m.p. 205-210 ºC (dec.); ^{1}H NMR (500 MHz,[D_7]-DMF): 8.77 (2H, s, *J* (^{195}Pt) = 44.8 Hz, H_g), 7.78 – 7.73 (2H, m, H_{i+f}), 7.62 –7.55 (4H, m, H_{d+e}), 7.15 (2H, m, H_b), 7.03 (2H, m, H_c), 6.90 – 6.82 (2H, m, H_a), 2.45 (6H, s, H_h); ^{13}C NMR (125 MHz, [D_7]-DMF): 173.7, 168.7, 151.3, 150.0, 140.8, 139.0, 136.8, 133.8, 130.8, 124.6, 123.8, 115.2, 17.8; LRESI-MS: *m/z* = 532 $[MH]^+$; HRESI-MS: *m/z* = 531.12649 (calc. for $C_{24}H_{20}N_2Pt$, 531.12687).

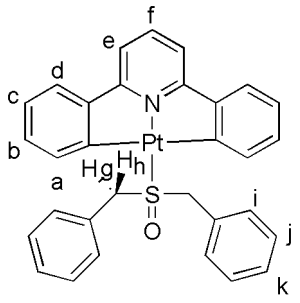

[**L**Pt(S(O)($CH_2Ph)_2$)]

To a yellow solution of [**L**Pt(DMSO)] (0.049 g, 0.098 mmol) in CH_2Cl_2 (10 mL) was added $S(O)(CH_2Ph)_2$ (0.044 g, 0.20 mmol), and the clear bright yellow solution was left stirring at ambient temperature for 18 h. The excess solvent was removed under reduced pressure and the resulting residue was subjected to flash column chromatography (1:1:0.01; CH_2Cl_2:hexane:NEt_3) and subsequent crystallisation from chloroform and hexane to give the desired product as a bright yellow solid. (0.051 g, 81%). m.p. 212-215 °C (dec.); ^{1}H NMR (500 MHz, [D_7]-DMF); δ = 7.95 – 7.93 (2H, m, H_d), 7.87 (1H, t, *J* = 8.0 Hz, H_f), 7.66 – 7.63 (4H, m, H_{c+e}), 7.58 – 7.57 (4H, m, H_i), 7.31 – 7.28 (6H, m, H_{j+k}), 7.20 – 7.17 (2H, m, H_b), 7.08 – 7.05 (2H, m, H_a), 5.25 (2H, d, *J* = 13.0 Hz, $H_{g/h}$), 5.06 (2H, d, *J* = 10 Hz, ^3J (^{195}Pt) = 42 Hz, $H_{g/h}$); ^{13}C NMR (125 MHz, [D_7]-DMF); 138.2 (2C), 122.4 (^3J (^{195}Pt) = 50 Hz), 113.7, 108.8 (^3J (^{195}Pt) = 42 Hz), 103.2, 101.9, 101.8, 100.0, 99.9, 96.0 (2C) 87.0 (^3J (^{195}Pt) = 28 Hz), 34.3 (^3J (^{195}Pt) = 58 Hz); LR-FABMS (3-NOBA matrix): *m/z* = 677 $[MNa]^+$, 655 $[MH]^+$; HR-FABMS (3-NOBA matrix); *m/z* = 655.13907 (calc. for $C_{31}H_{26}ONPtS$, 655.13883).

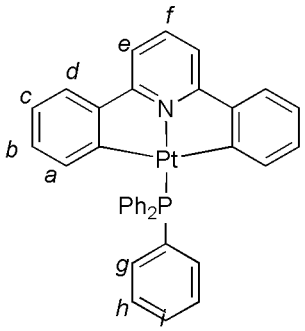

[**L**Pt(PPh_3)]

[**L**Pt(DMSO)] (0.50 g, 1.00 mmol) was dissolved in $CHCl_3$ (20 mL) and to this solution was added PPh_3 (0.26 g, 1.00 mmol). The reaction mixture was then left stirring for 1 min and then the excess solvent was removed under reduced pressure. The product was isolated as a bright yellow solid after flash column chromatography (1:1:0.01; CH_2Cl_2:hexane:NEt_3). Crystals suitable for X-ray crystallography were

grown *via* slow diffusion of di-isopropyl ether into a saturated solution of the desired complex in chloroform to give bright orange crystals. (0.63 g, 93%). m.p. 239 °C (dec.); ^{1}H NMR (500 MHz, CD_2Cl_2): 7.83 – 7.79 (6H, m, H_g), 7.68 (1H, t, J = 7.5 Hz, H_f), 7.45 – 7.34 (13H, m, $H_{d+e+h+i}$), 6.90 – 6.87 (2H, m, H_c), 6.63 – 6.60 (2H, m, H_b), 6.23 (2H, q, J = 7.5 Hz, J (^{195}Pt) = 26 Hz, H_a); ^{13}C NMR (125 MHz, CD_2Cl_2): 166.8 (J (^{195}Pt) = 116 Hz), 166.2, 166.1, 151.3 (2C) (J (^{195}Pt) = 50 Hz), 140.8, 139.0 (2C) (J (^{195}Pt) = 104 Hz), 135.7 (J (^{195}Pt) = 60 Hz), 135.6 (^{3}J (^{195}Pt) = 60 Hz), 132.7 (J (^{195}Pt) = 60 Hz), 132.2 (J (^{195}Pt) = 45 Hz), 130.9 (2C), 129.8 (J (^{195}Pt) = 66 Hz), 128.5, 128.4, 124.1 (J (^{195}Pt) = 51 Hz), 123.8, 115.2 (2C) (J (^{195}Pt) = 45 Hz); ESI-MS *m/z*: 687.0 ([M-H]$^+$); LRESI-MS: *m/z* = 687 [M]$^+$; HRESI-MS: *m/z* = 687.15193 (calc. for $C_{35}H_{27}NPtP$, 687.15234).

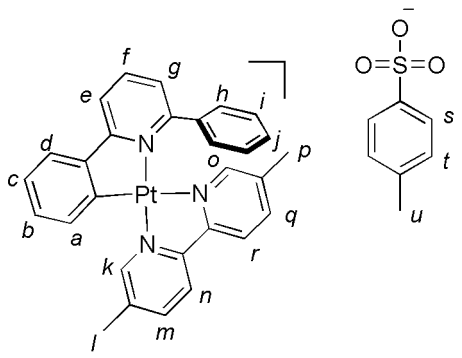

[H**L**Pt(dmbipy)]OTs

To a solution of [**L**Pt(DMSO)] (0.50 g, 10.0 mmol) in CH_2Cl_2 (30 mL) was added 5,5`-dimethyl-2,2`bipyridyl.TsOH (0.37 g, 10.0 mmol) and the reaction mixture stirred at RT for 5 minutes. After this time, the solution was concentrated down to ~ 3 mL under reduced pressure and upon the slow addition of hexane the desired product precipitated from solution as a bright yellow solid. The crude solid was filtered off and collected. Crystals suitable for X-ray crystallography were grown *via* slow diffusion of diisopropyl ether into a saturated solution of the desired complex in chloroform. (0.48 g, 78%) ^{1}H NMR (500 MHz, [D_7]-DMF); δ = 9.47 (1H, s, H_k), 8.73 (1H, s, H_o), 8.59 – 8.50 (3H, m, H_{m+q+f}), 8.44 – 8.38 (4H, m, H_{i+n+g}), 8.07 – 7.98 (4H, m, H_{h+j+r}), 7.66 – 7.62 (3H, m, H_{e+t}), 7.38 – 7.25 (3H, m, H_{b+c+d}), 7.28

(1H, m, H_a), 7.11 (2H, d, ^3J = 8.0 Hz, H_s), 2.71 (3H, s, H_l), 2.32 (3H, s, H_u), 2.29 (3H, s, H_p); ^{13}C NMR (125 MHz, [D_7]-DMF); 167.6, 160.7, 155.9, 153.5, 151.6, 150.1, 148.3, 148.0, 142.5, 141.9, 141.2, 140.6, 139.7, 138.7, 138.1, 137.9, 133.0, 131.3, 130.8, 129.8, 128.6, 128.5, 126.6, 126.1, 125.7, 125.3, 124.2, 122.9, 119.1, 21.1, 18.4 (2C); LRESI-MS: *m/z* = 611 $[M]^+$; HRESI-MS: *m/z* = 611.17716 (calc. for $C_{29}H_{26}N_3Pt$, 611.17690).

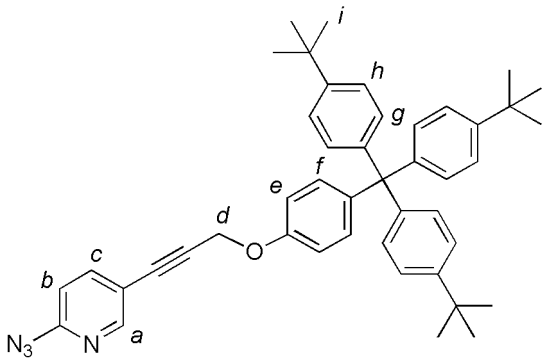

79

To a solution of **86** (0.22 g, 0.34 mmol) in DMF (5 mL) was added sodium azide (0.066 g, 1.0 mmol) and the reaction mixture was stirred at 120°C for 18 h. H_2O (1 x 15 mL) was added to the reaction mixture and the aqueous phase was extracted with CH_2Cl_2 (3 x 20 mL). The organic phases were combined, dried over $MgSO_4$ and then filtered off. The excess solvent was removed under reduced pressure and the resulting residue purified by flash column chromatography on silica (93:7; CH_2Cl_2:EtOAc) and the resulting solid was recrystallised from ethanol to give desired product as a white solid, (0.091 g, 41%). ^{1}H NMR (400 MHz, $CDCl_3$); δ = 8.89 (1H, s, H_a), 8.15 (1H, d, *J* = 6.8 Hz, $H_{b/c}$), 7.42 (1H, d, *J* = 6.8 Hz, $H_{b/c}$), 7.25 – 7.23 (6H, m, H_g), 7.12 (2H, d, *J* = 7.2 Hz, H_f), 7.13 – 7.06 (6H, m, H_h), 6.89 (2H, d, *J* = 7.2 Hz, H_e), 5.22 (2H, s, H_d), 1.30 (27H, s, H_i); ^{13}C NMR (100 MHz, $CDCl_3$);

171.2, 155.6, 151.6, 148.5, 148.3, 143.9, 140.8, 137.7, 132.4, 130.7, 124.4, 124.0, 113.3, 63.1, 60.4, 34.3, 31.4, 21.1, 14.2; LRESI-MS: *m/z* = 697 $[M-K]^+$; HRESI-MS; *m/z* = 697.33342 (calc. for $C_{45}H_{46}ON_4K$, 697.33142).

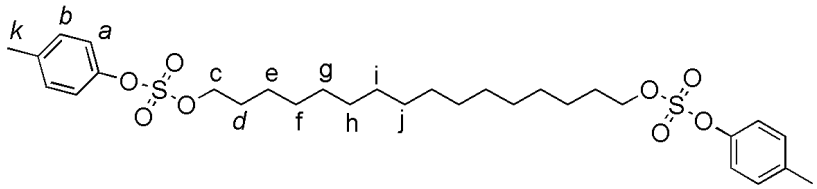

81

To a solution of 1,16-hexadecanediol (1.00 g, 3.9 mmol) and *p*-tosylchloride (1.6 g, 8.5 mmol) in THF (25 mL) was added *N*-methylmorpholine (1.6 g, 15 mmol) to give a cloudy yellow solution. The reaction mixture was left to stir at ambient temperature for five days. The solvent was removed under reduced pressure and to the resulting residue was added CH_2Cl_2 (200 mL). The organic layer was washed with 1 M $NaHCO_3$ (3 x 50 mL), 1 M HCl (3 x 50 mL) and deionized water (3 x 50 mL). The organic phase was dried over $MgSO_4$, filtered, concentrated under reduced pressure then purified by flash column chromatography (3:1; hexane:CH_2Cl_2) providing the desired product as a white solid. m.p. 75-77 °C; ^{1}H NMR (400 MHz, $CDCl_3$); δ = 7.80 (4H, d, *J* = 8.0, H_a), 7.35 (4H, d, *J* = 8.0, H_b), 4.02 (4H, t, *J* = 6.4, H_c), 2.45 (6H, s, H_k), 1.69 – 1.59 (4H, m, H_d), 1.29 – 1.21 (24H, m, H_{e-j}); ^{13}C NMR (100 MHz, $CDCl_3$); 144.6, 133.2, 129.8, 127.9, 70.7, 29.6, 29.6, 29.5, 29.4, 28.9, 28.8, 25.3, 21.6; LRESI-MS: *m/z* = 256 $[M-(OTs)_2]^+$; HRESI-MS: *m/z* = 257.24838 (calc. for $C_{16}H_{33}O_2$, 257.24860).

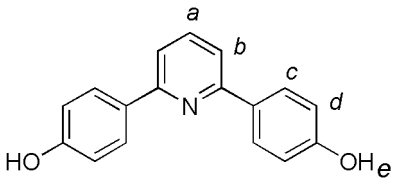

82

Isopropanol (50 mL) was added to potassium tertbutoxide (3.4 g, 44 mmol) and [trans-Dichloro(1,3-bis-(2,6-diisopropylphenyl)imidazolylidinium)(3-chloro-pyridine)palladium] (0.60 g, 0.88 mmol). The reaction was stirred at ambient temperature until a colour change from yellow to red/brown was observed (~10 min). 2,6-Dibromopyridine (4.2 g, 18 mmol) and 4-hydroxyphenylboronic acid (5.0 g, 36 mmol) were added as solids, and the reaction flask was resealed and purged with nitrogen. The reaction mixture was stirred at room temperature for 12 h, then quenched with aqueous saturated NH_4Cl solution (100 mL) and extracted with EtOAc (3 x 100 mL). The combined organic fractions were dried over $MgSO_4$, filtered, concentrated under reduced pressure and then purified by flash column chromatography (3:1; Et_2O:CH_2Cl_2) providing the desired product as an off-white solid. (3.3 g, 53 %) m.p. 222-226 °C; ^{1}H NMR (400 MHz, CD_3OD); δ = 7.98 – 7.94 (4H, m, H_c), 7.78 (1H, t, *J* = 8.0 Hz, H_a), 7.60 (2H, d, *J* = 8.0 Hz, H_b), 6.10 – 6.89 (4H, m, H_d), 4.87 (2H, s, br, H_e); ^{13}C NMR (100 MHz, CD_3OD); 159.8, 158.2, 138.9, 132.4, 129.5, 118.3, 116.5; LR-FABMS (3-NOBA matrix): *m/z* = 263 $[MH]^+$; HR-FABMS (3-NOBA matrix); *m/z* = 263.09510 (calc. for $C_{17}H_{13}O_2N$, 263.09518).

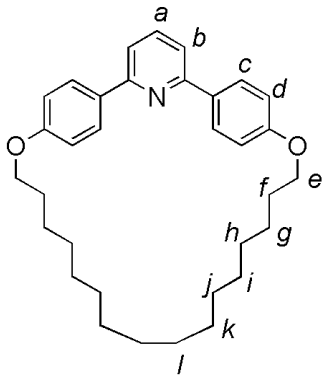

H_2**L8**[6]

81 (1.6 g, 4.6 mmol), **82** (2.3 g, 4.6 mmol) and K_2CO_3 (8.3 g, 60 mmol) were dissolved in anhydrous DMF (800 mL) under an atmosphere of N_2. The reaction

mixture was stirred at 100 °C for 48 h. The solvent was removed under reduced pressure, the resulting residue was dissolved in CH_2Cl_2 (150 mL) and washed with an aq. sat. NH_4Cl solution (2 x 75 mL). The organic layer was dried over $MgSO_4$, filtered, concentrated under reduced pressure and the crude residue was then purified by flash column chromatography (CH_2Cl_2:ether; 3:1) to give the desired product as a white solid, (0.91 g, 41%). m.p. 212-215 °C (dec.); ^{1}H NMR (500 MHz, $CDCl_3$); δ = 8.01 (4H, d, *J* = 9.0 Hz, H_c), 7.73 (1H, t, *J* = 7.5 Hz, H_a), 7.56 (2H, d, *J* = 7.5 Hz, H_b), 7.00 (4H, d, *J* = 9.0 Hz, H_d), 4.03 (4H, t, *J* = 6.5 Hz, H_e), 1.83 – 1.77 (4H, m, H_f), 1.55 – 1.50 (4H, m, H_g), 1.37 – 1.27 (20H, m, $H_{h+i+j+k+l}$); ^{13}C NMR (125 MHz, $CDCl_3$); 160.0, 156.3, 137.2, 132.0, 128.1, 117.0, 114.6, 68.0, 29.5, 29.4 (3C) 29.2, 29.1, 25.9; LRESI-MS: *m/z* = 485 $[MH]^+$; HRESI-MS; *m/z* = 485.32891 (calc. for $C_{33}H_{43}O_2N$, 485.328

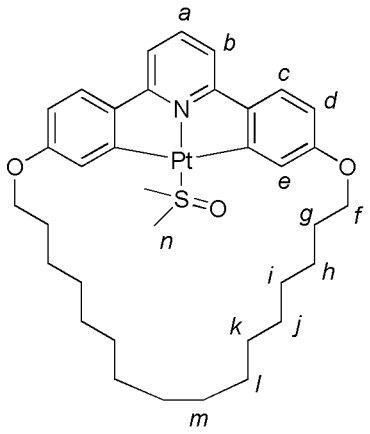

[L8Pt(DMSO)]

H_2**L8** (0.13 g, 0.26 mmol) was dissolved in acetic acid (20 mL) to which $K_2[PtCl_4]$ (0.11 g, 0.25 mmol), dissolved in H_2O (8 mL), was added dropwise to give a light rose coloured inhomogeneous solution. The mixture was refluxed for 3 days upon which time the red colour of the Pt salt had disappeared. The yellow precipitate which had formed was filtered off and washed with water (10 mL), acetone (5 mL), Et_2O (5 mL) and hexane (10 mL). The yellow solid was then dissolved in DMSO (4 mL) and K_2CO_3 (0.14 g, 1.00 mmol) and H_2O (4 mL) were added and the mixture heated to 90 ºC for 3 hr. Upon the addition of water (50 mL) the product precipitated from solution as a bright yellow solid. Flash column chromatography (CH_2Cl_2) and recrystallisation (CH_2Cl_2:hexane) gave the product as a bright yellow solid. (0.024 g,

12%). (^{1}H NMR 400 MHz, $CDCl_3$): 7.52 (1H, t, J = 8.0 Hz, H_a), 7.46 (2H, d, ^4J = 2.4 Hz, H_e), 7.40 (2H, d, J = 8.4 Hz, H_c), 7.06 (2H, d, J =8.0 Hz, H_b), 6.64 (2H, dd, J = 8.4 Hz, ^4J = 2.4 Hz, H_d), 4.19 (4H, t, J =7.2 Hz, H_f), 3.72 (6H, s, J(^{195}Pt) = 26 Hz, H_n); 1.79 – 1.56 (4H,m, H_g), 1.44 – 1.42 (4H, m, H_h), 1.40 – 1.25 (20H, m, $H_{i+j+k+l+m}$), (^{13}C NMR 400 MHz, $CDCl_3$): 168.2, 166.4, 160.5, 142.2, 141.0, 126.1, 121.2, 113.4, 113.1, 68.4, 48.4, 30.2, 30.0, 29.9, 29.8, 29.4, 28.5, 25.7; LRESI-MS: m/z = 757 $[MH]^+$; HRESI-MS; m/z = 757.29854 (calc. for $C_{35}H_{48}O_3NPtS$, 757.29972).

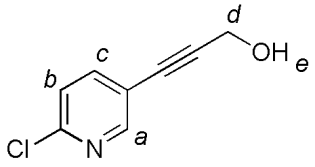

84

To a solution of 2-chloro-5-iodo-pyridine (1.0 g, 4.2 mmol) in THF (15 mL) and NEt_3 (7 mL), was added copper(I) iodide (0.048 g, 0.25 mmol) and $Pd(Ph_3)_4$ (0.15 g, 0.13 mmol). Propargyl alcohol (0.23 g, 4.2 mmol) was then added to the reaction and the mixture was stirred in the absence of light for 20 h at room temperature. After this time, the excess solvent was removed under reduced pressure. The resulting residue was dissolved in EtOAc (100 mL) and washed with saturated aqueous NH_4Cl (3 x 50 mL). The aqueous phase was extracted with EtOAc (3 x 50 mL) and the combined organic extracts were washed with brine (50 mL) and dried over Na_2SO_4. The excess solvent was removed under reduced pressure and the resulting residue purified by flash column chromatography (Et_2O) providing the desired compound as a pale yellow solid (0.64 g, 91%). m.p. 62-66 °C; ^{1}H NMR (400 MHz, $CDCl_3$); δ = 8.46 (1H, d, ^4J = 2.0 Hz, H_a), 7.68 – 7.66 (1H, m, $H_{b/c}$), 7.31 – 7.29 (1H, m, $H_{b/c}$), 4.52 (2H, s, H_d), 1.98 (1H, s, br, H_e); ^{13}C NMR (100M Hz, $CDCl_3$); 152.2,

150.8, 141.1, 123.9, 118.6, 91.8, 81.1, 51.5; LR-FABMS (3-NOBA matrix): *m/z* = 168 $[MH]^+$; HR-FABMS (3-NOBA matrix); *m/z* = 167.01384 (calc. for C_8H_6OCl, 167.01434).

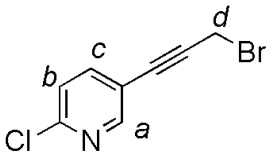

85

To a solution of **84** (2.5 g, 15 mmol) and CBr_4 (5.5 g, 17 mmol) in CH_2Cl_2 (300 mL) at 0 °C was added PPh_3 (4.4 g, 17 mmol). The solution was allowed to warm to RT and was then stirred at room temperature for 18 h. The excess solvent was removed under reduced pressure and the crude residue was purified by flash column chromatography (Ether: Et_2O 1:1) to give the desired product as off-white solid. (0.78 g, 23%). ^{1}H NMR (400 MHz, $CDCl_3$); δ = 8.46 (1H, d, ^4J = 2.0 Hz, H_a), 7.69 – 7.66 (1H, m, $H_{b/c}$), 7.31- 7.29 (1H, m, $H_{b/c}$), 4.13 (2H, s, H_d); ^{13}C NMR (100 MHz, $CDCl_3$); 152.3, 151.1, 141.2, 123.9, 118.2, 88.7, 81.9, 14.1; LR-FABMS (3-NOBA matrix): *m/z* = 228 $[M-H]^-$; HR-FABMS (3-NOBA matrix); *m/z* = 228.93001 (calc. for C_8H_5NBrCl, 228.92994).

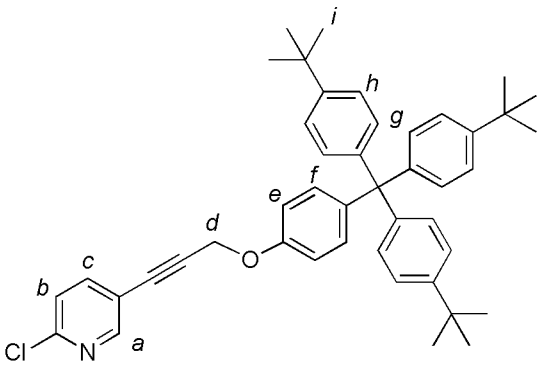

86

To a solution of **85** (0.70 g, 3.1 mmol) and 4-[tris-(4-*tert*-butylphenyl)methyl]phenol[22] (1.5 g, 3.1 mmol) in butanone (100 mL) was added K_2CO_3 (3.9 g, 30 mmol) and the resulting mixture was heated at reflux for 36 h. After this time, the reaction was filtered through celite, and the resultant solution concentrated down under reduced pressure. The crude residue was purified by column chromatography (hexane:CH_2Cl_2; 1:1) to give the desired product as an off-

white solid. (1.6 g, 79%). m.p. 216-219 °C; ^{1}H NMR (400 MHz, $CDCl_3$); δ = 8.45 (1H, d, ^{4}J = 2.0 Hz, H_a), 7.68 (1H, dd, J = 8.0 Hz, ^{4}J = 2.0 Hz, H_c), 7.30 – 7.22 (7H, m, H_{b+g}), 7.14 (2H, d, J = 9.2 Hz, H_f), 7.09 – 7.06 (6H, m, H_h), 6.85 (2H, d, J = 9.2 Hz, H_e), 4.89 (2H, s, H_d), 1.30 (27H, s, H_i); ^{13}C NMR (100 MHz, $CDCl_3$); 155.5, 152.3, 151.0, 148.4, 144.0, 141.2, 140.7, 132.3, 130.7, 124.1, 123.9, 118.4, 113.4, 88.8, 82.5, 63.1, 56.4, 34.3, 31.4; LRESI-MS: *m/z* = 654 $[M-H]^-$; HRESI-MS; *m/z* = 653.34222 (calc. for $C_{45}H_{48}NOCl$, 653.34189).

7.2.9 Exchange Reactions for Chapter Five

a) [LPt(PyH)] +dmbipy + TsOH ⟶ [HLPt(dmbipy)]OTs + PyH

To a solution of [**L**Pt(PyH)] (3.5 mg, 7.0 μmol) in [D_6]-acetone/CD_2Cl_2; 1:1 (0.4 mL) at 298 K was added TsOH (1.3 mg, 7.0 μmol) and a lightening of the solution was observed after the reaction mixture was agitated for one min. The subsequent addition of dmbipy (1.2 mg, 7.0 μmol) to the reaction mixture and agitation for one min led to a darkening of the solution to clear bright yellow and the ^{1}H NMR spectrum was recorded.

b) [LPt(PyNMe$_2$)] + dmbipy + TsOH ⟶ [HLPt(dmbipy)]OTs + PyNMe$_2$

To a solution of [**L**Pt(PyNMe$_2$)] (4.3 mg, 7.9 μmol) in [D_6]-acetone/CD_2Cl_2; 1:1 (0.45 mL) at 298 K was added TsOH (1.5 mg, 7.9 μmol) and a lightening of the solution was observed after the reaction mixture was agitated for one min. The subsequent addition of dmbipy (1.5 mg, 7.9 μmol) to the reaction mixture and agitation for one min led to a darkening of the solution to clear bright yellow and the ^{1}H NMR spectrum was recorded.

c) [LPt(S(O)($CH_2Ph)_2$)] + dmbipy.TsOH $\rightleftharpoons$ [HLPt(dmbipy)]OTs +S(O)($CH_2Ph)_2$

Method (a) direct addition of dmbipy·2TsOH.

To a solution of [**L**Pt(S(O)($CH_2Ph)_2$)] (4.1 mg, 6.3 μmol) in [D_7]-DMF (0.4 mL) at 298 K was added dmbipy.TsOH (2.2 mg, 6.3 μmol). The mixture was agitated for one minute to give a clear bright yellow solution and the ^{1}H NMR spectrum was recorded to show quantitative displacement of S(O)($CH_2Ph)_2$ and formation of [H**L**Pt(dmbipy)]OTs in a quantitative yield. Then P_1-^{t}Bu (7.3 mg, 31 μmol) was added directly to the NMR tube and the reaction mixture agitated for one min and left 12 h at 298 K and the ^{1}H NMR spectrum recorded at regular intervals until no further was observed.

Method (b) sequential addition of TsOH and dmbipy.

To a solution of [**L**Pt(S(O)($CH_2Ph)_2$)] (4.1 mg, 6.3 μmol) in [D_7]-DMF (0.4 mL) at 298 K was added TsOH (1.19 mg, 6.3 μmol) and a lightening of the solution was observed after the reaction mixture was agitated for one min. The subsequent addition of dmbipy (1.15 mg, 6.3 μmol) to the reaction mixture and agitation for one min led to a darkening of the solution to clear bright yellow and the ^{1}H NMR spectrum was recorded. ^{1}H NMR spectrum showed the quantitative displacement of S(O)($CH_2Ph)_2$ and formation of [H**L**Pt(dmbipy)]OTs in a quantitative yield. Then P_1-^{t}Bu (7.3 mg, 31 μmol) was added directly to the NMR tube and the reaction mixture agitated for one min and left 12 h at 298 K and the ^{1}H NMR spectrum recorded at regular intervals until no further was observed.

d) [LPt(3,5-Lut)] + dmbipy.TsOH $\rightleftharpoons$ [HLPt(dmbipy)]OTs + 3,5-Lut

Method (a) direct addition of dmbipy·2TsOH.

To a solution of [**L**Pt(3,5-Lut)] (3.2 mg, 6.0 μmol) in [D_7]-DMF (0.35 mL) was added dmbipy.TsOH (2.2 mg, 6.0 μmol). The mixture was agitated for one min to give a clear bright yellow solution and the ^{1}H NMR spectrum was recorded. The spectrum showed the formation of [H**L**Pt(dmbipy)]OTs. Then P_1-^{t}Bu (7.1 mg, 30 μmol) was added directly to the NMR tube and the reaction mixture agitated for one

min and left 12 h at 298 K and the ^{1}H NMR spectrum recorded at regular intervals until no further was observed.

Method (b) sequential addition of TsOH and dmbipy.

To a solution of in [**L**Pt(3,5-Lut)] (3.2 mg, 6.0 μmol) [D_7]-DMF (0.35 mL) at 298 K was added TsOH (1.15 mg, 6.0 μmol) and a lightening of the solution was observed after the reaction mixture was agitated for one min. The subsequent addition of dmbipy (1.11 mg, 6.25 μmol) to the reaction mixture and agitation for one min led to a darkening of the solution to clear bright yellow and the ^{1}H NMR spectrum was recorded. Then P_1-^{t}Bu (7.1 mg, 30 μmol) was added directly to the NMR tube and the reaction mixture agitated for one min and left 12 h at 298 K and the ^{1}H NMR spectrum recorded at regular intervals until no further was observed

e) [LPt(PPh_3)] + dmbipy.TsOH

Method (a) direct addition of dmbipy·2TsOH.

To a solution of [**L**Pt(PPh_3)] (4.3 mg, 6.3 μmol) in [D_7]-DMF (0.4 mL) was added dmbipy.TsOH (2.3 mg, 6.3 μmol). The mixture was agitated for one min to give a clear bright yellow solution and the ^{1}H NMR spectrum was recorded.

Method (b) sequential addition of TsOH and dmbipy.

To a solution of in [**L**Pt(PPh_3)] (4.3 mg, 6.3 μmol) [D_7]-DMF (0.4 mL) at 298 K was added TsOH (1.2 mg, 6.3 μmol) and a lightening of the solution was observed after the reaction mixture was agitated for one min. The subsequent addition of dmbipy (1.2 mg, 6.3 μmol) to the reaction mixture and agitation for one min led to a darkening of the solution to clear bright yellow and the ^{1}H NMR spectrum was recorded.

Crystal data and structure refinement for [LPt(3,5-Lut)], [LPt(PPh_3)] and [HLPt(dmbipy)OTs].

Structural data were collected at 93 K using a Rigaku Mercury diffractometer (MM007 high-flux RA/MoKa radiation, confocal optic). All data collection

employed narrow frames (0.3-1.0) to obtain at least a full hemisphere of data. Intensities were corrected for Lorentz polarisation and absorption effects (multiple equivalent reflections). The structures were solved by direct methods, non-hydrogen atoms were refined anisotropically with CH protons being refined in riding geometries (SHELXTL) against F^2.

Table 7.15 Crystal data and structure refinement for [**L**Pt(3,5-Lut)].

Identification code	[**L**Pt(3,5-Lut)]	
Empirical formula	C24 H20 N2 Pt	
Formula weight	531.51	
Temperature	93(2) K	
Wavelength	0.71073 Å	
Crystal system	Monoclinic	
Space group	P2(1)/n	
Unit cell dimensions	a = 7.402(2) Å	α = 90°.
	b = 18.424(5) Å	β = 90.431(10)°.
	c = 13.588(4) Å	γ = 90°.
Volume	1853.1(10) $Å^3$	
Z	4	
Density (calculated)	1.905 Mg/m^3	
Absorption coefficient	7.583 mm^{-1}	
F(000)	1024	
Crystal size	0.10 x 0.10 x 0.03 mm^3	
Theta range for data collection	1.86 to 25.33°.	
Index ranges	-7<=h<=8, -18<=k<=22, -16<=l<=16	
Reflections collected	11348	
Independent reflections	3343 [R(int) = 0.0525]	
Completeness to theta = 25.00°	99.1 %	
Absorption correction	Multiscan	
Max. and min. transmission	1.000 and 0.579	
Refinement method	Full-matrix least-squares on F^2	
Data / restraints / parameters	3343 / 0 / 246	
Goodness-of-fit on F^2	1.064	

Final R indices [I>2sigma(I)]	R1 = 0.0302, wR2 = 0.0684
R indices (all data)	R1 = 0.0414, wR2 = 0.0756
Largest diff. peak and hole	1.467 and -2.092 e.Å^{-3}

Table 7.16 Crystal data and structure refinement for [**L**Pt(PPh$_3$)].

Identification code	[**L**Pt(PPh$_3$)]	
Empirical formula	C35 H26 N P Pt	
Formula weight	686.63	
Temperature	93(2) K	
Wavelength	0.71073 Å	
Crystal system	Monoclinic	
Space group	P2(1)/c	
Unit cell dimensions	a = 13.981(7) Å	α = 90°.
	b = 9.441(5) Å	β = 95.771(9)°.
	c = 20.635(8) Å	γ = 90°.
Volume	2710(2) Å^3	
Z	4	
Density (calculated)	1.683 Mg/m^3	
Absorption coefficient	5.262 mm^{-1}	
F(000)	1344	
Crystal size	0.2000 x 0.1000 x 0.0500 mm^3	
Theta range for data collection	2.34 to 25.34°.	
Index ranges	-16<=h<=15, -11<=k<=11, -24<=l<=22	
Reflections collected	25318	
Independent reflections	4919 [R(int) = 0.0636]	
Completeness to theta = 25.00°	99.3 %	
Absorption correction	Multiscan	
Max. and min. transmission	1.0000 and 0.5740	
Refinement method	Full-matrix least-squares on F^2	
Data / restraints / parameters	4919 / 0 / 343	
Goodness-of-fit on F^2	0.823	

Final R indices [I>2sigma(I)]	R1 = 0.0286, wR2 = 0.0743
R indices (all data)	R1 = 0.0303, wR2 = 0.0766
Largest diff. peak and hole	1.119 and -1.511 e.Å^{-3}

Table 6.17 Crystal data and structure refinement for [H**L**Pt(dmbipy)]OTs.2CHCl$_3$.

Identification code	[H**L**Pt(dmbipy)]OTs.2CHCl$_3$	
Empirical formula	C38 H33 Cl6 N3 O3 Pt S	
Formula weight	1019.52	
Temperature	93(2) K	
Wavelength	0.71073 Å	
Crystal system	Monoclinic	
Space group	P2(1)/c	
Unit cell dimensions	a = 16.521(4) Å	α = 90°.
	b = 14.330(3) Å	β = 115.215(5)°.
	c = 17.844(4) Å	γ = 90°.
Volume	3821.8(14) Å^3	
Z	4	
Density (calculated)	1.772 Mg/m^3	
Absorption coefficient	4.188 mm^{-1}	
F(000)	2008	
Crystal size	0.10 x 0.06 x 0.06 mm^3	
Theta range for data collection	2.30 to 25.36°.	
Index ranges	-18<=h<=19, -13<=k<=17, -20<=l<=21	
Reflections collected	23501	
Independent reflections	6874 [R(int) = 0.0535]	
Completeness to theta = 25.00°	98.6 %	
Absorption correction	Multiscan	
Max. and min. transmission	1.0000 and 0.725	
Refinement method	Full-matrix least-squares on F^2	
Data / restraints / parameters	6874 / 6 / 472	
Goodness-of-fit on F^2	1.116	
Final R indices [I>2sigma(I)]	R1 = 0.0606, wR2 = 0.1515	
R indices (all data)	R1 = 0.0696, wR2 = 0.1583	
Largest diff. peak and hole	2.479 and -2.569 e.Å^{-3}	

7.3. References

[1] D. H. Cai, D. L. Hughes, T. R. Verhoeven; *Tetrahedron Lett.,* 1996, **37**, 2537.

[2] T. Bunlaksananusurn, K. Polburn, P. Knochel; *Angew. Chem. Int. Ed.,* 2003, **42**, 3941.

[3] (a) G. W. V. Cave, F. P. Fanizzi, R. J. Deeth, W. Errington, J. P. Rourke, *Organometallics*, 2000, **19**, 1355; (b) J. D. Crowley, I. M. Steele, B. Bosnich, *Inorg. Chem.,* 2005, **44**, 2989.

[4] G. T. Morgan, F. H. Burstall; *J. Chem. Soc.,* 1934, 965.

[5] H. Nikol, H. -B. Bürgi, K. I. Hardcastle, H. B. Gray, *Inorg. Chem.* 1995, **34**, 6319.

[6] V. Aucagne, J. Berna, J. D. Crowley, S. M. Goldup, K. D. Hanni, D. A. Leigh, P. J. Lusby, V. E. Ronaldson, A. M. Z. Slawin, A. Viterisi, D. B. Walker, *J. Am. Chem. Soc.,* 2007, **129**, 11950.